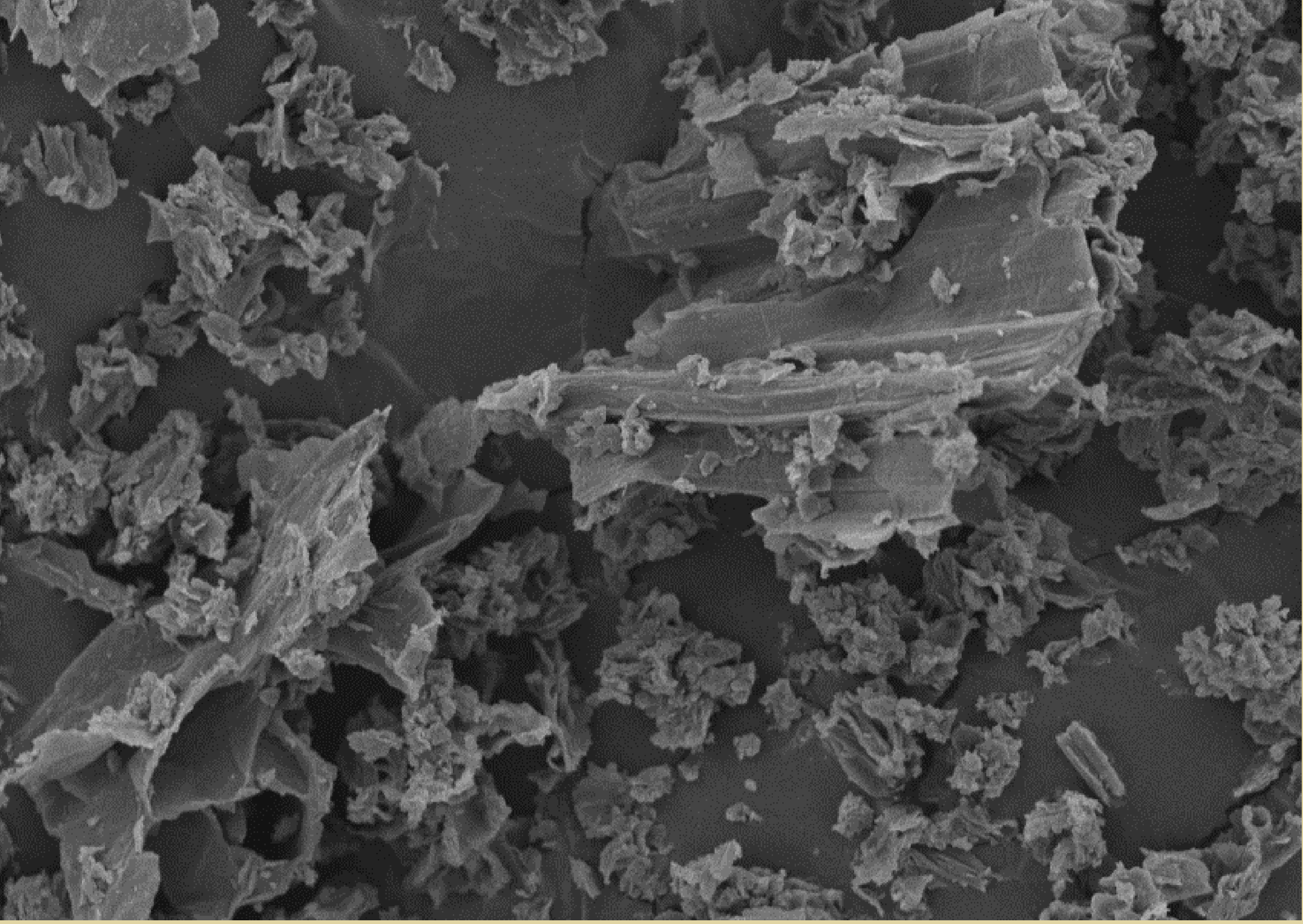

Fábio Luís Ribeiro Branco

Controlled Modification of Graphene by Living Radical Polymerization

Master Degree Thesis in Chemical Engineering, supervised by Doctor Jorge F. J. Coelho, by Doctor Arménio C. Serra and by Master Francisco T. A. Catalão, submitted to the Faculty of Science and Tecnology of the University of Coimbra.

September 2014

UNIVERSIDADE DE COIMBRA

Fábio Luís Ribeiro Branco

Controlled modification of Graphene by Living Radical Polymerization

Master Degree Thesis in the scientific area of Chemical Engineering, supervised by Doctor Jorge F. J. Coelho, by Doctor Arménio C. Serra and by Master Francisco T. A. Catalão, submitted to the Faculty of Science and Technology of the University of Coimbra

Supervisors:

PhD Jorge F. J. Coelho

PhD Arménio C. Serra

Host institutions:

CEMUC - Centre for Mechanical Engineering, Department of Chemical Engineering, Faculty of Sciences and Technology of the University of Coimbra

Coimbra

2014

· U C ·

UNIVERSIDADE DE COIMBRA

Acknowledgements

This work is the culmination of a long academic journey, in which I grew up as a person and as a professional. Many people were involved in this learning process, from professionals to friends and family. I would like to take this opportunity to thank to all these people.

To all the professionals that, since the nursery school to the fifth year of the graduate course, taught me all the scientific knowledge that allowed me to achieve this point of my academic career.

To my supervisors, Ph.D. Jorge F. J. Coelho and Ph.D. Arménio C. Serra, for the help, support, for all the trust they have placed in me and for the opportunity and privilege of working on a Research Group in which the excellence is the level that prevails.

A very special thank to the Master Francisco Catalão for the tirelessly help and support, he was always present, on the good and bad moments, always informed, always applied. I can state that without him this work would be far more complex.

To all the members of the Polymer Research Group, in particular to Master Joana Mendes, that were always available to help and for providing an excellent working environment.

To all my friends and family who have contributed, during all my life, for my happiness and growth as a citizen. They are an important part of my life.

To my parents for giving me the best conditions to arrive until this stage of my life. I thank, from the bottom of my heart, all the teachings and education that they provided me, I believe that they make me a better, and most important, a most prepared person.

Finally, to my sweet Inês Serôdio, a very special person in my life that has in my heart a special place forever. She is my strength in the moments of weakness, my calm and peace in the moments of stress, my happiness in the moments of sorrow. Thank you for your patience, support, understanding and dedication.

A huge thank you to everyone.

Abstract

The main goal of this work was to study some experimental approaches to accomplish the controlled modification of Graphene oxide (GO) with polymer brushes by using controlled polymerization techniques, CLRP (Controlled / Living Radical Polymerization).

Some CLRP reactions were firstly conducted in homogeneous medium by applying the Supplemental Activator and Reducing Agent Atom Transfer Radical Polymerization (SARA ATRP) technique. The work plan was inserted in two projects underway in the Polymer group of the Department of Chemical Engineering, University of Coimbra. One project a synergistic effect between the ionic liquid 1-butyl-3-methylimidazolium hexafluorophosphate (BMIM-PF_6) and dimethyl sulfoxide (DMSO) mixtures was discovered for the SARA ATRP of methyl acrylate (MA) using as catalytic system of sodium dithionate ($Na_2S_2O_4$) and $CuBr_2$ / Me_6TREN (Me_6TREN: tris [2 (dimethylamino) ethyl] amine) at room temperature. In the second project, it was discovered that sulfolane is an efficient and universal solvent for copper mediated atom transfer radical (co) polymerization of acrylates, methacrylates, styrene (Sty) and vinyl chloride (VC).

GO was firstly functionalized with initiator molecules. Two methods reported in the literature with α-bromo isobutyrylbromide (BIBB) were tested: modification of carboxyl (-COOH) and hydroxyl (-OH) groups of GO or only –OH groups of GO. Through X-ray photoelectron spectroscopy (XPS) it was determined the amount of bromine atoms (Br) covalently bonded to GO (0.34 mmol per gram of GO with first method and 0.51 to 0.72 mmol of Br per gram of GO with second method).

The graft copolymerization of Sty from GO macroinitiators using the SARA ATRP catalyzed by Cu (0) wire/TREN (Tris(2-aminoethyl)amine) were carried out and resulted in an uncontrolled polymerization, and the polystyrene (PS) was found detached. It was impossible to understand the scientific reason behind this result during the course of this work.

The SARA ATRP of MA catalysed by Cu (0) wire/Me_6TREN was also studied. PMA was polymerized from the surface of GO, with molecular weights around 30 kDa and dispersity values lower than 1.5. The results suggest that it was possible to polymerize PMA from the surface of GO apparently with good control over the “grafting-from” polymerization, using a catalytic system developed in our department that uses low concentrations of catalyst.

Additional experiments using free initiator molecules (also known as sacrificial initiator) carried out revealed that only free polymer chains were produced.

Resumo

O principal objetivo deste trabalho foi estudar algumas abordagens experimentais para realizar a modificação controlada de grafeno oxidado (GO) com cadeias poliméricas, recorrendo a técnicas de polimerização controlada, CLRP (Controlled/Living Radical Polymerization).

Algumas reações CLRP foram conduzidas em meio homogéneo, aplicando a técnica *Supplemental Activator Reducing Agent Atom Tranfer Radical Polymerization* (SARA ATRP). Estas reações foram realizadas no âmbito de dois projetos do grupo de Polímeros do Departamento de Engenharia Química da Universidade de Coimbra. Num projeto um efeito sinérgico entre misturas do líquido iónico hexafluorofosfato de 1-butil-3-metilimidazólio (BMIM-PF$_6$) e dimetilsulfóxido (DMSO) foi descoberto para a SARA ATRP de acrilato de metilo (MA), utilizando como sistema catalítico ditionato de sódio ($Na_2S_2O_4$) e $CuBr_2$/Me$_6$TREN (Me$_6$TREN: tris [2 (dimetilamino) etil] amina) à temperatura ambiente. No segundo projeto, foi descoberto que o sulfolano é um solvente eficaz e universal para a (co)polimerização ATRP de acrilatos, metacrilatos, estireno (Sty) e cloreto de vinilo (VC) catalisada por cobre.

Inicialmente o GO foi funcionalizado com moléculas de iniciador. Dois métodos reportados na literatura com α-bromo isobutyrylbromide (BIBB) foram testados: modificação dos grupos carboxilo (-COOH) e hidroxilo (-OH) do GO ou apenas dos grupos -OH. Através de espectroscopia fotoelectrónica de raios-X (XPS), determinou-se a quantidade de átomos de bromo (Br) ligados covalentemente ao GO (0.34 mmol por grama de GO com o primeiro método e 0.51-0.72 mmol de Br por grama de GO com o segundo método).

Foram conduzidas reações de copolimerizações de Sty a partir dos macroiniciadores de GO utilizando a SARA ATRP catalisada por Cu (0) em fio/TREN (Tris(2-aminoethyl)amine), obtendo-se polimerizações descontroladas e poliestireno (PS) não ligado. No decorrer deste trabalho não foi possível compreender a razão científica por trás deste resultado.

Foi também estudada a SARA ATRP de MA catalisada por Cu (0) em fio / Me$_6$TREN. Poli metil acrilato (PMA) foi polimerizado a partir da superfície do GO, tendo-se determinado pesos moleculares de aproximadamente 30 kDa e valores de polidispersividade inferiores a 1.5. Os resultados sugerem que foi possível polimerizar PMA a partir da superfície de GO de uma forma aparentemente controlada, utilizando um sistema catalítico desenvolvido no nosso departamento que utiliza baixas concentrações de catalisador.

Foram ainda realizadas experiencias usando moléculas de iniciador livre (também conhecido como *Sacrificial Initiator*) obtendo-se apenas cadeias poliméricas livres.

Thesis Outline

Since the discovery of graphene in 2004, achieved by Konstantin Novoselov, Andre Geim and co-workers, the interest in the use of such carbon nanomaterial in diverse areas has grown dramatically as result of their outstanding electrical, thermal and mechanical properties. Many studies have been conducted to functionalize graphene with oxygen containing species (yielding the graphene oxide (GO)) and organic species, such as polymers, in order to improve its compatibility with various types of solvents and organic materials. The ultimate goal of these modifications is to produce nanocomposites with unique properties.

Within the scope of this dissertation, some experimental approaches were explored to accomplish the controlled modification of GO with polymer brushes by using controlled polymerization techniques, CLRP (Controlled / Living Radical Polymerization).

In the beginning of this work GO was experimentally unknown to us. In addition, I, in particular, hadn't any experience in laboratorial techniques, namely in CLRP experiments. Considering this, to gain some experience in the CLRP (theoretical and experimental) some polymerizations were carried out in homogeneous medium by applying the CLRP technique Supplemental Activator and Reducing Agent Atom Transfer Radical Polymerization (SARA ATRP). These reactions were conducted under scope of two projects developed by the Polymer Research Group of the Department of Chemical Engineering, University of Coimbra originating two publications in *ACS Macro Letters*. The articles published and the respective supporting information (SI) are shown in Appendices C, D, E and F.

After acquiring some experience in CLRP we started to work with GO. Before polymerize from its surface was necessary to functionalize it with alkyl bromide groups. Two methods reported in the literature were tested. Preliminary reactions were carried out in other to understand which one of the methods could provide more functionalization of GO. In the end of this step the method through which was possible to attach more bromide molecules was used to produce significant amounts of macroinitiator (GO-Br) for future polymerizations. This was our first contact with GO, which means that some problems were found and overcome. A significant part of the semester was taken with this stage. In Chapter 2 section 2.1 is presented all the work developed with the objective of functionalize GO with initiator molecules. A brief description of the various reactions, the main results and decisions are exposed in this Chapter.

After GO-Br yielded, in the final phase of the work, diverse "grafting-from" CLRP reactions were carried out using different monomers and catalytic systems with the goal of produce polymer brushes in the GO's surface. Preliminary polymerizations and one system reported in the literature were conducted aiming to gain some experience in polymerizations from GO and to understand the suitable procedures to conduct such reactions with success. Finally, SARA ATRP reactions from the surface of GO-Br were carried out employing one system that uses low concentrations of catalysts, in order to achieve the main goal of the work. In addition, some reactions using free initiator molecules (also known as sacrificial initiator) were carried out, aiming to improve the control over the grafting polymerization. In Chapter 2 section 2.2 are presented possible polymerization techniques from GO's surface reported in the literature, the experiments carried out and the respective results and conclusions.

In Chapter 3 are presented all the materials and procedures used in the different experiments carried out and all the characterization techniques employed to evaluate the success of the reactions. Finally, some suggestions for future works as well as the main conclusions of this work are exposed in Chapter 4.

Nomenclature

$Đ$	Dispersity
$M_{monomer}$	Monomer molecular weight
$M_{Initiator}$	Initiator molecular weight
$\bar{M}_n$	Number-average molecular weight
$\bar{M}_{n,GPC}$	Number-average molecular weight determine by GPC
$\bar{M}_{n,th}$	Theoretical number-average molecular weight, calculated from ^{1}H NMR
$\bar{M}_w$	Weigh-average molecular weight
^{1}H NMR	Proton NMR spectroscopy
AA	Acrylamide molecular imprinted polymer
AFM	Atom force microscopy
APTES	(3-aminopropyl) triethoxysilane
ARGET ATRP	Activators Regenerated by Electron Transfer
ATRA	Atom Transfer Radical Addition
ATRP	Atom Transfer Radical Polymerization
BE	Binding Energy
BEB	1-bromoethylbenzene
BIBB	α-bromoisobutyryl bromide
BMIM-PF_6	1-butyl-3 methylimidazolium hexafluorophosphate
BPMODA	Bis(2-pyridylmethyl)octadecylamine
Bpy	2,2'-Bipyridine
Br	Bromine
C	Catalyst
CD	3-((4-hydroxybutoxy)dimethylsilyl)propyl methacrylate
CLRP	Controlled Living Radical Polymerization
CuBr	Copper(I) bromide
$CuBr_2$	Copper(II) bromide
DMSO	Dimethyl sulfoxide
DP	Degree of polymerization

e-ATRP	Electrochemically mediated ATRP
EBiB	Ethyl α-bromoisobutyrate
EBPA	Ethyl α-bromophenylacetate (EBPA)
EDC.HCL	N-(3-(dimethylamino)propyl)-N’-ethylcarbodiimide hydrochloride
EDMA	Ethylene glycol dimethacrylate
ESCA	Electron Spectroscopy for Chemical Analysis
FRP	Free Radical Polymerization
FTIR-ATR	Fourier transform infrared spectroscopy - Attenuated total reflection
GO	Graphene oxide
GO-Br	Graphene oxide modified with initiator moieties (BIBB)
GPC	Gel permeation chromatography
HEA	hydroxy ethyl acrylate
HMTETA	1,1,4,7,10,10 hexylmethyltriethylenetetramine
HPSEC	High performance size-exclusion chromatography
HRTEM	High resolution transmission electron microscopy
I	Initiator
ICAR ATRP	Initiators for continuous actrivator regeneration
IR	Infrared
k_{act}	Constant rate of activation
k_{deact}	Constant rate of deactivation
k_{exch}	Constant rate of exchange
k_p	Constant rate of propagation
k_p^{app}	Apparent constant rate of propagation
k_t	Constant rate of termination
L	Ligand
M	Monomer
MA	Methyl acrylate
m_i	Initial mass
m_f	Final mass
MMA	Methyl methacrylate
MALDI-TOF	Matrix Assisted Laser Desorption Ionization – Time Of Flight – Mass Spectrometry
Me_6TREN	Tris(2-(dimethylamino)ethyl)amine
MPS	3-(trimethoxysilyl)propyl methacrylate

MW	Molecular weight
NHS	N-Hydroxysuccinimide
NMP	Nitroxide mediated polymerization
P4VP	Poly(4-vinylpyridine)
PAM	Propionamide
PAA	Poly(acrylic acid)
PBA	Poly(butyl acrylate)
PDMA	Poly(dimethylamino ethyl methacrylate)
PDMAEMA	Poly((2-N,N-dimethylamino)ethyl methacrylate)
PDMAEA	Poly(dimethyl amino-ethyl acrylate)
PE	Polyethylene
PEMA	Poly(2-(ethyl(phenyl)amino)ethyl methacrylate)
PMA	Poly(methyl acrylate)
PMAAm	Poly(methacrylamine)
PMDETA	N,N,N,N,N-Pentamethyldiethylenetriamine
PMMA	Poly(methyl methacrylate)
PNIPAm	Poly(N-isopropylacrylamide)
PP	Polypropylene
PPEGEEMA	Poly[poly(ethylene glycol) ethyl ether methacrylate]
ppm	Parts per million
PS	Polystyrene
PSSS	Poly(sodium 4-styrenesulfonate)
PtBA	Poly(ter-butyl acrylate)
PtMA	Poly(ter-butyl methacrylate)
PVFD	Poly(vinylidene fluoride)
PVK	Poly(N-vinylcarbazole)
RA	Reducing Agent
RAFT	Reversible Addition-Fragmentation Chain Transfer
RDRP	Reversible-deactivation radical polymerization methods
Rel%	Relative percentage
rGO	Reduced graphene oxide
VC	Vinyl chloride
SARA ATRP	Supplemental Activator and Reducing Agent Atom Transfer Radical Polymerization

SEM	Scanning electron microscopy
SET-LRP	Single-Electron Transfer Living Radical Polymerization
SFRP	Stable free radical polymerization
SIP	Surface initiated polymerization
Sty	Styrene
T	Temperature
$TBAPF_6$	Tetrabutylammonium hexafluorophosphate
TEA	Triethylamine
TGA	Thermogravimetric analysis
Tg	Glass transition temperature
TREN	Tris(2-aminoethyl)amine
XPS	X-ray photoelectron spectroscopy
XRD	X-ray diffraction

Contents

Acknowledgements III

Abstract V

Resumo VII

Thesis Outline IX

Nomenclature XI

Contents XV

List of Figures XVII

List of Tables XXIII

Chapter 1 1

1. Theoretical Introduction 1
    - 1.1. The Graphene species – from Graphite to Graphene 3
    - 1.2. Functionalization of GO with Polymer Brushes - Strategies 9
    - 1.3. CLRP - Fundamentals 11
        - 1.3.1. Origins of CLRP 12
        - 1.3.2. CLRP approaches 15
        - 1.3.3. ATRP and its evolution 17
    - 1.4. “Grafting-from” - State of the Art 19

Chapter 2 25

2. GO - Controlled modification 25
    - 2.1. Preparation of GO for future polymerization 26
        - 2.1.1. Preliminary reactions: Modification of –OH groups vs Modification of both –OH and –COOH groups 29
        - 2.1.2. Main esterification reactions 40
        - 2.1.3. Problems and solutions 47
    - 2.2. Polymerization from the surface of GO - “grafting-from” 49
        - 2.2.1. Step 1 – The dream of a non-reported system on the first attempt 50
        - 2.2.2. Step 2 - Understand the problems and eliminate variables/parameters (Reproduction of one reported system) 53
        - 2.2.3. Step 3 - SARA ATRP of MA catalysed by Cu(0):Me_6TREN = wire:1.1 from the GO’s surface in DMF at 60 ºC 59

Chapter 3 69

3. Experimental 69
    - 3.1. Materials 69
        - 3.1.1. Used in the preparation of GO for future polymerizations 69
        - 3.1.2. Used for polymerizations from the surface of GO 69
        - 3.1.3. Solvents and reactants purification 70

3.2. Apparatus and Characterization techniques.. 70
3.3. Procedures.. 72
3.3.1. Functionalization of GO with initiator moieties using both hydroxyl and carboxyl acid groups 72
3.3.2. Functionalization of GO with initiator moieties (GO-Br) using only hydroxyl groups (-OH) 73
3.3.3. Polymerization from the surface of GO 74
3.3.4. Cleavage of polymer chains from the surface of GO 77
Chapter 4 79
4. Conclusions and Future work 79
Chapter 5 83
5. Bibliography... 83

Appendices.. 93
Appendix A – Methods to produce GO 93
Appendix B – Determination of the conversion, $M_{n,th}$ and k_p^{app}... 95
Appendix C – Article “Synergistic Effect of 1-Butyl-3-methylimidazolium Hexafluorophosphate and DMSO in the SARA ATRP at Room Temperature Affording Very Fast Reactions and Polymers with Very Low Dispersity”.. 99
Appendix D – SI of the article “Synergistic Effect of 1-Butyl-3-methylimidazolium Hexafluorophosphate and DMSO in the SARA ATRP at Room Temperature Affording Very Fast Reactions and Polymers with Very Low Dispersity”.. 107
Appendix E – Article “Sulfolane – an Efficient and Universal Solvent for Copper Mediated Atom Transfer Radical (co)Polymerization of Acrylates, Methacrylates, Styrene and Vinyl Chloride.”... 123
Appendix F – SI of the article “Sulfolane – an Efficient and Universal Solvent for Copper Mediated Atom Transfer Radical (co)Polymerization of Acrylates, Methacrylates, Styrene and Vinyl Chloride.”.. 129
Appendix G – Reactions Tables for the different modifications realized to GO............... 155
Appendix H – Preliminary reactions results 163
Appendix I – NanoInnova Technologies analysis 173
Appendix J – Control tests to esterification reaction 177
Appendix K – Main esterification reactions 183
Appendix L – Preliminary polymerization reactions characterization 187
Appendix M – Polymerization reactions, reproduction of one reported system 191
Appendix N – “Grafting-from” in the presence of sacrificial initiator 195
Appendix O – Chemical structures 201

List of Figures

Figure 1. Schematic representation of Graphite Structure. Adapted from reference [27]..........4

Figure 2. a) Graphene powder. b) Schematic representation of Graphene structure, adapted from reference [7]..........5

Figure 3. Schematic structure of GO. Reproduced from reference [40]. 7

Figure 4. Structures and pathway of graphite, graphite oxide, GO, rGO and graphene. Reproduced from reference [9]..........8

Figure 5. Scheme representing the two main approaches to functionalize GO with polymer brushes. 10

Figure 6. Schematic representation of ethylene monomer, polyethylene (PE) and its respective repeating unit. 12

Figure 7. Schematic representation of CLRP reactions, in which k_p, k_{deact}, k_{act} and k_t represent the propagation rate, deactivation rate, activation rate and termination rate, respectively. Adapted from reference [89]. 15

Figure 8. Schematic representation of RAFT mechanism. k_t, k_{exch} and k_p represent the rate of termination, rate of chain exchange and rate of propagation, respectively. Reproduced from reference [94]..........16

Figure 9. General mechanism of ATRP. k_{act}, k_{deact}, k_p and k_t represent the activation rate, deactivation rate, propagation rate and termination rate, respectively. 17

Figure 10. Schematic representation of the pathway to modify the GO with initiator and after polymerize from its surface PS, PBA and PMMA. Reproduced from reference [24]. 22

Figure 11. Schematic representation of the attachment of initiator using only hydroxyl groups. 27

Figure 12. Schematic representation of the attachment of initiator moieties using both carboxyl and hydroxyl groups. 28

Figure 13. IR spectrum of Original GO FB_NIT. 33

Figure 14. TGA curve of original GO FB_NIT..........34

Figure 15. XPS spectrum of original GO FB_NIT..........35

Figure 16. XPS spectrum of FB_NIT. a) Deconvoluted peaks for C1s and b) Deconvoluted peaks for O1s. 36

Figure 17. IR spectrum of a) Original GO FB_NIT; b) Esterification product Br_G08; c) Esterification/amidation product Br_G09. 38

Figure 18. TGA curves of GO FB_NIT (solid line), esterification product Br_G08 (short dashed line) and esterification/amidation product Br_G09 (long dashed line). 39

Figure 19. IR spectrum of a) Original GO FB_NIT; b) Esterification product Br_G10. 41

Figure 20. TGA curves of GO FB_NIT (solid line) and esterification product Br_G10 (short dashed line). 43

Figure 21. Br3d high resolution spectrum of esterification product Br_G10. 44

Figure 22. XPS spectrum of esterification product Br_G10. 45

Figure 23. Br3d hight resolution spectrum of esterification product Br_G11. 47

Figure 24. FTIR spectrum of a) Esterified product Br_G10 and washed polymerization products from the SARA ATRP of Sty catalyzed by Cu(0) wire/TREN in DMF at 80 ºC with different target DPs: b) DP = 602, c) DP = 250 and d) DP = 500. 56

Figure 25. (Left) TGA curves obtained for the esterified GO used (solid line) and for the various washed polymerization products obtained from the SARA ATRP of Sty in DMF at 80 ºC having different target DPs: DP = 602 (short dashed line), DP = 250 (long dashed line) and DP = 500 (broken double dashed line). (Right) Typical ^{1}H NMR obtained for the respective washed products. 57

Figure 26. FTIR spectra of a) Esterified product Br_G10, c) Esterified product Br_G11 and washed polymerization products yielded in the SARA ATRP of MA from the surface of GO in DMF at 60 ºC catalysed by Cu(0) wire/Me$_6$TREN: b) polymerized from the macroinitiator Br_G10 and d) polymerized from the macroinitiator Br_G11. 61

Figure 27. (Left) TGA curves of macroinitiator Br_G10 (solid line) and of its washed SARA ATRP product (dashed line). (Right) TGA curves of macroinitiator Br_G11 (solid line) and of its washed SARA ATRP product (dashed line.) 62

Figure 28. ^{1}H NMR spectra of PMA attached to the surface of GO, acquired in CDCl$_3$. 1 – Washed SARA ATRP product polymerized from the macroinitiator Br_G10 and 2 – Washed SARA ATRP product polymerized from the macroinitiator Br_G11. 63

Figure 29. GPC traces of the detached PMA recovered from the saponification reactions. a) PMA polymerized from the surface of the macroinitiator Br_G10 and b) PMA polymerized from the surface of the macroinitiator Br_G11. The molecular weights, $M_{n,GPC}$, and the dispersity values were calculated through the OmniSEC software using the conventional calibration. 65

Figure 30. SEM images of (A) original graphene oxide magnification 1000x, (B) original graphene oxide magnification 3500x, (C) GO modified with PMA brushes magnification 1000x and (D) GO modified with PMA brushes 10000x. 67

Figure 31. Dispersion of (A) original GO, (B) GO-Br and (C) GO functionalized with PMA brushes in DMF with a concentration of about 1.0 mg/mL. 67

Figure 32. Scheme with the reactions pathway followed during the experimental work. 81

Figure B1. ^{1}H NMR of a sample collected during the SARA ATRP of MA in DMF, used to determine monomer conversion and $M_{n,th}$. 96
Figure B2. Example of a kinetic plot of ln[M_0]/[M] vs Time used to evaluate the first-order kinetic of the reaction with respect to the monomer concentration and to determine the k_p^{app}. 97
Figure H1. IR spectrum of a) Original GO, Oxi_Porto1; b) Esterification/amidation product Br_G01 and c) Esterification product Br_G02. 163
Figure H2. IR spectrum of Original GO Oxi_Porto2. 163
Figure H3. TGA curves of Original GO Oxi_Porto2. 164
Figure H4. IR spectrum of a) Original GO Oxi_Porto2; b) Esterification product Br_G03; c) Esterification/amidation product Br_G04 and d) Esterification product Br_G05. 165
Figure H5. TGA curves of a) Oxi_Porto2 (solid line); b) Esterification product Br_G03 (short dashed line); c) Esterification/amidation product Br_G04 (long dashed line) and d) Esterification product Br_G05 (broken double dashed line). 166
Figure H6. IR spectrum of a) Original GO Oxi_Porto2; b) Esterification product Br_G06 and c) Esterification product Br_G07. 167
Figure H7. TGA curves of original GO Oxi_Porto2, esterification product Br_G06 and esterification product Br_G07. 168
Figure H8. Comparison between a) FB_NIT and b) Oxi_Porto2. 168
Figure H9. Comparison between TGA curves of GO FB_NIT and Oxi_Porto2. 169
Figure H10. XPS spectrum of esterifications/amidation product Br_G09. 170
Figure H11. Br3d High resolution spectrum of Br_G09 esterification/amidation product. 170
Figure H12. Comparison between the IR spectra from the esterifications product Br_G10 acquired using the FTIR analysis in a) ATR mode and b) KBr mode. 172
Figure J1. IR spectrum of a) FB_NIT; b) Control test nº 1 (only TEA) and c) Control test nº 2 (only BIBB). 177
Figure J2. TGA curves of GO FB_NIT (solid line), control test nº 1 (only TEA, short dash line) and control test nº 2 (only BIBB, long dash line). 179
Figure J3. IR spectrum of a) Control test nº 2; b) Esterification product Br_G10 and c) Esterification product Br_G11. 180
Figure J4. TGA curves of control test nº 2, esterification product Br_G10 and esterification product Br_G11. 181
Figure K1. IR spectrum of a) GO FB_NIT and b) Esterification product Br_G11. 183
Figure K2. TGA curves of original GO (solid line) and esterifications product Br_G11 (dashed line). 184

Figure K3. XPS spectrum of the esterified GO Br_G11.. 185

Figure L1. FTIR spectra obtained for the different polymerization preliminary reactions. a) (top) esterified product Br_G06; a) (middle) esterified product Br_G07; a) (bottom) esterified product Br_G08. b) (top) and b) (middle) product obtained from the ATRP of MA catalysed by CuBr:Me_6TREN in DMF at 30ºC and c) (top) and b) (bottom) product obtained from the SARA ATRP of MA catalysed by Cu(0):$CuBr_2$:Me_6TREN in DMF at 30 ºC................................. 187

Figure L2. TGA results obtained for the different polymerization preliminary reactions. (solid line, top) esterified product Br_G06; (solid line, middle) esterified product Br_G07; (solid line, bottom) esterified product Br_G08. (short dashed line, top) and b) (dashed line, middle) products obtained from the ATRP of MA catalysed by CuBr:Me_6TREN in DMF at 30ºC and (long dashed line, top) and (dashed line, bottom) products obtained from the SARA ATRP of MA catalysed by Cu(0):$CuBr_2$:Me_6TREN in DMF at 30 ºC. 188

Figure L3. Typical ^{1}H NMR acquired for the washed powders of the various preliminary polymerization reactions. 189

Figure M1. FTIR spectra of a) Esterified product GO-Br and of the precipitates obtained from the SARA ATRP of Sty catalyzed by Cu(0) wire/TREN in DMF at 80 ºC with different target DPs, b) DP = 602, c) DP = 250, d) DP = 500. 191

Figure M2. (Left) TGA curves obtained for the esterified GO used as raw material (solid line) and for the various precipitates obtained from the SARA ATRP of Sty in DMF at 80 ºC having different target DPs; DP = 602 (short dashed line), DP = 250 (long dashed line) and DP = 500 (broken double dashed line). (Right) Typical ^{1}H NMR obtained for the respective precipitates. 192

Figure M3. GPC traces of the polymers recovered from the supernatants with diferente target DPs; a) DP = 602, b) DP = 250 and c) DP = 500. The molecular weights, $M_{n,GPC}$, and the dispersity values were calculated through the software OmniSEC using the TRiSEC calibration. 193

Figure N1. GPC traces of free PMA obtained in the SARA ATP of MA catalyzed by Cu(0) wire/Me6TREN in DMF at 60 ºC in heterogeneous medium. Kinetic points: (left) I – 2h, Mn,GPC= 28 kDa, Đ = 1.14 ; II – 4h, Mn,GPC= 53 kDa, Đ = 1.20; End – 7inh, Mn,GPC = 55 kDa, Đ = 1.33 and (right) I – 0.5h, Mn,GPC = 24 kDa, Đ = 1.16 ; II – 1h, Mn,GPC= 41 kDa, Đ = 1.15; End – 2h, Mn,GPC = 49 kDa, Đ =1.29 . The molecular weights and the dispersity values were measured in OmniSec software using the TriSec calibration. 196

Figure N2. Second reaction conducted with sacrificial initiator. (left) Kinetic plot of conversion and ln[M_0]/[M] vs Time and (right) plot of number average molecular weight, $M_{n,GPC}$, and dispersity values, Đ, vs theoretical number average molecular weight, $M_{n,th}$, for SARA ATRP of PMA catalysed with Cu(0) wire/Me6TREN in DMF at 60ºC. 197

Figure N3. First reaction conducted with sacrificial initiator. (left) Kinetic plot of conversion and ln[M_0]/[M] vs Time and (right) plot of number average molecular weight, $M_{n,GPC}$, and dispersity values, Đ, vs theoretical number average molecular weight, $M_{n,th}$, for SARA ATRP of PMA catalysed with Cu(0) wire/Me6TREN in DMF at 60ºC. 197

Figure N4. FTIR spectra pf a) GO-Br (Br_G11) and b), c) washed products obtained from the two SARA ATRP of MA in the presence of GO-Br using sacrificial initiator. 198

Figure N5. (Left) TGA curves obtained for the esterified GO used as raw material (solid line) and for the two washed products obtained from the SARA ATRP of MA catalysed by Cu(0) wire/Me_6TREN at 60 ºC. (Right) ^{1}H NMR obtained for the respective washed powders collected from the two polymerizations. 199

List of Tables

Table 1. Properties of graphene and potential applications. 6
Table 2. ATRP variations and their features. 18
Table 3. Non CLRP methods reported for grafting polymers from graphene and its derivatives. 20
Table 4. Articles published that report the grafting of polymers from graphene and its derivatives through RAFT polymerization. 20
Table 5. Articles published that report the grafting of polymers from graphene and its derivatives through ATRP and respectively derivatives polymerization techniques. 23
Table 6. First functionalization reactions carried out to attach the initiator moieties to the surface of GO Oxi_Porto1. 30
Table 7. Preliminary functionalization reactions realized during the semester to attach the initiator moieties to the surface of GO Oxi_Porto2. 31
Table 8. Esterification reactions conducted to GO Oxi_Porto2, following the Lee method [24]. 32
Table 9. XPS elemental quantification of FB_NIT. 35
Table 10. C1s, O1s and S2p3/2 high resolution spectra / binding energy assignments. 36
Table 11. Final preliminary esterifications reactions using the GO FB_NIT as raw material. 37
Table 12. Main esterification reactions realized to attach initiator molecules to the surface of GO. 41
Table 13. XPS elemental quantification of esterification product Br_G10. 43
Table 14. Preliminary polymerization reactions in DMF at 30 ºC. 50
Table 15. SARA ATRP of Sty catalysed by Cu(0) wire/TREN, systems based in the literature [24]. 54
Table 16. SARA ATRP of MA catalyzed by Cu(0) wire/Me6TREN in DMF in at 60 ºC 60
Table 17. Weight losses measured for the macroinitiators Br_G10 and Br_G11 and for the respective washed products obtained through the SARA ATRP of MA catalysed by Cu(0) wire/Me6TREN in DMF at 60 ºC. 62

Table A1. Main oxidation methods to prepare GO. Contents adapted from reference [40]. 93
Table G1. Amounts and ratios used to determine the quantities of reactants used in esterification reactions, following the work developed reported [24]. 155
Table G2. Amounts and ratios used to determine the quantities of reactants used in esterification/amidation reactions, following the work reported in the literature. [23]. 156

Table G3. Amounts of monomers, catalyst and ligands used in some of the articles found. Research for typical ratios of catalysts and ligands used in the literature. 157

Table G4. Amounts and ratios used to determine the quantities of reactants used in preliminary polymerization reactions, following the work developed by Gonçalves et al. [10]............... 159

Table G5. Amounts and ratios used to determine the quantities of reactants used in SARA ATRP of Sty catalysed by Cu(0) wire/TREN [24]. 161

Table G6. Amounts and ratios used to determine the quantities of reactants used in SARA ATRP of MA catalysed by Cu(0) wire/Me_6TREN from the surface of GO. 162

Table H1. Elemental quantification obtained from the XPS analysis conducted to the esterifications amidation product Br_G09. 171

Table K1. Elemental quantification obtained from the XPS analysis for the esterifications product Br_G11.. 184

Chapter 1

1. Theoretical Introduction

"a little word with a big potential… That word is "nano"."

Ratner, M. and Ratner D. [1]

The word *nano* has been revolutionizing the scientific world, since some years nanotechnologies, nanoscience and nanomaterials have attracted an enormous attentions from the academia and industrial world, in diverse areas (energy, life science, health, automotive industry, mobility, information, communication, chemistry, environment, consumer goods and agriculture). Nanotechnologies and nanoscience explore and manipulate matter at the nanoscale, dealing with new materials that possesses in its composition some kind of nanostructure. A certain structure is considered nanostructure when it includes at least one dimension at the nanoscale, from 1 to 100 nm [1].

When the size of some materials is reduced to the nanoscale, the properties of these materials can drastically change, mainly due to the relatively larger surface area when compared to the same mass of material at the large scale and also due to quantum effects [2]. Therefore, with the discovery of new materials with enhanced and distinct properties the "Nanoareas" opened the doors to a new revolution in the science, society and economy [1].

One of the types of nanomaterials that has attracted more attentions in the last three decades, is the carbon based nanomaterials, like carbon nanotubes, fullerenes and graphene [3, 4]. These materials possess unique electrical, optical, thermal, mechanical and chemical properties [3].

Graphene is the most recent carbon nanomaterial discovered (in 2004 by A. Geim and K. Novoselov at the University of Manchester), and due to its astonishing properties it has gradually becoming the star of the carbon nanomaterials and the main subject for carbon nanomaterials researchers [4-8]. Such carbon nanomaterial can be combined with other materials with distinct chemical and physical properties, like polymers, metals and others, originating composites with unique and enhanced mechanical, thermal and chemical properties [5].

With the goal of improving the properties of polymers through the construction of composites and hybrid materials, researchers have tried to combine these organic compounds with other inorganic fillers like silica, clay and reinforced fibres. In recent years, materials with nanometric dimensions, due to its unique properties, have been combined with polymers yielding novel polymer nanocomposites that exhibit better mechanical, thermal, optical and electrical properties than polymers used in their pure form [9]. The discovery of graphene, a material with extraordinary and useful properties for several scientific fields, provide scientists with a new nanofiller [10-15]. It is important to note that in order to use graphene as a nanofiller it is, in many cases, necessary to functionalize its surface, since in its pristine form, this material is very difficult to disperse due to its great tendency to form granular aggregates, which will jeopardize the properties of nanocomposites [16]. One of the ways to overcome such problem is to attach oxygenated species to its surface, like hydroxyl, carboxyl and epoxy groups, obtaining the graphene oxide (GO) [17, 18].

Polymer nanocomposites with graphene and GO can be produced by various processing methods such as melt mixing [19, 20], latex technology [21], solution processing [19, 22], in *situ* polymerization [10, 14, 19, 23-26], among others polymerization techniques [9]. For the purpose of this work the focus will be set on *in situ* polymerization.

Having in mind the extraordinary properties of graphene and GO, the improvements that this materials can bring to polymers, and the vast experience in polymer synthesis[1] of the Polymer Research Group (where this project was carried out) the main goal of this work was to synthesize polymer nanocomposites, through *in situ* Controlled/Living Radical Polymerization (CLRP) from GO's surface, and explore new polymerization systems using low concentrations of catalysts.

The graphene research field, as already mentioned, is a recent area and in our Department of Chemical Engineering, University of Coimbra, it is not only a recent area but a completely new and unfamiliar research area. To the best of our knowledge, nobody has worked with graphene, so far, and even in Portugal there are only a few research groups that deal with this material (University of Porto and University of Aveiro). Considering this, by achieving the main goal of this work a new perspective of working towards the development of graphene research area are accomplishing. This new perspective is focused on trying to understand how to work properly with this carbon nanomaterial; how it behaves when submitted to a reaction medium; constructing a good logistic platform to work with graphene and GO, namely instruments and characterization techniques necessary to analyse all the reaction results; trying to find the problems associated with its use and explore/clarify other questions that may arise during the research.

---

[1] The Polymer Research Group of Department of Chemical Engineering, University of Coimbra, has numerous works reported and several collaborations with industries (see some work developed in http://www.uc.pt/fctuc/deq/polymer)

To achieve the main goal of this work some partial objectives were defined:

1. Understand the fundamentals (theoretical and practical) of controlled/living radical polymerization. CLRP reactions in homogeneous media were carried out in the framework of two projects of the Polymer Research Group;
2. Functionalization of GO with bromide moieties to be used as macroinitiator. Understand the fundamentals and the procedures to attach initiator molecules to GO's surface with success.
3. The third partial objective was to understand the suitable procedures to conduct polymerization reactions from the surface of GO (previously modified with initiator) correctly and with success.
4. Finally, in order to achieve the main goal of the project, the fourth goal was to polymerize from GO's surface with new monomers and new catalytic systems.

1.1. The Graphene species – from Graphite to Graphene

Nowadays, graphite is a well-known allotrope of carbon, named by Abraham Gottlob Werner in 1789, that is widely used in writing and drawing for many decades. The first pencils were manufactured in the 15th century in England [27]. Besides this well-known application, graphite can be used to produce a considerable range of materials such as strong fibres, lubricants, gas-tight barriers, gas adsorbers and recently nanomaterials like graphene [6, 27]. It is the most stable form of carbon under standard conditions [28].

Graphite, as can be seen in Figure 1, has in its composition various parallel plane layers of carbon atoms bonded to each other in an hexagonal shape by a sp^2 bond. These layers are stacked and bonded one each another by weak *Van dar Waals* bond resulting in a separation distance of 0.335 nm [27]. Within the basal planes, each carbon atom is bonded to three neighbour atoms forming a honeycomb lattice that can be considered as an infinite two-dimensional molecule [29]. The unique structure of graphite, mainly due to the presence of delocalized electrons in the sp^2-hybridized carbon, yields good thermal and electrical conductivity and others interesting chemical, mechanical and physical properties [27, 28].

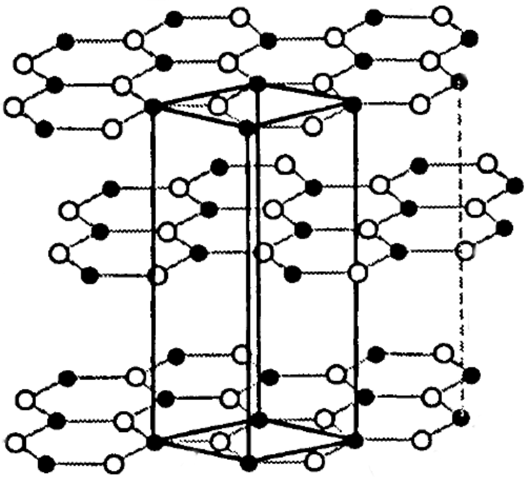

Figure 1. Schematic representation of Graphite Structure. Adapted from reference [27].

"New star of the material world"

Neil Savage [4]

In 2004 Konstantin Novoselov, Andre Geim and co-workers at the University of Manchester discovered a new carbon nanomaterial that has been attracting an enormous attention from the scientific world in the last years, due to its extraordinary properties and to the abundance of graphite, one of its possible raw materials [4-6, 15]. A. Geim and K. Novoselov proved that is possible to isolate the planes of graphite, through a Scotch tape method, thus obtaining a single atomic layer of carbon, denominated graphene. This discovery was recognized by the Royal Swedish Academy of Sciences with the Nobel Price of Physics in 2010 [4-6, 30, 31]. Graphene is already experimentally studied for over 50 years, but before 2004 scientists believed that planar graphene, as other 2D crystals, would not exist in free state, thinking that it was unstable and, in the case of graphene, it formed curved structures such as fullerenes, soot and carbon nanotubes [4, 6, 8]. Therefore, graphene is no more than a single atomic sheet composed only by carbon atoms that are organized in a honeycomb (hexagonal) lattice. These atoms are bonded to three other carbon atoms through a sp^2 bond, like in graphite layer planes (Figure 2) [5, 6, 8, 18]. Graphene can be seen as a basic building block for other allotropes of carbon, for example, if we roll the graphene sheet into a 1D we will obtain a carbon nanotube [8, 18].

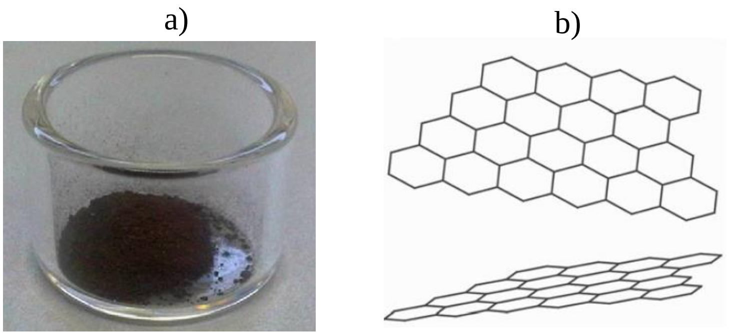

Figure 2. a) Graphene powder. b) Schematic representation of Graphene structure, adapted from reference [7].

Strictly speaking graphene and other 2D crystals, as mentioned above, are a sheet of just a single atoms thick, but in reality a 2D crystal can be constituted by more than one layer packed with each other. In this phase it is important to understand how many layers are necessary to construct a 3D structure and, with this in mind, be able to distinguish between single-, double-, few-layered graphene and graphite. The number of layers is determined by the evaluation of the electronic structure of carbon material. When more than two layers are packed the electronic spectra becomes complex because of the appearance of various charge carriers and due to the overlapping of the conducting and valence bands, only single layered and bilayered graphene have a simple electronic spectra. Based on electronic spectra, B. Partoens and F. M. Peeters, in 2006, proved that with 10 layers the electronic structure was already corresponding to the bulk graphite behaviour, so in this work the graphene considered has always less than 10 layers of carbon atoms [8, 32].

“Graphene is phenomenally strong, thin, flexible, transparent and conductive — and applications beckon”

Neil Savage [4]

The unique structure of graphene gives it outstanding electrical, thermal, optical and mechanical properties, and as result of this graphene is, in the majority of the papers, presented as a wonderful material that has numerous possible applications.

The primary and most valuable property of graphene is its electric conductivity [33]. Alongside with the discovery of graphene, in 2004, A. Geim and K. Novoselov studied the electronic properties of a few-layered graphene for the first time [6]. These scientist observed an ambipolar field effect in a few-layered graphene and have proved that 2D electronic transport is ballistic at submicrometer distances. When graphene is submitted to an electrical potential difference, electrons move through it as if they have no mass. In addition, at room temperature, they can travel without scattering during a long time. [4, 6, 34]. This new carbon nanomaterial has 100 times more electron mobility than silicon, a material sometimes used as comparison because nowadays it has been dominating the semiconductors industry [4].

In addition to its extraordinary electric conductivity graphene retains also other unique characteristics. It is also a good thermal conductor, higher than cooper and better than diamond, the best heat conductor until graphene discovery [4, 35, 36]. Graphene is 100 times stronger than steel and, furthermore, it has a good elasticity, since it can be easily stretched without breaking as other hardy materials, and turning it very useful as a reinforcement filler in diverse composite materials [4, 37]. Its thickness of one-atom gives it interesting optical properties and good transparency, graphene has an absorbance of only 2.3%, which turns this material very promising for flexible screens and other optical applications [34, 38]. Finely, the tightly packed arrangement of carbon atoms in the graphene layer provides this nanomaterial with exceptional barrier capacities, to better understand, not even an atom of helium, the smallest atom known, can pass through it [4].

In Table 1 are summarized the properties of graphene.

Table 1. Properties of graphene and potential applications.

Property	Value	Comparison
High Electron mobility at r.t.	200 000 $cm^2 V^{-1} s^{-1}$ [39]	100x more than silicon
High Electric conductivity	~6000 $S cm^{-1}$ [40]	-
High Thermal Conductivity	~ 3080-5150 $W m^{-1} K^{-1}$ [36]	Copper (400 $W m^{-1} K^{-1}$)
Large Surface Area	2630 m^2g^{-1} [41]	-
Tensile strength	125 – 130 GPa [37]	100x stronger than steel
Young modulus	1 TPa [37]	-
Absorbance	2.3% [34]	-

Although seeming easy, it is very difficult to produce large quantities of graphene at industrial scales with the Scotch tape method. Furthermore, it is very difficult to disperse pristine graphene in other solid materials and solvents, because its sheets have a great tendency to form granular aggregates due to its surface area, small quantity of functional groups in the surface and due to the strong π-π and *Van der Waals* interactions, resulting in a bad distribution and decreasing the properties of the final material [9, 17, 40]. One of the ways to solve this problem is to functionalize the pristine graphene with oxygenated species, like hydroxyl, carboxyl and epoxy groups, obtaining the so called GO . This oxygenated material can be easily dispersed and mixed with other materials and can also be more easily obtained from graphite than pure graphene [17].

Several methods to obtain graphene and GO have been investigated, including chemical vapour deposition [42], chemical exfoliation [15, 24], thermal exfoliation [43, 44] and carbon nanotubes cutting [45]. In Appendix A is shown a table with the main methods, reported in the literature, to produce GO. Among all the methods the most reported are the “top-down” chemical exfoliation routes, like Hummer’s method, modified Hummer’s method and Staudenmaier method [9, 40]. This three methods share the same basic principle, the difference between them lies on some reactants used and on reaction conditions. In chemical exfoliation routes, previously mentioned, the raw material is graphite, in many cases natural graphite [17]. The graphite is submitted to harsh conditions promoted by the strong oxidising agents used in the reactions. This processes intercalates between graphite layers oxygenated species, like hydroxyl groups, carboxyl, epoxy and others [9]. The oxygenated groups reduce the *Van dar Waals* interaction that exist between the different planes of graphite, producing an expanded graphite denominated graphite oxide [17]. After, a dispersion of graphite oxide, in many cases in water, it is placed in an ultrasound bath, in order to achieve its exfoliation and obtain isolated layers of GO (Figure 3) [9].

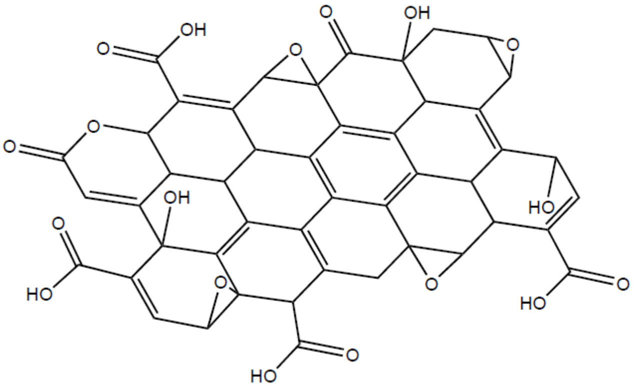

Figure 3. Schematic structure of GO. Reproduced from reference [40].

Despite GO is more easily dispersed in other materials and solvents than pure graphene, it should be stressed that with the functionalization of graphene layers some of the most interesting properties of pure graphene can be lost or reduced, namely its electrical conductivity [46]. The extraordinary electric conductivity of pure graphene is ascribed to the sp^2 carbon-carbon bonds [6]. When graphene is functionalized, sp^2 bonds are disrupted to form sp^3 bonds with oxygenated species, leading to a decrease in the density of delocalized electrons and, consequently, to a reduction of the electrical conductivity of carbon nanosheets. This problem can be significantly overlapped by reducing the number of oxygenated species in GO’s surface, restoring its π-network and yielding reduced graphene oxide (rGO) [46]. rGO has less electrical conductivity than pure graphene, because complete reduction is very difficult, but considerably higher conductivity than GO [40]. The most common reduction process uses hydrazine hydrate, a strong reducing agent, and it is used when the interest is to obtain a final product with properties as similar as possible to pure graphene and when the methods used to obtain isolated layers of carbon are the “top-down” chemical exfoliation ones, the most promising, so far, to produce exfoliated chemical modified graphene platelets (CMG) from graphite at a large scale [40, 46]. Figure 4 shows the schematic structures and pathway from graphite to graphene’s species.

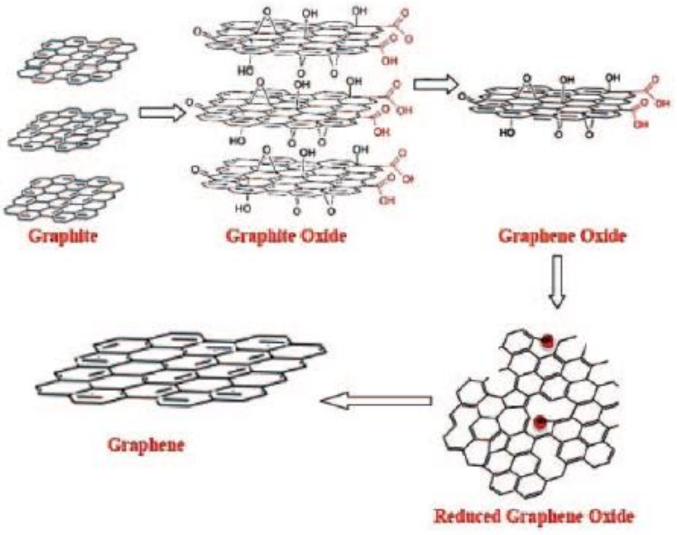

Figure 4. Structures and pathway of graphite, graphite oxide, GO, rGO and graphene. Reproduced from reference [9].

The experiments realized within the framework of this projects used as main raw material GO. This product firstly was kindly supplied by the University of Porto and was later purchased from NanoInnova Technologies.

1.2. Functionalization of GO with Polymer Brushes - Strategies

Graphene or GO can be combined with other materials with distinct chemical and physical properties to produce nanocomposites with remarkable and unique properties and performances. One of the most interesting and powerful composites are the ones that combine organic materials (e.g. polymers) with inorganic materials (e.g. graphene or silica), which can take advantage of the best of both worlds, for example the good electrical conductivity and mechanical resistance of inorganic materials and the good biocompatibility of some organic constituents.

As already proved these carbon nanomaterials can improve the final properties of the polymers when combined [9]. In addition, the interest in improvement of polymer properties is great, because these organic materials are widely used, mainly due to their easy processing, relatively low cost, great variety of chemical structures and properties, and also by their capability to be recycled and biodegradable [47]. However, to yield a final nanocomposite with desired properties it is fundamental to ensure a good compatibility of graphene with various polymer matrices and with common solvents, in order to obtain a homogeneous distribution of the graphene in the dispersion medium. One way to improve the compatibility and to modify graphene (or GO) to be used in a wide range of applications is the attachment of organic compounds to its surface, namely polymer chains (brushes). Since pure graphene is mostly free of functional groups on its surface, attachment of polymer chains is very difficult. Therefore, the most used precursor for this type of organic functionalization is GO having oxygen reactive groups capable of being modified with polymer chains by different approaches [48].

To date, the routes used to modify GO with polymer brushes can be classified in two main categories, “grafting-to” and “grafting-from” approaches [9, 40, 48]. In the first one, polymers previously synthetized normally by CLRP are attached to GO by various chemical reactions. In the “grafting-from” approach GO, in some cases graphene or rGO, is used as macroinitiator and polymers are grown from the surface, this process is known as Surface Initiated Polymerization (SIP) [47].

Figure 5 illustrate the two main approaches employed to functionalize GO with polymeric chains.

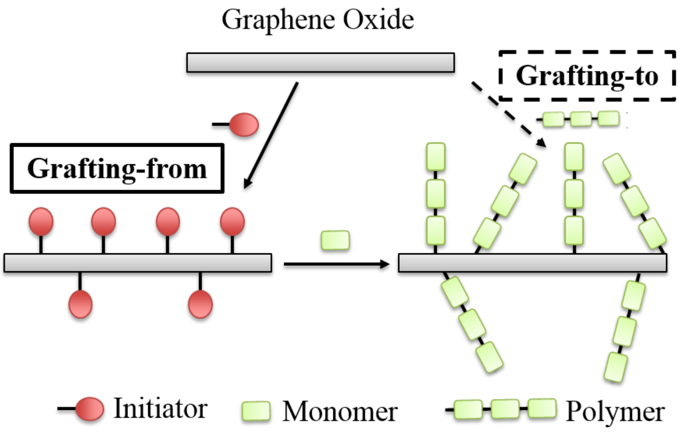

Figure 5. Scheme representing the two main approaches to functionalize GO with polymer brushes.

In "grafting-to" approach polymers can be attached to GO by either non-covalent (ex:. GO/end functionalized polymers π-π interactions, ionic interactions or Van der Waals forces) or covalent linkage [49]. Covalent functionalization of GO, through "grafting-to" methodology, can be achieved by diverse types of chemical reactions, like esterification [50], amidation [51], "click" chemistry [52] and radical coupling [53]. When polymers are bonded covalently to the surface of graphene, its graphitic sp^2 domains are considerably destroyed, and consequently properties of graphene are negatively affected. In contrast, non-covalent functionalization preserves these important sp^2 domains. However, the hybrid material is unstable and it is difficult to control the attachment of graphene to polymer chains [40].

The "Grafting-to" approach is more versatile method that is particularly useful to attach polymers that cannot be polymerized from the surface of graphene or GO [40, 48]. Nevertheless, the possible steric hindrance, especially for polymers with high molecular weighs, difficults the preparation of high density grafted graphene [10, 15, 24, 54]. Therefore, despite the "grafting-to" method allowance of better control over polymer structure, "grafting-from" methodology is considerably advantageous, because it allows to prepare higher molecular weight brushes, higher grafting density, and the control over the structure of polymers is good [40, 48]. With surface initiated polymerization the steric effects, verified in the "grafting-to" approach, can be greatly suppressed [54].

After analysing the existent literature the "grafting-from" approach was selected for this work, since from theoretically standpoint, it is easier to control the grafting density of polymers attached to GO and also to attach polymers with higher molecular weight with relatively good control. Having this in mind, in the project presented in this dissertation our main focus was synthesis of polymers from the surface of GO using the "grafting-from" approach.

1.3. CLRP - Fundamentals

As already mentioned, in “grafting-from” methodology, polymer chains (brushes) are grown from the surface of graphene’s species, like GO or rGO . Normally, polymerization takes places from initiator molecules that are previously attached to the surface of graphene’s species [10, 23-26, 55, 56]. In the literature we can find numerous strategies to conduct such “grafting-from” polymerizations [10, 15, 23-26, 54, 56-87]. One of the differences between the reports published are in the polymerization mechanism employed.

CLRP is the most employed method to grow polymers from the surface of graphene and its derivatives, mainly due to the ability to control the structures of polymers and to produce polymers with narrow dispersity (*Đ*) [47]. With this in mind, in this work, CLRP methodologies were employed to functionalize GO with polymeric chains and because of this it is important to present some important fundamental concepts, about CLRP techniques, that will be important to understand the work developed.

“It is hard to visualize today’s world with all its luxury and comfort without man-made polymeric materials.”

Ebewele, R. O. [88]

All around the world, in forests, oceans, animals and in each one of us there are large molecules, built up by the repetition of small chemical units, denominated polymers. In addition to natural polymers that exist in nature and are the building blocks of many living forms, like cellulose and starch we can find man-made polymers like polystyrene (synthetic polymer), and natural polymers modified by the human being like cellulose acetate (artificial polymers) . Such macromolecular structures are created through polymerization reactions, in which several single molecules (monomers), of the same or different type, are combined. Polymers having in their composition different types of monomers are called *copolymers*, instead of *homopolymers* which are only composed by one type of monomer [88].

It is important to note that a monomer is the isolated molecule and a repeating unit is the unit repeated along the polymer chains (Figure 6). The number of repeating units in a given polymeric chain gives the degree of polymerization, which multiplied by the molecular weight of the monomers gives the molecular weight of polymer, MW [88].

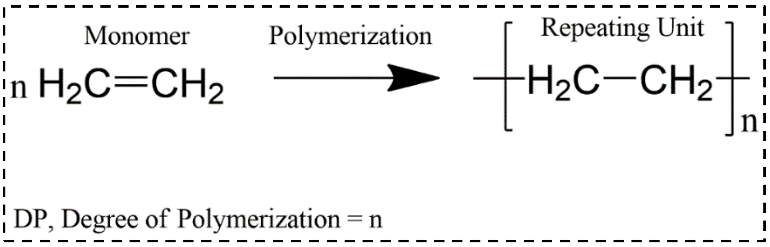

Figure 6. Schematic representation of ethylene monomer, polyethylene (PE) and its respective repeating unit.

When one polymerization reaction is carried out, the produced polymer chains do not present the same length and, consequently, have different molecular weights. Considering this, in the end of the polymerization we can find a distribution of molecular weights, which is usually well characterized through three parameters: number-average molecular weight, $\overline{M}_n$, weigh-average molecular weight, $\overline{M}_w$, and dispersity, $Đ = \overline{M}_w/\overline{M}_n$. The first parameter is based on the number of macromolecules with a certain size, the second is a weighted average that takes in account the weight of each chain, and the last parameter gives information about how broad is the distribution of polymer chain lengths in a sample. Higher dispersity index's indicates a broader molecular weight distribution [88].

Polymerization reactions can be classified as step-growth reactions or chain-growth reactions according to the mechanism of polymer construction. In step-growth reactions monomers, oligomers or other long molecules are randomly combined yielding increasing molecules like dimers, trimers or, at the end of the reaction, macromolecules . In chain-growth reactions monomers are gradually added to an active species, like free radicals and anionic or cationic species [88].

1.3.1. Origins of CLRP

Two types of chain-growth reactions were at the foundation of controlled living radical polymerization, to be exact free radical polymerization (FRP) and living anionic polymerization, reported by Michael Szwarc in 1956 as the first type of "living" polymerization which allowed the production of block copolymers [89, 90]. Notice that after the discovery of anionic polymerization other important studies for the development of CLRP were conducted [89].

The growing mechanism of polymer chains and the existing reactions in CLRP are very similar to the ones in FRP. Both use free radicals as active species to build up polymers [89, 91].

FRP, also known as conventional radical polymerization, has been widely used to prepare high molecular weight polymers for about eighty years and it is responsible for the annual production of 100 million tons of polymers [89, 91, 92]. FRP is relatively easy to use at industrial scale due to its ability to synthesize several types of vinyl monomers, in a broad range of conditions and temperatures. By this method, it is possible to polymerize at temperatures between -80 and 250 ºC using both homogeneous systems, like bulk or solution, and heterogeneous, like suspension or emulsion systems . Furthermore, it is also possible to build copolymers with different properties according to the quantities of co-monomers used [89].

FRP and CLRP both need initiator molecules, responsible for the generation of free radicals, and unsaturated monomer molecules, the basic building blocks of polymers. In both techniques, all throughout the polymerization, four different steps can be distinguished [91, 93]:

1. **Initiation** – primary radicals (R•) are created by homolytic cission of organic compounds, when submitted to temperature (thermal initiators), radiation (photoinitiators), or through redox reactions. After this, the double bond of monomers (M) is attacked by radicals (R•), initiating the polymerization;

$$R - R \rightarrow 2R \bullet \tag{1}$$

$$R \bullet + \mathrm{M} \rightarrow \mathrm{RM} \bullet \tag{2}$$

2. **Propagation** – monomers are continuously added to the growing radicals (P_n•)[2];

$$RM \bullet + \mathrm{n\ M} \rightarrow P_n \bullet \tag{3}$$

3. **Termination** – two growing chains are combined yielding a final dead polymeric chain. Two types of termination processes are well described, namely coupling and disproportionation;

$$\text{[Coupling]: } P_n \bullet + P_m \bullet \rightarrow P_{n+m} \tag{4}$$

$$\text{[Disproportionation]: } P_n \bullet + P_m \bullet \rightarrow P_n + P_m \tag{5}$$

4. **Chain Transfer** – this is an additional reaction in which the active centre is transferred to another active specie. Such phenomenon can occur not only to the polymer but also to the monomer or to a chain transfer agent, intentionally introduced in the system to control the length of chains.

---

[2] “n” represent the number of monomers added to the polymeric chain

In FRP molecular weights of polymers increase rapidly in the beginning of the reaction, monomer is consumed slowly and at the end of polymerization is often left unreacted monomer [89, 91]. Additionally, under steady state conditions, the rate of initiation is equal to the rate of termination and these are about 1000 times slower than propagation rate. Termination reactions by disproportionation or coupling are very fast and the average life of propagating chains is in the order of 1s, too short to define the structure of polymers, end functionalization or to construct complex architectures like block copolymers [89].

The evolution of human civilization and the continuing desire of man for intellectual progress and for new tailored materials with unique properties, brought the necessity to control the structure of polymers, as, for example, produce block copolymers or polymers with low dispersity and defined molecular weights. The features of conventional radical polymerization do not allow such control, mainly due to higher rates of initiation and termination compared to the rates of propagation, which led to the research for new polymerization techniques [91].

With the discovery of anionic polymerization Szwarc introduced a new concept which enabled to control the structure of polymers. His pioneer work found out that with the elimination of transfer and termination reactions it is possible to obtain polymers with defined end-groups and to construct block copolymers with sequential addition of more monomer during the polymerization [90]. Since then, various techniques were explored trying to achieve control by free-radical means, because ionic polymerizations cannot be extended to many types of monomers and require hard conditions. Thereby, a new category of polymerization techniques appeared, known as CLRP. Despite CLRP can be subdivided in various types of polymerization techniques, all methods have the same basic principle. The control over the structure of polymers is achieved by establishing a dynamic equilibrium between propagating radicals and dormant species, that cannot be terminated (Figure 7) [93]. Furthermore, lifetime of growing chains is higher in CLRP (~1s FRP and ~1h CLRP), chains grow all at the same time, due to a combination of fast initiation (LRP = 0.1 – 10 ms and FRP = 1 s) and negligible termination and transfer reactions. The concentration of active species in the system is maintained at low levels during all polymerization, as result of the continuous deactivation reaction [89, 91].

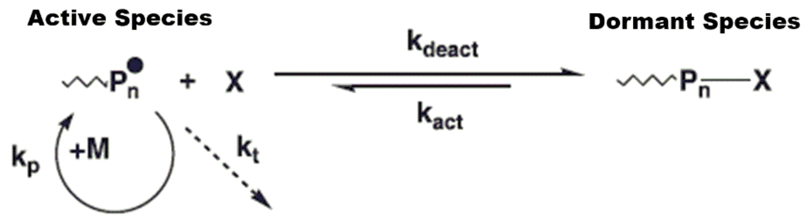

Figure 7. Schematic representation of CLRP reactions, in which k_p, k_{deact}, k_{act} and k_t represent the propagation rate, deactivation rate, activation rate and termination rate, respectively. Adapted from reference [89].

One polymerization is considered controlled/"living" when four standards are achieved [88, 91, 93]:

i) Fisrt-order kinetics with respect to monomer concentration, which means that in semi logarithmic coordinates it must present a linear kinetic plot;

$\ln\left(\frac{[M]_0}{[M]}\right) vs\ time = linear\ function$, in which $[M]_0$ and $[M]$ are the monomer concentration for t = 0 and t = t, respectively (6)

ii) Linear evolution of the degree of polymerization with conversion;

$DP = \frac{\Delta[M]}{[I]_0}$, in which $\Delta[M]$ represents the reacted monomer and $[I]_0$ the initial concentration of initiator (7)

iii) Dispersity, Đ, must decrease with conversion and should be narrow, identical to the Poisson distribution;

$$Đ = \bar{M}_w/\bar{M}_n \approx 1 + 1/DP \qquad (10)$$

iv) Chains should possess end-functionality, this means if more monomer is supplied to the reaction they should continue to grow.

1.3.2. CLRP approaches

Diverse systems can be used to achieve the equilibrium between dormant and active species using different structures for dormant species and chemistry of exchange [91]. Atom transfer radical polymerization (ATRP), stable free radical polymerization (SFRP), also known as nitroxide-mediated polymerization (NMP), and reversible addition-fragmentation chain transfer (RAFT) are the most promising methods of CLRP [94].

In RAFT systems chain transfer agents are introduced in the reaction medium. These compounds are responsible for the change of the active center of propagation for another active species, playing the role of dormant species, because they are present in much larger concentration than radical initiators (Figure 8) [95-97]. RAFT is the closest type of CLRP to FRP, following the typical FRP kinetics, and can be used with a larger range of monomers, which give to this technique a practical character [89, 91]. However, transfer agents are normally expensive and in many cases are not available in market. In addition, some of these transfer agents have poor stability, are toxics and can lead to some problems of toxicity, colour and odour in final polymers [89].

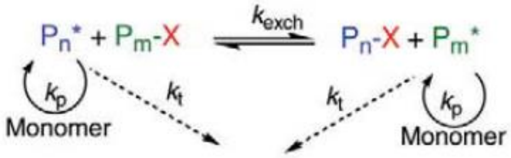

Figure 8. Schematic representation of RAFT mechanism. k_t, k_{exch} *and* k_p *represent the rate of termination, rate of chain exchange and rate of propagation, respectively. Reproduced from reference [94].*

While in RAFT polymerizations radicals are involved in a degenerative exchange mechanism, shown in Figure 8, in the other two techniques, ATRP and SFRP, they are reversibly trapped in a deactivation/activation process, as can be seen in Figure 7 [89].

The last two techniques use the concept of persistent radical effect (PRE), in which propagating radicals ($P_n\bullet$) are converted into dormant species (P_n-X) reacting with persistent radical (X), with a deactivation rate of k_{deact}. Species X are denominated persistent radicals because they only react with growing radicals and never with radicals of the same type. The selectivity of persistent radicals results in an irreversible accumulation of these species, caused by the termination reaction (k_t) that involves the reaction of growing radicals with each other. This increase in concentration of persistent radicals balances the equilibrium of the reaction to the side of the dormant species, leading to a decrease in radical's concentration as well as in the probability of termination, that can be assumed negligible [89, 93].

The main differences between SFRP and ATRP are in the species used as persistent radicals and in the mechanism to activate dormant species, with a constant rate of activation k_{act}. In SFRP species X are stable radicals as, for example, nitroxides (in NMP) or metalloradicals [98, 99]. With regard to the mechanism, in SFRP dormant species can be activated spontaneously or thermally and in ATRP are activated by transition metal catalysts in their high oxidation state, namely X-Cu$^{(II)}$ [89, 100]. SFRP uses pure organic systems and can be used in several monomers. However, it is necessary higher amounts of controlling compounds, in many cases potentially toxic, it is difficult to produce polymers with good end-functionality and normally it is necessary high temperatures to carry out the polymerizations [89]. ATRP has some disadvantages regarding SFRP, like the necessity of removal of the transition metal complexes and the protection required by acidic monomers. However, numerous advantages of this method turned it the most often used. In ATRP a range of monomers can be polymerized in a wide range of reaction conditions (diverse temperatures and different media), it is simple to construct polymeric chains with active terminals, gel effect can be avoided, block copolymerization can be realized in any order and reactants, like initiators and catalysts, are commercially available [94].

1.3.3. ATRP and its evolution

In ATRP, the equilibrium between dormant species and propagating radicals is reached by using a catalytic system (Mt^m/L). This system is a stable complex composed by a transition metal (Mt^m), normally in its lower oxidation state, and a ligand (L). In this type of polymerization it is also necessary an alkyl halide initiator/macroinitiator (P_n-X). With these elements in the reaction medium, the dormant species (P_n-X) periodically activated by the transition metal complex in its lower oxidation state (Mt^m/L), yielding propagating radicals (P_n•) and the respective transition metal complex in its higher oxidation state, coordinated with the halogen specie ($X\text{-}Mt^{m+1}/L$), with a constant rate of activation k_{act}. After this, growing radicals can propagate (k_p) or terminate (k_t), however when termination occurs the concentration of deactivator-transition metal complex in its higher oxidation state increases, and consequently, propagating radicals are rapidly trapped producing again dormant alkyl halide species and activator-transition metal complex in its lower oxidation state. This mechanism assures low concentration of radicals and a negligible termination rate, since the constant rate of activation is considerably lower than the constant rate of deactivation [92, 93].

In Figure 9 is represented the general schematic mechanism of ATRP.

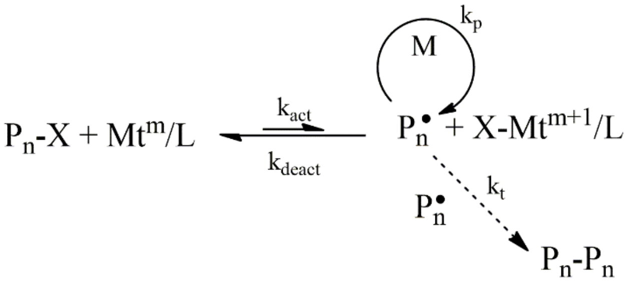

Figure 9. General mechanism of ATRP. k_{act}, k_{deact}, k_p and k_t represent the activation rate, deactivation rate, propagation rate and termination rate, respectively.

A wide range of transition metals in combination with different ligands (normally nitrogen-based ligands) can be employed, like Cu, Fe, Ru, Mo, amongst others [92, 100-102]. Cu-based transition metal complexes have been the most often used, because has been proved that these complexes are the most efficient catalysts for diverse monomers and reaction media [92, 100].

The conventional ATRP process uses concentrations of catalysts usually in the order of 1000 parts per million (ppm) [103]. Catalysts normally used in conventional ATRP are toxic, like copper catalysts, and have to be removed after polymerization [92]. With this in mind, since the discovery of ATRP scientists have been searching for ATRP variations that use less quantities of catalysts or "green" transition metals like iron. Regarding this, new ATRP variations, employing less than 100 ppm, of catalysts were reported and are today under study for polymerization of diverse monomers in different conditions and reactions media [92, 103].

Currently, there are five variations of ATRP which are most commonly used: activator regenerated by electron transfer (ARGET ATRP) that use inorganic or organic reducing agents [104]; initiators for continuous activator regeneration (ICAR ATRP), employ conventional thermal radical initiators [105]; electrochemically mediated ATRP (*e*-ATRP), use electrical current as reducing agent [106]; supplemental activator and reducing agent (SARA ATRP), zerovalent transition metals are used [102, 107] and single electron transfer-living radical polymerization (SET-LRP) [108], similar to SARA ATRP .

In Table 2 are summarized all variations mentioned and main features.

Table 2. ATRP variations and their features.

ATRP Variation	Representative Scheme[a]	Features
ARGET ATRP [109]	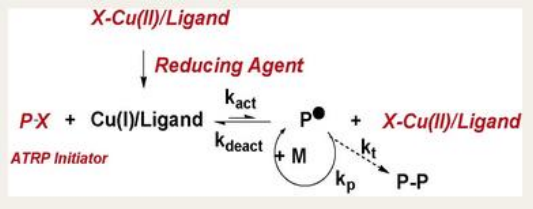 X-Cu(II)/Ligand Reducing Agent P-X + Cu(I)/Ligand ATRP Initiator k_{act} k_{deact} P• + X-Cu(II)/Ligand + M k_p k_t P-P	- Use low amounts of catalysts; - Use reducing agents, that regenerate the catalyst; - Catalysts induced side reactions are diminished; - Activator is regenerated by electron transfer
ICAR ATRP [92]	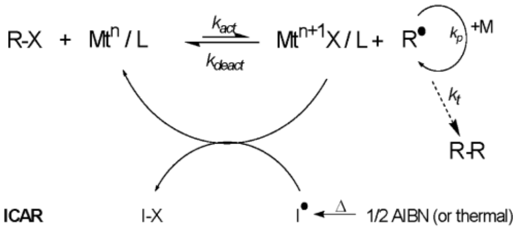 R-X + Mtⁿ / L k_{act} k_{deact} Mtⁿ⁺¹X / L + R• k_p +M k_t R-R ICAR I-X I• Δ 1/2 AIBN (or thermal)	- Source of organic free radicals is used (ex:. AIBN); - Activator is regenerated by the organic free radicals; - 5 to 50 ppm of catalyst was used with success - Kinetic similar to the RAFT; - Rate of polymerization established by the rate of decomposition of the organic initiator
***e*-ATRP [92]**	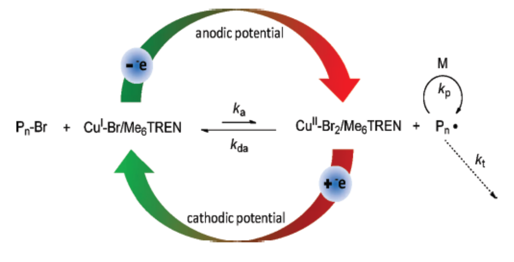 anodic potential - e P_n-Br + Cu^I-Br/Me₆TREN k_a k_{da} Cu^{II}-Br₂/Me₆TREN + P_n• M k_p k_t + e cathodic potential	- Don't use chemicals like reducing agents; - The electrons (from electrical current) regenerate the catalysts;

[a] Images were reproduced from the references mentioned.

Table 2. (Continued)

ATRP Variation	Representative Scheme[a]	Features
SARA ATRP **[103]**	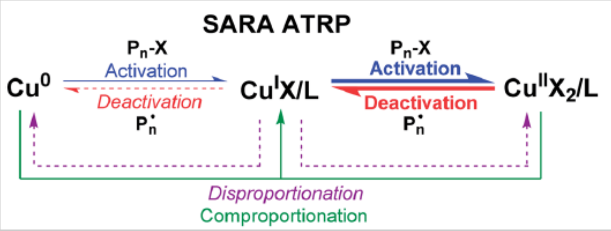 SARA ATRP Cu^0 P_n-X Activation Deactivation $P_n^\bullet$ Cu^IX/L P_n-X Activation Deactivation $P_n^\bullet$ $Cu^{II}X_2/L$ Disproportionation Comproportionation	- Use zerovalent transition metals or inorganic sulfites; - Activation by Cu(I) and deactivation by Cu(II); - Cu^0 act as reducing agent and supplemental activator of alkyl halides; - Activation of alkyl halides occurs by inner sphere electron transfer (ISET).
SET-LRP **[103]**	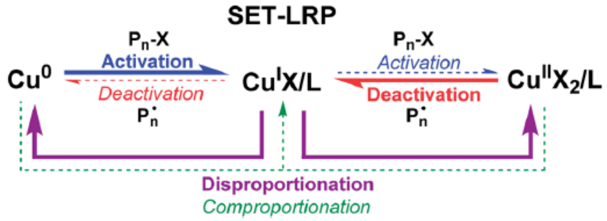 SET-LRP Cu^0 P_n-X Activation Deactivation $P_n^\bullet$ Cu^IX/L P_n-X Activation Deactivation $P_n^\bullet$ $Cu^{II}X_2/L$ Disproportionation Comproportionation	- Cu^0 is exclusively an activator of alkyl halides; - Activation of alkyl halides occurs by outer sphere electron transfer (OSET); - Cu(I) undergoes instantaneous disproportionation to Cu^0 and Cu(II)

[a] Images were reproduced from the references mentioned.

It is important to note that in the schemes representing the SARA ATRP and SET-LRP models, shown in Table 2, bold arrows represent the most relevant reactions, solid arrows indicate supplemental reactions and, finally, dashed lines represent reactions that can be neglected. These two mechanisms are identical and are normally applied to classify polymerizations that use zerovalent transitions metals, namely Cu^0. Nowadays, it is still in debate which is the most correct model to describe the role of Cu^0 in the polymerization mechanism. In the literature is possible to find the two nomenclatures to describe similar systems [103]. For example, in the graphene research area the most often used classification is SET-LRP [60-62]. However, in this work the systems catalysed by Cu^0 zerovalent transition metal are classified as SARA ATRP systems, since it is the mechanism supported by the Polymer Research Group where this work was done and that are recently supported by Konkolewicz, D. and co-workers through diverse experimental and theoretical data [100, 103].

1.4. "Grafting-from" - State of the Art

Given the fact that our focus was the "grafting-from" approach and after some fundamentals about CLRP have been exposed, it is important at this stage to present the state of the art of the area.

Although CLRP methods are the most employed to functionalize graphene and GO with polymers, other alternative strategies can be found, like in *situ* Ziegler-Nata polymerization, in *situ* condensation or in *situ* FRP [76, 78-80]. For example, in 2010 was reported the first example of “grafting-from” polymer chains through in *situ* Ziegler-Nata polymerization [76]. In this work, GO was first functionalized with a Ziegler-Nata catalyst and after, polypropylene (PP) was polymerized from the surface of GO, producing a nanocomposite that revealed good dispersion in a PP matrix and high electrical conductivity.

Table 3 shows some reports in which polymer chains were attached to the surface of GO by using alterative techniques.

Table 3. Non CLRP methods reported for grafting polymers from graphene and its derivatives.

Ref.	Year	Type of Graphene	Polymer attached	Polymerization mechanism
[78]	2012	GO	Hydrogel	FRP
[80]	2011	rGO	PU	Condensation
[79]	2010	GO	PMMA	FRP
[76]	2010	GO	PP	Ziegler-Natta

To date, in the field of polymerization from graphene species ATRP and RAFT polymerization are the most studied methods [10, 15, 23-26, 40, 47, 48, 54, 56-75, 81-87]. ATRP has several advantages including the ability to synthetize polymers from a wide range of monomers with complex structure, good control over *Đ*, high end functionality, employs commercial available compounds and uses mild reaction condictions [10, 15, 23-26, 47, 54, 56-73].

In Table 4 are summarized several papers that reported the functionalization of graphene species with polymer chains using RAFT polymerization.

Table 4. Articles published that report the grafting of polymers from graphene and its derivatives through RAFT polymerization.

Ref.	Year	Type of Graphene	Polymer attached	Polymerization mechanism
[85]	2012	rGO	PNIPAm	RAFT
[74]	2012	GO	PS	RAFT
[81]	2012	GO	PS	RAFT
[82]	2012	rGO	PDMAEA, PAA, PS	RAFT
[86]	2012	Graphene	PS, PMMA, PMA, P4VP and PDMA	RAFT
[83]	2012	GO	PS, PNIPAm, PMA, PtBA and PDMA	RAFT
[75]	2011	GO	PS	RAFT
[87]	2011	GO	PVK	RAFT
[84]	2010	GO	PMAAm	RAFT

In the several reports that describe the use of ATRP to grow polymers from the surface of the graphene species, it is possible to find several differences, as, for example, in the monomers polymerized, in the catalytic system and in the strategy employed to functionalize graphene with the initiator moieties.

One of the first papers published report the polymerization of PDMAEMA chains by ATRP [23]. The carboxyl groups of GO were converted to amine groups through an amidation reaction, between GO and 1,3-diaminopropane, in the presence of N-hydroxysuccinimide (NHS) and N-(3-(dimethylamino)propyl)-N'-ethylcarbodiimide hydrochloride (EDC.HCl). In a second step, amine and hydroxyl groups were used to graft the initiator α-bromoisobutyryl bromide (BIBB) via one reaction catalysed by triethylamine (TEA). For the ATRP of PDMAEMA they used as catalyst copper bromide (CuBr) and as ligand N,N,N,N,N-pentamethyldiethylenetriamine (PMDETA). Several characterization techniques, like Fourier transform infrared spectroscopy (FTIR), thermogravimetric analysis (TGA), X-ray photoelectron spectroscopy (XPS) and transmission electron microscopy (TEM), were carried out to prove the success of the polymerization. In other work the same strategy was employed to afford a nanocomposite of GO/poly(sodium 4-styrenesulfonate) (GO/PSSS) with good catalytic activity for the synthesis of isoamyl benzoate [25].

Lee and co-workers used a similar approach, but instead modifying both the carboxyl groups and hydroxyl groups of GO, only hydroxyl groups were used to attach the initiator BIBB, through esterification reaction, also catalysed by TEA (Figure 10). As catalytic system Cu(0) wire and tris(2-aminoethyl)amine (TREN) in dimethylformamide (DMF) at 80 ºC was used. In this report, diverse polymers were attached, namely polystyrene (PS), poly(methyl methacrylate) (PMMA) and poly(butyl acrylate) (PBA). The particularity of this work is the deep characterization of the GO grafted with initiator by XPS, TGA and elemental analysis (EA). It was proved that the ATRP reactions proceed in a control manner with different types of monomers and the modified GO gave a stable dispersion in DMF, chloroform ($CHCl_3$), toluene and dichloromethane (CH_2Cl_2) [24]. A PDMAEMA thermoresponsive polymer was attached to the surface of GO via ATRP following the same strategy applied by the previous authors [24] to attach the initiator to GO (Figure 10), but a different catalytic system (CuBr/PMDETA in DMF at 60 ºC) was used [26].

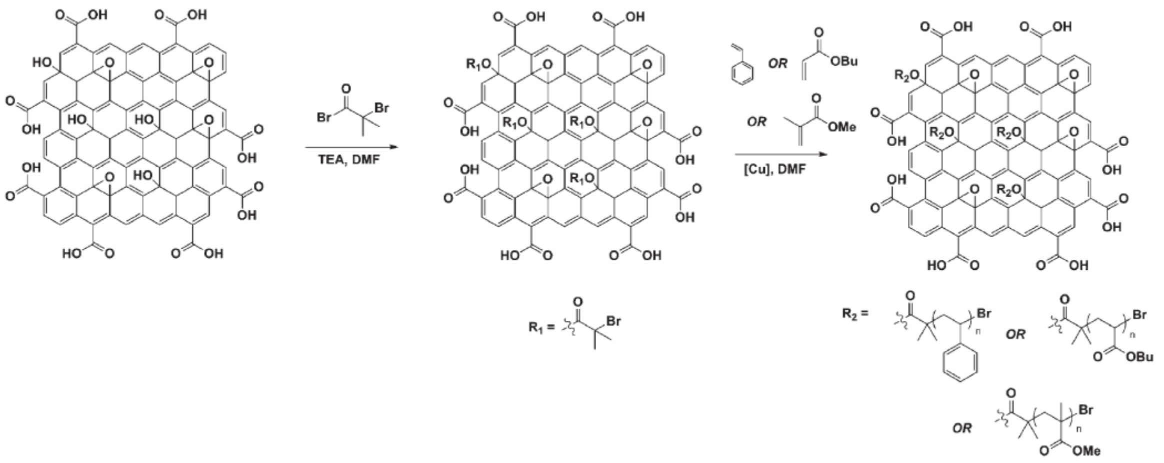

Figure 10. Schematic representation of the pathway to modify the GO with initiator and after polymerize from its surface PS, PBA and PMMA. Reproduced from reference [24].

A completely different approach to functionalize GO with initiator moieties was reported. First, the authors carried out an esterification reaction between the carboxyl acid of the GO and ethylene glycol and then reacted the modified GO with BIBB in the presence of TEA and dimethylaminopyridine. Then, GO modified with BIBB was suspended in DMF and the polymerization of methyl methacrylate (MMA) was conducted in the presence of CuBr and PMDETA, at 65ºC. In this experiment, composite films of PMMA with different percentages of GO modified with PMMA (GO-PMMA) were produced, and was concluded that loadings of 1% (w/w) of GO-PMMA are effective reinforcing agents [10].

A technique previously used to graft initiator moieties to carbon nanotubes was applied for the CLRP from graphene surfaces [15, 47]. rGO was prepared through the reaction of GO with hydrazine hydrate. The grafting density of PS chains was controlled through the concentration of a diazonium salt (reactants: 2-(4-aminophenyl) ethanol and isoamyl nitrite) during the grafting process of the initiator and through the monomer concentration during the ATRP reaction. The initiator 2-bromopropionyl bromide was grafted through the hydroxyl groups, resulting from the coupling of the diazonium salt, by an esterification reaction realized in the presence of triethanolamine. Different chain lengths were polymerized from rGO surface via polymerization catalysed by CuBr and PMDETA using as solvent 1,2-dichlorobenzene at 110ºC and in the presence of free initiator. The grafting polymer chains showed an increase in glass transition temperature (Tg) and a composite film of PS produced with 2 % (w/w) of rGO modified with PS revealed an increase in thermal conductivity compared to pure PS [15]. Wang and co-workers also functionalized rGO with initiator through a diazonium addition reaction followed by an esterification between the hydroxyl groups and the initiator BIBB [72]. After the modification, the polymerization of poly(2-(ethyl(phenyl)amino)ethyl methacrylate)

(PEMA) was performed with CuBr/1,1,4,7,10,10 hexylmethyltriethylenetetramine (HMTETA) in 1,2-dichlorobenzen at 80 ºC.

In the field of the graphene modifications, in addition to the conventional ATRP, also have been used ATRP variations using low concentrations of catalysts to perform the "grafting" CLRP reactions. One reported ATRP variation was the SET-LRP, which achieves high polymerization rates at low temperatures and high end group fidelity [40, 61]. One example was reported for the polymerization of poly(tert-butyl methactylate) (PtBMA) [60]. The authors polymerized PtBMA from the surface of rGO using as catalytic system Cu(0) wire and tris(2-(dimethylamino)ethyl)amine (Me_6TREN) in dimethylsulfoxide (DMSO) at 25ºC. To attach the initiator, 2-bromopropionyl bromide, to the rGO they used one methodology already mentioned above[15].

Between the most recent reports is the research made by Roghani-Mamaqani, H. and Haddadi-Asl, V., published in 2014 [54]. The major difference from the works previously presented is the functionalization of GO with (3-aminopropyl) triethoxysilane (APTES) through the hydroxyl groups of GO by a coupling reaction. The next step was to attach the BIBB to APTES, in the presence of TEA, and then PS brushes were grown with CuBr and PMDETA in DMF at 110 ºC.

Previously it was presented a briefly overview from some of the most referred papers published so far, trying to show some of the main differences that can be found in the literature. However, many other reports were produced.

In Table 5 are summarized the most important reports in the area, which deal with ATRP strategies to grafting polymers (brushes) from the surface of graphene and its derivatives.

Table 5. Articles published that report the grafting of polymers from graphene and its derivatives through ATRP and respectively derivatives polymerization techniques.

Ref.	Year	Type of Graphene	Polymer attached	Polymerization mechanism
[54]	2014	GO	PS	ATRP
[70]	2014	rGO	PS[3]	ATRP
[65]	2014	GO	AA[4]	ATRP
[67]	2014	GO	BEB, PS, PVDF	ATRA
[26]	2013	GO	PDMAEMA	ATRP
[25]	2013	GO	PSSS	ATRP

---

[3] Before polymerization graphene was functionalized with different amounts of CD.

[4] Reactants used: PAM; functional monomer HEA; EDMA as crosslinking agent and acetonitrile as solvent and dispersion medium.

Table 5. (Continued)

Ref.	**Year**	**Type of Graphene**	**Polymer attached**	**Polymerization mechanism**
[56]	2013	GO	PMA	ATRP
[71]	2013	GO	PS[5]	ATRP
[57]	2012	rGO	PtBA[6]	ATRP
[64]	2012	GO	PDMAEMA	ATRP
[73]	2012	GO	PNIPAm	ATRP
[68]	2012	rGO	PNIPAm	ATRP
[58]	2012	GO	PDMAEMA	ATRP
[62]	2012	GO	PNIPAm	SET-LRP
[55]	2012	rGO	PMA	ATRP
[69]	2011	rGO	PMMA, PS	ATRP
[61]	2011	GO	PPEGEEMA	SET-LRP
[60]	2011	rGO	PtBMA	SET-LRP
[72]	2011	rGO	PEMA	ATRP
[24]	2010	GO	PS, PMMA, PBA	ATRP
[15]	2010	rGO	PS	ATRP
[10]	2010	GO	PMMA	ATRP
[66]	2010	GO	PMMA	ATRP
[63]	2009	GO	PS	ATRP
[23]	2009	GO	PDMAEMA	ATRP

---

[5] GO was modified with MPS by a silane coupling reaction and was polymerized with PS.

[6] By subsequente hydrolysis of rGO-PtBA tert-butyl groups were prepared water-dispersible rGO-PAA.

Chapter 2

2. GO - Controlled modification

The main goal of this work was to polymerize from the surface of GO. However, in the beginning, graphene, GO or any other type of graphene species were experimentally unknown to us. To the best of our knowledge, this was the first project in the graphene research area in our department. To override this background and in order to gain some experience before ensuing the polymerization processes with GO, the first step was to learn how to conduct CLRP reactions in the laboratory and, with this, improve the experimental and theoretical knowledge in CLRP.

The learning process started in the beginning of the first semester of this academic year, 2013/2014, with the involvement in two CLRP projects of the Polymer Research Group of the Department of Chemical Engineering, University of Coimbra. Throughout the year, several CLRP reactions were carried out and the evolution of the research was followed closely.

In both projects were tested new solvents and solvents combinations for controlled polymerization using the SARA ATRP mechanism. In the first one, an unusual synergistic effect between 1-butyl-3 methylimidazolium hexafluorophosphate (BMIM-PF_6) and DMSO mixtures was examined for the SARA ATRP of MA at room temperature. This study was published in *ACS Macro Letters* [100]. In the second project, also published in *ACS Macro Letters*, it was proposed sulfolane as an universal solvent for the SARA ATRP of acrylates, methacrylates, Sty and vinyl chloride (VC) at room temperature [110].

These two research projects, alongside with my thesis advisors Doctor. Jorge F. J. Coelho and Doctor Arménio C. Serra, were conducted by Master Joana P. Mendes, Master Carlos M. R. Abreu, Master Patricia V. Mendonça, Doctor Tamaz Guliashvilli from CEMUC, Department of Chemical Engineering, University of Coimbra, and Doctor Anatoliy V. Popov from Department of Radiology, University of Pennsylvania.

In Appendices C to F are presented the two papers published and the respective Supporting Information (SI).

After a semester gaining some experience in CLRP reactions, in the beginning of the second semester of this academic year the work with GO was started. In this Chapter 2 is presented the work developed with GO, namely all decisions, results and the respective interpretations.

Throughout the work diverse steps were taken in order to achieve the final goal, namely the CLRP from GO using systems which use low concentrations of catalysts. Regarding this, the chapter is divided in two parts: the preparation of GO for future polymerization and the polymerization from the surface of GO.

The purpose of this work was to polymerize from GO, however, in order to grow polymers from it, it is necessary to modify its surface with initiator moieties, which will be responsible for generating radical species starting the polymerization. Considering this, the first part of this chapter concerns to the functionalization of GO with initiator molecules. Such modifications were realized according to procedures reported in the literature [23-26].

In the second part of the chapter are exposed the results and the respective discussions of the polymerization from GO and are explained the scientific path followed during the course of the work. Preliminary polymerizations were conducted reproducing some of the systems reported in the literature, i.e., using the same monomers, catalysts, ligands and reactant ratios [10, 23, 24]. Finally, the polymerizations from GO surface were carried out using systems studied by our research group, like the systems presented in Appendix E.

2.1. Preparation of GO for future polymerization

The preparation of GO for future polymerization consists in the covalent attachment of initiator molecules to the surface of the oxidized carbon nanomaterial. Diverse methodologies to realize such modification can be found in the literature, as for example, the attachment of ATRP initiators by esterification with the hydroxyl groups of GO or by esterification and amidation reactions using both hydroxyl and carboxyl groups [23-26]. It is also possible to increase the number of hydroxyl groups through an epoxide ring-opening, followed by esterification reaction between initiator molecules and hydroxyl groups [61].

Gonçalves and co-workers introduced hydroxyl groups in GO by reacting the carboxyl groups with thionyl chloride and ethylene glycol. Final functionalization with ATRP initiator was also achieved by esterification [10]. Other strategy reported consists in the reduction of GO with hydrazine hydrate, in order to remove the oxygen-containing species from its surface, followed by introduction of hydroxyl groups through a diazonium coupling reaction. After this, hydroxyl groups were reacted with initiator molecules also by an esterification reaction [15, 60]. In addition, other methodologies can be found in the literature [54-62, 64-73].

In general, the functionalization of GO with initiator molecules is achieved by a final esterification reaction between hydroxyl groups existing in its surface and free ATRP initiator molecules. The main difference between the different methodologies concerns the treatment of GO, in order to control/increase the amount of initiator moieties covalently bonded to the carbon nanosheets.

In this work, the initiator moieties were attached to GO following two reported approaches, in order to understand which one could be more successful. After some preliminary reactions it was established the use of the most promising methodology. One of the strategies employed was reported by Lee and co-workers. In this methodology only hydroxyl groups of GO were modified through an esterification reaction at room temperature catalysed by TEA (Figure 11) [24]. In the second strategy followed, first carboxyl groups were converted to amine groups reacting the GO with 1,3-diaminopropane in the presence of NHS and EDC.HCl and, in a second step, amine and hydroxyl groups were reacted with initiator molecules in the presence of TEA at 90 ºC. This methodology was reported by Yang and co-workers [23].

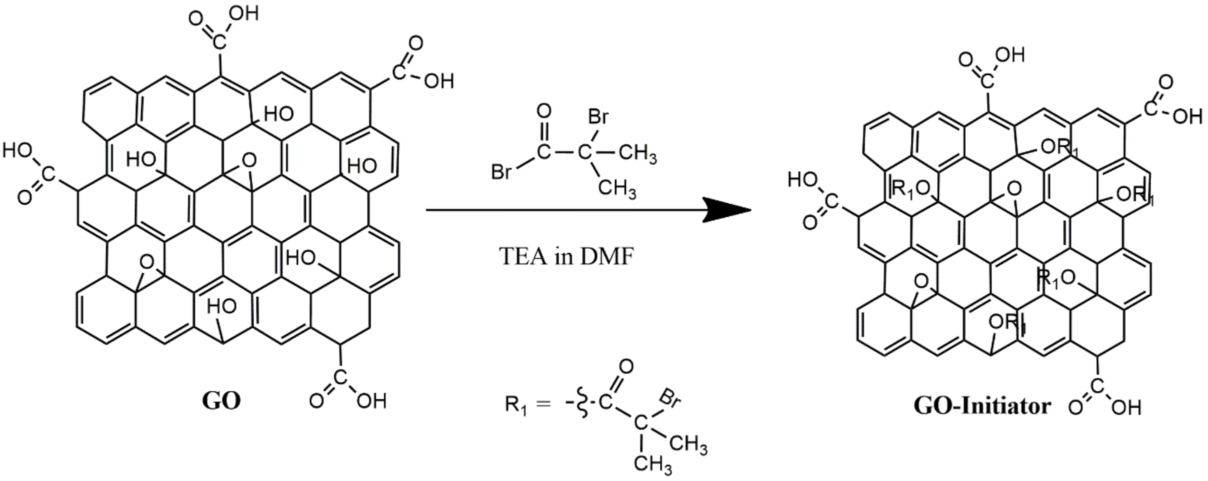

Figure 11. Schematic representation of the attachment of initiator using only hydroxyl groups.

In order to facilitate the discussion presented below, was defined a nomenclature for the two methods. From this point, the method in which only the hydroxyl groups of GO were modified will be denominated as Lee method and the other strategy that use both hydroxyl groups and carboxyl groups of GO will be referred as Yang method.

It is important to note that in the literature is possible to find most recent papers that report the use of the Lee method and Yang method to attach the initiator molecules to the surface of GO, only the amounts of reactants are reformed remained the other parameters unchanged [25, 26].

The scheme of the reaction pathways for the two methodologies used are shown in Figure 11 and Figure 12, respectively, and all the procedures are described in chapter 3.

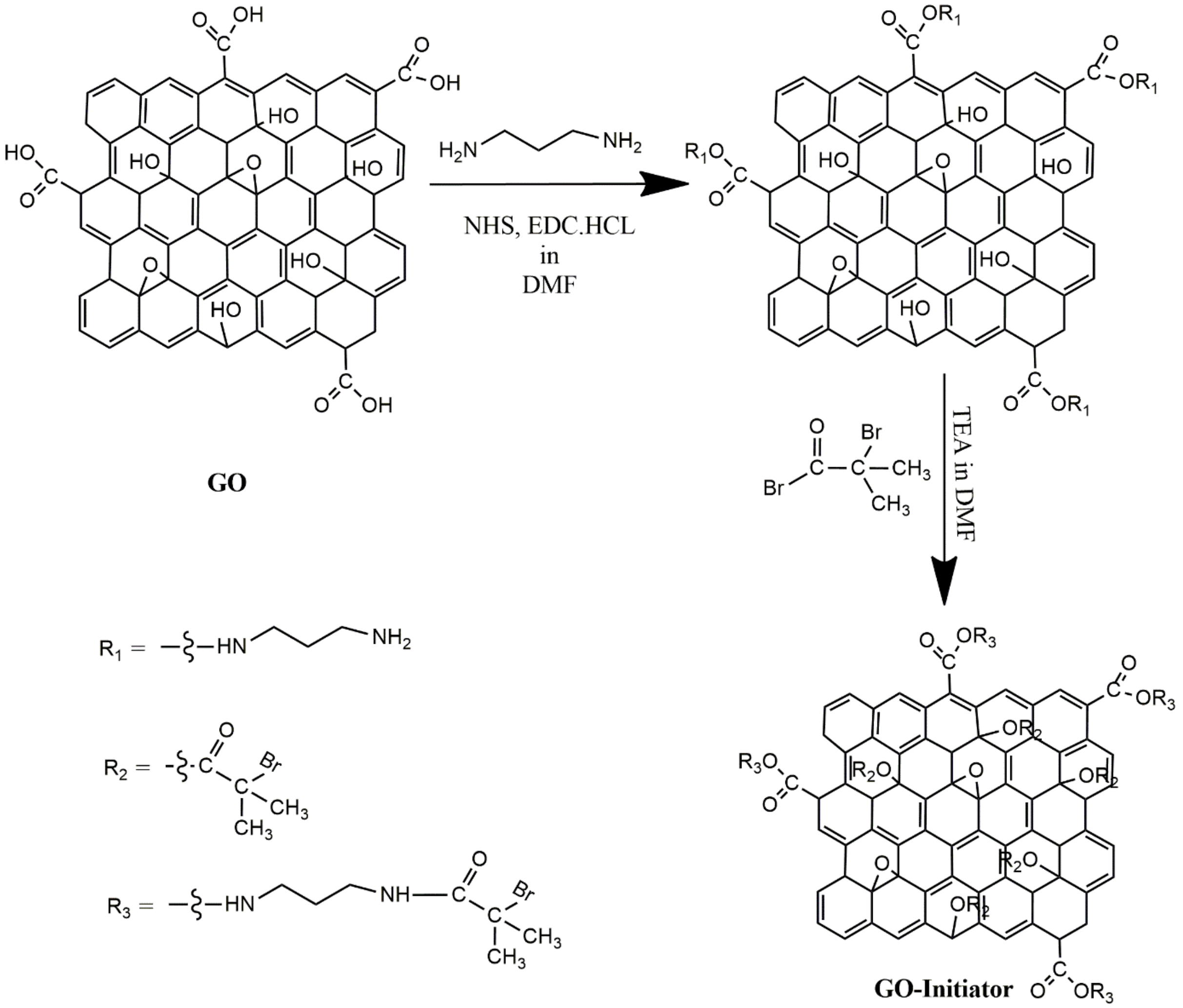

Figure 12. Schematic representation of the attachment of initiator moieties using both carboxyl and hydroxyl groups.

Considering the time consumption and the main objective, to test a wide number of methods reported was impossible. Therefore, only two of the methods described in the literature were reproduced [23-26]. Some of the reasons that made choose these two methodologies were the knowledge acquired about the reactions and procedures described in the references as well as the availability of the reactants in our department. In addition, the number of reactions required to achieve the final GO modified with initiator moieties was also an important factor. For example, in the Lee method initiator molecules were attached to GO only by an esterification reaction, a type of reaction that was already conducted in our group, which gave to us some confidence in the methodology [24, 26]. Additionally, the article was easy to understand, the procedures were well described and different characterization techniques were used to prove the attachment of initiator molecules to the GO surface. As an alternative, GO was reduced before the attachment of the initiator moieties to its surface, in order to remove the oxygen-containing groups. After this hydroxyl groups were introduced in the rGO with different grafting densities, by using different concentrations of a diazonium salt, and, only after this steps, initiator molecules were attached to GO [63]. This process was promising, because it allows an easy control over the grafting density of the polymer. However, the number of reactions was relatively high which increase the probability of failure and up to date, in our group, this type of reactions has never been done, which increased the probability of failure even further. Considering this, the last method described was one of the reported methods that was decided not to reproduce in this phase. For similar reasons other methods were excluded. The previous methods are only examples to better illustrate the choices.

It is remarkable to note that, in this phase, the control over the grafting density of the polymer brushes was not a critical factor. It was of extreme importance to choose a straightforward method in order to introduce with success the initiator molecules in the GO surface and to proceed to polymerization.

In short, the Lee method and the Yang method were selected because were simple to understand and well described. We felt confidence with the reactions described and few resources and mild reaction conditions were required.

As initiator was used, in all the procedures, BIBB, because it was the most reported initiator and suitable for SIP, it could be bonded to the basal planes of GO or to the edges using diverse approaches. Moreover, it had proved to be able to initiate with success the polymerization of a wide range of monomers from diverse types of surfaces [10, 23-26, 47, 54-58, 61, 64, 68, 69, 73, 111-117].

In these reactions three types of GO were used. The two firstly, mainly for preliminary reactions, were kindly supplied by the University of Porto, Department of Chemical Engineering (codes: Oxi_Porto1 and Oxi_Porto2), and afterwards GO was purchased from NanoInnova Technologies SL (code: FB_NIT), located in Spain.

2.1.1. Preliminary reactions: Modification of –OH groups vs Modification of both –OH and –COOH groups

Preliminary reactions were conducted in order to understand which one of the two selected methods was more successful in the modification of GO with initiator molecules. As previously mentioned, in this reactions, was used as raw material the GO (Oxi_Porto1 and Oxi_Porto2) kindly supplied by the Department of Chemical Engineering, University of Porto. This was our first contact with graphene species, namely GO. Until this phase, the behaviour of GO when submitted to reactions was unknown for us. Having this in mind and also the small quantities available, in the first reactions were used low amounts of GO, in order to acquire some experience in such functionalization process, understand the problems that this carbon nanomaterial could cause, learn how to deal with it and mainly to evaluate if the final product was correctly functionalized with initiator molecules.

Two reactions were conducted using the GO Oxi_Porto1 (Table 6). In the experiment labelled as Br_G01 was reproduced the Yang method, modifying both carboxyl and hydroxyl groups existing in GO [23]. In the other reaction, Br_G02, only hydroxyl groups were modified following the Lee method [24]. All the procedures were carried out as described in the mentioned, only the scale of the reactions and the quantities of reactants used were changed, having as base the ratios between the different reactants (Appendix G, Table G1 and Table G2). The detailed description of all procedures used is exposed in the Chapter 3.

Table 6. First functionalization reactions carried out to attach the initiator moieties to the surface of GO Oxi_Porto1.

Entry	Rx Code	GO	Groups modified	m_i (mg)	m_f (mg)	Analysis
1	Br_G01	Oxi_Porto1	-OH and -COOH	10	9.1	FTIR-ATR
2	Br_G02	Oxi_Porto1	Hydroxyl (-OH)	30	12.8	FTIR-ATR

Due to the low amounts of GO used (Table 6) the final products of the reactions Br_G01 and Br_G02 were only analysed by Fourier transform infrared spectroscopy - Attenuated total reflection (FTIR-ATR) and the results were not conclusive in respect to the success of GO functionalization (Appendix H, Figure H1). However, some important observations were taken from these experiments. Regarding to the GO Oxi_Porto1, the characteristic band at 2500-3500 cm^{-1}, attributed to the hydroxyl stretching vibration of O-H groups, was not visible, which was an indication that most probably the graphene used had a low degree of oxidation [23, 26, 40, 56, 61, 62]. The curve corresponding to the product of the esterification/amidation reaction Br_G01 revealed many defined peaks (Appendix H, Figure H1). This observation suggested that the product contained traces of solvents or reactants and also that the washing process had to be improved. The Infrared (IR) peaks of the esterification product Br_G02 were very similar to the peaks of the original GO. Probably some modification was not achieved, because of the lack of hydroxyl groups in GO surface.

After the first two reactions, a new GO (Oxi_Porto2) was supplied again by the University of Porto. Aiming to understand if the GO had hydroxyl groups and other oxygenated species in its surface, before realizing any type of reaction, it was characterized by FTIR-ATR and TGA (Appendix H, Figure H2 and Figure H3). The FTIR and TGA results allowed us to conclude that the GO Oxi_Porto2 possessed in its surface oxygen-containing groups likely to be functionalized with initiator moieties.

Having in account that previous reactions were not conclusive, three reactions were carried out using as raw material the oxidized carbon nanomaterial Oxi_Porto2 (Table 7). The reactions were carried out, again using low amounts of GO, aiming to understand which one of the selected methods could give us more probabilities of success in the attachment of initiator molecules to the GO surface. In the reactions denominated as Br_G03 and Br_G05 was reproduced the Lee method, and in the reaction Br_G04 the Yang method was followed. At this time the product Br_G04 was washed exhaustively with ethanol to remove all the traces of solvents and reactants.

Table 7. Preliminary functionalization reactions realized during the semester to attach the initiator moieties to the surface of GO Oxi_Porto2.

Entry	Rx Code	GO	Groups modified	m_i (mg)	m_f (mg)	Analysis
1	Br_G03	Oxi_Porto2	Hydroxyl (-OH)	50	34.1	FTIR-ATR, TGA
2	Br_G04	Oxi_Porto2	-OH and -COOH	50	40.03	FTIR-ATR, TGA
3	Br_G05	Oxi_Porto2	Hydroxyl (-OH)	50	32.37	FTIR-ATR, TGA

By comparing between the results obtained for original Oxi_Porto2, esterification product Br_G03 and esterification/amidation product Br_G04, was concluded that the modifications in GO were higher when the Lee method was employed. The FTIR-ATR and TGA results are shown in Appendix H (Figure H4 and Figure H5).

The esterification named as Br_G05 was carried out to gain some experience in the selected method and to evaluate its reproducibility. As can be seen in Figure H5 and Figure H4 (Appendix H) the results obtained in this reaction were very similar to the obtained in the esterification reaction Br_G03, meaning that probably the modifications generated in GO were the same and that we had been able to reproduce the final modified product.

At this stage, the results obtained (Appendix H) led us to select the Lee method as the most promising for the functionalization of GO with initiator moieties. Therefore, two esterification reactions were conducted using higher amounts of GO (Table 8). After characterization, the products of these reactions were used in future polymerizations (Section 2.2.1).

Table 8. Esterification reactions conducted to GO Oxi_Porto2, following the Lee method [24].

Entry	Rx Code	GO	Groups modified	m_i (mg)	m_f (mg)	Analysis
1	Br_G06	Oxi_Porto2	Hydroxyl (-OH)	151.8	123.67	FTIR-ATR; TGA
2	Br_G07	Oxi_Porto2	Hydroxyl (-OH)	165.7	113.3	FTIR-ATR; TGA

The FTIR-ATR and TGA results obtained for the esterification products Br_G06 and Br_G07 were very similar to the results obtained in the previous esterification reactions (Appendix H, Figure H6 and Figure H7). It is important to mention that these esterification products were used for polymerizations without knowing the amount of bromine in the sample and also without having certainties about the covalent attachment of BIBB to the GO surface.

One of the characterization techniques that provides information about the quantities of bromine (Br) in GO and if this element is covalently bonded to GO is the XPS, also known as Electron Spectroscopy for Chemical Analysis (ESCA). This technique measures the elemental composition in the surface of the material, producing important information about the bonding environment, like functional groups, within the material [40]. XPS is an expensive technique that is not available in our department (the lowest price found was 45€/h and the average time of one analysis is about 1 hour). Considering that, XPS was only used when considerable amounts of GO were submitted to esterification, i.e., when we had significant amounts of final esterified product enough for diverse polymerizations and not only for one or two as in the case of Br_G06 and Br_G07.

At this stage was assumed that the quantities of Br existing in GO were identical to the reported in the literature and, in preliminary polymerization reactions, were followed the reactant ratios used in systems reported. The goal of this strategy was to test the esterification products as macroinitiators for polymerization reactions, in order to understand if the ATRP initiator was present in the GO surface. We were working on the assumption that if polymer was obtained at the end of the polymerization reaction it could indicate that probably the esterification reactions were successful.

In the middle of the second semester, the GO (FB_NIT) purchased at NanoInnova arrived to our department, the main raw material for this work. As before, with GO Oxi_Porto2, the FB_NIT was characterized through FTIR, TGA and, additionally, through XPS. The characterization realized to the purchased GO had as main goal to evaluate if the analysis realized by us and our partners were in agreement with the producer analysis (Appendix I) and compare this new raw material with the previous, namely Oxi_Porto2.

In the FTIR spectrum of GO FB_NIT (Figure 13), is well-visible the characteristic O-H stretching vibration band centred at 3376 cm^{-1} [23, 56]. The two peaks at 1723 and 1619 cm^{-1} illustrate the C=O vibration from carbonyl/carboxyl groups and C=C vibration from the aromatic skeletons of GO, respectively [13, 56, 61, 62, 118]. The C-OH vibration, C-O vibration from epoxy groups and C-O vibration from alkoxy groups are visible at 1362, 1226 and 1058 cm^{-1}, respectively [56, 61, 118].

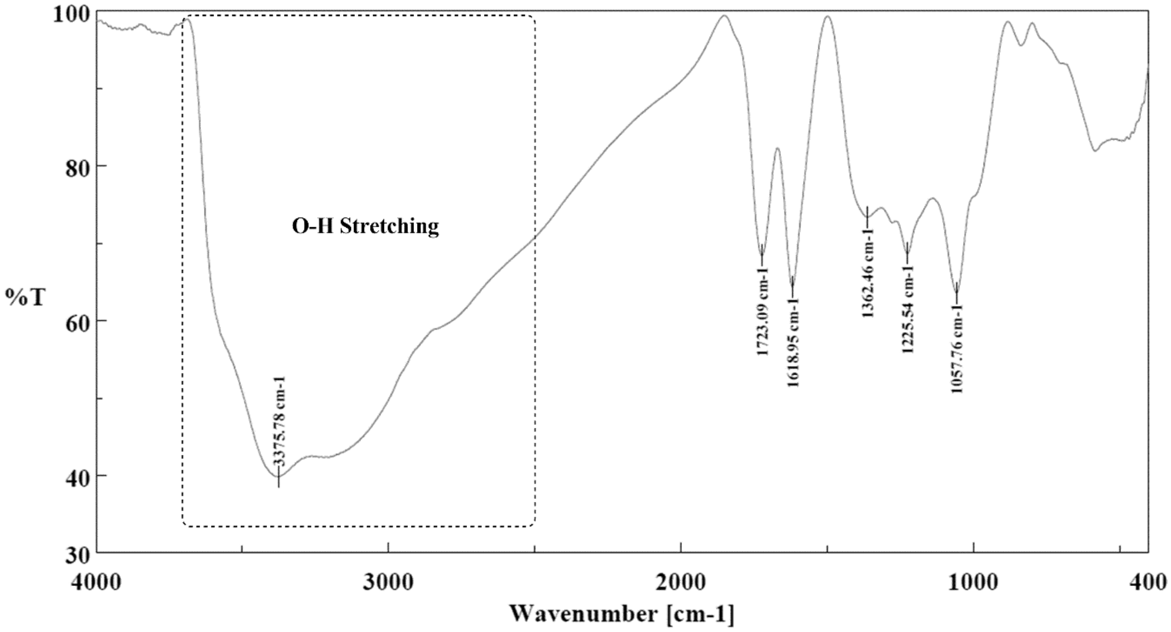

Figure 13. IR spectrum of Original GO FB_NIT.

TGA analysis of FB_NIT also revealed that the nanomaterial possessed numerous oxygen-containing groups in its surface (Figure 14). The TGA curve of original GO FB_NIT revealed a first weight loss of about 12% around 100ºC, which we believe to be associated to the loss of water molecules that were absorbed in the hydrophilic GO’s structure [24, 56]. The main weight loss of about 30% was observed between 121 and 353ºC and was mainly attributed to the decomposition of labile oxygenated species like hydroxyl, carboxyl and epoxy groups that were released in the form of carbon oxides, namely CO and CO_2 [24, 61, 62]. Above 353ºC the weight loss was roughly constant and was probably due to the decomposition of most stable species and of part of the carbon structure.

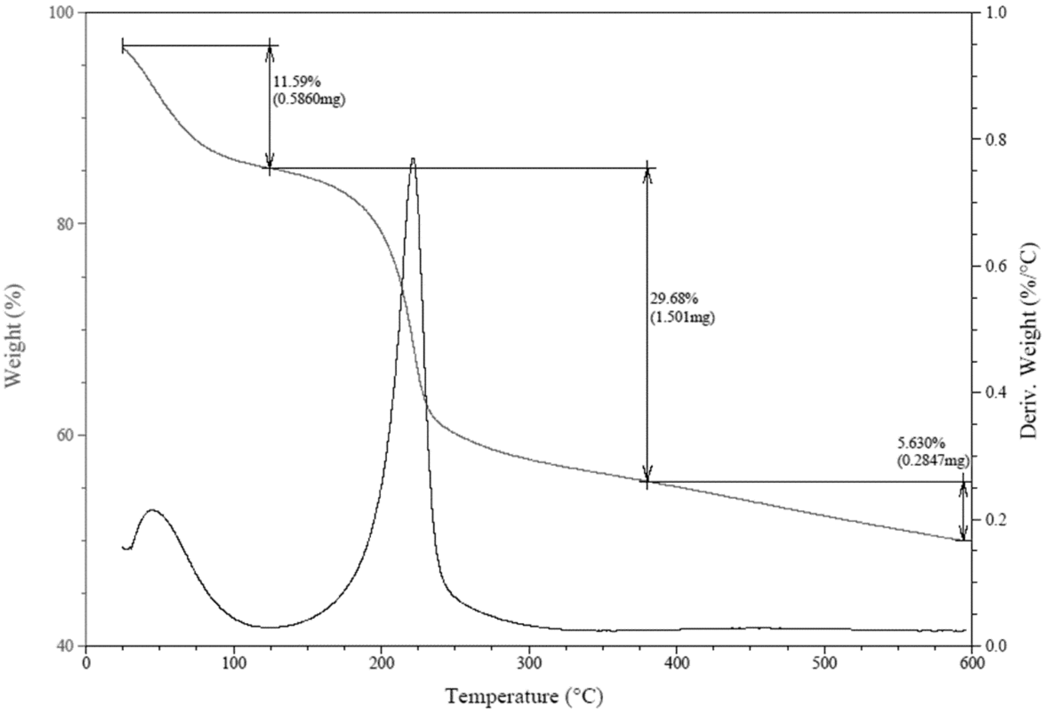

Figure 14. TGA curve of original GO FB_NIT.

Finally, the XPS results, presented in Figure 15, Figure 16, Table 9 and Table 10 provided information about the types of bonds existing in the sample (qualitative and quantitative information) and also provided an elemental quantification. As expected, the XPS results supported the FTIR and TGA results, since it also revealed a significant degree of oxidation.

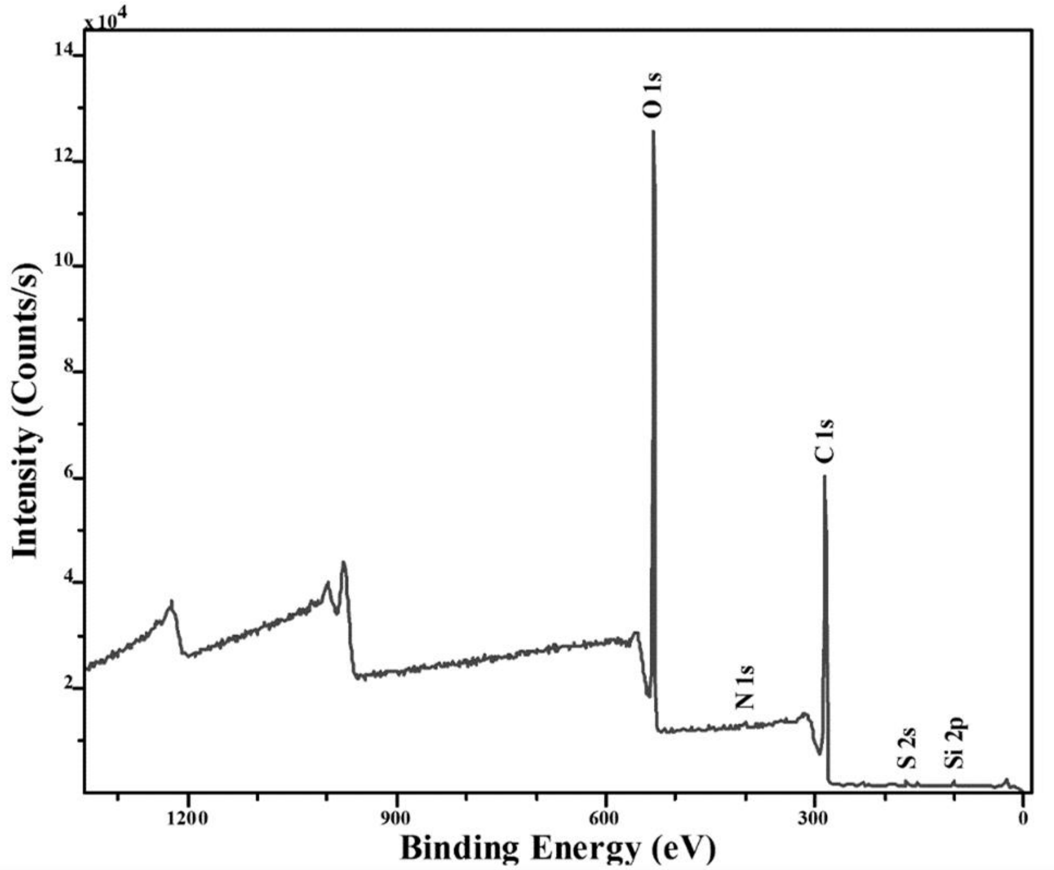

Figure 15. XPS spectrum of original GO FB_NIT.

Elemental quantification (Figure 15 and Table 9) revealed numerous oxygen-containing species and also traces of silicon (Si), sulphur (S) and nitrogen (N) that may result from the oxidation process.

Table 9. XPS elemental quantification of FB_NIT.

Code	%	C	O	Si	S	N	O/C Ratio
FB_NIT	atom	65.40	31.65	1.55	0.59	0.81	0.484
	w/w	57.52	37.08	3.19	1.39	0.83	-

The deconvolution of the C1s high resolution spectrum revealed the presence of carbon atoms in three different chemical environments, namely C-O at 286.6 eV, C-C/C-H sp^2 contribution at 284.4 eV and C=O at 288.4 eV (Figure 16). It was also registered the O1s high resolution spectrum (Figure 16, right) and the respective deconvoluted peaks, which revealed that the oxygen was found mainly in the C-O bonding environment, however the C1s high resolution spectrum also revealed the existence of oxygen atoms in the C=O chemical environment.

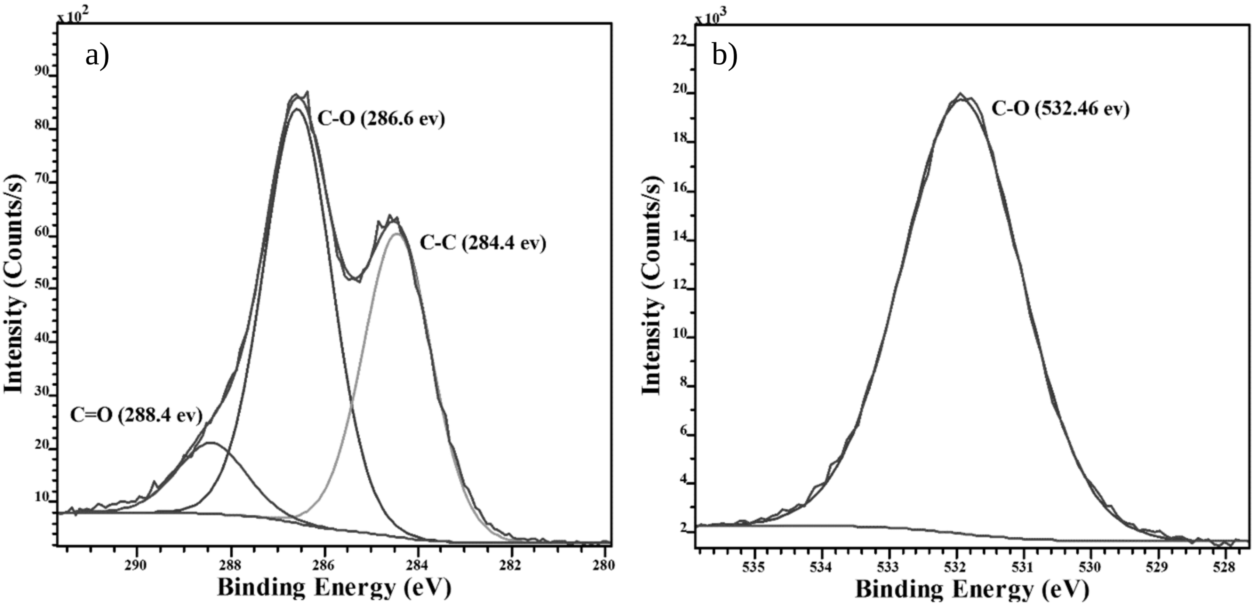

Figure 16. XPS spectrum of FB_NIT. a) Deconvoluted peaks for C1s and b) Deconvoluted peaks for O1s.

Table 10 summarizes the different chemical environments found in the FB_NIT and the respective assignments.

Table 10. C1s, O1s and S2p3/2 high resolution spectra / binding energy assignments.

Code		**C1s**			**O1s**	**S2p3/2**
FB_NIT	chemical environment	C-C/C-H sp^2 contribution	C-O	C=O	Mainly C-O	SO_4^{-2}
	Binding Energy (BE) (eV)	284.4	286.6	288.4	532.46	168.44

The results obtained from the different characterization techniques realized to the original FB_NIT were in agreement with the results realized by the producer, presented in Appendix I.

This means that we can state with some confidence that the characterization techniques conducted by us and our partners were accurate.

In Appendix H (Figure H8 and Figure H9) are presented comparisons between the results obtained for the GO Oxi_Porto2 and FB_NIT. Such comparisons showed that the results attained for the two raw materials were considerably different, namely in the FTIR spectra. We believe that such differences can be ascribed to different degrees of oxidation existing in the materials.

Knowing that the amount and the type of oxygen-containing species existing in the GO surface could influence the degree of modification achieved by the esterification/amidation reactions, we decided to reproduce again the two methodologies, but now using the purchased FB_NIT as raw material. With these reactions we had in mind to decide definitely which would be the main method used in this work, to produce GO modified with initiator molecules (GO-Br) in higher amounts for various polymerization reactions.

The two reactions are presented in Table 11 and the respective results (FTIR and TGA) are presented in Figure 17 and Figure 18. In the reaction Br_G08 was reproduced the Lee method, instead of the reaction Br_G09 reproduced the Yang method, modifying both carboxyl and hydroxyl groups from the GO [23-26].

Table 11. Final preliminary esterifications reactions using the GO FB_NIT as raw material.

Entry	Rx Code	GO	Groups modified	m_i (mg)	m_f (mg)	Analysis
1	Br_G08	FB_NIT	Hydroxyl (-OH)	103	80.31	FTIR-ATR; TGA
2	Br_G09	FB_NIT	-OH and -COOH	101	103.4	FTIR-ATR; TGA; XPS
3	Br_teste01	FB_NIT	-	12	-	FTIR-KBr; TGA
4	Br_teste02	FB_NIT	Hydroxyl (-OH)	11	-	FTIR-KBr; TGA

The results obtained from the reactions Br_G08 and Br_G09 led to the same conclusions. Once again the Lee method provided higher modifications in GO than the other. An interesting fact was the similarity between the IR spectrum obtained for the esterification product Br_G08 and the IR spectra of the previous esterification products (Br_G03, Br_G05, Br_G06 and Br_G07), presenting drastic changes when compared to the spectrum of the original GO.

Focusing on the characteristic O-H stretching vibration band at 3680-2500 cm^{-1} for the hydroxyl and carboxyl groups, was observed that although it was not visible in the esterification product Br_G08 (Figure 17, curve b)) in the esterification/amidation product Br_G09 it was detected (Figure 17, curve c)). The appearance of such band in the Br_G09 product probably reveals that even after esterification and amidation reactions some hydroxyl groups remained in the surface of GO. Instead, in the Br_G08 IR spectrum, the disappearance of the O-H band might means that mostly of the hydroxyl groups were replaced by BIBB molecules, through ester linkage. This observation was the main reason which led to select the Lee method as the most promising method for the functionalization of GO with initiator moieties.

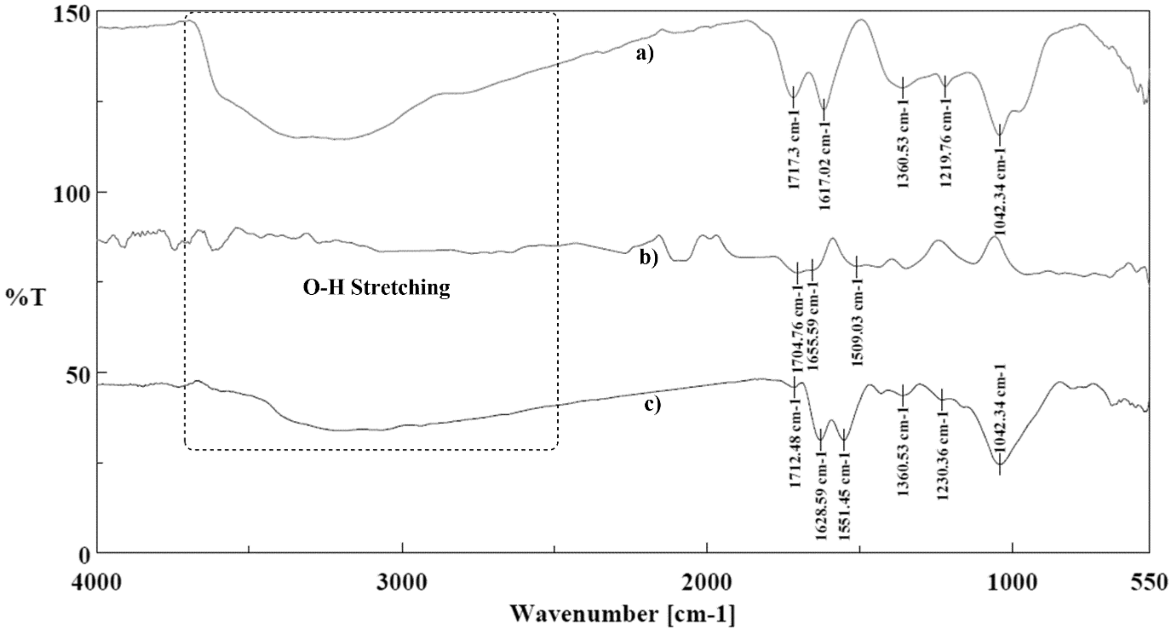

Figure 17. IR spectrum of a) Original GO FB_NIT; b) Esterification product Br_G08; c) Esterification/amidation product Br_G09.

In addition to the differences found in the O-H band, there were also other peaks changes and new peak appearances in both modified products.

For both of these systems there was the presence of amines (TEA when the Lee method was used and TEA and 1,3-diaminepropane in the Yang method) and bromine acids (BIBB in both methods) in the reaction medium. It is known that amines can react with carboxyl acids and epoxy groups from the GO yielding amine linkages (-CNHOC-) [23, 25, 119-121]. On the other hand, acid groups, bromine acid groups from BIBB molecules to be precise, can react with hydroxyl and amine groups producing esters and amine bonds, respectively [23-26]. Also, based on the FTIR results of two control tests conducted meanwhile (Appendix J) was observed that TEA can react with carboxyl acids of GO through an acid-base reaction producing a quaternary ammonium salt [122]. With this in mind, most probably the changes observed in the IR peaks representing carboxyl, epoxy and alkoxy groups were mainly due to reactions that may occurred between the different oxygen-containing species and the amines presented in the medium (TEA and 1,3 diaminepropane) as well as with the BIBB initiator molecules.

For example, when the Yang method was employed the FTIR spectrum (Figure 17, curve c)) clearly showed that carboxyl groups of GO reacted with the amines added to the reaction medium, yielding amine linkages. Two peaks illustrate such modification, namely the peaks at 1712 and 1551 cm^{-1} [121]. The first one was associated to the C=O vibration from carbonyl/carboxyl groups of the GO that, as expected, decreased its intensity when compared with the same peak shown in the original GO IR spectrum at 1717 cm^{-1} (Figure 17, curve a)) [121]. The C=O associated to the new amine linkage shifted its position to lower wave lengths and probably was overlapped by the C=C vibration peak at 1628 cm^{-1} from the aromatic skeletons [121, 123]. The peak at 1551 cm^{-1} was associated to the N-H vibration from the amines introduced in the GO [11, 121].

The identification of the IR peaks obtained from the esterification product Br_G08 (Figure 17, curve b)) was not so obvious, as result of the higher modification observed comparatively to the original GO spectrum and to the arrangement of the peaks (broad and bad defined). In order to understand the drastic changes observed in the IR spectra of the different esterification products were realized two control tests (Appendix J) and the FTIR analysis were carried out using KBr pellets. These options are discussed in the Problems and solutions section presented in this chapter.

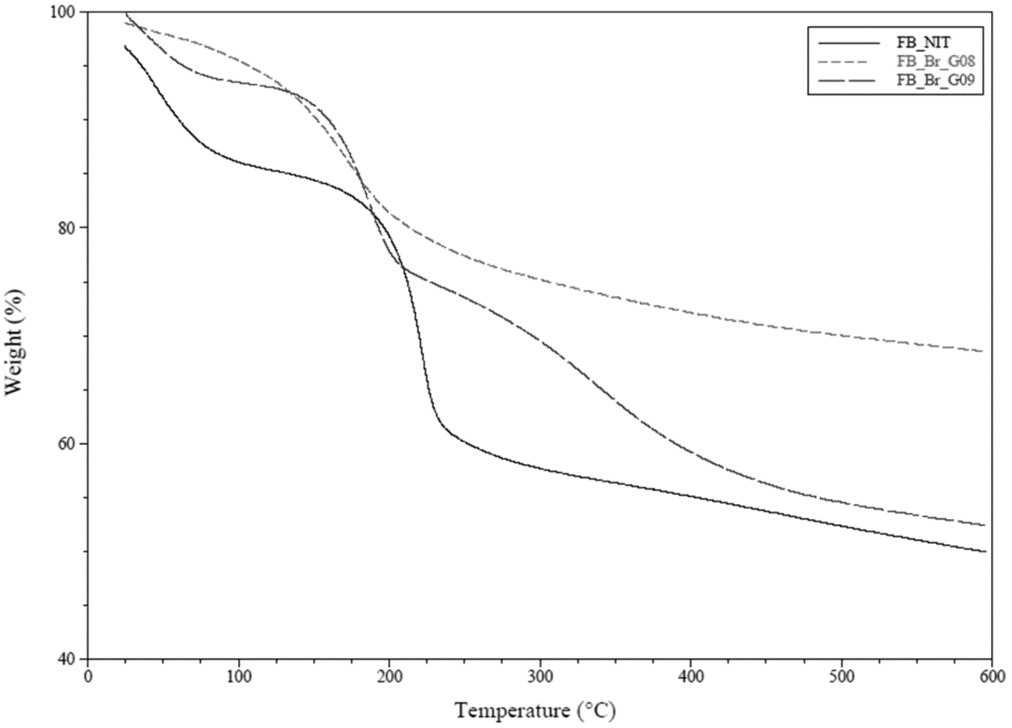

Figure 18. TGA curves of GO FB_NIT (solid line), esterification product Br_G08 (short dashed line) and esterification/amidation product Br_G09 (long dashed line).

The TGA results presented in Figure 18 also revealed that the Br_G09 product presents more labile species in its surface, probably oxygen-containing species and some new attached molecules (amines and BIBB). The total weight loss observed was of about 47%, very similar to the GO FB_NIT weight loss, however with a different decomposition pattern, as result of the introduction of the amines in the surface of GO. Instead, in the Br_G08 product the weight loss was only of about 30% revealing a decomposition pattern completely different from the previous and following the decomposition pattern reported in the literature [24].

In our opinion, and having as main focus the O-H vibration band, the lower modification achieved when using the Yang method, resulted from using lower quantities of BIBB when compared to the quantities of GO employed in the Lee method. As can be seen in (Appendix G, Table G1 and Table G2) the Lee method uses 4× more BIBB than the Yang method.

It is important to note that the esterified products obtained from the reaction Br_G08 were also used for preliminary reactions as the previous products. In the same way, and for the same reasons, they were used without knowing the quantity of bromine present in GO’s surface.

In summary, we chosen the Lee method as the main methodology to functionalize GO FB_NIT with initiator moieties, having as base the results presented and considering that such methodology required less reactants, less time and mild reaction conditions than the other.

In a later phase of the work, one sample of the esterification/amidation product Br_G09 was sent to XPS analysis, alongside with samples of the subsequent esterifications conducted, and the content of Br covalently bonded in the sample was determined to be 2.74% (w/w), which corresponds to a 0.034 mmol of initiator per 100 mg of GO. This result supported our decision, since the quantity of Br in the samples was higher when the Lee method was employed, as can be seen next. The XPS results of the product Br_G09 are presented in Appendix H (Figure H10, Figure H11 and Table H1).

2.1.2. Main esterification reactions

After the acquisition of some laboratorial experience with GO, namely in the esterification reactions, and the selection of the method for this functionalization step, new esterification reactions were conducted using higher amounts of GO (Table 12). With these reactions GO-Br was prepared and characterized through FTIR in KBr mode (FTIR-KBr), TGA and XPS. With all the characterization accomplished, such intermediate products were used as macroinitiators for ATRP reactions.

Table 12. Main esterification reactions realized to attach initiator molecules to the surface of GO.

Entry	Rx Code	GO	Groups modified	m_i (mg)	m_f (mg)	Analysis
12	Br_G10	FB_NIT	Hydroxyl (-OH)	601	523.73	FTIR- KBr; TGA; XPS
13	Br_G11	FB_NIT	Hydroxyl (-OH)	500	477.8	FTIR- KBr; TGA; XPS

Depending on the amounts required for the polymerization reactions realized throughout the experimental work, the main esterification reactions were conducted in different batches using amounts of original GO ranging from 500 mg to 1 g.

Having into account that the results of the different batches were similar, in this section are presented and discussed only the results obtained for one of the main esterification reactions carried out. Regarding the other esterification reactions (the results are not showed in this section but can be found in Appendix K) only some modifications employed to the procedures and to the reactant ratios reported are mentioned and discussed [24].

The first main esterification reaction (Br_G10; Table 12, entry 1) was carried out exactly as described in the article (Lee method [24]), i.e., using the same steps, procedures, reactant ratios and reaction conditions [24, 26]. In Figure 19 to Figure 22 are presented the FTIR spectra of the esterified product Br_G10 and of its carbon raw material FB_NIT, the TGA curves and the XPS analysis results, respectively.

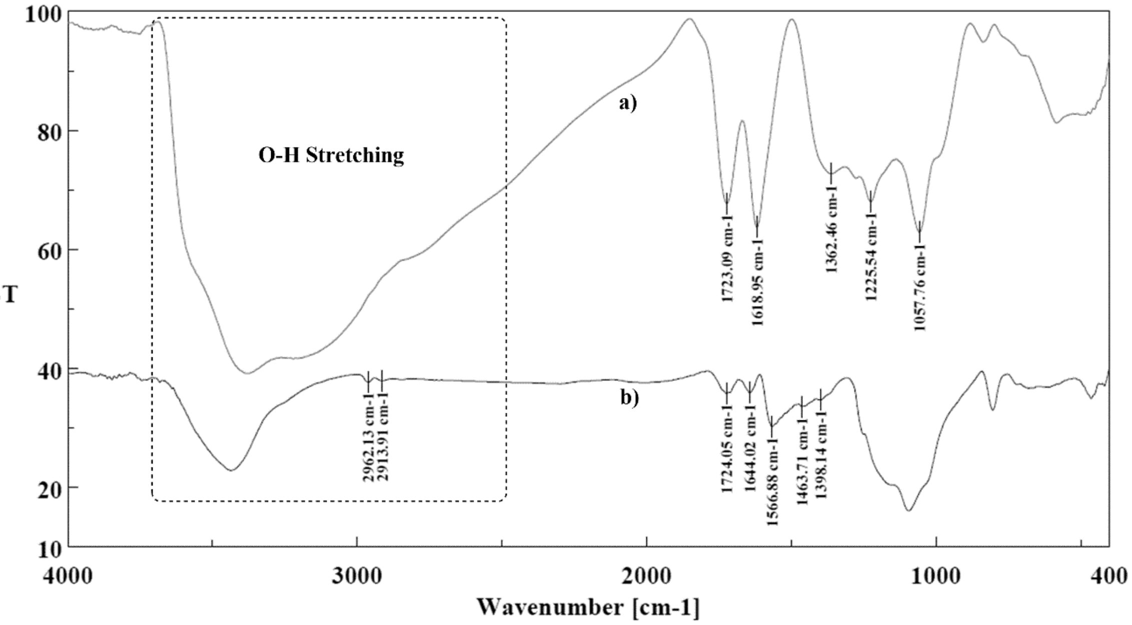

Figure 19. IR spectrum of a) Original GO FB_NIT; b) Esterification product Br_G10.

From the FTIR spectrum shown in Figure 19 (curve b)) was observed that the O-H stretching vibration band disappeared, indicating that almost all –OH groups of the original GO were replaced by new compounds. The broad peak that remained at about 3500 cm^{-1} can be due to some water traces, adsorbed in KBr powder or in the sample. According to our analysis, the disappearance of the O-H vibration band mainly resulted from the esterification reaction that occurred between the initiator molecules and the hydroxyl groups from GO.

Through the esterification reaction new ester bonds (GO-O-CO-C$(CH_3)_2$Br) were produced. These bonds were attributed to the new peak that appeared at 1644 cm^{-1} (Figure 19, curve b)) as result of the C=O vibration from the ester groups bonded to the aromatic rings of GO (conjugated esters). The peaks at 2962, 2914, 1464 and 1398 cm^{-1} are also evidences of the presence of initiator moieties. The first two peaks are due to the C-H vibrations from the methyl groups ($-CH_3$) of BIBB and the last two peaks result from the C-C vibration of the alkane structure from initiator molecules [54, 123].

Another important peak that shift its position after esterification reactions was the C=C vibration peak, changing from 1618 cm^{-1}, in original GO, to 1567 cm^{-1}, in esterification product Br_G10. Such modification probably resulted from some interactions that may have occurred between the new attached molecules and the aromatic skeletons and also due some reduction that took place during the esterification process, as reported in the literature [24-26].

The peak at 1724 cm^{-1} (Figure 19, curve b)) representing the C=O vibration from the carboxyl/carbonyl groups of GO, decreased of intensity. As mentioned aboved, is maintained that TEA reacted with the –OH groups of the carboxyl acids through an acid-base reaction, yielding a quaternary ammonium salt [122]. Such reaction converted the carboxyl acids groups to carboxylate ions, shifting the C=O vibration peak for low wave lengths (around 1600 cm^{-1}) [122, 123]. Is important to stress one more time, which the conclusions about the FTIR spectra were achieved based on the results of two control tests exposed in Appendix J.

The TGA and XPS results, presented in Figure 20, Figure 21 and Table 13, supported the FTIR analysis previously shown.

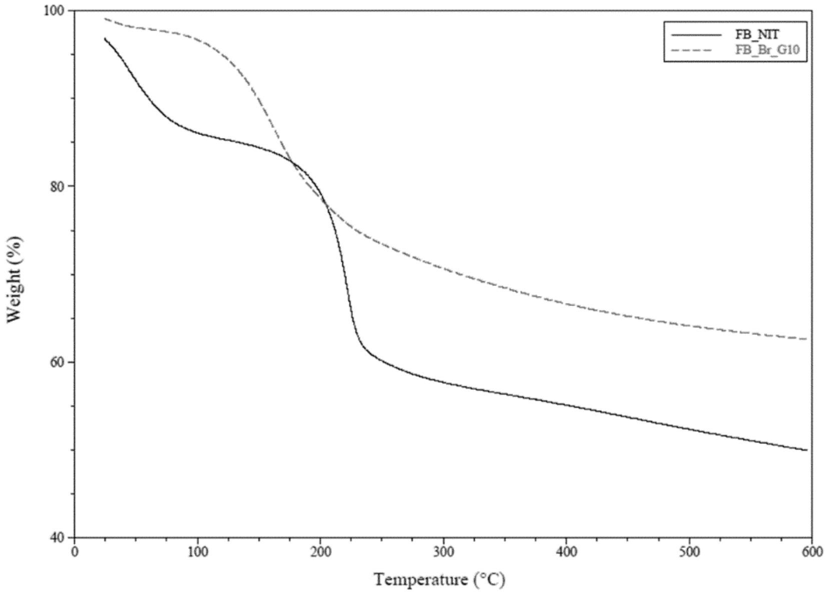

Figure 20. TGA curves of GO FB_NIT (solid line) and esterification product Br_G10 (short dashed line).

After the esterification reactions, the washed and dried product only revealed one level of weight loss, as observed in the literature [24]. In addition, the weight loss measured, of about 37%, was significantly lower than the total weight loss calculated for the purchased FB_NIT, of about 47%. It is important to note that in the TGA curve of the esterified product (Figure 20, dashed line) was not observed a significantly weight loss around 100ºC as in the original GO, indicating that a significant part of the water adsorbed in the GO structure was removed during the esterification reaction. This fact is the main justification for the lower total weight loss measured for the esterified product. The GO-Br revealed the main weight loss between 120 and 300ºC, as result of the decomposition of the oxygen containing groups and initiator molecules presented in its surface [24].

Table 13. XPS elemental quantification of esterification product Br_G10.

Code	%	C	O	Br	Si	S	N	O/C Ratio
FB_NIT	atom	65.40	31.65	-	1.55	0.59	0.81	0.484
	w/w	57.52	37.08	-	3.19	1.39	0.83	-
Br_G10	atom	81.67	12.66	1.74	0.98	0.12	2.84	0.155
	w/w	70.39	14.53	9.98	1.97	0.28	2.85	-

The amount of initiator was calculated, by XPS analysis, to be 9.98 % (w/w) (Table 13), meaning that for every 100 mg of GO there are 0.125 mmol of Br. However, the Br3d high resolution spectra conducted to the Br element (Figure 21) revealed two peaks with different binding energies, indicating that part of the Br was detached from the GO's surface in the form of bromine salts (Br^- species) [124]. Considering this, the total amount of Br covalently linked to GO was calculated to represent only 57.83% of the total Br, which corresponds to 0.072 mmol of initiator (Br) per 100 mg of GO (or 1.01 atom % ⇔ 5.77% (w/w)). This result besides proving that BIBB moieties were covalently linked to GO also revealed that the washing process needed improvement.

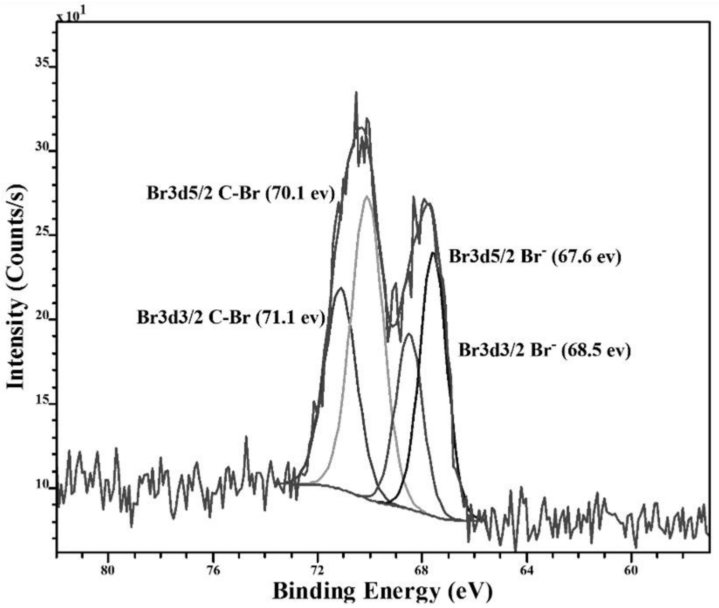

Figure 21. Br3d high resolution spectrum of esterification product Br_G10.

In addition, the XPS results revealed that the percentage of oxygen existing in the surface of GO diminished during the esterification reactions from 37% (w/w) to 15% (w/w), approximately. On the other hand, the carbon percentage in the sample increased, from 58% to 70% (w/w) approximately (Table 13). These results are in agreement with the FTIR results and with the results reported in the literature, indicating that during the esterification reactions some reduction of the oxide functionality presented on the GO surface occurred [24-26]. The mechanism behind the reduction observed was not clearly understood, since the procedures were carried out using low temperatures, soft reaction conditions, and theoretically in the esterification mechanism the oxygen species from GO are not removed, but for each initiator molecule bonded to the GO surface is added one oxygen atom. From our point of view, the decrease in the oxygen percentage is not necessarily due to diminish of number of oxygen atoms in the sample, through the removal of the oxygen atoms. This is probably associated to the attachment of new species, like BIBB and TEA molecules, with more carbon atoms than oxygen atoms, leading to the decrease of the O/C ratio.

During the experimental work it was observed that the GO-Br was hydrophobic, contrarily to the original GO, one more fact that supported the suspected loss of the oxygen functionality during the esterification reactions. This observation is justified with the substitution of the –OH groups from the hydroxyl and carboxyl acids existing in the GO's surface by new hydrophobic molecules, decreasing the hydrophilicity of the carbon nanomaterial (new molecules in the surface of the functionalized GO: GO-OH were replaced by GO-O-CO–C$(CH_3)_2$Br and GO-COOH by GO-CO-$O^-$$NHEt_3^+$).

Finally, other important result that was obtained from the elemental quantification acquired from the XPS analysis was the increase observed in the percentage of nitrogen (N) presented in the esterified sample (from 0.83% to 2.85% (w/w)). Such increase in the quantity of nitrogen supports the theory that TEA can react with some of the oxygen-containing species of GO, namely with the carboxyl acids groups as previously explained.

Figure 22 shows the survey spectrum acquired from the XPS analysis carried out to the esterification product Br_G10.

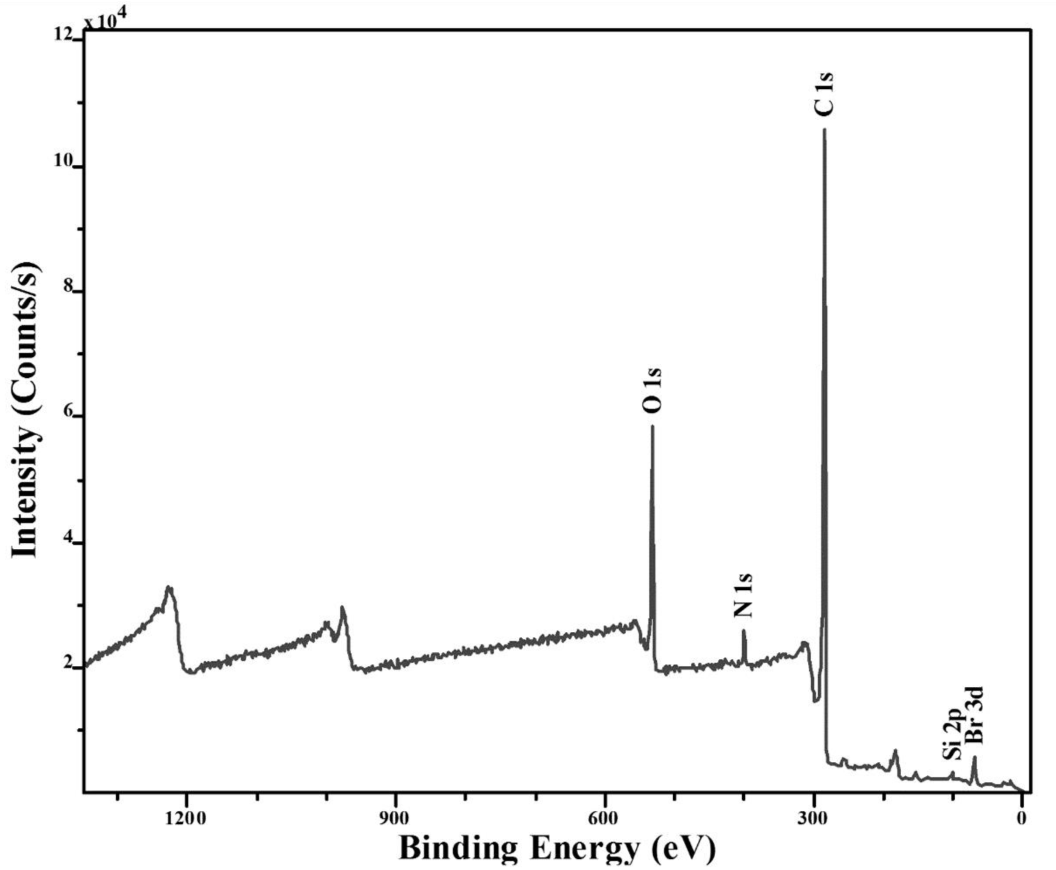

Figure 22. XPS spectrum of esterification product Br_G10.

In summary, the results obtained from the three characterization techniques conducted, allowed to conclude that the esterification reaction labelled as Br_G10 was successful, meaning that through this reaction some initiator molecules of BIBB were covalently attached to the surface of GO and that the GO-Br could be used as a polymerization macroinitiator.

Throughout the work, in addition to the esterification reaction previously shown, it was necessary to conduct one more esterification reaction, Br_G11 (Table 12, entry 2).

Aiming to reduce the quantity of BIBB used to functionalize the surface of GO, the second main esterification reaction was carried out using only half of the quantity of BIBB used in the original Lee method [24] as well as in the esterification reaction Br_G10. However, considering that there could be a loss of TEA by reaction with the carboxyl acids and to compensate the lower quantities of BIBB, higher TEA/BIBB ratio than in the previous reactions was used. Following the ratios reported in other works that used lower quantities of initiator molecules, in the esterification reaction Br_G11, the TEA/BIBB ratio was changed to 1/1 (previous ratio = 0.59/1) [58, 61].

The results are shown and analysed in Appendix K. The changes in the reactant ratios had no significant effect on the final esterified product, which means that lower quantities of BIBB can be used. The esterification product Br_G11 was also evaluated by FTIR-KBr, TGA and XPS (Appendix K). The FTIR spectrum was very similar to the spectrum of the previous esterification product, presenting all the same modifications and the same new peaks when compared to the original GO. The TGA results were also similar, however the weight loss measured was higher (about 42%), which might mean that more oxygen-containing species remained in the surface of the carbon nanomaterial. Finally, the XPS results revealed that the amount of initiator by weight was 5.21% (w/w) approximately, corresponding to 0.065 mmol of initiator (Br) per 100 mg of GO. The quantity of bromine salts (Br^- species) was only 22% of the total Br (Covalently bonded Br = 4.08% (w/w) ⇔0.051 mmol per 100 mg of GO), indicating that the washing process was improved but not enough to remove all the salts (Figure 23) [124].The elemental quantification also revealed a decrease in the quantity of oxygen atoms and an increase in the nitrogen content.

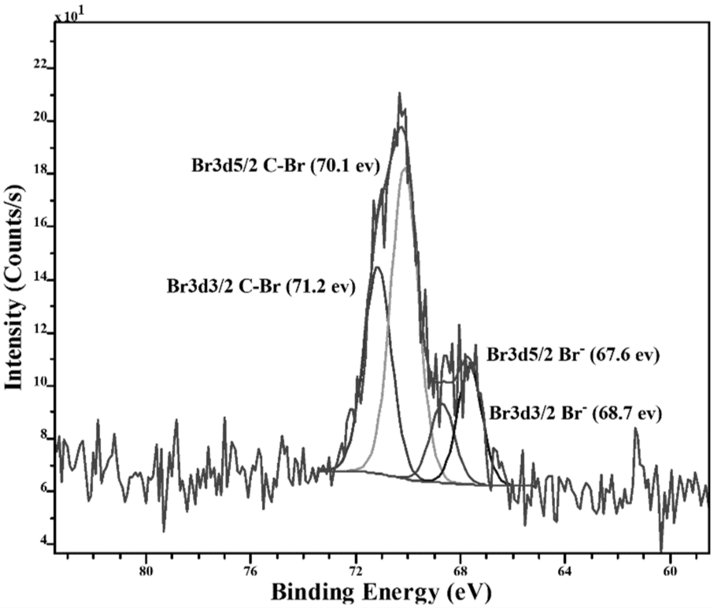

Figure 23. Br3d hight resolution spectrum of esterification product Br_G11.

Having in mind the results of the two main esterification reactions, it is possible to sustain that some reproducibility was achieved, obtaining similar esterified products with initiator moieties covalently bonded to the surface of GO likely to be polymerized.

2.1.3. Problems and solutions

One of the main difficulties of this work was the interpretation of IR spectra from the diverse products, only the IR peaks of the original GO were completely identified and clearly understood. The FTIR-ATR spectra presented broad bands instead of defined peaks, with low intensities, and were considerably different from the spectra found in the literature as well as different of each other. [23, 26, 56, 61, 62]. In addition, the characteristic bond for the attachment of initiator moieties to GO is an ester bond (O-C=O). This bond appears in the same region of the C=O vibration from carbonyl/carboxyl groups existing in GO surface (~1750-1600), making it very difficult to identify the C=O vibration resulting from an ester linkage. [40]. Considering this, the interpretation of IR spectra from the functionalized GO was a difficult task. To overcome this issue, firstly the analyses were focused on the most well-defined band, the O-H stretching vibration band at 2500-3500 cm^{-1} from hydroxyl groups. If the modification with ATRP initiator was successful the O-H stretching vibration band should decrease or even disappear, as result of the esterification reaction [26, 56]. This methodology was used in the reactions realized with the GO Oxi_Porto2, until the characterization of the new GO FB_NIT.

With the acquisition of GO FB_NIT, it was possible to achieve new conclusions concerning the FTIR analysis. The modifications observed in the FTIR-ATR spectra of the GO-Br relatively to the original GO were severe. As can be seen in Figure 17, in addition to the disappearance of the O-H stretching vibration band, all the other peaks (corresponding to the carboxy, epoxy and alkoxy groups) also suffered important changes. With the goal of clearly understanding the modifications made to the GO resulting from the esterification reactions, two strategies were followed:

- Was started to make the FTIR analysis in KBr mode. The samples were mixed with a KBr powder and compressed in order to obtain compact and transparent pellets.
- Two control tests were conducted to the esterification reaction. All the procedures were realized as in regular esterification reactions, however in the first test it was only used TEA and in the second test only BIBB was used.

The FTIR analysis using the KBr mode gives more definition in the IR peaks and in some cases can detect more peaks than the FTIR analysis when employed in ATR mode. In this work the KBr mode was used in all reactions realized subsequently to the esterification reaction Br_G09. Also in the results of this work the FTIR spectra acquired in KBr mode revealed more defined peaks than in ATR, which facilitated the analysis. In Appendix H (Figure H12), it is plotted a comparison between a spectrum obtained in ATR mode and another one acquire using KBr pellets.

The control tests realized allowed to understand the influence of TEA and BIBB in the modification of GO. Through the FTIR spectra and TGA curves obtained from the product of test number one (Appendix J, Figure J1 and Figure J2) was concluded that TEA probably reacted with the carboxyl and epoxy groups originating new peaks resulting from the formation of a quaternary ammonium salt and also leading to the decrease of the C=O and epoxy peaks, all the other peaks remained practically unmodified.

As expected, having in mind that TEA was only a catalyst, with the second test was observed that BIBB can react when introduced alone in the reaction medium, however the modification in O-H vibration band was lower than when used in the presence of TEA. In addition, two peaks in the C=O vibration zone were observed, probably due to the appearance of new ester bonds and the C=C vibration peak, from the aromatic skeletons, suffered some deviation during the esterification reaction as result of some reduction that might have occurred [24-26, 125]. In Appendix J, it can be found a more detailed discussion of the results of these control tests realized, which were very helpful in the FTIR interpretation exposed in this work.

Other problems were found during this stage of the work, namely the separation of GO from the reaction mixture and the washing process. Different processes were tested, like centrifugation, dialysis or filtration. The success of the washing process was evaluated by weighting the dried product, by FTIR and finally through XPS analysis. Was concluded that the most suitable process to wash GO after functionalization is through filtration. Was used a sintered disc filter funnel (Duran), with nominal maximum pore size ranging between 1.0-1.6 µm. The doubt if GO was being lost through the filter was upraised, considering that the filtrate presented a black colour. However, when it was washed in other reactions the filtrate was clear, indicating that practically all the graphene was retained by the filter.

2.2. Polymerization from the surface of GO - “grafting-from”

In the previous section (2.1) were described the diverse reactions, and the respective results, realized with the goal of producing functionalized GO with ATRP initiator molecules. With the GO-Br prepared the next step was trying to produce surface initiated polymer brushes on the GO nanosheets, through the well-known CLRP technique ATRP.

The functionalization of GO with polymer brushes has proven to be an important field of research, with many scientists investigating and reporting diverse ways to achieve such functionalization [10, 15, 23-26, 54-87]. The reasons behind the relevance given to this kind of modification are the low compatibility of pure graphene and GO with polymer matrices and the outstanding mechanical, thermal and electrical properties presented by the graphene/polymer nanocomposites when compared with pure polymers [9, 40, 47].

As mentioned on the introduction of this work, to date, diverse variations of the ATRP technique were reported, differing from each other in the species and in the mechanism used to establish the equilibrium between the dormant and active species, responsible for the control over the polymerization reactions [89, 92, 94]. In this work the focus was the SARA ATRP. This method was chosen having in mind that it allows a good control over the polymer structure, while it requires low concentrations of catalysts, with a rapid rate of polymerization and soft reaction conditions [61, 100-102, 110, 126]. The amounts of catalyst can be reduced to ppm levels when SARA ATRP techniques is employed, because the use of reducing agents allows the Cu(I) species to be continuously regenerating during the polymerization process [100]. In addition, there was an interest from the research group to test some previously studied SARA ATRP systems in the CLRP from the GO’s surface, as for example the system presented in Appendix E. Recalling that the goal was to find polymerization systems for the “grafting-from” approach of growing polymer brushes on GO's surface not reported so far, which required low concentrations of catalysts [100, 102].

In the course of the research and according to the results obtained different ways and strategies were followed. In this section are presented and discussed the diverse polymerization reactions carried out during all the research work as well as the respective results. The reactions are exposed according to the different strategies adopted.

2.2.1. Step 1 – The dream of a non-reported system on the first attempt

As first step, the ATRP of MA using two distinct catalytic systems was tested (Table 14). One used as catalyst CuBr and as ligand Me_6TREN, with a molar ratio CuBr:Me_6TREN = 1:1.1; the other employed as catalysts Cu(0)/$CuBr_2$ and as ligand Me_6TREN, using the molar ratio Cu(0):$CuBr_2$:Me_6TREN = wire:0.1:1.1. In both systems DMF was the solvent chosen and the reactions were carried out at 30 ºC.

Table 14 shows the two catalytic systems tested in the first ATRP reactions carried out, the macroinitiators used in each system, the characterization techniques employed to evaluate the success of the polymerization and the respective conclusion.

Table 14. Preliminary polymerization reactions in DMF at 30 ºC.

Entry	**GO-Initiator**	**Monomer**	**Catalytic System**[a]	**Results**[b,c]
1	Br_G06, Br_G07	MA	[CuBr]:[Me6TREN] = 1:1.1	n.p.
2	Br_G06, Br_G08	MA	[Cu(0)]:[$CuBr_2$]:[Me6TREN] = wire:0.1:1.1	n.p.

[a] Molar ratios. [b] n.p. = no polymer obtained. [c] The products of the polymerizations were characterized through FTIR, TGA and ^1H NMR.

MA was the monomer used for preliminary reactions because it is normally a monomer easy to polymerize with good control and commonly used as a model monomer in several types of systems, solvents and experiments with success [56, 100-102, 104, 114, 126-131]. In addition, it was not extensively explored for the "grafting-from" polymerizations from GO [56]. Also, MA can be easily copolymerized with other monomers originating interesting block copolymers and revealing good control over the copolymerization reactions, even when realized from surfaces [114, 130].

From previous esterification reactions and from the literature it was possible to conclude that DMF is one of the aprotic polar solvents that allows the achievement of a good dispersion of

GO in the reaction medium, being this a crucial factor for the success of the diverse reactions [10, 24-26, 54, 60, 70, 71]. Having this in mind and that MA, PMA and the catalytic systems were soluble in DMF such solvent was also used in polymerization reactions.

In the references found in the literature, which describe the surface initiated ATRP from GO, CuBr is the most reported catalyst [10, 15, 23, 25, 26, 54, 55, 57, 58, 61-64, 68-73, 132]. Considering the success of reported polymerizations and in order to gain some experience in polymerization reactions with GO, CuBr was employed as catalyst in the preliminary reactions (Table 14, entry 1).

The choice of an appropriate ligand is a crucial factor for the success of a CLRP reaction. Ligand species have as primary role to solubilize the transition metal salts in the reaction mixture and to adjust the redox potential of the metal center providing an appropriate activity and dynamics for the repetitive halogen exchange reactions. This is achieved through the formation of a Catalyst/Ligand ATRP complex (Mt^m/L) [133]. Considering this, Me_6TREN was used as ligand because it already proved to be suitable for the ATRP of MA catalysed by copper based catalysts, assuring good control over the polymerization of PMA in diverse systems [100-102, 127, 129].

With the goal of this work in mind, in addition to the ATRP reactions carried out using CuBr as catalyst, in parallel experiments SARA ATRP reactions of MA were conducted, employing one catalytic system studied in our department, Cu(0) wire and $CuBr_2$/Me_6TREN at 30 ºC (Table 14, entry 2) [110]. To the best of our knowledge, this system was not reported so far in the polymerization reactions conducted from the surface of GO. In homogenous reaction conditions, the system allowed very good control over the polymerizations, namely for acrylate monomers, while using low amounts of catalysts (< 100 ppm). The good control achieved in homogeneous mediums was reflected by the low dispersity values ($Đ$ ~1.05) , the first-order kinetics with respect to the concentration of monomer and the similar values of theoretical molecular weight calculated from ^{1}H NMR, $M_{n,th}$, and molecular weight measured from GPC, $M_{n,GPC}$ [110]. These results fulfil the standards that characterize a CLRP (standards exposed in the introduction of this dissertation). Having in account the interesting behaviour of the referred system in homogenous medium, the interest to evaluate its capabilities to control polymerization reactions carried out in heterogeneous media, like the polymerization from the surface of GO, was considerable. Also the ratios and temperature were defined having in mind the success achieved in SARA ATRP reactions in homogeneous medium reported in previous works [100, 110].

Preliminary polymerizations used as macroinitiators the GO-Br obtained from the preliminary esterification reactions (Br_G06, Br_G07 and Br_G08 as shown in Table 14). As already mentioned in this dissertation, these macroinitiators were not completely characterized, remaining the doubt if ATRP initiator was covalently bonded to the GO's surface. Also in this phase of the work, were unknown the amounts of initiator present in the esterified GOs. With these reactions, we were working on the assumption that if polymer was attached to the surface of GO, probably, the esterification reactions would have been successful.

Considering the small information about the initiator moieties presented in the macroinitiators surface, it was necessary to use typical amounts of catalysts and ligands obtained from the reported systems. In order to find such typical values a research had to be conducted, however, in general it was not found a logic relationship between the amounts of GO (or the amount of initiator molecules bonded to the surface of GO) and the amounts of catalyst and ligands reported (Appendix G, Table G3 shows the results of the research). From one article to another, the ratios between the mass of catalyst and the mass of GO (or between the moles of initiator moieties and the moles of catalyst) were considerably different. It was not clear how the majority of the ratios used were determined and if such amounts of catalysts and ligands were optimized, since there were no reports studying the influence of different catalytic systems in the functionalization of GO with polymer brushes through the "grafting-from" methodology. With this background, to define the amounts of catalysts, were followed the quantities of CuBr reported in the work developed by Gonçalves and co-workers [10]. This reported system was used as reference because it used the same initiator, it was identical to one of the systems tested in the first polymerizations, the monomer polymerized (MMA) was similar to the monomer tested (MA) and, mainly, because it reported a GPC curve revealing that the polymerization was success, with very good control, showing a dispersity value of 1.09 (a hydrolysis reaction with potassium hydroxide (KOH) was carried out to cleave the ester linkage existing between GO and polymer chains) [10].

The amounts of catalysts used in the experiments of this work were calculated based on the ratio between the mass of CuBr and the mass of GO used in the reference mentioned [10]. Also, the quantity of solvent added to dilute the reaction mixture (and to disperse GO) was determined following the concentration of GO relatively to the solvent used by the same authors, in mg/mL [10]. The reasoning and calculations adopted to determine the amounts of reactants handled are explained in Appendix G (below Table G4) and were established setting the amount of GO in a determined value of interest. All the procedures used in this phase of the work are described in the Chapter 3.

From all the results was easy to conclude that all the reactions conducted were unsuccessful, meaning that no polymer was obtained. By analysing the FTIR spectra of GO recovered from the polymerization medium, it was not observed any significant modification in the IR peaks when compared to the original GO spectrum. Regarding TGA, in general the weight loss measured was very similar to the weight loss of the original GO, and the ^{1}H NMR results show no peaks corresponding to the PMA protons in $CDCl_3$ at about 3.7, 2.30, 1.94, 1.67 and 1.56 ppm [100]. The FTIR, TGA and ^{1}H NMR results are shown in Appendix L.

Many factors may have been in the origin of the failure of these preliminary reactions. Firstly, the covalent attachment of the BIBB molecules to GO was not confirmed, which means that one of the reasons for the failure could be the lack of initiators in the GO's surface. Other factor could be the degasing process used in this initial phase of the work. If a residual amount of oxygen remains in the polymerization medium radicals will be trapped by oxygen molecules and polymerization will be inhibited. As can be seen in the Section 3.3.3, the degasing processes were realized only by bubbling the reaction mixture and monomer with nitrogen (N_2). In a normal controlled polymerization reactions realized in our department the degasing process involve successive freeze-vacuum-thaw cycles and purging the reactor with nitrogen. In our opinion, the bubbling process realized was not enough to remove all the oxygen traces.

In addition to the previous factors, more complex parameters might have influenced the polymerization, like the temperature (could be too low), the catalytic system and the amounts of catalysts and ligands used.

After the failure of all the preliminary reactions, many questions and doubts about the experiments carried out appeared. The success of the esterification reactions questioned as well as the procedures used in the polymerization reactions. The great number of dubious variables and parameters made practically impossible to find the sources of failure. Such panorama led to redefine the strategy, in order to better understand what could be the best way to polymerize from the surface of GO.

2.2.2. Step 2 - Understand the problems and eliminate variables/parameters (Reproduction of one reported system)

After the failure in the first approach, a new strategy was defined. GO-Br macroinitiators (Br_G10 and Br_G11) were produced and characterized by diverse techniques, namely XPS.

The goal was to build up certainties about the functionalization of GO with ATRP initiator molecules and to determine the amount of initiator attached to the modified carbon nanosheets.

To better understand the influence of the reaction conditions, including temperature, and the catalytic system one work reported in the literature was reproduced, using the same system (monomer, catalyst, ligand, solvent and temperature), the same reactants ratios and the same procedures [24]. Following the mentioned work various SARA ATRP reactions of Sty catalysed by Cu(0) wire/TREN in DMF at 80ºC during 20h were carried out (Table 15 entry 1) and after, according to the results, the reaction temperatures and the system parameters (molar ratios and solvent) were being changed, in order to understand its influence in the polymerization products (Table 15 entries 2-4).

Table 15. SARA ATRP of Sty catalysed by Cu(0) wire/TREN, systems based in the literature [24].

Entry	**GO-Initiator**	**Monomer**	**Catalytic System**[b]	**Result**[c,d]
1	Br_G10, Br_G11	Sty[a]	[Cu(0)]:[TREN] in DMF at 80 ºC	u.d.p.
2	Br_G11	Sty (DP = 250)	[Cu(0)]:[TREN] in DMF at 60 ºC	u.d.p.
3	Br_G10	Sty (DP = 500)	[Cu(0)]:[TREN] = wire:1.1 in Sulfolane at 80 ºC	u.d.p.
4	Br_G11	Sty (DP = 500)	[Cu(0)]:[TREN] = wire:1.1 in Sulfolane at 60 ºC	n.

[a] Different monomer amounts were used: 1 - using the quantities of the article, 2 - defining a target DP of 250, 3 – defining a target DP of 500. [b] Molar ratios defined relatively to the moles of initiator existing in the GO-Br. [c] n. = no polymer obtained; u.d.p = uncontrolled detached polymer. [d] The products were analysed through FTIR, TGA, ^{1}H NMR and GPC.

The system reported was reproduced because the modifications of GO with initiator moieties were performed according to the procedures described by the same authors, which means that probably the macroinitiators prepared in this work were identical to their macroinitiator. In addition, the authors proved the attachment of polymer brushes to the GO's surface by using several characterization techniques and also the control achieved over the polymerization ($Đ$ < 1.5), after analysing the polymer chains cleaved from the GO through GPC analysis (saponification reaction with sodium hydroxide (NaOH) was employed to break the ester linkages between GO and polymer chains) [24].

Considering that in the procedure reproduced nothing was referred about the degasing of the reaction mixture, this important process was changed. From this point, the removal of the oxygen from the reaction mixture was achieved by successive freeze-vacuum-thaw cycles and purging the reactor with nitrogen in the end of the degasing it. Since this methodology was the most used in our department we had more confidence and experience in the process. The freeze-vacuum-thaw cycles technique was not used until now because of the theory that the freezing of the reaction mixture could destabilize the dispersion, however, this idea was tested and the dispersion remained very stable even after the degasing process.

Three distinct reactions were carried out using different quantities of monomer (Sty) (Table 15, entry 1). The relative quantities of GO and ligand used were exactly the same as used in the work followed (Appendix G, Table G5). [24]. The goal with these experiments was to evaluate if the target molecular weight was achieved and therefore examine the efficiency of the initiator sites. Considering that, at the moment, the amounts of initiator molecules in GO were known (given by the presence of Br atoms) it was possible to define target degrees of polymerizations (DP). Two DPs were stablished (250 and 500) and in the first experiment it was used the amount of Sty used in the paper reproduced (5 mL for 100 mg of GO) [24], calculating the respective target DP based on the moles of Br atoms existing in 100 mg of GO-Br (DP = 602). All these reactions were conducted at 80ºC in DMF during 20 h and were catalysed by a Cu(0) wire and TREN. The amounts of monomer, catalysts and ligands are shown in Appendix G (Table G5).

The reactions were stopped by exposing the reaction mixture to air and, cooling the reactor in a cold water bath, the final black solution was added to an excess of ethanol, in order to precipitate the polymer produced, remove the residual unreacted monomer and the catalytic system. Through this procedure it was possible to evaluate, at that moment, if polymer was produced or not. When there was polymer, a grey/black precipitate was observed otherwise GO spreads itself in the ethanol, producing an opaque (dark) dispersion.

The precipitates obtained were dried and analysed by ^{1}H NMR, FTIR and TGA (Appendix M). The results proved that PS was obtained. After the characterization, the dried precipitates were diluted in DMF, 50 mg/mL, and centrifuged at 4000 rpm during 30 min, diverse times (three to five times), to remove possible free polymer chains produced during the polymerization[7]. At the end of the washing process the deposited black powders were dried and subsequently analysed through FTIR, TGA and ^{1}H NMR (Figure 24 and Figure 25). The supernatants were poured into an excess of ethanol in order to precipitate and to recover the free polymer chains for future analysis.

---

[7] The wash can also be accomplished by diluting the precipitates (or the final reaction mixture) in DMF followed by filtration of the solution and during this process add diverse times DMF or other good solvent of the polymer, assuring that all the free polymer chains are removed.

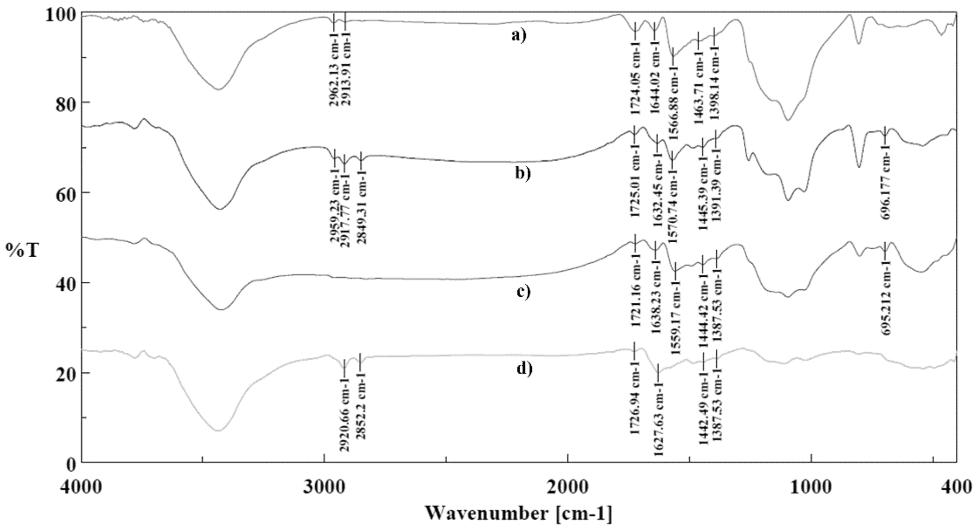

Figure 24. FTIR spectrum of a) Esterified product Br_G10 and washed polymerization products from the SARA ATRP of Sty catalyzed by Cu(0) wire/TREN in DMF at 80 ºC with different target DPs: b) DP = 602, c) DP = 250 and d) DP = 500.

The results obtained from the FTIR, TGA and ^{1}H NMR analysis (Figure 24 and Figure 25) conducted to the dried and washed powders, deposited in the Eppendorfs, revealed no presence of polymer. The only characterization technique in which some indications of polymer were observed was in the TGA, which revealed a slight weight loss around 400 ºC, probably due to the decomposition of PS chains [24]. However, taking into account the results reported in the literature [24], the weight loss observed was not significant and could result from some polymer chains that remained adsorbed in the surface of GO even after the washing process. In addition, the FTIR spectra of the washed polymerization products were very similar to the IR spectrum of the GO-Br used as raw material and the ^{1}H NMR showed no peaks of the PS protons in $CDCl_3$ at 6.00-7.50 and 2.0-1.25 ppm [24, 134]. The comparison between the FTIR, TGA and ^{1}H NMR results obtained for the precipitates (Appendix M, Figure M1 and Figure M2) and the results obtained for the washed products (Figure 24 and Figure 25) revealed that almost all the PS was separated from the carbon nanomaterial during the washing process.

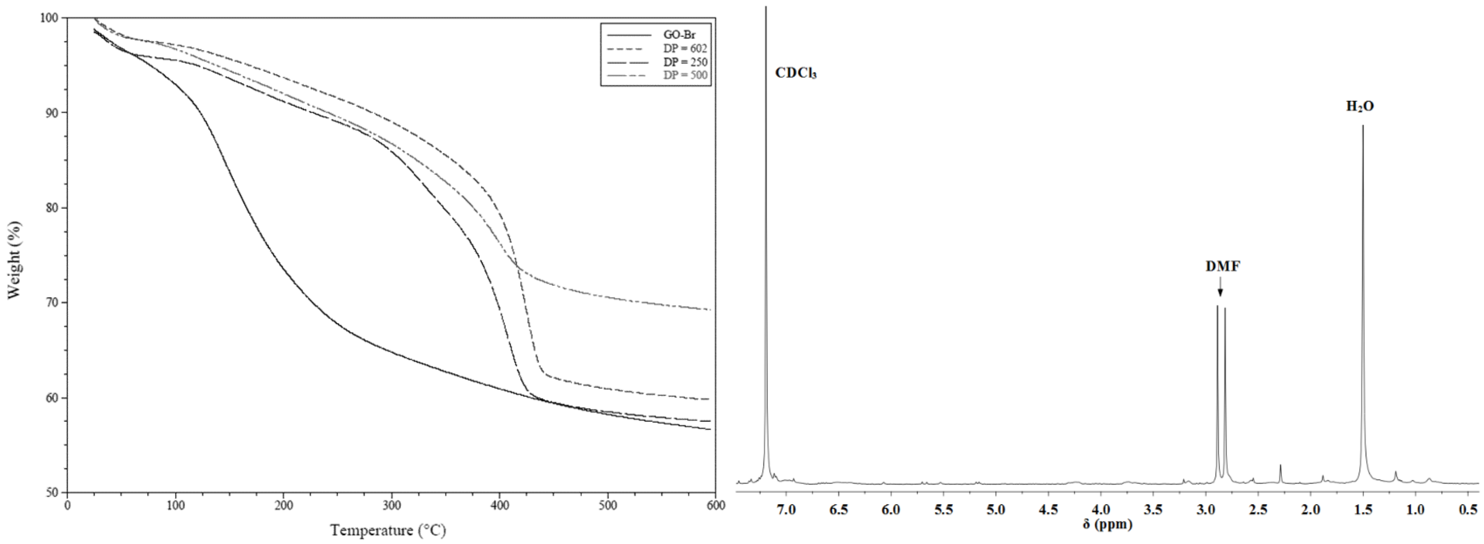

Figure 25. (Left) TGA curves obtained for the esterified GO used (solid line) and for the various washed polymerization products obtained from the SARA ATRP of Sty in DMF at 80 ºC having different target DPs: DP = 602 (short dashed line), DP = 250 (long dashed line) and DP = 500 (broken double dashed line). (Right) Typical ^{1}*H NMR obtained for the respective washed products.*

The group of results previously referred allowed to conclude that the PS produced was detached from GO's surface. The question that appeared was: "How only free polymer chains were produced and why wasn't possible to produce attached polymer brushes?". Aiming to better understand the origin of free polymer, an analysis to the polymers recovered from the supernatants was made by GPC (after diluted in THF, 5-10 mg/mL, and filtered through a 0.22 µm PTFE filter). From this analysis it was possible to observe that the free PS produced presented high molecular weight ($M_{n,GPC}$ > 200 kDa) and high dispersity values ($Đ$ > 2), which meant that the three type of reactions that reproduced the system reported [24] yielded uncontrolled detached PS (GPC curves shown in Appendix M, Figure M3). It is important to stress that all the three distinct reactions were conducted in duplicate using different macroinitiators (Br_G11 and Br_G10) and the results were exactly the same, revealing that the problem was not associated to the macroinitiator used.

It is well known that PS owns diverse issues that reduce the control over its polymerization, like low propagation rates at low temperatures, occurrence of irreversible termination reactions and thermal self-initiation at high temperature [89, 110, 134-136].

From our point of view, the uncontrolled PS homo-polymer could be due to the high temperatures used (80 ºC), that probably induced the self-initiation of the Sty monomer. Trying to overcome this problem, one SARA-ATRP of Sty catalysed by Cu(0) wire/TREN in DMF using a lower temperature (60ºC) (Table 15, entry 2) was carried out. The temperature was decreased only to 60 ºC because of the low propagation rates for low reaction temperatures already reported in the polymerization of this monomer [134]. The low concentration of initiator sites along with the low temperatures could completely inhibit the grafting polymerization. The amount of catalyst, ligand and solvent was the same as previously and a target degree of polymerization of 250 was established.

In Appendix E is presented a system developed in our group in which PS was polymerized in homogeneous medium at different temperatures (30, 60 and 90 ºC) with good control. The SARA ATRP of Sty catalysed by Cu(0):PMDETA = wire:1.1 in sulfolane was conducted without problems of thermal self-initiation or controllability. Having in mind these results, and the universal character of sulfolane, as well as the changes in the reaction temperature, sulfolane was used, maintaining the molar ratios presented in Appendix E for the polymerization of Sty from the surface of GO. The molar ratios of catalyst and ligand were defined based on the moles of Br atoms existing in the GO-Br macroinitiator. The volume of sulfolane used to dilute the reaction mixture (and disperse GO) was equal to the volume of DMF used in the previous reactions, to guarantee a good dispersion of GO. It is remarkable to note that GO-Br dispersed very well in sulfolane either by ultrasonication or magnetic stirring.

The results were similar for all the procedures, i.e., PS was obtained, however, it was detached from GO and uncontrolled. Was not possible to clearly understand why the grafting of PS brushes from the surface of GO was not achieved through the reactions conducted until this phase of the work, since several authors reported the polymerization of PS from the surface of GO with good control and dealing with temperatures higher than 80 ºC [24, 54, 70, 71]. The procedures described in the articles were followed and the polymer brushes were not obtained. Various hypotheses for the failure of the procedures were brought up:

- Thermal self-initiation. Was the first reason found for the homo-polymerization, however, in some way was discarded by the works reported [24, 54, 70, 71];
- Low availability of the initiator sites that difficult the initiation step of the polymerization and promote the homo-polymerization of Sty. This inaccessibility could result, for instance, from a poor dispersion of GO-Br in the reaction mixture or from low concentration of initiator moieties. One of the difficulties of this work was to understand when GO was well dispersed, i.e., how to evaluate the quality/stability of the dispersion;
- Free initiator, molecules of BIBB that remained adsorbed on the surface of GO after the esterification. Since BIBB also presents the halogen terminal (Br), if the homo-

polymerization was due to such molecules it would be somewhat controlled. Furthermore, in the literature it was referred that the polymerization products were washed to remove possible “free” polymer chains (probably as result of free initiator traces) and the control over the polymerization was achieved as well as the attachment of polymer chains to the GO’s surface [10, 15, 23-26, 54-73, 132].

Although the failure in the grafting of PS brushes from the GO’s surface it was possible to better understand the procedures necessary to conduct the polymerization reactions, namely, how to realize the degasing with more confidence, how to evaluate the obtainment of polymer and its attachment status and also how to realize the purification of the final graphene, resulting from the polymerization reactions.

The experiments conducted until this phase revealed that the CLRP from the surface of GO is not so easy as it appears in the literature, many questions are behind the success shown in the broad literature published, namely the origin of the free polymer chains. We believe that these polymer chains could be originated from residues of free initiator molecules that are adsorbed on the GO’s structure and could not be removed by the extensive washing procedures. However, to the best of our knowledge, the influence of this polymer chains in polymerization was never mentioned or studied.

Considering the problems found in the “grafting-from” polymerization of Sty, and the known issues of this monomer, the strategy was changed one more time. Taking into consideration the experience and the deeper knowledge acquired about the GO-Br macroinitiators, the model monomer MA was again the chosen one.

2.2.3. *Step 3 - SARA ATRP of MA catalysed by Cu(0):Me$_6$TREN = wire:1.1 from the GO’s surface in DMF at 60 ºC*

In the last phase of the work, MA was, once again, used as monomer for the SARA ATRP from the surface of GO. As mentioned before, this monomer was chosen because it is a monomer easy to polymerize in a controlled way and does not present the same kind of issues that Sty does. In the beginning of the work it was already used, however many variables and parameters were dubious. At this stage of the work where the macroinitiators used (Br_G10 and Br_G11) were well characterized and the polymerization procedures were relatively well understood it was time to give it another try.

The SARA ATRP of MA was catalysed by Cu(0) and Me_6TREN in DMF at 60 ºC (Table 16, entry 1). The amounts of reactants were defined based on the moles of initiator moieties (Br) existing in the GO's surface (determined from XPS analysis). Following previous works developed in the research group, the molar ratio [GO-Br]:[Cu(0)]:[Me_6TREN] employed was 1:wire:1.1 (Table 16) [100, 110]. The amount of monomer (MA) was stablished, also comparatively to the moles of initiator moieties employed in each reaction, in order to obtain a target degree of polymerization of 500 (for a monomer conversion of 100%). The DP of 500 was defined to use a high target molecular weight (or DP) to ensure that the resulting polymer brushes had a significant chain length.

In Table 16 are summarized the SARA ATRP reactions of MA conducted from the surface of GO-Br.

Table 16. SARA ATRP of MA catalyzed by Cu(0) wire/Me_6TREN in DMF in at 60 ºC

Entry	**GO-Br**	**Monomer**	**Catalytic System**[a]	**Result**[b,c]
1	Br_G10, Br_G11	MA (DP = 500)	[GO-Br]:[Cu(0)]:[Me_6TREN] = 1:wire:1.1	a.p.
2	Br_G11	MA (DP = 500)	[EBiB+GO-Br]:[Cu(0)]:[Me_6TREN] = 1:wire:1.1	c.d.p.

[a] Molar ratios. [b] a.p. = attached polymer and c.d.p = controlled detached polymer obtained. [c] The polymerization products were analysed by FTIR, TGA, ^1H NMR, GPC

The catalytic system Cu(0) wire/Me_6TREN was used for the reasons already exposed in previous section 2.2.1. The SARA ATRP reactions carried out in sulfolane, presented in Appendix E, are an example of controlled polymerizations in which Cu(0) and Me_6TREN were used as catalytic system for the polymerization of acrylate monomers (MA and MMA). In addition, this catalytic system was also reported in the area of the "grafting-from" polymerizations of GO to grow polymer brushes of acrylate monomers [60].

The temperatures of these last polymerizations were set at 60 ºC, based on the temperature reported in the literature to polymerize MA from the GO's surface [56]. ATRP reactions from the surface of GO at low temperatures were already reported, for example at room temperature [55, 60-62]. However, considering the previous problems and aiming to facilitate and to accelerate the "grafting-from" polymerization process, was used a temperature that assures higher activation, $k_{act,}$, and propagation rates, k_p^{app}. In the literature was reported that the activation rates, k_{act}, of diverse initiators increase with temperature [137]. Some works shown that with higher reaction temperatures, higher propagation rates (k_p^{app}) were achieved [110, 134].

The SARA ATRP of MA was carried out in duplicate using two different macroinitiators, as shown in Table 16 (entry 1). The polymerization products obtained from these reactions were precipitated in water to evaluate if PMA was produced and to remove unreacted monomer as well as the catalytic system. In all reactions a black and sticky precipitate was obtained, indicating that polymer was produced. The precipitates were dried in a vacuum oven at 40 ºC and, subsequently, exhaustively washed with DMF and Tetrahydrofuran (THF) by successive centrifugation/redispersion cycles, to remove the possible "free" polymer chains produced. As realized in previous reactions, the deposited and washed powders were dried and firstly analysed through FTIR, TGA and ^{1}H NMR. The results obtained from the analysis conducted to the washed powders are shown in Figure 26 to Figure 28.

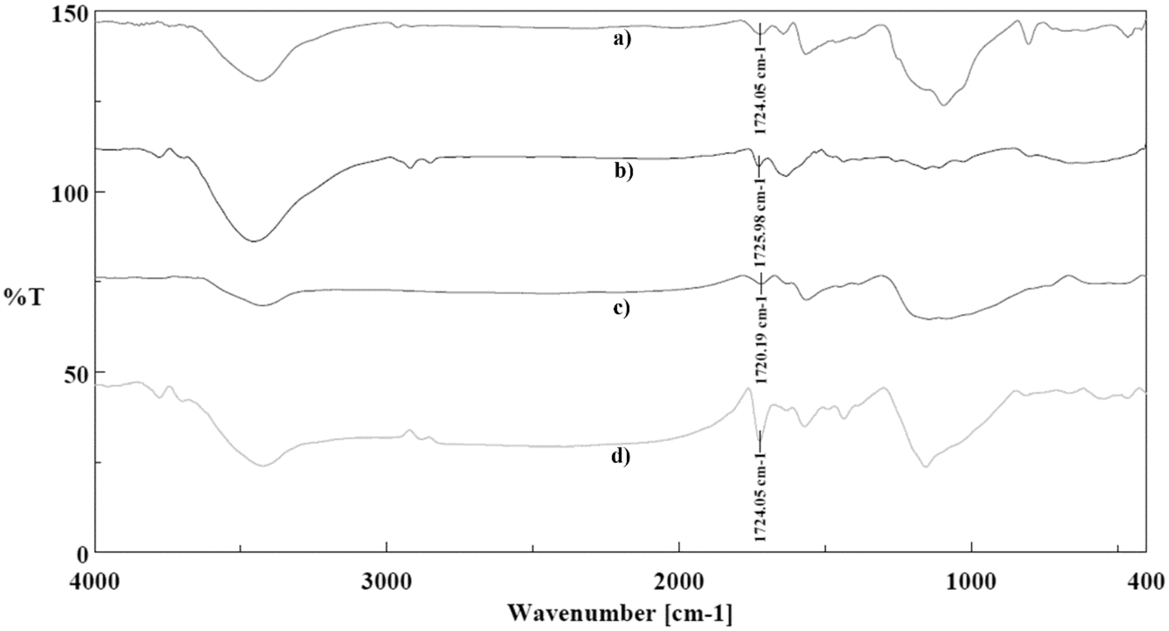

Figure 26. FTIR spectra of a) Esterified product Br_G10, c) Esterified product Br_G11 and washed polymerization products yielded in the SARA ATRP of MA from the surface of GO in DMF at 60 ºC catalysed by Cu(0) wire/Me$_6$TREN: b) polymerized from the macroinitiator Br_G10 and d) polymerized from the macroinitiator Br_G11.

Figure 26 show FTIR spectra of two macroinitiators (Br_G10, curve a) and Br_G11, curve c)) and two washed products recovered from the reaction mixture. Variations observed in the peak at about 1725 cm^{-1} provided the first evidences that PMA chains were attached to the surface of GO macroinitiators. This peak shows the presence of C=O vibrations from ester groups. Through the comparison of the IR curves of macroinitiators and washed polymerization products, mainly curve c) with curve d) (Figure 26), it was possible to conclude that the C=O peak increased its intensity becoming more sharp and defined after SARA ATRP reactions.

These changes were associated to the presence of –COOCH$_3$ groups (ester group) from the PMA chains introduced in the surface of the carbon nanomaterial.

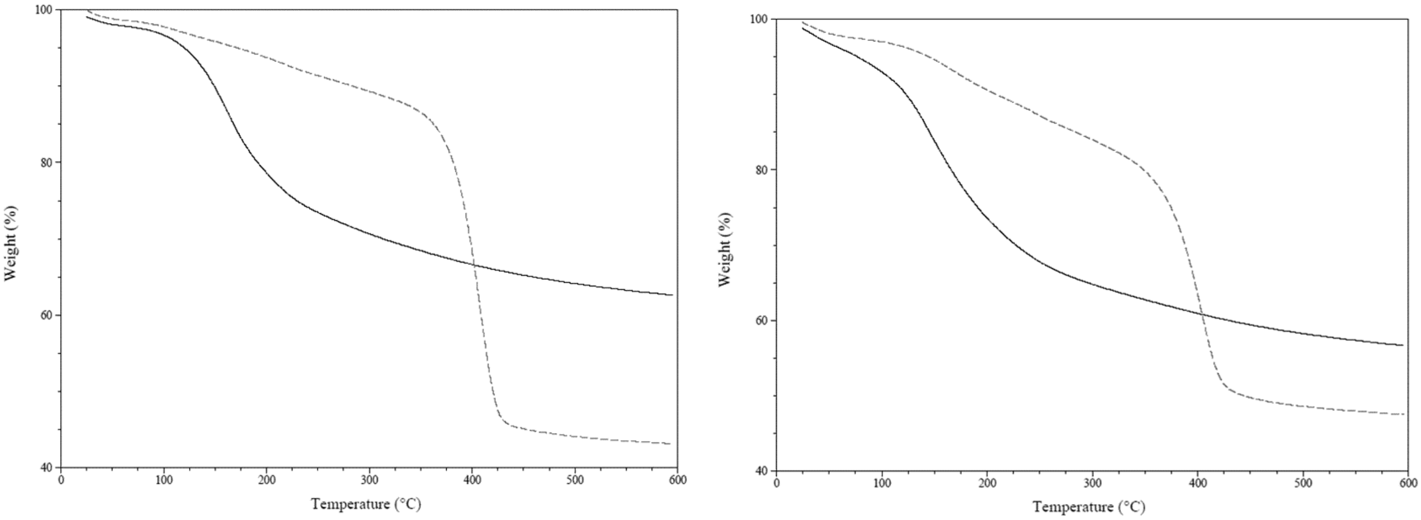

Figure 27. (Left) TGA curves of macroinitiator Br_G10 (solid line) and of its washed SARA ATRP product (dashed line). (Right) TGA curves of macroinitiator Br_G11 (solid line) and of its washed SARA ATRP product (dashed line.)

TGA was studied to evaluate the thermal stability of the washed SARA ATRP products, supposedly functionalized with PMA chains (Figure 27). TGA curves of the polymerization products (dashed lines) revealed a main and significant weight loss at around 400 ºC, having a decomposition pattern completely different from its macroinitiators (solid lines). In the literature, it was found that PMA typical decomposes at about 400 ºC, following a decomposition pattern very similar to the obtained in the TGA results shown in this work (Figure 27) [138]. Considering this information, the weight loss observed around 400 ºC was associated to the presence of PMA chains in the surface of GO, providing one evidence of the success achieved in the grafting reactions. In Table 17 are shown the weight losses measured for the different products obtained in this phase of the work.

Table 17. Weight losses measured for the macroinitiators Br_G10 and Br_G11 and for the respective washed products obtained through the SARA ATRP of MA catalysed by Cu(0) wire/Me6TREN in DMF at 60 ºC.

Macroinitiator	Weight loss (%)	SARA ATRP products weight loss (%)
Br_G10	36.52	56.83
Br_G11	42.23	52.16

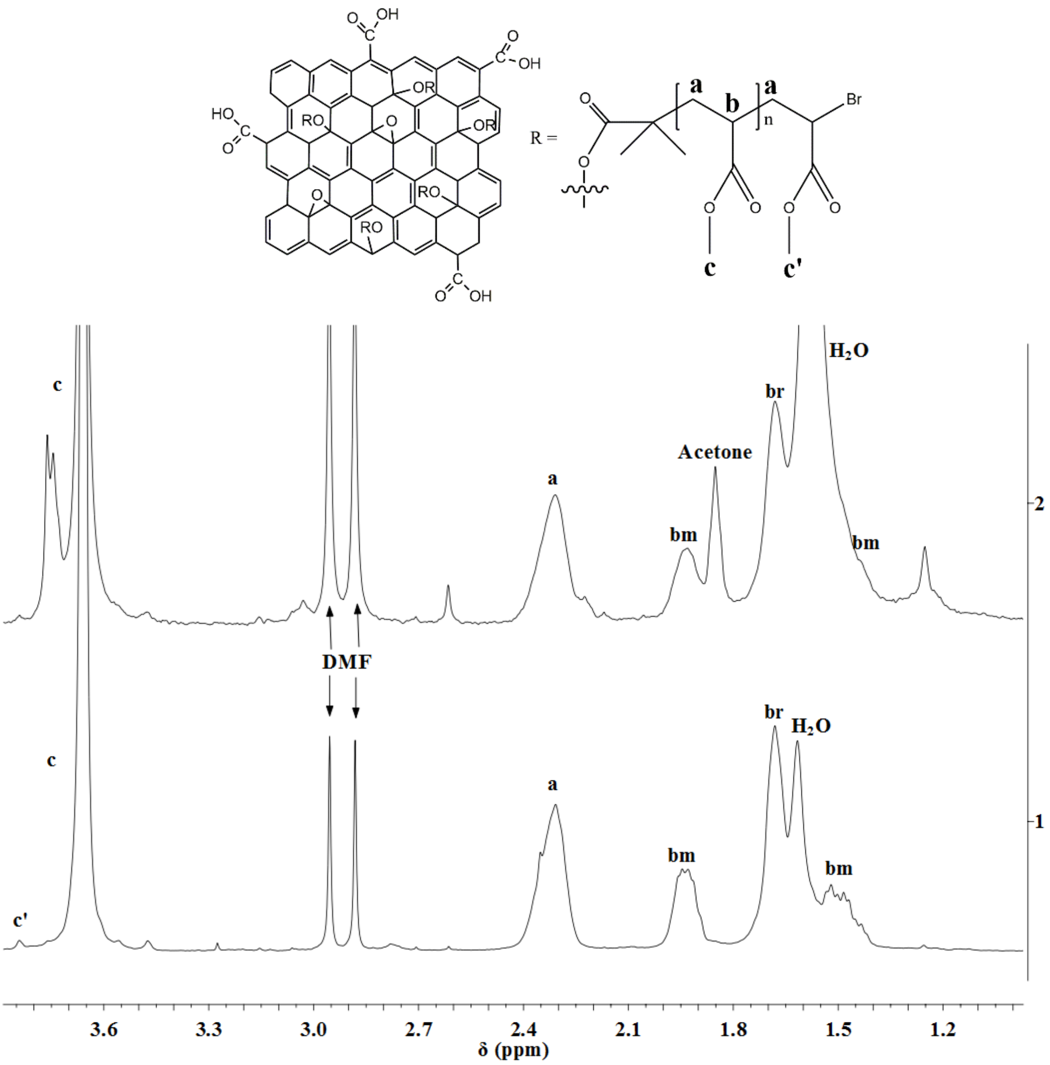

Figure 28. ^{1}H NMR spectra of PMA attached to the surface of GO, acquired in $CDCl_3$. 1 – Washed SARA ATRP product polymerized from the macroinitiator Br_G10 and 2 – Washed SARA ATRP product polymerized from the macroinitiator Br_G11.

^{1}H NMR was recorded in $CDCl_3$ to evaluate the synthesis of PMA chains on the surface of the macroinitiators (Figure 28). The most intense peak that appeared at 3.7-3.6 ppm, peak **c**, resulted from the $–COOCH_{3\mathbf{c}}$ protons of PMA. The peak **a** at 2.4-2.2 ppm correspond to 2 protons of $–CH_{2\mathbf{a}}–$. Finally, peaks **bm**, **br** and **bm** at about 1.95, 1.68 and 1.52 ppm, respectively, were attributed to **b** protons of $–CH_{\mathbf{b}}(COOCH_3)$- groups [100, 102, 126, 129]. The signals **br** and **bm** represent the fractions of syndiotactic and isotactic diads, respectively [100]. All the aforementioned peaks confirmed that PMA chains were produced through the SARA ATRP of MA from the surface of GO-Br.

After the confirmation that PMA was grown from the surface of GO, by the three characterization techniques previously exposed, the next step was to evaluate the control achieved over the polymerization and the molecular weight of the polymer brushes. For this evaluation, it was necessary to detach the polymer chains from the surface of the carbon nanosheets, in order to analyse the surface initiated PMA through GPC.

The polymer chains were bonded to the surface of GO through ester linkages. It is known that such bond can be cleaved through hydrolysis, either acid hydrolysis or basic hydrolysis (also known as saponification) [139]. Aiming to cleave the ester bond existing between GO and the polymer chains two methodologies were found in the literature [10, 24, 111]. One of the methodologies, KOH was the alkali employed to realize the saponification of the polymer chains attached to GO [10, 111]. On the other, was reported the use of NaOH as alkali to achieve the saponification of the surface initiated polymer chains [24]. Both methodologies were tested, however only when KOH was used, it was possible to obtain detached polymer. It is important to note that in both procedures, it was very difficult to dissolve the alkali in the solvents mentioned in the reports (THF and DMF) [10, 24, 111]. To dissolve KOH in THF it was necessary to add some water droplets to the solid alkali before the addition of the solvent. Having in mind the quantities of NaOH used (300 mg) it was not possible to use the same strategy as before, which means that the total dissolution of the solid alkali in DMF was not achieved. The procedures used to conduct the two saponification methodologies are described in Chapter 3.

The reaction mixtures obtained from the saponification reactions with KOH were filtered through a 0.22 µm PTFE filter (Whatman), to remove the GO platelets, and concentrated by evaporation. After this, the residues were diluted with THF, filtered through a 0.22 µm PTFE filter (Whatman) and analysed through GPC. Figure 29 shows the GPC traces of the two detached PMA obtained from the SARA ATRP of MA grafted from the macroinitiators Br_G10 and Br_G11.

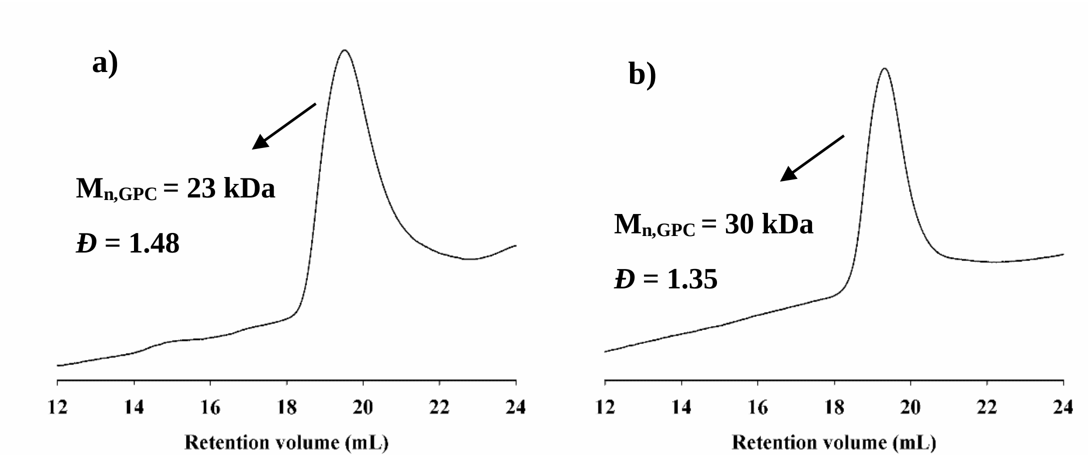

Figure 29. GPC traces of the detached PMA recovered from the saponification reactions. a) PMA polymerized from the surface of the macroinitiator Br_G10 and b) PMA polymerized from the surface of the macroinitiator Br_G11. The molecular weights, $M_{n,GPC}$, and the dispersity values were calculated through the OmniSEC software using the conventional calibration.

From GPC traces the $M_{n,GPC}$ determined were 23 and 30 kDa and the *Đ* values 1.48 and 1.35 for PMA polymerized from the surface of the macroinitiator Br_G10 and from the macroinitiator Br_G11, respectively. The dispersity values are relatively low (*Đ*< 1.5) and provided evidences that the SARA ATRP of MA from the surface of GO carried out in a control manner. In addition, the *Đ* obtained in the SARA ATRP reactions developed in this work are similar to various values reported in the literature [24, 57, 58, 61].

Although the evidences of controlled polymerizations, provided by the *Đ*, it is important to note that it is not possible to affirm that the SARA ATRP reactions had controlled/"living" character. The standards that define if a polymerization is controlled were not all verified, like the agreement between the $M_{n,th}$ and the $M_{n,GPC}$ as well as the first order kinetics with respect to the monomer conversion. In the literature, this study is in some cases realized by adding free initiator molecules, known as sacrificial initiator, to the heterogeneous reaction medium [61, 62]. These free polymers are recovered from the reactions mixture and directly analysed by ^{1}H NMR and GPC, as in normal controlled polymerization reactions, shown for example in Appendices C to F. The control over the polymerization is evaluated based on the results acquired for the free polymers, assuming that the grafted polymers had the same growing behaviour [57, 58]. Theoretically according to the CLRP mechanism, free polymers initiated by sacrificial initiator possess almost the same molecular weight and *Đ* as those grafted onto the surface of the carbon macroinitiator [61, 62].

Although use of sacrificial initiator could raise also some questions this approach was tested (Table 16, entry 2). However, when sacrificial initiator was added to the reaction medium, polymer brushes were not polymerized from the surface of GO. Probably the easy accessibility of the free initiator molecules compared to the attached initiator molecules avoided the initiation from the last. The results probably reveal that the efficiency of the macroinitiators prepared in this work was low, as already seen in the polymerization of Sty. In Appendix N are presented more details about the SARA ATRP of MA from the surface of GO in DMF at 60 ºC using sacrificial initiator.

Considering the results obtained with sacrificial initiator, the improvement and the analysis of the control achieved over the polymerization process was not completely fulfilled, however, in future works these issues must be well clearly explored. Alternative strategies to the sacrificial initiator should be explored. For example, to achieve a better control over the grafting polymerization one hypothesis could be the addition of $CuBr_2$ to the reaction medium, to increase the amount of deactivator species in the beginning of the polymerization and overcome the initial lack of this kind of species as result of the low concentrations of initiator. This strategy was already reported and well-studied for ATRP polymerizations from silicon surfaces [114].

Considering the results of the previous characterization techniques, one of the GOs functionalized with PMA brushes was additionally analysed through SEM. A dispersion test was also conducted.

SEM was realized to observe the morphology of the carbon nanomaterials. Figure 30 displays SEM images of original GO (FB_NIT) and GO functionalized with PMA brushes. The well packed layers of GO can be seen in Figure 30B. Although the presence of PMA was not clearly visible in SEM images, it was possible to observe some modifications in the morphology and dimensions of the GO particles. The original GO particles are bigger and more agglomerates were perceptible, as can be seen through the comparison between Figure 30A and Figure 30C. In addition, a smoother surface was observed in original GO nanosheets (comparison between Figure 30B and Figure 30D). Without certainties we believe that the agglomerate identified by the white circle, in Figure 30D, might be PMA attached to the GO surface.

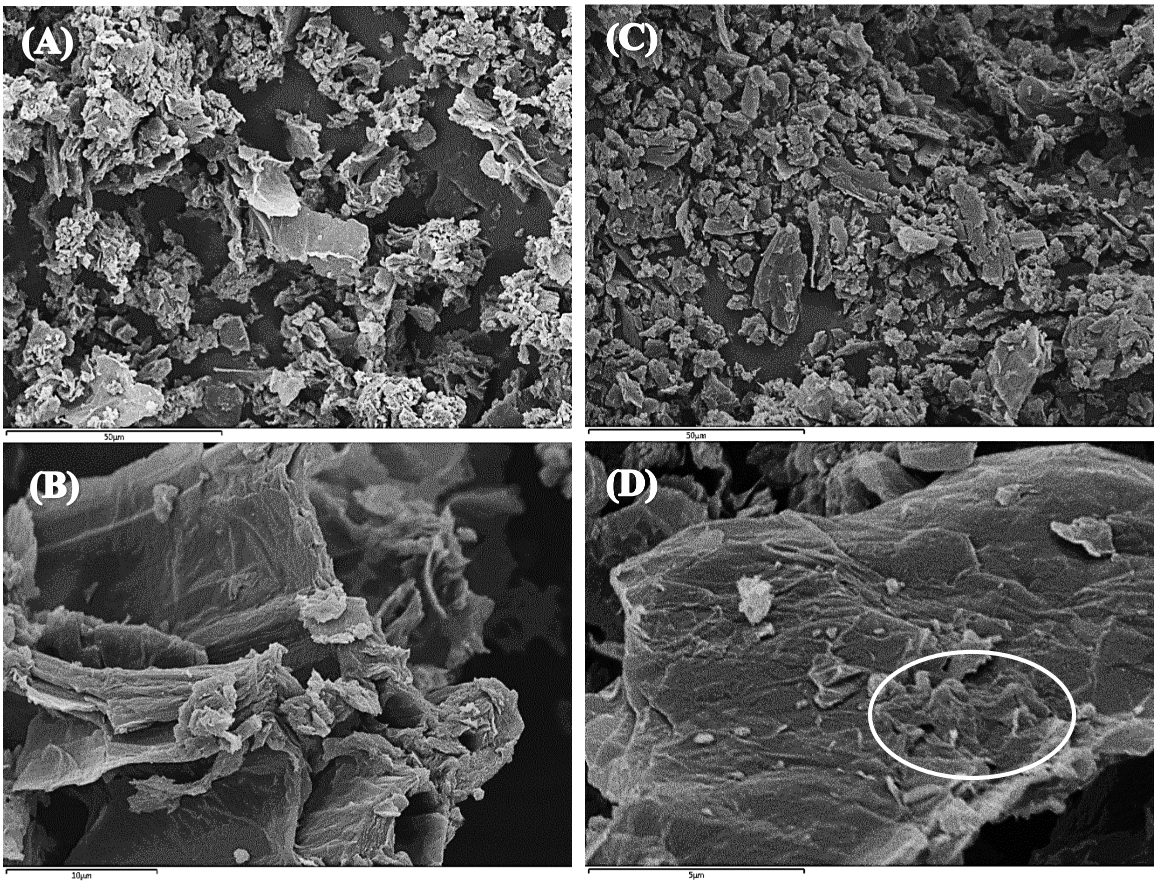

Figure 30. SEM images of (A) original graphene oxide magnification 1000x, (B) original graphene oxide magnification 3500x, (C) GO modified with PMA brushes magnification 1000x and (D) GO modified with PMA brushes 10000x.

Figure 31 shows dispersions of original GO, GO-Br and GO functionalized with PMA brushes in DMF, about 1 mg/mL. In order to equalize the conditions to all samples, the mixtures were all stirred overnight using an orbital stirrer. From the images is clear that the dispersion of GO in DMF improved with its functionalization. The dispersion of original GO, Figure 31A, was the poorest of all dispersions, instead, when GO was functionalized with PMA chains its dispersion in DMF was easy, originating a black dark colloidal dispersion (Figure 31C). This test also provided visible evidences that GO was functionalized with PMA polymer brushes.

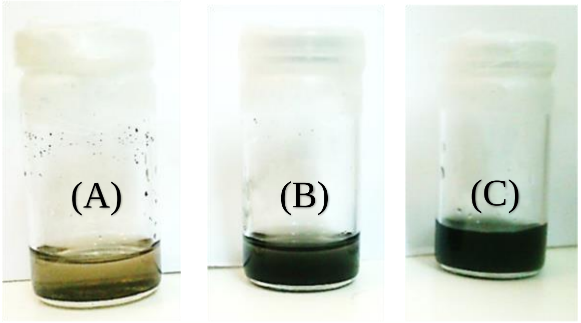

Figure 31. Dispersion of (A) original GO, (B) GO-Br and (C) GO functionalized with PMA brushes in DMF with a concentration of about 1.0 mg/mL.

In summary, SARA ATRP of MA catalysed by Cu(0) wire/Me_6TREN in DMF at 60 ºC were conducted using GO previously modified with initiator moieties as macroinitiator. The GO powders, recovered from the reaction mixture, were exhaustibly washed, dried and analysed by diverse characterization techniques. The results revealed that PMA brushes with molecular weights of about 30 kDa and *Đ* lower than 1.5 were grown from the surface of GO.

It is important to note that, although the final results obtained show some success, many problems were found and improvements must continue to be made because some crucial issues remained unclear, like the failure in the SARA ATRP of Sty and in the use of sacrificial initiator to control the grafting polymerizations.

Chapter 3

3. Experimental

3.1. Materials

In a preliminary phase of the work, GO was kindly supplied by the Department of Chemical Engineering, University of Porto, and after was purchased from NanoInnova Technologies SL, Spain.

3.1.1. Used in the preparation of GO for future polymerizations

N-Hydroxysuccinimide (NHS) (98+%; Acros Organics), N-(3-(dimethylamino)propyl)-N'-ethylcarbodiimide hydrochloride (EDC.HCl) (purum, ≥98.0%; Sigma-Aldrich), 1,3-diaminopropane (≥99%; Sigma-Aldrich), α-bromo isobutyrylbromide (BIBB) (98%; Aldrich) and chloroform ($CHCl_3$) (99.98%, stabilized with amylene; Fisher Chemical) were used as received. Dimethylformamide (DMF) (99.99%; Fisher Chemical) and triethylamine (TEA) (≥99%; Sigma-Aldrich) were purified following the procedures described in the sub-point "Solvents and reactants purification", presented in this chapter.

3.1.2. Used for polymerizations from the surface of GO

Methyl Acrylate (MA) (99% stabilized; Acros) and Styrene (Sty) (+99%; Sigma-Aldrich) were passed over a sand/alumina column before use, to remove the radical inhibitor. Ethyl 2-bromoisobutyrate (EBiB) (98%; Sigma-Aldrich), tris(2-aminoethyl)amine (TREN) (96%; Sigma-Aldrich), copper (II) bromide ($CuBr_2$) (+99% extra pure, anhydrous; Acros), N,N,N′,N″,N″-pentamethyldiethylenetriamine (PMDETA) (99%; Aldrich), dimethylformamide (DMF) (99.8%; Sigma-Aldrich), sulfolane (+99%; Acros), tetrahydrofuran (THF) (99.99%, stabilized with ca. 0.0025% BAT; Fisher Chemical), hidróxido de sódio (NaOH) (98%, pellets; Panreac), potassium hydroxide (KOH) (98%, flakes; Sigma-Aldrich), deutered chloroform ($CDCl_3$) (+1 % tetramethylsilane (TMS); Euriso-top) and polystyrene (PS) standards (Polymer Laboratories) were used as received. Copper (I) bromide (CuBr) (98%; Sigma-Aldrich) was purified by washing with glacial acetic acid, filtered, washed with ethanol and dried in a vacuum oven at 40 ºC. Tris[2-(dimethylamino)ethyl]amine (Me6TREN) was synthesized by the researchers of the Polymer Research Group (In which this work was developed), according the procedures described in the literature [140]. Metallic copper (Cu(0) wire, d = 1mm; Sigma-Aldrich) was washed with nitric acid and subsequently rinsed with acetone (or methanol) and dried in an oven at 50 ºC. Tetrahydrofuran (THF, high-performance liquid chromatography (HPLC) grade; Panreac) was filtered (0.2 μm filter) under reduced pressure before use.

3.1.3. Solvents and reactants purification

The reactant BIBB, initiator attached to the surface of GO, easily react with water. Considering this, was fundamental to conduct the esterification reactions in the absence of water as far as possible. Aiming to minimise loss of BIBB molecules in secondary reactions with water, was necessary to dry all the other solvents and reactants that could lead significant water traces to the reaction medium. In addition, was necessary to carry out the esterification reactions under controlled atmosphere as well as add BIBB under the same atmosphere conditions (in this work the reactor was purged with nitrogen (N_2)).

All the solvents and reactants were dried having as base procedures described in the literature [141].

DMF was treated with calcium oxide (CaO) previously activated at 500 ºC. The mixture was decanted and after was added NaOH, stirring during 1h. Finally, DMF was decanted, distilled and stored over 4Å molecular sieves.

TEA was distilled and stored over 4Å molecular sieves.

3.2. Apparatus and Characterization techniques

Throughout the experimental work different equipment and characterization techniques were used to conduct some steps of the reactions and to evaluate its products. In this section are presented all the apparatus used and described the various characterization techniques (equipment and conditions).

In some steps of the experiments, namely before esterification reactions, was necessary to disperse the GO in the solvent using ultrasons. For this task was used a Crest Tru-Sweep ultrasonic cleaner, model 275D with a frequency of 42-45 kHz and a sonic power from 10 to 90 W.

The centrifugations realized during this work were performed in a Rotofix 32 A; Hettich, Zentrifugen.

In preliminary reactions the FTIR spectra were recorded in ATR mode using a Jasco FT/IR-4200 spectrometer, equipped with a golden gate single reflection diamond ATR. The spectra were recorded using a resolution of 4 cm^{-1} and 64 interferograms. After some reactions, was concluded that the IR spectra obtained were more perceptible when FTIR analysis was carried out in KBr mode. This means that the various GO samples were mixed with a KBr powder (Aldrich, 99%, FT-IR grade) and compressed to obtain compact and transparent pellets. The pellets were prepared in a die with 7 mm.

The chemical stability of the samples were evaluated through TGA, in order to evaluate the attachment of new molecules to the surface of GO, namely initiator molecules and polymer chains. The samples were heated from 25ºC to 600 ºC at a heating rate of 10 ºC/min under a nitrogen flow of 100 mL/min on a SDT Q500, Thermal Analysis (TA) Instruments. The TGA curves and the weigh losses were measured using the Universal Analysis 2000 software, TA Instruments. TGA analysis were performed by Dr. Maria João at *Centro de Investigação em Engenharia dos Processos Químicos e dos Produtos da Floresta* (CIEPQPF, University of Coimbra).

To determine the presence of Br atoms in the samples after esterification reactions and also to evaluate if the Br were covalently bonded to the GO’s surface the esterified products and its raw materials were characterized by XPS. Analysis of the samples was performed using a Thermo Scientific K-Alpha ESCA instrument equipped with aluminium Kα monochromatized radiation at 1486.6 eV X-ray source. Due the no conductor nature of samples was necessary to use an electron flood gun to minimize surface charging. Neutralization of the surface charge was performed by using both a low energy flood gun (electrons in the range 0 to 14 eV) and a low energy Argon ions gun. The XPS measurements were carried out using monochromatic Al-Ka radiation (hn=1486.6 eV). Photoelectrons were collected from a take-off angle of 90º relative to the sample surface. The measurement was done in a Constant Analyser Energy mode (CAE) with a 100 eV pass energy for survey spectra and 20eV pass energy for high resolution spectra. Surface elemental composition was determined using the standard Scofield photoemission cross sections. The XPS data were obtained by Dr. Carmen Serra Rodrigues at Servicio Nanotecnología y Análisis de Superficies, Centro de Apoyo Científico y Tecnologíco a la Investigación (C.A.C.T.I., University of Vigo, Spain).

The presence of polymer chains in the surface of GO and its structures were also evaluated by ^{1}H NMR. 400 MHz ^{1}H NMR spectra of GO-Polymers were recorded on a Bruker Avance III 400 MHz spectrometer, with a 5-mm TIX triple resonance detection probe, in $CDCl_3$ with

TMS as an internal standard. The ^{1}H NMR data were obtained at the Nuclear Magnetic Resonance Laboratory of the Coimbra Chemistry Centre (http://www.nmrccc.uc.pt), University of Coimbra.

To evaluate the control over the structure of the synthesized polymers as well as to determine its molecular weight was used Gel Permeation Chromatography / Size Exclusion Chromatography (GPC/SEC). The chromatographic parameters of the samples were determined using high performance size-exclusion chromatography (HPSEC); Viscotek (Viscotek TDAmax) with a differential viscometer (DV); right-angle laser-light scattering (RALLS) (Viscotek); low-angle laser-light scattering (LALLS) (Viscotek) and refractive index (RI) detectors. The column consisted of a PL 10 mm guard column (50 × 7.5 mm2) followed by one Viscotek T200 column (6 µm), one MIXED-E PLgel column (3 µm) and one MIXED-C PLgel column (5 µm). An HPLC dual piston pump was set at a flow rate of 1 mL/min. The eluent, THF, was previously filtered through a 0.2 µm filter. The system was also equipped with an on-line degasser. The tests were done at 30 ºC using an Elder CH-150 heater. Before the injection (100 µL), the samples were filtered through a polytetrafluoroethylene (PTFE) membrane with 0.2 µm pore. The system was calibrated with narrow PS standards. The dn/dc was determined as 0.063 for PMA and 0.185 for PS. The number-average molecular weight ($M_{n,GPC}$) and dispersity ($Đ$) of synthesized polymers were determined by multidetectors calibration using OmniSEC software version: 4.6.1.354.

SEM was employed to analyse the morphology of the GO and the diverse products yielded during the experimental work. SEM observations were conducted on a scanning microscope JSM-5310, Jeol. Samples were sputter coated with gold and attached to a carbon felt support. SEM analysis were carried out by Dr. António Fonseca at Intituto Pedro Nunes (IPN, Coimbra).

3.3. Procedures

In this section are well described all the experimental procedures employed during the research conducted in this work. The molecular structures of the various compounds used in the laboratory are shown in Appendix O.

3.3.1. Functionalization of GO with initiator moieties using both hydroxyl and carboxyl acid groups

The functionalization of GO with initiator moieties using either the –OH and –COOH groups from the GO were realized following the procedures described in the literature [23, 25].

GO (100 mg) and dry DMF (25 mL) were placed in a 100 mL round-bottomed flask. The carbon nanomaterial were dispersed in DMF by ultrosonication during 2 h (sonic power: 90 W). The dispersion was cooled putting the flask in an ice bath, then, NHS (342 mg, 3 mmol) and EDC.HCl (575 mg, 3 mmol) were added to the dispersion at ~0ºC. After stirring during 2 h (600-700 rpm), 1,3-diaminopropane (0.380 mL) was added, the flask was sealed and the reaction mixture stirred (600-700 rpm) overnight at room temperature (25 ºC). The final mixture was filtered through a sintered disc filter funnel (Duran) (nominal maximum pore size ranging between 1.0-1.6 µm) washed with water and ethanol and dried in a vacuum oven at 40 ºC, during 12 h.

The dried product obtained from the previous reaction was loaded in a 100 mL three-neck flask along with dry DMF (25 mL). One more time, GO was dispersed in the solvent by ultrasonication during 1 h (sonic power: 90 W). Then, the dispersion was cooled to ~0 ºC and TEA (1.05 mL, 7.53 mmol) was carefully added under stirring (600-700 rpm). The flask was putted under controlled atmosphere (purged with nitrogen (N_2)) and BIBB (0.62 mL, 5.02 mmol) was added dropwise to the reaction medium at ~0 ºC, using an addition funnel. After stirring the dispersion during 2 h at 0 ºC the flask was immersed in an oil bath at 90 ºC and the colloidal suspension was stirred (600-700 rpm) during 24 h with a condenser. The final product was filtered through a sintered disc filter funnel (Duran, pore size 1.0-1.6 µm), exhaustively washed with ethanol and dried in a vacuum oven at 40ºC during 12 h to obtain the final macroinitiator GO-Br (103.4 mg).

3.3.2. Functionalization of GO with initiator moieties (GO-Br) using only hydroxyl groups (-OH)

The procedures described in this sub-point were based in the literature [24, 26, 61, 62]. During the work were used, in the esterification reactions, different reactants and solvents ratios. However, all the procedures were realized as follow exposed, only the amounts of reactants and solvents used were altered.

GO (500 mg) and dry DMF (25 mL) were loaded in a three-neck flask. A colloidal suspension were prepared putting the mixture in an ultrasonic bath (sonic power: 90 W) during 1 h. The flask was immersed in an ice bath and TEA (4.23 mL, 30 mmol) was carefully added to the colloidal dispersion. Then, BIBB (3.75 mL, 30 mmol) was added dropwise to the dispersion at 0ºC, under controlled atmosphere (flask purged with N_2) and using an addition funnel or an airtight syringe. The reaction mixture was stirred (600-700 rpm) for 2 h at ~0ºC and at room temperature during 24 h (25 ºC). The suspension was filtered using a sintered disc filter funnel (Duran, pore size 1.0-1.6 µm). During the filtration the product was washed with chloroform and deionized water to remove the salts formed during the esterification reaction (mainly in the form of $Br^-NEt_3^+$). Finally, the GO-Br, was dried in a vacuum oven at 40 ºC during 24 h to obtain 477 mg.

3.3.3. Polymerization from the surface of GO

In this point are described typical procedures used to polymerize from the surface of GO-Br. Throughout the experimental work different strategies were used, depending on the phase of the work, the experience acquired and the results obtained.

Next are presented the typical procedures to polymerize from the surface of GO used in the different phases of the work.

- **Step 1 - Typical Procedure for the SARA ATRP of MA from the GO surface in DMF, catalyzed by [Cu(0)]/[$CuBr_2$]/[Me6TREN] = wire/0.1/1.1**

GO-Br (47 mg) and DMF (1 mL) were loaded in a Schlenk tube reactor. The mixture were stirred (400-500 rpm) at room temperature for 20-30 min to disperse the modified carbon nanomaterial. Then, a mixture of $CuBr_2$ (1.42 mg, 0.006 mmol), Me_6TREN (18.65 µL, 0.07 mmol) and DMF (1 mL) along with Cu(0) wire (5 cm) were added to the dispersion, the reactor was sealed with a rubber septum and bubbled with N_2 for 30 min. MA (689.11 µL, 7.65 mmol) was bubbled with nitrogen, in a vial sealed with a rubber septum, during 30 min and added to the reactor mixture under a constant flow of nitrogen using an airtight syringe. The Schlenk tube reactor containing the reaction mixture was placed in a water bath at 30 ºC with stirring (500-600 rpm) for 2 days. The reaction was stopped by exposing the mixture to air. The final GO was purified by successive centrifugation/redispersion cycles using $CHCl_3$, until obtain a clear supernatant. The centrifugation were carried out using 4000 rpm for 10 min and the redispersion were achieved submitting the falcon with the solvent and the deposited GO to a vortex stirrer. The washed powders were dried in a vacuum oven at 40ºC for 24 h.

The FTIR, ^1H NMR and TGA results revealed no presence of significant amounts of polymer in the final products obtained from the reactions conducted using this procedures.

- **Step 2 and 3 - Typical Procedure for the SARA ATRP of Sty from the GO surface in DMF, catalyzed by [Cu(0)]/[TREN] (Reproduction of the polymerization reported [24])**

GO-Br (100 mg, 0.051 mmol of Br) and DMF (5 mL), previously bubbled with N_2 (10-15 min), were loaded in a Schlenk reactor. The mixture were stirred (400-500 rpm) at room temperature for 20-30 min to disperse the modified carbon nanomaterial. Then, Sty (5 mL, 43.49 mmol), TREN (75 µL, 0.25 mmol) and Cu(0) wire (5 cm) were added to the dispersion and the reactor was sealed and frozen in liquid nitrogen. The Schlenk reactor was deoxygenated with four freeze-vacuum-thaw cycles and purged with nitrogen. After this, it was placed in an oil bath at 80 ºC with stirring (500-600 rpm) for 20 h. The reaction was stopped by exposing the mixture to air and cooling the reactor in a water bath. The final reaction mixture was precipitated in ethanol, filtered, washed with ethanol until obtain a clear filtrate and dried in a vacuum oven at 40 ºC. The dried product was dispersed in DMF (50 mg/mL) and centrifuged during 30 min at 4000 rpm to remove possible "free" polymer chains. The deposited GO was dried in a vacuum oven at 40ºC for 24 h and the supernatant was added to an excess of ethanol to evaluate if detached polymer was produced.

In the experiments realized according this procedures was obtained polymer, since when the final reaction mixture was added to ethanol a grey precipitate was formed. However, after centrifugation, when the supernatant was added to ethanol a significant precipitate was formed, indicating that detached polymer chains were produced during the polymerization reaction. In addition, the ^{1}H NMR of the washed GO revealed no presence of PS chains. The polymer obtained from the supernatant, was dried in a vacuum oven at 40 ºC during 12 h and, then, dissolved in THF (10 mg/mL) to characterize through GPC analysis and in $CDCl_3$ (10 mg/mL) for ^{1}H NMR analysis. The results revealed that uncontrolled polymer was formed in solution.

Having in mind that Sty can easily auto polymerize at high temperatures, new reactions were conducted using lower temperatures (60 ºC). Also were carried out polymerization using sulfolane as solvent and different molar ratios. All the procedures were followed as previously described, only the reaction temperature and the reactant ratios were changed. The final results were very similar to the previous obtained at higher temperatures.

- **Step 4 - Typical Procedure for the SARA ATRP of MA (DP = 500) from the GO surface in DMF, catalyzed by [Cu(0)]/[Me_6TREN] = wire/1.1**

GO-Br (100 mg, 0.051 mmol of Br) and DMF (5 mL), previously bubbled with N_2 (10-15 min), were loaded in a Schlenk reactor. The mixture were stirred (400-500 rpm) at room temperature for 20-30 min to disperse the modified carbon nanomaterial. Then, MA (2.30 mL, 25.52 mmol), Me_6TREN (15.01 µL, 0.056 mmol) and Cu(0) wire (5 cm) were added to the dispersion and the reactor was sealed and frozen in liquid nitrogen. The Schlenk reactor was deoxygenated with four freeze-vacuum-thaw cycles and purged with nitrogen. After this, it was placed in an oil bath at 60 ºC with stirring (500-600 rpm) for 24 h. The reaction was stopped by exposing the mixture to air and cooling the reactor in a water bath. The final reaction mixture was precipitated in water and filtered/decanted. Subsequently, the product was diverse times washed with water until obtain a clear filtrate/decanted and dried in a vacuum oven at 40 ºC. The dried product was dispersed in DMF (50 mg/mL) and centrifuged during 30 min at 4000 rpm to remove possible “free” polymer chains. The washing process were realized by successive centrifugation/redispersion cycles in DMF and THF. The deposited GO was dried in a vacuum oven at 40ºC for 24 h.

In the experiments realized according this procedures was obtained polymer, since when the final reaction mixture was added to water a black and sticky precipitate was formed. The dried washed GO was dissolved in $CDCl_3$ (10 mg/mL) for ^{1}H NMR analysis and was analysed by TGA. The results revealed that polymer chains were attached to the surface of GO.

- **Step 5 - Typical Procedure for the SARA ATRP of MA (DP = 500) from the GO surface with sacrificial initiator in DMF, catalyzed by [Cu(0)]/[Me_6TREN] = wire/1.1**

GO-Br (100 mg, 0.051 mmol of Br) and a mixture of EBiB (7.49 µL, 0.051 mmol) and DMF (5 mL), previously bubbled with N_2 (10-15 min), were loaded in a Schlenk reactor. The mixture were stirred (400-500 rpm) at room temperature for 20-30 min to disperse the modified carbon nanomaterial. Then, a mixture of MA (4.60 mL, 51.04 mmol) and Me_6TREN (30.01 µL, 0.11 mmol) along with a Cu(0) wire (5 cm) were added to the dispersion and the reactor was sealed and frozen in liquid nitrogen. The Schlenk reactor was deoxygenated with four freeze-vacuum-thaw cycles and purged with nitrogen. After this, it was placed in an oil bath at 60 ºC with stirring (500-600 rpm) for 24 h. The reaction was stopped by exposing the mixture to air and cooling the reactor in a water bath. Throughout the polymerization, different samples were collected through an airtight syringe while purging the side arm of the Schlenk reactor with N_2. Each sample were diluted with THF, filtered two times through a PTFE filter with 0.2 µm pore and analysed by GPC and ^1H NMR. The final reaction mixture was precipitated in water and filtered/decanted. Subsequently, the product was diverse times washed with water until obtain a clear filtrate/decanted and dried in a vacuum oven at 40 ºC. The dried product was dispersed in DMF (50 mg/mL) and centrifuged during 30 min at 4000 rpm to remove the "free" polymer chains. The deposited GO was dried in a vacuum oven at 40ºC for 24 h. The supernatant was passed through a sand/alumina column, precipitated in water and dried in a vacuum oven at 40 ºC. The dried "free" polymer chains were dissolved in THF (10 mg/mL) for GPC analysis and in $CDCl_3$ (10 mg/mL) for ^1H NMR characterization.

3.3.4. Cleavage of polymer chains from the surface of GO

The goal of this work was not only to polymerize from the surface of GO, but polymerize from GO in a control manner, yielding polymer chains with defined molecular weights and low dispersity ($Đ << 2$). Considering this, was fundamental to evaluate the structures of the polymer chains attached to the surface of the carbon nanomaterial through GPC analyses. In order to realize such characterization technique was necessary to detach the polymer chains from the GO's surface, cleaving the ester linkage that bonded the polymer chains to GO.

Different methodologies were employed trying to achieve the saponification (basic hydrolysis) of the ester linkage.

- **Detachment of polymer chains from GO using NaOH**

The procedures were followed as described in the literature [24].

GO modified with polymer chains (25 mg) and DMF (5 mL) were loaded in a 25 mL round-bottomed flask. NaOH (300 mg) was added to the suspension, the flask was sealed, purged with nitrogen and stirred (500-600 rpm) at 80 ºC for 96 h. The final reaction mixture was filtered through a sintered disc filter funnel (Duran, pore size 1.0-1.6 µm). The filtrate was added to ethanol to precipitate the polymer. The solids were isolated by filtration (sintered disc filter funnel (Duran, pore size 1.0-1.6 µm)) or by decantation and washed diverse times with ethanol and deionized water to remove the traces of base. When polymer was obtained, it was dried in a vacuum oven at 40 ºC, then, dissolved in THF (10 mg/mL) for GPC analysis and in $CDCl_3$ (10 mg/mL) for ^1H NMR analysis.

- **Detachment of polymer chains from GO using KOH**

The procedures described in this section were reported in the mentioned references [10, 111].

GO modified with polymer chains (20 mg), THF (3 mL) and KOH (8 mg) were loaded in a 5 mL reactor flask. The reactor was equipped with a condenser, purged with N_2 and placed in an oil bath at 50 ºC with stirring (500-600 rpm) overnight. The final reaction mixture was quenched with ethanol (2-3 mL) and filtered through a 0.2 μm PTFE filter (Whatman) and diluted with THF for GPC analysis.

Chapter 4

4. Conclusions and Future work

In this work, controlled modification of GO by CLRP was studied, having in account the growing interest in graphene and its derivative nanomaterials.

In a preliminary phase of the work SARA ATRP reactions conducted in homogeneous medium were studied aiming to gain some experience in CLRP techniques. These reactions were carried out alongside with various researchers of the Polymer Research Group from the Department of Chemical Engineering, University of Coimbra and interesting results were obtained originating two publications in *ACS Macro Letters*.

An unusual synergistic effect between BMIM-PF_6, an ionic liquid, and DMSO mixtures was reported for the SARA ATRP of MA catalysed by $Na_2S_2O_4$ and $CuBr_2$/Me_6TREN at room temperature. In a parallel work, it was discovered that sulfolane, a common and industrial solvent, is an efficient and universal solvent for copper mediated atom transfer radical (co)polymerization of acrylates, methacrylates, Sty and VC.

In the second and main phase of the work were investigated methods to polymerize from the surface of GO in a control manner, through CLRP reactions.

Before the actual polymerizations, it was necessary to functionalize the surface of GO with initiator moieties. Two processes described in the literature were followed. One methodology consisted on reacting 1,3-diaminopropane with –COOH groups of GO through an amidation reaction at room temperature catalysed by NHS and EDC.HCl and, finally, BIBB molecules were attached to the surface of GO through the modification of –OH groups of GO and amine groups previously introduced, reaction conducted at 90 ºC catalysed by TEA (2.74% (w/w) Br covalently bonded to GO). The second method involved just a reaction between BIBB molecules and –OH groups of GO by an esterification reaction at room temperature catalysed by TEA (4.08 to 5.77% (w/w) Br covalently bonded to GO).

After analysing the GO-Br products through FTIR, TGA and XPS it was proved that the esterification/amidation reactions were successful and that the second method (which only used –OH groups of GO) yielded a great amount of initiator molecules attached to the GO’s surface. We believe that the results were due to the higher amounts of BIBB used in this method. A reduction of the oxide functionality of GO was observed after esterification reactions, in accordance with the results reported in the literature. Additionally, the interpretations of the IR peaks of the esterified products were very difficult, as result of the great modifications observed. Through two experiments and FTIR analysis was demonstrated that TEA can react with some of the oxygen containing species, namely with carboxyl groups. Other issues related to the washing process of the esterified products and its purification upraised during the work, namely the complete removal of the salts and traces of reactants resulting from the esterification reactions which was never achieved.

In the last phase of the work, SARA ATRP reactions catalysed by Cu(0) wire/Me_6TREN in DMF at 60 ºC were conducted from the surface of GO. The final purified powders were analysed through FTIR, TGA, ^1H NMR, GPC,XPS and SEM and the results revealed that polymer brushes with molecular weights of about 30 kDa and dispersity values lower than 1.5 were grown from the surface of GO. Although this final positive results, diverse problems and issues were found during the course of this work. Several systems reported in the literature were reproduced and detached uncontrolled polymer chains were obtained. Also sacrificial initiator was used, in the SARA ATRP of MA from GO's surface, in order to improve the control over the reactions and the result was detached polymer. These results led us to believe that, probably, the efficiency of the macroinitiators prepared was low, since when some external factor (homo-polymerization due to high temperatures or free initiator) competed with the attached initiator molecules the controlled grafting reaction was inhibited.

In Figure 32 is presented a scheme to summarize the diverse polymerization reactions carried out during this work and to illustrate the diverse approaches adopted to achieve the goal of this dissertation.

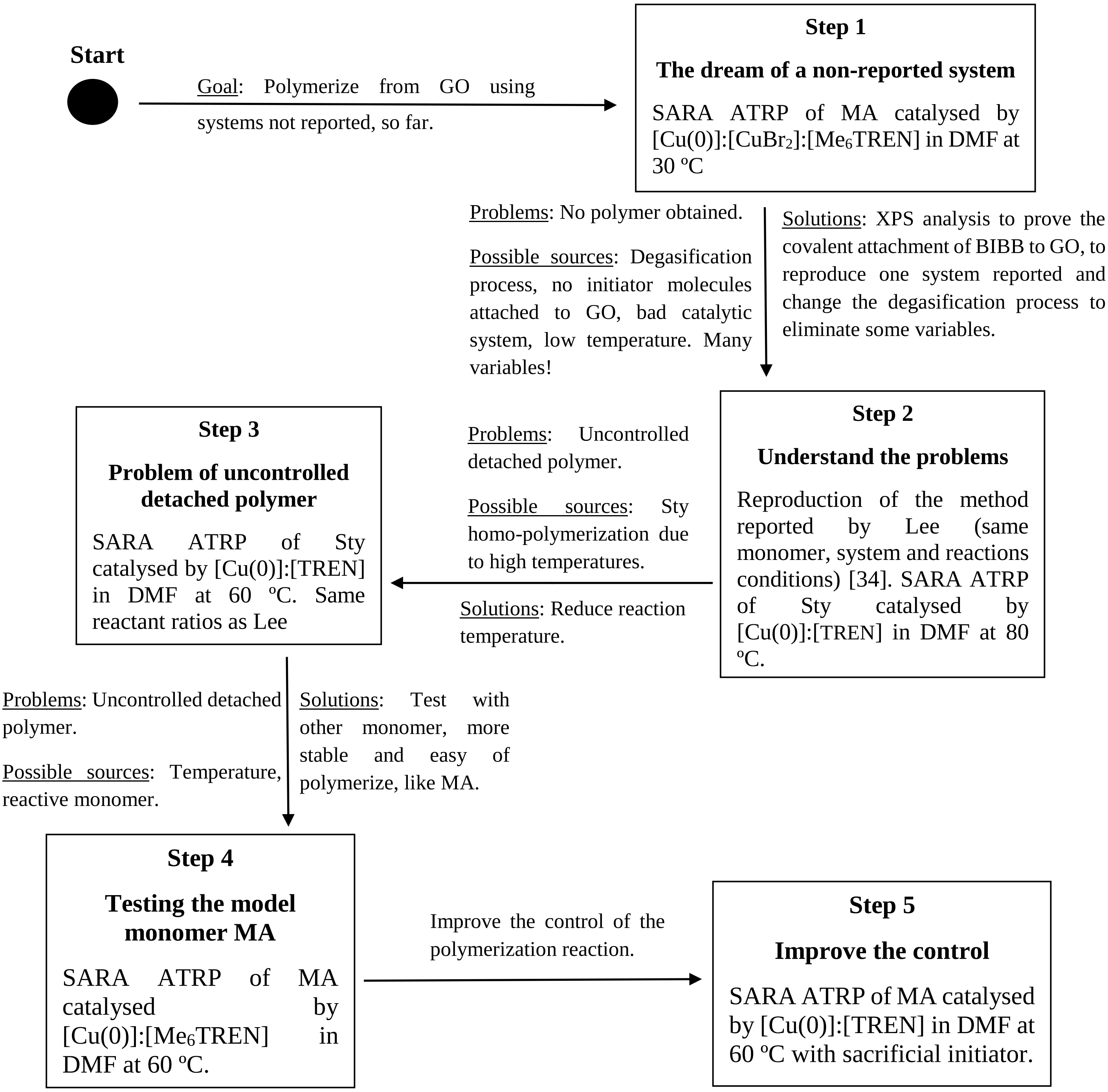

Start

Goal: Polymerize from GO using systems not reported, so far.

Step 1

The dream of a non-reported system

SARA ATRP of MA catalysed by [Cu(0)]:[$CuBr_2$]:[Me_6TREN] in DMF at 30 ºC

Problems: No polymer obtained.

Possible sources: Degasification process, no initiator molecules attached to GO, bad catalytic system, low temperature. Many variables!

Solutions: XPS analysis to prove the covalent attachment of BIBB to GO, to reproduce one system reported and change the degasification process to eliminate some variables.

Step 2

Understand the problems

Reproduction of the method reported by Lee (same monomer, system and reactions conditions) [34]. SARA ATRP of Sty catalysed by [Cu(0)]:[TREN] in DMF at 80 ºC.

Problems: Uncontrolled detached polymer.

Possible sources: Sty homo-polymerization due to high temperatures.

Solutions: Reduce reaction temperature.

Step 3

Problem of uncontrolled detached polymer

SARA ATRP of Sty catalysed by [Cu(0)]:[TREN] in DMF at 60 ºC. Same reactant ratios as Lee

Problems: Uncontrolled detached polymer.

Possible sources: Temperature, reactive monomer.

Solutions: Test with other monomer, more stable and easy of polymerize, like MA.

Step 4

Testing the model monomer MA

SARA ATRP of MA catalysed by [Cu(0)]:[Me_6TREN] in DMF at 60 ºC.

Improve the control of the polymerization reaction.

Step 5

Improve the control

SARA ATRP of MA catalysed by [Cu(0)]:[TREN] in DMF at 60 ºC with sacrificial initiator.

Figure 32. Scheme with the reactions pathway followed during the experimental work.

The balance of the work developed is positive, besides the various problems we had to overcome and the experience acquired about GO and its functionalization. However, the goals of the work were not completely achieved and further research has to be done on this field.

In future work, the evaluation of the control achieved over the grafting polymerizations requires further and more detailed studies. In our opinion, the demonstration of the control achieved over the grafting polymerizations should be a primary interest point when working in this area.

The methods used in this work to cleave polymer chains from GO’s surface revealed some problems of solubilisation of the alkali in the solvents and were not deeply studied, which means that, in the case of PMA, the hydrolysis can also attacked the ester groups of PMA degrading its structure. A more detailed study should be done about these saponification reactions in order to better understand all the problems they brought up. We also believe that this future study should have the concern to try to find out more methods to cleave the polymer chains from GO surface, without the polymer degradation. For example, study the possibility of attaching photolabile initiator molecules to the surface of GO that after the polymerization reactions could be degraded when exposed to UV irradiation. The use of these photolabile initiators to grow polymers from surfaces was already reported [142].

An interesting study to be carried out in future could be a detailed research about the influences of the catalytic systems in the control over the polymerization process achieved in the grafting polymerizations and optimizing the amounts of catalysts employed as well as test new catalysts like zero valent iron (Fe(0)) and the incorporation of $CuBr_2$ to improve the control.

An additional characterization that should be carried out in future works is the measurement of the conductivities of the different graphene species produced, since the high electrical conductivity of graphene is its most popular property.

Finally, from our point of view other less used methods for the functionalization of graphene can also be explored. Interesting reactions that may be able to ensure the maintenance of the extraordinary electrical conductivities of graphene are the 1,3-dipolar cycloadditions. In these reactions hydroxyl groups are introduced in the graphene nanosheets without disrupting the sp^2 structure of graphene. To the best of our knowledge, only two works reported the use of these chemical reactions to functionalize graphene with oxygen containing species [55, 143].

Chapter 5

5. Bibliography

[1] M. Ratner and D. Ratner, *Nanotechnology: a gentle introduction to the next big idea*: Prentice Hall Press, 2002.

[2] Y. Gogotsi, *Carbon Nanomaterials*. Drexel University, Philadelphia, Pennsylvania, USA: Taylor and Francis Group, LLC, 2006.

[3] D. Jariwala, V. K. Sangwan, L. J. Lauhon, T. J. Marks, and M. C. Hersam, "Carbon nanomaterials for electronics, optoelectronics, photovoltaics, and sensing," *Chemical Society Reviews*, vol. 42, pp. 2824-2860, 2013.

[4] S. Neil, "Materials science: Super carbon," *Nature*, vol. 483, 2012.

[5] K. P. Loh, Q. Bao, P. K. Ang, and J. Yang, "The chemistry of graphene," *Journal of Materials Chemistry*, vol. 20, pp. 2277-2289, 2010.

[6] K. S. Novoselov, A. K. Geim, S. V. Morozov, D. Jiang, Y. Zhang, S. V. Dubonos, *et al.*, "Electric Field Effect in Atomically Thin Carbon Films," *Science*, vol. 306, pp. 666-669, October 22, 2004 2004.

[7] L. Rodriguez-Perez, M. a. A. Herranz, and N. Martin, "The chemistry of pristine graphene," *Chemical Communications*, vol. 49, pp. 3721-3735, 2013.

[8] A. K. Geim and K. S. Novoselov, "The rise of graphene," *Nature Materials*, vol. 6, pp. 183-191, 2007.

[9] N. Saravanan, R. Rajasekar, S. Mahalakshmi, T. Sathishkumar, K. S. K. Sasikumar, and S. Sahoo, "Graphene and modified graphene-based polymer nanocomposites – A review," *Journal of Reinforced Plastics and Composites*, February 20, 2014 2014.

[10] G. Goncalves, P. A. A. P. Marques, A. Barros-Timmons, I. Bdkin, M. K. Singh, N. Emami, *et al.*, "Graphene oxide modified with PMMA via ATRP as a reinforcement filler," *Journal of Materials Chemistry*, vol. 20, pp. 9927-9934, 2010.

[11] W. Li, X.-Z. Tang, H.-B. Zhang, Z.-G. Jiang, Z.-Z. Yu, X.-S. Du, *et al.*, "Simultaneous surface functionalization and reduction of graphene oxide with octadecylamine for electrically conductive polystyrene composites," *Carbon*, vol. 49, pp. 4724-4730, 11// 2011.

[12] P.-P. Zuo, H.-F. Feng, Z.-Z. Xu, L.-F. Zhang, Y.-L. Zhang, W. Xia, *et al.*, "Fabrication of biocompatible and mechanically reinforced graphene oxide-chitosan nanocomposite films," *Chemistry Central Journal*, vol. 7, pp. 1-11, 2013/02/25 2013.

[13] N. Minoo, W. Jing, A. Abbas, K. Hamid, H. Nishar, L. Lu Hua, *et al.*, "Mechanical Property and Structure of Covalent Functionalised Graphene/Epoxy Nanocomposites," *Scientific Reports*, vol. 4, 2014.

[14] M. A. Rafiee, J. Rafiee, Z. Wang, H. Song, Z.-Z. Yu, and N. Koratkar, "Enhanced Mechanical Properties of Nanocomposites at Low Graphene Content," *ACS Nano*, vol. 3, pp. 3884-3890, 2009/12/22 2009.

[15] M. Fang, K. Wang, H. Lu, Y. Yang, and S. Nutt, "Single-layer graphene nanosheets with controlled grafting of polymer chains," *Journal of Materials Chemistry*, vol. 20, pp. 1982-1992, 2010.

[16] N. A. Kotov, "Materials science: Carbon sheet solutions," *Nature*, vol. 442, pp. 254-255, 07/20/print 2006.

[17] O. C. Compton and S. T. Nguyen, "Graphene Oxide, Highly Reduced Graphene Oxide, and Graphene: Versatile Building Blocks for Carbon-Based Materials," *Small*, vol. 6, pp. 711-723, 2010.

[18] H. Kim, A. A. Abdala, and C. W. Macosko, "Graphene/Polymer Nanocomposites," *Macromolecules,* vol. 43, pp. 6515-6530, 2010/08/24 2010.

[19] H. Kim, Y. Miura, and C. W. Macosko, "Graphene/Polyurethane Nanocomposites for Improved Gas Barrier and Electrical Conductivity," *Chemistry of Materials,* vol. 22, pp. 3441-3450, 2010/06/08 2010.

[20] H. Kim and C. W. Macosko, "Morphology and Properties of Polyester/Exfoliated Graphite Nanocomposites," *Macromolecules,* vol. 41, pp. 3317-3327, 2008/05/01 2008.

[21] E. Tkalya, M. Ghislandi, A. Alekseev, C. Koning, and J. Loos, "Latex-based concept for the preparation of graphene-based polymer nanocomposites," *Journal of Materials Chemistry,* vol. 20, pp. 3035-3039, 2010.

[22] J. Liang, Y. Huang, L. Zhang, Y. Wang, Y. Ma, T. Guo*, et al.*, "Molecular-Level Dispersion of Graphene into Poly(vinyl alcohol) and Effective Reinforcement of their Nanocomposites," *Advanced Functional Materials,* vol. 19, pp. 2297-2302, 2009.

[23] Y. Yang, J. Wang, J. Zhang, J. Liu, X. Yang, and H. Zhao, "Exfoliated Graphite Oxide Decorated by PDMAEMA Chains and Polymer Particles," *Langmuir,* vol. 25, pp. 11808-11814, 2009/10/06 2009.

[24] S. H. Lee, D. R. Dreyer, J. An, A. Velamakanni, R. D. Piner, S. Park*, et al.*, "Polymer Brushes via Controlled, Surface-Initiated Atom Transfer Radical Polymerization (ATRP) from Graphene Oxide," *Macromolecular Rapid Communications,* vol. 31, pp. 281-288, 2010.

[25] X. Sun, W. Wang, T. Wu, H. Qiu, X. Wang, and J. Gao, "Grafting of graphene oxide with poly(sodium 4-styrenesulfonate) by atom transfer radical polymerization," *Materials Chemistry and Physics,* vol. 138, pp. 434-439, 3/15/ 2013.

[26] W. Yuan, J. Wang, T. Shen, and J. Ren, "Surface modification of graphene oxide with thermoresponsive polymers via atom transfer radical polymerization: Transition from LCST to UCST," *Materials Letters,* vol. 107, pp. 243-246, 9/15/ 2013.

[27] H. O. Pierson, "3 - Graphite Structure and Properties," in *Handbook of Carbon, Graphite, Diamonds and Fullerenes*, H. O. Pierson, Ed., ed Oxford: William Andrew Publishing, 1993, pp. 43-69.

[28] A. Krueger, "Carbon – Element of Many Faces," in *Carbon Materials and Nanotechnology*, ed: Wiley-VCH Verlag GmbH & Co. KGaA, 2010, pp. 1-32.

[29] D. D. L. Chung, "Review Graphite," *Journal of Materials Science,* vol. 37, pp. 1475-1489, 2002/04/01 2002.

[30] K. S. Novoselov, D. Jiang, F. Schedin, T. J. Booth, V. V. Khotkevich, S. V. Morozov*, et al.*, "Two-dimensional atomic crystals," *Proceedings of the National Academy of Sciences of the United States of America,* vol. 102, pp. 10451-10453, July 26, 2005 2005.

[31] B. Herb, "Graphene," *Nature,* vol. 483, 2012.

[32] B. Partoens and F. M. Peeters, "From graphene to graphite: Electronic structure around the K point," *Physical Review B,* vol. 74, p. 075404, 08/02/ 2006.

[33] W. Wei and X. Qu, "Extraordinary physical properties of functionalized graphene," *Small,* vol. 8, pp. 2138-51, Jul 23 2012.

[34] M. J. Allen, V. C. Tung, and R. B. Kaner, "Honeycomb Carbon: A Review of Graphene," *Chemical Reviews,* vol. 110, pp. 132-145, 2010/01/13 2009.

[35] A. A. Balandin, "Thermal properties of graphene and nanostructured carbon materials," *Nat Mater,* vol. 10, pp. 569-581, 08//print 2011.

[36] S. Ghosh, I. Calizo, D. Teweldebrhan, E. P. Pokatilov, D. L. Nika, A. A. Balandin*, et al.*, "Extremely high thermal conductivity of graphene: Prospects for thermal management applications in nanoelectronic circuits," *Applied Physics Letters,* vol. 92, pp. -, 2008.

[37] C. Lee, X. Wei, J. W. Kysar, and J. Hone, "Measurement of the Elastic Properties and Intrinsic Strength of Monolayer Graphene," *Science,* vol. 321, pp. 385-388, July 18, 2008 2008.

[38] R. R. Nair, P. Blake, A. N. Grigorenko, K. S. Novoselov, T. J. Booth, T. Stauber, *et al.*, "Fine Structure Constant Defines Visual Transparency of Graphene," *Science,* vol. 320, p. 1308, June 6, 2008 2008.

[39] X. Du, I. Skachko, A. Barker, and E. Y. Andrei, "Approaching ballistic transport in suspended graphene," *Nat Nano,* vol. 3, pp. 491-495, 08//print 2008.

[40] S. C. Thickett and P. B. Zetterlund, "Functionalization of Graphene Oxide for the Production of Novel Graphene-Based Polymeric and Colloidal Materials," *Current Organic Chemistry,* vol. 17, pp. 956-974, // 2013.

[41] M. D. Stoller, S. Park, Y. Zhu, J. An, and R. S. Ruoff, "Graphene-Based Ultracapacitors," *Nano Letters,* vol. 8, pp. 3498-3502, 2008/10/08 2008.

[42] Z.-Y. Juang, C.-Y. Wu, A.-Y. Lu, C.-Y. Su, K.-C. Leou, F.-R. Chen, *et al.*, "Graphene synthesis by chemical vapor deposition and transfer by a roll-to-roll process," *Carbon,* vol. 48, pp. 3169-3174, 9// 2010.

[43] H.-B. Zhang, J.-W. Wang, Q. Yan, W.-G. Zheng, C. Chen, and Z.-Z. Yu, "Vacuum-assisted synthesis of graphene from thermal exfoliation and reduction of graphite oxide," *Journal of Materials Chemistry,* vol. 21, pp. 5392-5397, 2011.

[44] C. Zhang, W. Lv, X. Xie, D. Tang, C. Liu, and Q.-H. Yang, "Towards low temperature thermal exfoliation of graphite oxide for graphene production," *Carbon,* vol. 62, pp. 11-24, 10// 2013.

[45] H. Wang, Y. Wang, Z. Hu, and X. Wang, "Cutting and Unzipping Multiwalled Carbon Nanotubes into Curved Graphene Nanosheets and Their Enhanced Supercapacitor Performance," *ACS Applied Materials & Interfaces,* vol. 4, pp. 6827-6834, 2012/12/26 2012.

[46] D. R. Dreyer, S. Park, C. W. Bielawski, and R. S. Ruoff, "The chemistry of graphene oxide," *Chemical Society Reviews,* vol. 39, pp. 228-240, 2010.

[47] H. J. Salavagione, G. Martínez, and G. Ellis, "Recent Advances in the Covalent Modification of Graphene With Polymers," *Macromolecular Rapid Communications,* vol. 32, pp. 1771-1789, 2011.

[48] R. K. Layek and A. K. Nandi, "A review on synthesis and properties of polymer functionalized graphene," *Polymer,* vol. 54, pp. 5087-5103, 8/23/ 2013.

[49] V. Georgakilas, M. Otyepka, A. B. Bourlinos, V. Chandra, N. Kim, K. C. Kemp, *et al.*, "Functionalization of Graphene: Covalent and Non-Covalent Approaches, Derivatives and Applications," *Chemical Reviews,* vol. 112, pp. 6156-6214, 2012/11/14 2012.

[50] D. Yu, Y. Yang, M. Durstock, J.-B. Baek, and L. Dai, "Soluble P3HT-Grafted Graphene for Efficient Bilayer−Heterojunction Photovoltaic Devices," *ACS Nano,* vol. 4, pp. 5633-5640, 2010/10/26 2010.

[51] D. Yu and L. Dai, "Self-Assembled Graphene/Carbon Nanotube Hybrid Films for Supercapacitors," *The Journal of Physical Chemistry Letters,* vol. 1, pp. 467-470, 2010/01/21 2009.

[52] Y. Pan, H. Bao, N. G. Sahoo, T. Wu, and L. Li, "Water-Soluble Poly(N-isopropylacrylamide)–Graphene Sheets Synthesized via Click Chemistry for Drug Delivery," *Advanced Functional Materials,* vol. 21, pp. 2754-2763, 2011.

[53] L. Kan, Z. Xu, and C. Gao, "General Avenue to Individually Dispersed Graphene Oxide-Based Two-Dimensional Molecular Brushes by Free Radical Polymerization," *Macromolecules,* vol. 44, pp. 444-452, 2011/02/08 2010.

[54] H. Roghani-Mamaqani and V. Haddadi-Asl, "In-plane functionalizing graphene nanolayers with polystyrene by atom transfer radical polymerization: Grafting from hydroxyl groups," *Polymer Composites,* vol. 35, pp. 386-395, 2014.

[55] B. Ou, Z. Zhou, Q. Liu, B. Liao, S. Yi, Y. Ou, *et al.*, "Covalent functionalization of graphene with poly(methyl methacrylate) by atom transfer radical polymerization at room temperature," *Polymer Chemistry*, vol. 3, pp. 2768-2775, 2012.

[56] X. Liu, H. Cheng, and Y. Liu, "Modifying graphite oxide with grafted methyl acrylate brushes for the attachment of magnetite nanoparticles," *Applied Surface Science*, vol. 280, pp. 235-239, 9/1/ 2013.

[57] J. M. Bak and H.-i. Lee, "pH-tunable aqueous dispersion of graphene nanocomposites functionalized with poly(acrylic acid) brushes," *Polymer*, vol. 53, pp. 4955-4960, 10/12/ 2012.

[58] J. M. Bak, T. Lee, E. Seo, Y. Lee, H. M. Jeong, B.-S. Kim, *et al.*, "Thermoresponsive graphene nanosheets by functionalization with polymer brushes," *Polymer*, vol. 53, pp. 316-323, 1/24/ 2012.

[59] L. Chang, S. Wu, S. Chen, and X. Li, "Preparation of graphene oxide–molecularly imprinted polymer composites via atom transfer radical polymerization," *Journal of Materials Science*, vol. 46, pp. 2024-2029, 2011/04/01 2011.

[60] X. Chen, L. Yuan, P. Yang, J. Hu, and D. Yang, "Covalent polymeric modification of graphene nanosheets via surface-initiated single-electron-transfer living radical polymerization," *Journal of Polymer Science Part A: Polymer Chemistry*, vol. 49, pp. 4977-4986, 2011.

[61] Y. Deng, Y. Li, J. Dai, M. Lang, and X. Huang, "Functionalization of graphene oxide towards thermo-sensitive nanocomposites via moderate in situ SET-LRP," *Journal of Polymer Science Part A: Polymer Chemistry*, vol. 49, pp. 4747-4755, 2011.

[62] Y. Deng, J. Z. Zhang, Y. Li, J. Hu, D. Yang, and X. Huang, "Thermoresponsive graphene oxide-PNIPAM nanocomposites with controllable grafting polymer chains via moderate in situ SET–LRP," *Journal of Polymer Science Part A: Polymer Chemistry*, vol. 50, pp. 4451-4458, 2012.

[63] M. Fang, K. Wang, H. Lu, Y. Yang, and S. Nutt, "Covalent polymer functionalization of graphene nanosheets and mechanical properties of composites," *Journal of Materials Chemistry*, vol. 19, pp. 7098-7105, 2009.

[64] T. Gao, Q. Ye, X. Pei, Y. Xia, and F. Zhou, "Grafting polymer brushes on graphene oxide for controlling surface charge states and templated synthesis of metal nanoparticles," *Journal of Applied Polymer Science*, vol. 127, pp. 3074-3083, 2013.

[65] J. Ji, X. Sun, X. Tian, Z. Li, and Y. Zhang, "Synthesis of Acrylamide Molecularly Imprinted Polymers Immobilized on Graphite Oxide through Surface-Initiated Atom Transfer Radical Polymerization," *Analytical Letters*, vol. 46, pp. 969-981, 2013/04/13 2012.

[66] R. K. Layek, S. Samanta, D. P. Chatterjee, and A. K. Nandi, "Physical and mechanical properties of poly(methyl methacrylate) -functionalized graphene/poly(vinylidine fluoride) nanocomposites: Piezoelectric β polymorph formation," *Polymer*, vol. 51, pp. 5846-5856, 11/12/ 2010.

[67] K.-J. Peng, K.-H. Wang, K.-Y. Hsu, and Y.-L. Liu, "Building up polymer architectures on graphene oxide sheet surfaces through sequential atom transfer radical polymerization," *Journal of Polymer Science Part A: Polymer Chemistry*, vol. 52, pp. 1588-1596, 2014.

[68] L. Ren, S. Huang, C. Zhang, R. Wang, W. Tjiu, and T. Liu, "Functionalization of graphene and grafting of temperature-responsive surfaces from graphene by ATRP “on water”," *Journal of Nanoparticle Research*, vol. 14, pp. 1-9, 2012/06/08 2012.

[69] L. Ren, X. Wang, S. Guo, and T. Liu, "Functionalization of thermally reduced graphene by in situ atom transfer radical polymerization," *Journal of Nanoparticle Research*, vol. 13, pp. 6389-6396, 2011/12/01 2011.

[70] H. Roghani-Mamaqani, V. Haddadi-Asl, K. Khezri, and M. Salami-Kalajahi, "Edge-functionalized graphene nanoplatelets with polystyrene by atom transfer radical polymerization: grafting through carboxyl groups," *Polymer International,* pp. n/a-n/a, 2014.

[71] H. Roghani-Mamaqani, V. Haddadi-Asl, K. Khezri, E. Zeinali, and M. Salami-Kalajahi, "In situ atom transfer radical polymerization of styrene to in-plane functionalize graphene nanolayers: grafting through hydroxyl groups," *Journal of Polymer Research,* vol. 21, pp. 1-11, 2013/12/14 2013.

[72] D. Wang, G. Ye, X. Wang, and X. Wang, "Graphene Functionalized with Azo Polymer Brushes: Surface-Initiated Polymerization and Photoresponsive Properties," *Advanced Materials,* vol. 23, pp. 1122-1125, 2011.

[73] S. Zhu, J. Li, Y. Chen, Z. Chen, C. Chen, Y. Li, *et al.*, "Grafting of graphene oxide with stimuli-responsive polymers by using ATRP for drug release," *Journal of Nanoparticle Research,* vol. 14, pp. 1-11, 2012/08/25 2012.

[74] H. M. Etmimi and R. D. Sanderson, "Synthesis and Characterization of Polystyrene-Graphite Nanocomposites via Surface Raft-Mediated Polymerization," *Advanced Materials Research,* vol. 463-464, pp. 527-532, February, 2012 2012.

[75] H. M. Etmimi, M. P. Tonge, and R. D. Sanderson, "Synthesis and characterization of polystyrene-graphite nanocomposites via surface RAFT-mediated miniemulsion polymerization," *Journal of Polymer Science Part A: Polymer Chemistry,* vol. 49, pp. 1621-1632, 2011.

[76] Y. Huang, Y. Qin, Y. Zhou, H. Niu, Z.-Z. Yu, and J.-Y. Dong, "Polypropylene/Graphene Oxide Nanocomposites Prepared by In Situ Ziegler−Natta Polymerization," *Chemistry of Materials,* vol. 22, pp. 4096-4102, 2010/07/13 2010.

[77] S. M. Kang, S. Park, D. Kim, S. Y. Park, R. S. Ruoff, and H. Lee, "Simultaneous Reduction and Surface Functionalization of Graphene Oxide by Mussel-Inspired Chemistry," *Advanced Functional Materials*, vol. 21, pp. 108-112, 2011.

[78] J. Liu, C. Chen, C. He, J. Zhao, X. Yang, and H. Wang, "Synthesis of Graphene Peroxide and Its Application in Fabricating Super Extensible and Highly Resilient Nanocomposite Hydrogels," *ACS Nano,* vol. 6, pp. 8194-8202, 2012/09/25 2012.

[79] K. P. Pramoda, H. Hussain, H. M. Koh, H. R. Tan, and C. B. He, "Covalent bonded polymer–graphene nanocomposites," *Journal of Polymer Science Part A: Polymer Chemistry,* vol. 48, pp. 4262-4267, 2010.

[80] X. Wang, Y. Hu, L. Song, H. Yang, W. Xing, and H. Lu, "In situ polymerization of graphene nanosheets and polyurethane with enhanced mechanical and thermal properties," *Journal of Materials Chemistry,* vol. 21, pp. 4222-4227, 2011.

[81] F. Beckert, C. Friedrich, R. Thomann, and R. Mülhaupt, "Sulfur-Functionalized Graphenes as Macro-Chain-Transfer and RAFT Agents for Producing Graphene Polymer Brushes and Polystyrene Nanocomposites," *Macromolecules,* vol. 45, pp. 7083-7090, 2012/09/11 2012.

[82] L. Cui, J. Liu, R. Wang, Z. Liu, and W. Yang, "A facile "graft from" method to prepare molecular-level dispersed graphene–polymer composites," *Journal of Polymer Science Part A: Polymer Chemistry,* vol. 50, pp. 4423-4432, 2012.

[83] K. Jiang, C. Ye, P. Zhang, X. Wang, and Y. Zhao, "One-Pot Controlled Synthesis of Homopolymers and Diblock Copolymers Grafted Graphene Oxide Using Couplable RAFT Agents," *Macromolecules,* vol. 45, pp. 1346-1355, 2012/02/14 2012.

[84] Y. Li, X. Li, C. Dong, J. Qi, and X. Han, "A graphene oxide-based molecularly imprinted polymer platform for detecting endocrine disrupting chemicals," *Carbon,* vol. 48, pp. 3427-3433, 10// 2010.

[85] Y. Yang, X. Song, L. Yuan, M. Li, J. Liu, R. Ji, *et al.*, "Synthesis of PNIPAM polymer brushes on reduced graphene oxide based on click chemistry and RAFT

polymerization," *Journal of Polymer Science Part A: Polymer Chemistry,* vol. 50, pp. 329-337, 2012.

[86] Y.-S. Ye, Y.-N. Chen, J.-S. Wang, J. Rick, Y.-J. Huang, F.-C. Chang*, et al.*, "Versatile Grafting Approaches to Functionalizing Individually Dispersed Graphene Nanosheets Using RAFT Polymerization and Click Chemistry," *Chemistry of Materials*, vol. 24, pp. 2987-2997, 2012/08/14 2012.

[87] B. Zhang, Y. Chen, L. Xu, L. Zeng, Y. He, E.-T. Kang, *et al.*, "Growing poly(N-vinylcarbazole) from the surface of graphene oxide via RAFT polymerization," *Journal of Polymer Science Part A: Polymer Chemistry,* vol. 49, pp. 2043-2050, 2011.

[88] R. O. Ebewele, *Polymer Science and Technology*. New York: CRC Press LLC, 2000.

[89] W. A. Braunecker and K. Matyjaszewski, "Controlled/living radical polymerization: Features, developments, and perspectives," *Progress in Polymer Science,* vol. 32, pp. 93-146, 1// 2007.

[90] M. Szwarc, "Living Polymers," *Nature,* vol. 178, pp. 1168-1169, 1956.

[91] K. Matyjaszewski and T. P. Davis, *Handbook of Radical Polymerization*: John Wiley & Sons, Inc., 2003.

[92] K. Matyjaszewski, "Atom Transfer Radical Polymerization (ATRP): Current Status and Future Perspectives," *Macromolecules,* vol. 45, pp. 4015-4039, 2012/05/22 2012.

[93] A. Goto and T. Fukuda, "Kinetics of living radical polymerization," *Progress in Polymer Science,* vol. 29, pp. 329-385, 4// 2004.

[94] K. Matyjaszewski and J. Spanswick, "Controlled/living radical polymerization," *Materials Today,* vol. 8, pp. 26-33, 3// 2005.

[95] G. Moad, E. Rizzardo, and S. H. Thang, "Living Radical Polymerization by the RAFT Process," *Australian Journal of Chemistry,* vol. 58, pp. 379-410, 2005.

[96] G. Moad, E. Rizzardo, and S. H. Thang, "Living Radical Polymerization by the RAFT Process – A Second Update," *Australian Journal of Chemistry,* vol. 62, pp. 1402-1472, 2009.

[97] J. Chiefari, Y. K. Chong, F. Ercole, J. Krstina, J. Jeffery, T. P. T. Le*, et al.*, "Living Free-Radical Polymerization by Reversible Addition−Fragmentation Chain Transfer: The RAFT Process," *Macromolecules*, vol. 31, pp. 5559-5562, 1998/08/01 1998.

[98] C. J. Hawker, A. W. Bosman, and E. Harth, "New Polymer Synthesis by Nitroxide Mediated Living Radical Polymerizations," *Chemical Reviews,* vol. 101, pp. 3661-3688, 2001/12/01 2001.

[99] B. B. Wayland, G. Poszmik, S. L. Mukerjee, and M. Fryd, "Living Radical Polymerization of Acrylates by Organocobalt Porphyrin Complexes," *Journal of the American Chemical Society,* vol. 116, pp. 7943-7944, 1994/08/01 1994.

[100] J. P. Mendes, F. Branco, C. M. R. Abreu, P. V. Mendonça, A. V. Popov, T. Guliashvili, *et al.*, "Synergistic Effect of 1-Butyl-3-methylimidazolium Hexafluorophosphate and DMSO in the SARA ATRP at Room Temperature Affording Very Fast Reactions and Polymers with Very Low Dispersity," *ACS Macro Letters*, pp. 544-547, 2014.

[101] C. M. R. Abreu, P. V. Mendonca, A. C. Serra, A. V. Popov, K. Matyjaszewski, T. Guliashvili*, et al.*, "Inorganic Sulfites: Efficient Reducing Agents and Supplemental Activators for Atom Transfer Radical Polymerization," *ACS Macro Letters,* vol. 1, pp. 1308-1311, Nov 2012.

[102] P. V. Mendonca, A. C. Serra, J. F. J. Coelho, A. V. Popov, and T. Guliashvili, "Ambient temperature rapid ATRP of methyl acrylate, methyl methacrylate and styrene in polar solvents with mixed transition metal catalyst system," *European Polymer Journal,* vol. 47, pp. 1460-1466, Jul 2011.

[103] D. Konkolewicz, Y. Wang, P. Krys, M. Zhong, A. A. Isse, A. Gennaro*, et al.*, "SARA ATRP or SET-LRP. End of controversy?," *Polymer Chemistry,* 2014.

[104] W. Jakubowski and K. Matyjaszewski, "Activators Regenerated by Electron Transfer for Atom-Transfer Radical Polymerization of (Meth)acrylates and Related Block Copolymers," *Angewandte Chemie,* vol. 118, pp. 4594-4598, 2006.

[105] K. Matyjaszewski, W. Jakubowski, K. Min, W. Tang, J. Huang, W. A. Braunecker*, et al.*, "Diminishing catalyst concentration in atom transfer radical polymerization with reducing agents," *Proceedings of the National Academy of Sciences,* vol. 103, pp. 15309-15314, October 17, 2006 2006.

[106] S. Hosseiny and P. van Rijn, "Surface Initiated Polymerizations via e-ATRP in Pure Water," *Polymers,* vol. 5, pp. 1229-1240, 2013.

[107] N. Bortolamei, A. A. Isse, A. J. D. Magenau, A. Gennaro, and K. Matyjaszewski, "Controlled Aqueous Atom Transfer Radical Polymerization with Electrochemical Generation of the Active Catalyst," *Angewandte Chemie International Edition,* vol. 50, pp. 11391-11394, 2011.

[108] M. J. Sienkowska, B. M. Rosen, and V. Percec, "SET-LRP of vinyl chloride initiated with CHBr3 in DMSO at 25 °C," *Journal of Polymer Science Part A: Polymer Chemistry,* vol. 47, pp. 4130-4140, 2009.

[109] M. P. Group. (27-08-2014). Available: http://www.cmu.edu/maty/atrp-how/procedures-for-initiation-of-ATRP/aget-atrp.html.

[110] J. P. Mendes, F. Branco, C. M. R. Abreu, P. V. Mendonça, A. C. Serra, A. V. Popov*, et al.*, "Sulfolane: an Efficient and Universal Solvent for Copper-Mediated Atom Transfer Radical (co)Polymerization of Acrylates, Methacrylates, Styrene, and Vinyl Chloride," *ACS Macro Letters,* pp. 858-861, 2014.

[111] D. Baskaran, J. W. Mays, and M. S. Bratcher, "Polymer-Grafted Multiwalled Carbon Nanotubes through Surface-Initiated Polymerization," *Angewandte Chemie International Edition,* vol. 43, pp. 2138-2142, 2004.

[112] Z. Yao, N. Braidy, G. A. Botton, and A. Adronov, "Polymerization from the Surface of Single-Walled Carbon Nanotubes − Preparation and Characterization of Nanocomposites," *Journal of the American Chemical Society,* vol. 125, pp. 16015-16024, 2003/12/01 2003.

[113] S. B. Lee, R. R. Koepsel, S. W. Morley, K. Matyjaszewski, Y. Sun, and A. J. Russell, "Permanent, Nonleaching Antibacterial Surfaces. 1. Synthesis by Atom Transfer Radical Polymerization," *Biomacromolecules,* vol. 5, pp. 877-882, 2004/05/01 2004.

[114] K. Matyjaszewski, P. J. Miller, N. Shukla, B. Immaraporn, A. Gelman, B. B. Luokala, *et al.*, "Polymers at Interfaces: Using Atom Transfer Radical Polymerization in the Controlled Growth of Homopolymers and Block Copolymers from Silicon Surfaces in the Absence of Untethered Sacrificial Initiator," *Macromolecules,* vol. 32, pp. 8716-8724, 1999/12/01 1999.

[115] H. Zhao, X. Kang, and L. Liu, "Comb−Coil Polymer Brushes on the Surface of Silica Nanoparticles," *Macromolecules,* vol. 38, pp. 10619-10622, 12/01 2005.

[116] S. Etienne, C. Becker, D. Ruch, B. Grignard, G. Cartigny, C. Detrembleur*, et al.*, "Effects of incorporation of modified silica nanoparticles on the mechanical and thermal properties of PMMA," *Journal of Thermal Analysis and Calorimetry,* vol. 87, pp. 101-104, 2007/01/01 2007.

[117] Y. Chen, C. Wang, J. Chen, X. Liu, and Z. Tong, "Growth of lightly crosslinked PHEMA brushes and capsule formation using pickering emulsion interface-initiated ATRP," *Journal of Polymer Science Part A: Polymer Chemistry,* vol. 47, pp. 1354-1367, 2009.

[118] J.-L. Chen and X.-P. Yan, "A dehydration and stabilizer-free approach to production of stable water dispersions of graphene nanosheets," *Journal of Materials Chemistry,* vol. 20, pp. 4328-4332, 2010.

[119] O. C. Compton, D. A. Dikin, K. W. Putz, L. C. Brinson, and S. T. Nguyen, "Electrically Conductive "Alkylated" Graphene Paper via Chemical Reduction of Amine-Functionalized Graphene Oxide Paper," *Advanced Materials,* vol. 22, pp. 892-896, 2010.

[120] Y. Chen, Q. Zhuang, X. Liu, J. Liu, S. Lin, and Z. Han, "Preparation of thermostable PBO/graphene nanocomposites with high dielectric constant," *Nanotechnology,* vol. 24, p. 245702, Jun 21 2013.

[121] S. K. Singh, M. K. Singh, P. P. Kulkarni, V. K. Sonkar, J. J. A. Grácio, and D. Dash, "Amine-Modified Graphene: Thrombo-Protective Safer Alternative to Graphene Oxide for Biomedical Applications," *ACS Nano,* vol. 6, pp. 2731-2740, 2012/03/27 2012.

[122] S. A. Lawrence, *Amines: Synthesis, Properties and Applications*. United Kingdom: Cambridge University Press, 2004.

[123] B. Optics, "Guide for Infrared Spectroscopy," GuideIFS.pdf, Ed., ed. http://www.bruker.com/nc/products/infrared-near-infrared-and-raman-spectroscopy/opus-software/downloads.html?cid=13999&did=50363&sechash=d949e96a: Bruker Optics, 2011.

[124] C. K. Chua and M. Pumera, "Renewal of sp2 bonds in graphene oxides via dehydrobromination," *Journal of Materials Chemistry,* vol. 22, pp. 23227-23231, 2012.

[125] J. Wang, S. Liang, L. Ma, S. Ding, X. Yu, L. Zhou*, et al.*, "One-pot synthesis of CdS-reduced graphene oxide 3D composites with enhanced photocatalytic properties," *CrystEngComm,* vol. 16, pp. 399-405, 2014.

[126] C. M. R. Abreu, A. C. Serra, A. V. Popov, K. Matyjaszewski, T. Guliashvili, and J. F. J. Coelho, "Ambient temperature rapid SARA ATRP of acrylates and methacrylates in alcohol-water solutions mediated by a mixed sulfite/Cu(ii)Br2 catalytic system," *Polymer Chemistry,* vol. 4, pp. 5629-5636, 2013.

[127] V. Percec, T. Guliashvili, J. S. Ladislaw, A. Wistrand, A. Stjerndahl, M. J. Sienkowska, *et al.*, "Ultrafast Synthesis of Ultrahigh Molar Mass Polymers by Metal-Catalyzed Living Radical Polymerization of Acrylates, Methacrylates, and Vinyl Chloride Mediated by SET at 25 °C," *Journal of the American Chemical Society,* vol. 128, pp. 14156-14165, 2006/11/01 2006.

[128] Y. Zhang, Y. Wang, and K. Matyjaszewski, "ATRP of Methyl Acrylate with Metallic Zinc, Magnesium, and Iron as Reducing Agents and Supplemental Activators," *Macromolecules,* vol. 44, pp. 683-685, Feb 22 2011.

[129] C. M. R. Abreu, P. V. Mendonca, A. C. Serra, J. F. J. Coelho, A. V. Popov, and T. Guliashvili, "Accelerated Ambient-Temperature ATRP of Methyl Acrylate in Alcohol-Water Solutions with a Mixed Transition-Metal Catalyst System," *Macromolecular Chemistry and Physics,* vol. 213, pp. 1677-1687, Aug 28 2012.

[130] T. Biedroń and P. Kubisa, "Atom transfer radical polymerization of acrylates in an ionic liquid: Synthesis of block copolymers," *Journal of Polymer Science Part A: Polymer Chemistry,* vol. 40, pp. 2799-2809, 2002.

[131] T. Guliashvili, P. V. Mendonça, A. C. Serra, A. V. Popov, and J. F. J. Coelho, "Copper-Mediated Controlled/"Living" Radical Polymerization in Polar Solvents: Insights into Some Relevant Mechanistic Aspects," *Chemistry – A European Journal,* vol. 18, pp. 4607-4612, 2012.

[132] M. Kumar, J. S. Chung, and S. H. Hur, "Controlled atom transfer radical polymerization of MMA onto the surface of high-density functionalized graphene oxide," *Nanoscale Research Letters,* vol. Volume 9, p. 9:345, 2014.

[133] M. P. Group. (15-08-2014).

[134] N. Rocha, P. V. Mendonca, J. P. Mendes, P. N. Simoes, A. V. Popov, T. Guliashvili*, et al.*, "Facile Synthesis of Well-Defined Telechelic Alkyne-Terminated Polystyrene in

Polar Media Using ATRP With Mixed Fe/Cu Transition Metal Catalyst," *Macromolecular Chemistry and Physics*, vol. 214, pp. 76-84, Jan 11 2013.

[135] F. R. Mayo, "The dimerization of styrene," *Journal of the American Chemical Society*, vol. 90, pp. 1289-1295, 1968/02/01 1968.

[136] K. S. Khuong, W. H. Jones, W. A. Pryor, and K. N. Houk, "The Mechanism of the Self-Initiated Thermal Polymerization of Styrene. Theoretical Solution of a Classic Problem," *Journal of the American Chemical Society*, vol. 127, pp. 1265-1277, 2005/02/01 2005.

[137] F. Seeliger and K. Matyjaszewski, "Temperature Effect on Activation Rate Constants in ATRP: New Mechanistic Insights into the Activation Process," *Macromolecules*, vol. 42, pp. 6050-6055, 2009/08/25 2009.

[138] W. Brostow, T. Datashvili, and P. Hackenberg Ken, "Synthesis and Characterization of Poly(methyl acrylate) + SiO2 Hybrids," in *e-Polymers* vol. 8, ed, 2008, p. 608.

[139] F. A. Carey, *Organic Chemistry*, 4th edition ed. United States of America: Mcgraw-Hill College, 2000.

[140] M. Ciampolini and N. Nardi, "Five-Coordinated High-Spin Complexes of Bivalent Cobalt, Nickel, andCopper with Tris(2-dimethylaminoethyl)amine," *Inorganic Chemistry*, vol. 5, pp. 41-44, 1966/01/01 1966.

[141] P. M. L. Cardoso, "Síntese de derivados de aminoácidos: ligandos quirais para catálise enantiosselectiva," Mestrado, Quimica, Universidade de Coimbra, 2010.

[142] C. Kang, R. M. Crockett, and N. D. Spencer, "Molecular-Weight Determination of Polymer Brushes Generated by SI-ATRP on Flat Surfaces," *Macromolecules*, vol. 47, pp. 269-275, 2014/01/14 2013.

[143] V. Georgakilas, A. B. Bourlinos, R. Zboril, T. A. Steriotis, P. Dallas, A. K. Stubos, *et al.*, "Organic functionalisation of graphenes," *Chemical Communications*, vol. 46, pp. 1766-1768, 2010.

[144] M. P. Group. (01-09-2014).

[145] M. Husseman, E. E. Malmström, M. McNamara, M. Mate, D. Mecerreyes, D. G. Benoit, *et al.*, "Controlled Synthesis of Polymer Brushes by “Living” Free Radical Polymerization Techniques," *Macromolecules*, vol. 32, pp. 1424-1431, 1999/03/01 1999.

[146] M. P. Group. (12 - 08 - 2014). Available: http://www.cmu.edu/maty/materials/Properties-of-well-defined/surfaces.html

Appendices

Appendix A – Methods to produce GO

.

Table A1. Main oxidation methods to prepare GO. Contents adapted from reference [40].

Method	Reactants	Reaction Time	Final C:O Ratio
Modified Hummers	NaNO3, KMnO4 and H2SO4	5 days	1.8
	K2S2O8, P2O5, H2SO4 KMnO4 and H2SO4	4 to 24 hours	1.3
Hummers	NaNO3, KMnO4 and H2SO4	2 to 10 hours	~2.20
Staudenmaier	KClO3, HNO3 and H2SO4	1 to 10 days	1.85
Brodie	KClO3 and HNO3	10 hours to 4 days	~ 2.20

Appendix B – Determination of the conversion, $M_{n,th}$ and k_p^{app}

Throughout this dissertation monomer conversions, theoretical number average molecular weights, $M_{n,th}$, and apparent propagation rates, k_p^{app}, values were presented, mainly in Appendices C to F and section 2.2. Such values were determined from the ^{1}H NMR results acquired from the kinetics studies realized to some of the CLRP reactions carried out during the experimental work. It is important to note that to determine these parameters it was necessary to collect diverse samples of the reaction mixtures at different times during the polymerizations. In this Appendix are shown examples to explain the reasoning and calculations realized to determine such important parameters.

- **Monomer conversion**

The conversion of monomer was calculated following the next equations:

$$Conversion = \frac{moles\ of\ polymer}{moles\ of\ polymer + moles\ monomer}$$

$$= 1 - \frac{moles\ of\ monomer}{moles\ of\ polymer + moles\ of\ monomer}$$

Monomer conversions were monitored using ^{1}H NMR spectroscopy. The areas of the peaks representing monomer and polymer protons are related to the amounts (concentration) of monomer and polymer existing in the sample analysed. Considering that the samples were extracted from the reaction mixtures and directly analysed, concentrations of monomer and polymer in the samples were equal to the concentrations of monomer and polymer in the reaction mixtures when the samples were collected. Through the relation between the areas of the peaks (determined by integration) representing monomer and the areas of the peaks representing polymer was possible to determine the monomer conversions for the various samples collected at different reaction times.

To better illustrate this, bellow are shown the procedures realized to determine the monomer conversion corresponding to one sample extracted from a SARA ATRP of MA.

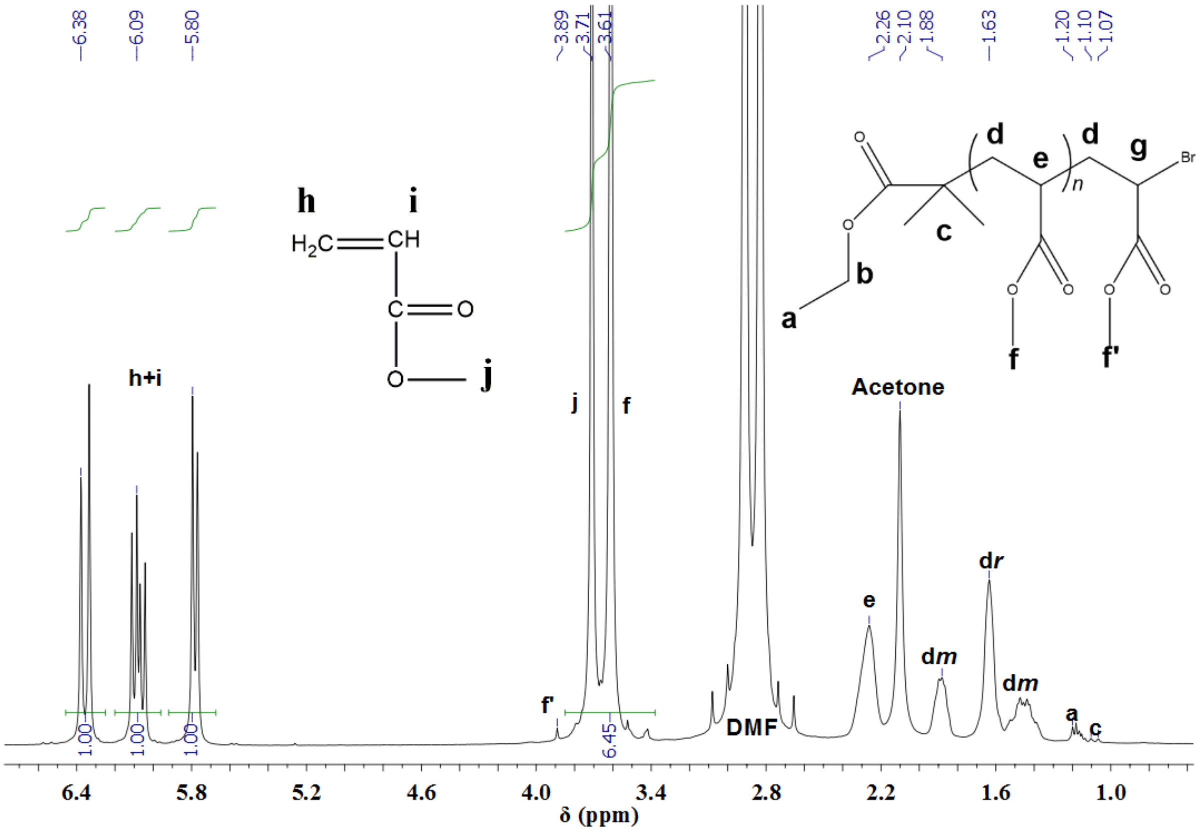

Figure B1. ^{1}H NMR of a sample collected during the SARA ATRP of MA in DMF, used to determine monomer conversion and $M_{n,th}$.

Monomer conversion of the sample presented in Figure B1 was determined using the integrals of the peaks at about 6.38, 6.09, 5.80 due to three protons **h** and **i** from MA monomer, using the integral of the peak at 3.71 ppm due to protons **j** from MA and the integral of the peaks at 3.61 and 3.89 ppm due to **f** and **f'** protons from PMA. Conversion was calculated through the equation presented as follow.

$$Conversion\ (\%) = 1 - \frac{(\int 6.38\, peak + \int 6.09\, peak + \int 5.80\, peak)/3}{(\int 3.89\, peak + \int 3.71\, peak + \int 3.61\, peak)/3} \times 100$$

$$= 1 - \frac{(1.00 + 1.00 + 1.00)/3}{6.45/3} \times 100 = 53\ \%$$

The previous calculations were made for the different samples collected.

- **Theoretical number average molecular weight, $M_{n,th}$**

After the calculation of the monomer conversions, theoretical number average molecular weights, $M_{n,th}$, were determined following the next equation.

$$M_{n,th} = Conversion \times DP \times M_{monomer} + M_{Initiator}$$

Using as example the results from the sample corresponding to the ^{1}H NMR of Figure B1,

$$M_{n,th} = 0.53 \times 494 \times 86.09 + 195.05 = 22.735\ kDa$$

As previously done with the conversions, $M_{n,th}$ was determined for the diverse collected samples.

- **Apparent propagation rate, k_p^{app}**

According to the mechanism of controlled/living radical polymerization, the reactions should present a first-order kinetics with respect to monomer concentration, which means that in semi logarithmic coordinates it must present a linear kinetic plot, as shown in Figure B2, and the progation rate, k_p^{app}, corresponds to the slope of the linear curve [89, 92].

Considering the mechanism of CLRP, the measured propagation rates were determined through the representation of $\ln([M_0]/[M])$ vs time. $\ln([M_0]/[M])$ was calculated through the equation:

$ln([M_0]/[M]) = 1 - Conversion$, with the conversions determined for the different collected samples.

Note that “Conversion” is the monomer conversion previously calculated. A linear regression was employed to the diverse points and the apparent propagation rates were found from the slope of the fitting line, as exemplified in Figure B2.

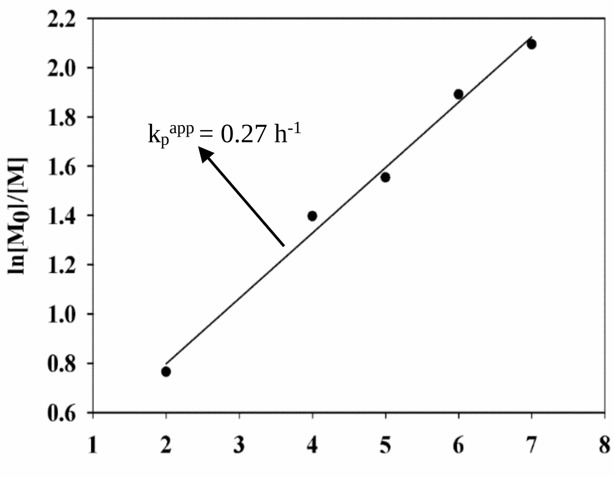

Figure B2. Example of a kinetic plot of ln[M$_0$]/[M] vs Time used to evaluate the first-order kinetic of the reaction with respect to the monomer concentration and to determine the k_p^{app}.

Appendix C – Article "Synergistic Effect of 1-Butyl-3-methylimidazolium Hexafluorophosphate and DMSO in the SARA ATRP at Room Temperature Affording Very Fast Reactions and Polymers with Very Low Dispersity"

The content of this Appendix are published in J. P. Mendes, F. Branco, C. M. R. Abreu, P. V. Mendonça, A. V. Popov, T. Guliashvili, et al., "Synergistic Effect of 1-Butyl-3-methylimidazolium Hexafluorophosphate and DMSO in the SARA ATRP at Room Temperature Affording Very Fast Reactions and Polymers with Very Low Dispersity," ACS Macro Letters, pp. 544-547, 2014.

Synergistic effect of 1-butyl-3-methylimidazolium hexafluorophosphate and DMSO in the SARA ATRP at room temperature affording very fast reactions and polymers with very low dispersity

Joana P. Mendes[†], Fábio Branco[†], Carlos M. R. Abreu[†], Patrícia V. Mendonça[†], Anatoliy V. Popov[‡], Tamaz Guliashvili[†]*, Arménio C. Serra[†] and Jorge F. J. Coelho[†]*

† CEMUC, Department of Chemical Engineering, University of Coimbra, 3030-790 Coimbra, Portugal

‡ Department of Radiology, University of Pennsylvania, Philadelphia, PA 19104, USA

ABSTRACT: An unusual synergistic effect between 1-butyl-3-methylimidazolium hexafluorophosphate (BMIM-PF_6) and dimethyl sulfoxide (DMSO) mixtures is reported for the supplemental activator and reducing agent atom transfer radical polymerization (SARA ATRP) of methyl acrylate (MA) using a catalytic system composed by sodium dithionate ($Na_2S_2O_4$) and $CuBr_2$/Me_6TREN (Me_6TREN: tris[2-(dimethylamino)ethyl]amine) at room temperature. To the best of our knowledge, the use of ionic liquids (IL) has never been reported for the SARA ATRP. The kinetic data obtained for a broad range of target molecular weights revealed very fast polymerization rates, low dispersity values (*Đ* < 1.05) and well-defined chain-end functionalities.

Atom transfer radical polymerization (ATRP) is one the most efficient, versatile and robust reversible deactivation radical polymerization (RDRP) techniques.[1] This method allows the synthesis of polymers having a vast range of specific functionalities with controlled molecular weight, architecture and topology.[2] ATRP is based on the use of a transition metal complex which mediates a fast equilibrium between dormant and active species (Scheme 1).

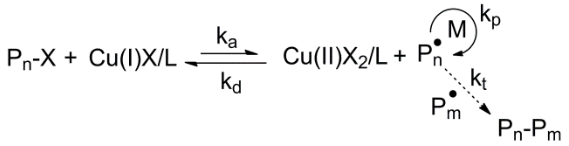

Scheme 1. General mechanism of ATRP.

Several transition metal complexes in combination with different ligands (typically nitrogen-based ligands) have been employed in ATRP,[3] being Cu-based the most used ones.[4] Aiming to reduce the amount of metal complexes required to control the polymerizations, new ATRP variations were proposed, such as: activators regenerated by electron transfer (ARGET) ATRP using inorganic or organic reducing agents;[5, 6] supplemental activator and reducing agent (SARA) ATRP involving the use of zerovalent transition metals[3, 5, 7-9] or inorganic sulfites;[10-12] initiators for continuous activator regeneration (ICAR) ATRP employing conventional thermal radical initiators; and electrochemically mediated ATRP (*e*-ATRP) that uses electrical current for the reduction process.[13] The use of reducing agents allows the continuous regeneration of Cu(I) species during the polymerization, lowering the amount of catalyst to ppm levels. Ionic liquids (IL) are a class of green solvents[14-16] that present important advantages over several conventional and harmful organic solvents. Among those, one can stress the possibility of tailoring the properties of the IL by varying the structures of both cation and anion, excellent solubility of polar substrates, low volatility, recyclability and compatibility with various organic compounds. Since the pioneer works of Haddleton,[17] Kubisa[18] and Matyjaszewski,[19] several reports have been published using IL as solvents for ATRP.[16, 20-23] The results revealed interesting features of these green solvents related to simplified separation of the polymer from the catalyst,[17, 19] controlled reactions in the absence of ligand, reduction of side reactions and catalytic effects.[20]

Here, we report the synergistic effect of dimethyl sulfoxide (DMSO) and 1-butyl-3-methylimidazolium hexafluorophosphate (BMIM-PF_6) in the SARA ATRP of methyl acrylate (MA) catalyzed by $Na_2S_2O_4$ and small amounts of $CuBr_2$/Me_6TREN (Me_6TREN: tris[2-(dimethylamino)ethyl]amine) deactivator complex at room temperature.

Preliminary experiments were performed using only BMIM-PF_6 as solvent for the MA polymerization, but no polymer was formed. This result can be justified based on the partial solubilization of the CuBr2/Me$_6$TREN complex and, most importantly, to the complete insolubility of the SARA agent ($Na_2S_2O_4$) in the BMIM-PF6, preventing the formation of Cu(I) activator species. With the introduction of DMSO as a co-solvent a controlled polymerization was observed. The kinetic plots of SARA ATRP carried out at room temperature in BMIM-PF$_6$/DMSO (ratio 5/95 and 50/50) catalyzed by $Na_2S_2O_4$/$CuBr_2$/Me$_6$TREN are presented in Figure 1 (a) and (b) and Table 1 (entry 2 and 4), respectively. The rate of polymerization (Figure 1) was first-order with respect to the concentration of monomer and the final conversion was close to 100%. The theoretical molecular weights were in very close agreement with $M_{n,GPC}$ for the full range of monomer conversions, which indicates a quantitative initiation and an excellent control during the entire course of the polymerization (Figure S1). Interesting, for a ratio BMIM-PF$_6$/DMSO of 50/50 (Figure 1 (b), Table 1 entry 4), the kinetic data allowed us to draw the same conclusions as the ones obtained for a ratio of 5/95. However, the reaction rate was 3 times faster for the ratio 50/50 (6 times faster than the obtained for pure DMSO, Table 1 entry 1). In order to determine the optimal ratio BMIM-PF$_6$/DMSO to afford fast polymerization while maintaining the living characteristics of the system, different ratios were investigated (Figure 2, Figure S2, Table 1, entries 1 to 6). Regardless the solvent ratio studied the control over the SARA ATRP of MA was perfect (*Đ* always below 1.07). Indeed, the only observed difference was the overall polymerization rate, which as refereed above was faster for the ratio DMSO/IL = 50/50. It is interesting to note that this ratio represents an optimum value for the mixture, which suggests that there is a synergistic effect between the two solvents (Figure S2).

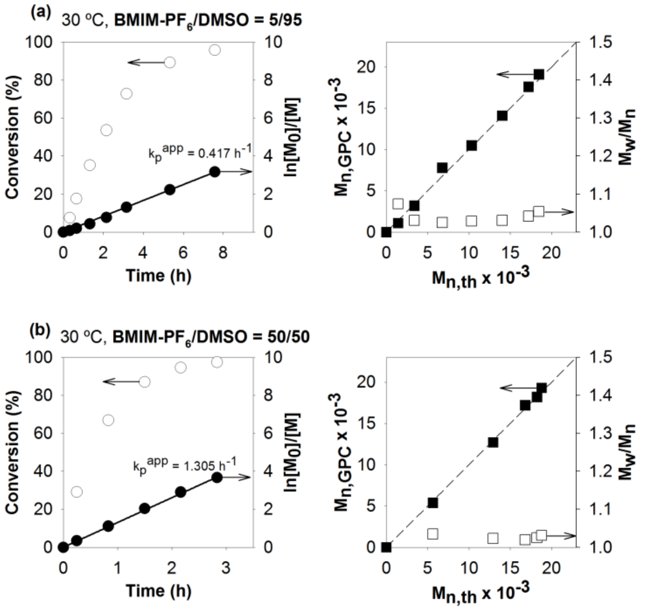

Figure 1. Kinetic plots of conversion and ln$[M]_0/[M]$ *vs*. time and plots of number average molecular weights ($M_{n,GPC}$) and *Đ* (M_w/M_n) *vs*. theoretical number average molecular weights ($M_{n,th}$) for the SARA ATRP of MA catalyzed by $Na_2S_2O_4$/$CuBr_2$//Me$_6$TREN in (a) BMIM-PF6/DMSO = 5/95 and (b) BMIM-PF$_6$/DMSO = 50/50. Conditions: $[MA]_0$/[solvent] = 2/1(v/v); $[MA]_0/[EBiB]_0/[Na_2S_2O_4]_0/[CuBr_2]_0/[Me_6TREN]_0$ = 222/1/1/0.1/0.1 (molar); T = 30 °C.

Considering the perfect miscibility of the BMIM-PF$_6$ and DMSO for the different mixtures, it is believed that the polarity values of the mixture may play an important role in the kinetics of the polymerization. In this regard, it was reported that mixtures of BMIM-PF$_6$ and tetraethylene glycol (TEG) exhibit unusual synergistic solvent effect, particularly a remarkable “hyperpolarity” for the mixture. In the presence of solvatochromic probes, as $E_T(33)$, polarity of the medium is always higher in the mixtures than in pure solvents reaching a maximum value for equimolar mixtures of the two solvents.[24]

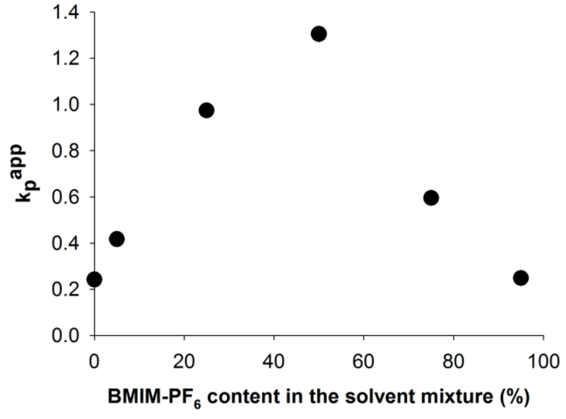

Figure 2. k_p^{app} values of the SARA ATRP of MA catalyzed by $Na_2S_2O_4$/$CuBr_2$/Me$_6$TREN in BMIM-PF$_6$/DMSO mixtures, for

different contents of BMIM-PF_6 in the reaction mixture. Conditions: $[MA]_0/[solvent] = 2/1$ (v/v); $[MA]_0/[EBiB]_0/[Na_2S_2O_4]_0/[CuBr_2]_0/[Me_6TREN]_0 = 222/1/1/0.1/0.1$ (molar); T = 30 °C

Using this analogy, absorbance spectra of Reichardt's dye (3o) were collected in BMIM-PF_6/DMSO (Figure S3) mixtures, showing that value of $E_T(30)$ for the different mixtures exceeds the value predicted by the simple mixture indicating that some synergistic effect occurs. On the other hand, the kinetic data using tetrabutylammonium hexafluorophosphate ($TBAPF_6$) was determined in order to evaluate if the previous results were due to the BMIM-PF_6 structure, or the speed up effect could be mainly due to the anion (PF_6). Using ratio $TBAPF_6$/DMSO (6/94) (Figure S4) the obtained k_p^{app} was 0.295 h^{-1}, higher than using pure DMSO but much lower than the value obtained for a mixture BMIM-PF_6/DMSO (5/95).

The effect of the target molecular weight on the control over the polymerization is a critical parameter that should be evaluated, since it could lead to possible solubility issues of the polymer in the reaction mixture. Therefore different targeted degrees of polymerization (DP) were investigated for the SARA ATRP of MA (Figure S5, Table 1 entries 4, 7 and 8) using a BMIM-PF_6/DMSO ratio of 50/50. As expected, the polymerization rate was higher for lower DP values, due to the higher number of growing radicals. It is worthwhile to mention that even for the highest DP = 1100, the PMA dispersity values remained very low ($Đ$ = 1.04). Additionally, a 4-arm initiator was used to evaluate the potential of the polymerization method in the synthesis of 4-arm star PMA (Figure S6). The results obtained regarding the kinetic data were similar to the ones described for the monofunctional initiator (Figure S7). Again, the final dispersity obtained for the star-shaped PMA was very low ($Đ$ = 1.04). On this matter, it should be mentioned that the GPC apparatus used is equipped with multi-detectors (light scattering, viscosimeter and refractive index), which allows a very accurate determination of the molecular weights, without the use of common calibration curves.[25] Table 1 summarizes the kinetic data obtained for SARA ATRP of MA in the presence of $Na_2S_2O_4/CuBr_2/Me_6TREN$ in BMIM-PF_6/DMSO mixtures at 30 °C. Independently of the BMIM-PF_6/DMSO ratio used, the polymer architecture or the target molecular weight, the reported system allowed the synthesis of well-defined PMA at room temperature with very low dispersity ($Đ < 1.1$) below the reported values using the same IL.[18] The efficiency of initiation is always close 100 %.

The level of control obtained under the different polymerization conditions investigated should be a direct consequence of three main aspects: high propagation rates; absence of side reactions, and fast reduction of Cu(II) species to Cu(I). On this matter, the use of IL is known to decrease the activation energy involved in the propagation steps due to high polarity.[26] The increase in the rate of polymerization was postulated based on a complex formation between the growing radicals and the IL.[27] The hypothesis was later confirmed by showing that when chiral IL were used more isotactic sequences were formed.[21] In contrast, the termination rate decreases[18] due to higher viscosity limiting the diffusion of radicals.[26] In order to evaluate viscosity of the solvent mixture BMIM-PF_6/DMSO, rheology tests were carried out (Figure S8). Indeed, it was observed no relevant variation of the viscosity up to a ratio 50/50. However, for higher contents of BMIM-PF_6 the increase of viscosity was found exponential. These results show that the observed maximum rate of polymerization (k_p^{app}) at 50/50 vol. % composition of BMIM-PF_6 /DMSO cannot be simply explained solely based on the viscosity changes and hence k_p/k_t value increase. We believe that while IL favors k_p/k_t increase (well-known fact), the role of DMSO seems to be more complex. Besides the influence on the reduction rate of Cu(II) to Cu(I) (highest rate observed for ratio 50/50– see Figure S9), the DMSO may also have an important role on the mechanism involving the radical generation. The data presented in this work suggests that the ideal balance of different factors described is observed for a ratio 50/50. The clear understanding of the full mechanism requires additional studies.

Table 1. Kinetic data for the SARA ATRP of MA in BMIM-PF$_6$/DMSO mixtures. Conditions: [MA]$_0$/[solvent] = 2/1 (v/v); [MA]$_0$/[EBiB]$_0$/[Na$_2$S$_2$O$_4$]$_0$/[CuBr$_2$]$_0$/[Me$_6$TREN]$_0$ = 222/1/1/0.1/0.1; T = 30 °C.

Entry	*BMIM-PF$_6$/DMSO ratio*	*Targeted DP*	*k_p^{app} (h^{-1})*	*Time (h)*	*Conv. (%) [a]*	*$M_{n,th}$ x 10^{-3} [a]*	*$M_{n,GPC}$ x 10^{-3} [a]*	*Đ*
1	*0/100*	*222*	*0.242*	*14*	*97*	*18.7*	*20.7*	*1.04*
2	*5/95*	*222*	*0.417*	*7.5*	*96*	*18.5*	*19.1*	*1.05*
3	*25/75*	*222*	*0.974*	*3.6*	*97*	*18.7*	*20.20*	*1.04*
4	*50/50*	*222*	*1.305*	*2.8*	*98*	*18.8*	*19.3*	*1.03*
5	*75/25*	*222*	*0.595*	*5.9*	*97*	*18.7*	*19.5*	*1.03*
6	*95/5*	*222*	*0.248*	*10.5*	*93*	*17.9*	*19.1*	*1.07*
7	*50/50*	*100*	*1.588*	*1.7*	*93*	*8.20*	*8.30*	*1.04*
8	*50/50*	*1100*	*0.053*	*23*	*58*	*56,1*	*51,2*	*1.04*

[a] Maximum monomer conversion obtained in the reaction

The “living” nature of the PMA-Br synthetized by the reported method was confirmed by doing a chain extension experiment (Figure S10), showing the complete movement of the macroiniatior GPC ($M_{n,GPC}$ = 6.9 x 10^3, *Đ* = 1.05) trace towards high molecular weight fractions. The chemical structure of the PMA-Br ($M_{n,GPC}$ = 6.9 x 10^3, *Đ* = 1.05) synthesized by SARA ATRP in BMIM-PF$_6$/DMSO = 50/50 was analyzed by and MALDI-TOF (Figures S11 and S12) and ^{1}H NMR spectroscopy (Figure S13). The results confirmed the expected structure and a high degree of chain-end functionality (92 %).

In conclusion, a synergistic effect of BMIM-PF$_6$/DMSO in the SARA ATRP of MA using Na$_2$S$_2$O$_4$/CuBr$_2$/Me$_6$TREN as the catalytic system is reported. The polymerization system allowed very fast polymerizations for a broad range of targeted molecular weights leading to polymers with very low dispersity values (*Đ* < 1.1).

ASSOCIATED CONTENT

Supporting Information. Materials, techniques, procedures, kinetic data and PMA ^{1}H NMR spectrum and MALDI-TOF data. This material is available free of charge via the Internet at http://pubs.acs.org.

AUTHOR INFORMATION

Corresponding Author

* Jorge F. J. Coelho – Email address: jcoelho@eq.uc.pt.
* Tamaz Guliashvili – Email address: tamazguliasvili@yahoo.com

Author Contributions

The manuscript was written through contributions of all authors. / All authors have given approval to the final version of the manuscript. / ‡These authors contributed equally.

Notes

The authors declare no competing financial interest

ACKNOWLEDGMENT

PVM acknowledges FCT-MCTES for her PhD scholarship (SFRH/BD/69152/2010). C.M.R.A. acknowledges FCT-MCTES for his Ph.D. scholarship (SFRH/BD/88528/2012). The authors acknowledge FCT-MCTES for funding (PTDC/EQU-EPR/098662/2008 and PTDC/EQU-EPR/114354/2009). The MALDI-TOF-MS data were obtained by Dr. Manuel Marcos Garcia and Dr. Paula Alvarez Chaver at Unidad de Espectrometria de Masas do Servicio de Determinación Estructural, Proteómica y Genómica, Centro de Apoyo Científico y Tecnologico a la Investigación (CACTI, University of Vigo, Spain). The ^{1}H NMR data were obtained at the Nuclear Magnetic Resonance Laboratory of the Coimbra Chemistry Centre (http://www.nmrccc.uc.pt), University of Coimbra, supported in part by grant REEQ/481/QUI/2006 from FCT, POCI-2010 and FEDER, Portugal. AVP’s research reported in this publication was supported by the National Center for Advancing Translational Sciences of the National Institutes of Health under award number UL1TR000003.

REFERENCES

1. Matyjaszewski, K. *Macromolecules* **2012,** 45, (10), 4015-4039.
2. Ouchi, M.; Terashima, T.; Sawamoto, M. *Chemical Reviews* **2009,** 109, (11), 4963-5050.
3. Mendonca, P. V.; Serra, A. C.; Coelho, J. F. J.; Popov, A. V.; Guliashvili, T. *European Polymer Journal* **2011,** 47, (7), 1460-1466.
4. Guliashvili, T.; Mendonça, P. V.; Serra, A. C.; Popov, A. V.; Coelho, J. F. J. *Chemistry – A European Journal* **2012,** 18, (15), 4607-4612.
5. Zhang, Y.; Wang, Y.; Matyjaszewski, K. *Macromolecules* **2011,** 44, (4), 683-685.
6. Jakubowski, W.; Min, K.; Matyjaszewski, K. *Macromolecules* **2005,** 39, (1), 39-45.
7. Abreu, C. M. R.; Mendonca, P. V.; Serra, A. C.; Coelho, J. F. J.; Popov, A. V.; Guliashvili, T. *Macromolecular Chemistry and Physics* **2012,** 213, (16), 1677-1687.
8. Cordeiro, R. A.; Rocha, N.; Mendes, J. P.; Matyjaszewski, K.; Guliashvili, T.; Serra, A. C.; Coelho, J. F. J. *Polymer Chemistry* **2013,** 4, (10), 3088-3097.
9. Rocha, N.; Mendonca, P. V.; Mendes, J. P.; Simoes, P. N.; Popov, A. V.; Guliashvili, T.; Serra, A. C.; Coelho, J. F. J. *Macromolecular Chemistry and Physics* **2013,** 214, (1), 76-84.
10. Abreu, C. M. R.; Mendonca, P. V.; Serra, A. C.; Popov, A. V.; Matyjaszewski, K.; Guliashvili, T.; Coelho, J. F. J. *ACS Macro Letters* **2012,** 1, (11), 1308-1311.
11. Abreu, C. M. R.; Serra, A. C.; Popov, A. V.; Matyjaszewski, K.; Guliashvili, T.; Coelho, J. F. J. *Polymer Chemistry* **2013,** 4, (23), 5629-5636.
12. Gois, J. R.; Rocha, N.; Popov, A.; Guliashvili, T.; Matyjaszewski, K.; Serra, A. C.; Coelho, J. *Polymer Chemistry* **2014**.
13. Magenau, A. J. D.; Strandwitz, N. C.; Gennaro, A.; Matyjaszewski, K. *Science* **2011,** 332, (6025), 81-84.
14. G. Huddleston, J.; D. Rogers, R. *Chemical Communications* **1998**, (16), 1765-1766.
15. Wheeler, C.; West, K. N.; Liotta, C. L.; Eckert, C. A. *Chemical Communications* **2001**, (10), 887-888.
16. Erdmenger, T.; Guerrero-Sanchez, C.; Vitz, J.; Hoogenboom, R.; Schubert, U. S. *Chemical Society Reviews* **2010,** 39, (8), 3317-3333.
17. Carmichael, A. J.; Haddleton, D. M.; Bon, S. A. F.; Seddon, K. R. *Chemical Communications* **2000**, (14), 1237-1238.
18. Biedroń, T.; Kubisa, P. *Macromolecular Rapid Communications* **2001,** 22, (15), 1237-1242.
19. Sarbu, T.; Matyjaszewski, K. *Macromolecular Chemistry and Physics* **2001,** 202, (17), 3379-3391.
20. Percec, V.; Grigoras, C. *Journal of Polymer Science Part A: Polymer Chemistry* **2005,** 43, (22), 5609-5619.
21. Biedroń, T.; Kubisa, P. *Journal of Polymer Science Part A: Polymer Chemistry* **2005,** 43, (15), 3454-3459.
22. Ma, H.; Wan, X.; Chen, X.; Zhou, Q.-F. *Journal of Polymer Science Part A: Polymer Chemistry* **2003,** 41, (1), 143-151.
23. Biedroń, T.; Kubisa, P. *Journal of Polymer Science Part A: Polymer Chemistry* **2002,** 40, (16), 2799-2809.
24. Sarkar, A.; Trivedi, S.; Baker, G. A.; Pandey, S. *The Journal of Physical Chemistry B* **2008,** 112, (47), 14927-14936.
25. Coelho, J. F. J.; Gonçalves, P. M. F. O.; Miranda, D.; Gil, M. H. *European Polymer Journal* **2006,** 42, (4), 751-763.
26. Harrisson, S.; Mackenzie, S. R.; Haddleton, D. M. *Macromolecules* **2003,** 36, (14), 5072-5075.
27. Harrisson, S.; Mackenzie, S. R.; Haddleton, D. M. *Chemical Communications* **2002**, (23), 2850-2851.

Appendix D – SI of the article "Synergistic Effect of 1-Butyl-3-methylimidazolium Hexafluorophosphate and DMSO in the SARA ATRP at Room Temperature Affording Very Fast Reactions and Polymers with Very Low Dispersity"

The content of this Appendix are published in J. P. Mendes, F. Branco, C. M. R. Abreu, P. V. Mendonça, A. V. Popov, T. Guliashvili, et al., "Synergistic Effect of 1-Butyl-3-methylimidazolium Hexafluorophosphate and DMSO in the SARA ATRP at Room Temperature Affording Very Fast Reactions and Polymers with Very Low Dispersity," ACS Macro Letters, pp. 544-547, 2014.

Supporting Information

Synergistic effect between 1-butyl-3-methylimidazolium hexafluorophosphate and DMSO in the SARA ATRP at room temperature affording very fast reactions and polymers with very low dispersity

Joana P. Mendes[†], Fábio Branco[†], Carlos M. R. Abreu[†], Patrícia V. Mendonça[†], Anatoliy V. Popov[‡], Tamaz Guliashvili[†]*, Arménio C. Serra[†] and Jorge F. J. Coelho[†]*

Materials

Methyl acrylate (MA) (99 % stabilized; Acros) was passed over a sand/alumina column before use to remove the radical inhibitor. Pentaerythritol tetrakis(2-bromoisobutyrate) (4f-BiB, 97 %; Sigma-Aldrich), copper(II) bromide ($CuBr_2$, +99 % extra pure, anhydrous; Acros), sodium hydrosulfite also known as sodium dithionite ($Na_2S_2O_4$, 85 %, technical grade; Aldrich), ethyl 2-bromoisobutyrate (EBiB, 98 %; Aldrich), N,N,N',N'',N''-pentamethyldiethylenetriamine (PMDETA, 99 %; Aldrich), tetrabutylammonium hexafluorophosphate ($TBAPF_6$, 98 %, Sigma-Aldrich), Reichardt's dye (30) (90 %, Sigma-Aldrich), deuterated chloroform ($CDCl_3$, +1% tetramethylsilane (TMS); Euriso-top), dimethyl sulfoxide (DMSO, +99.8 % extra pure; Acros), 1-butyl-3-methylimidazolium hexafluorophosphate ($BMIM\text{-}PF_6$, > 98 %; TCI (Tokyo Chemical Industry Co. LTD)), polystyrene (PS) standards (Polymer Laboratories), 2-(4-hydroxyphenylazo)benzoic acid (HABA, 99.5 %; Sigma Aldrich), 2,5-dihydroxybenzoic acid (DHB, > 99 %; Sigma Aldrich) were used as received. Tetrahydrofuran (THF, high-performance liquid chromatography (HPLC) grade; Panreac) was filtered (0.2 µm filter) under reduced pressure before use. Me_6TREN was synthesized according the procedure described in the literature.[1]

Techniques

The chromatographic parameters of the samples were determined using high performance size-exclusion chromatography (HPSEC); Viscotek (Viscotek TDAmax) with a differential viscometer (DV); right-angle laser-light scattering (RALLS) (Viscotek); low-angle laser-light scattering (LALLS) (Viscotek) and refractive index (RI) detectors. The column set consisted in a PL 10 mm guard column (50 × 7.5 mm^2) followed by one Viscotek T200 column (6 µm), one MIXED-E PLgel column (3 µm) and one MIXED-C PLgel column (5 µm). A HPLC dual piston pump was set at a flow rate of 1 mL/min. The eluent, THF, was previously filtered through a 0.2 µm filter. The system was also equipped with an on-line degasser. The tests were done at 30 °C using an Elder CH-150 heater. Before the injection (100 µL), the samples were filtered through a polytetrafluoroethylene (PTFE) membrane with 0.2 µm pore. The system was calibrated with narrow polystyrene (PS) standards. The *dn/dc* of PMA was determined as 0.063. The number-average molecular weight ($M_{n,GPC}$) and dispersity (*Đ*) of synthesized polymers were determined by multidetectors calibration using OmniSEC software version: 4.6.1.354.

400 MHz ^1H NMR spectra of the reaction mixture samples were recorded on a Bruker Avance III 400 MHz spectrometer, with a 5-mm TIX triple resonance detection probe, in $CDCl_3$ with TMS as an internal standard. Conversion of the monomer was determined by integration of monomer and polymer peaks using MestRenova software version: 6.0.2-5475.

The PMA samples were dissolved in THF at a concentration of 10 mg/mL for the MALDI-TOF-MS analysis and DHB and HABA (0.05 M in THF) were used as matrices. The dried-droplet samples preparation technique was used to obtain a 1:1 ratio (sample/matrix); an aliquot of 1 µL of each sample was directly spotted on the MTP AnchorChip TM 600/384 TF MALDI target, BrukerDaltonik (Bremen Germany) and, before the sample dried, 1 µL of matrix solution in THF was added and the mixture allowed to dry at room temperature, to allow matrix crystallization. External mass calibration was performed with a peptide calibration standard (PSCII) for the range 700-3000 (9 mass calibration points), 0.5 µL of the calibration solution and matrix previously mixed in an Eppendorf tube (1:2, v/v) were applied directly on the target and allowed to dry at room temperature. Mass spectra were recorded using an Autoflex III smartbeam 1 MALDI-TOF-MS mass spectrometer BrukerDaltonik (Bremen Germany) operating in the linear and reflectron positive ion mode. Ions were formed upon irradiation by a smartbeam laser using a frequency of 200 Hz. Each mass spectrum was produced by averaging 2500 laser shots collected across the whole sample spot surface by screening and in the range m/z 500-12500. The laser irradiance was set to 35-40% (relative scale 0-100) arbitrary units according to the corresponding threshold required for the applied matrix systems.

The UV/Vis studies were performed with a Jasco V-530 spectrophotometer. The analyses were carried out in the 350–1100 nm range at room temperature (rt).

Procedures

Typical Procedure for the [$Na_2S_2O_4$]/[$CuBr_2$]/[Me_6TREN] = 1/0.1/0.1 catalyzed SARA ATRP of MA (DP=222) in BMIM-PF_6/DMSO = 50/50 (v/v)

In a typical SARA ATRP polymerization of MA, $Na_2S_2O_4$ (30.62 mg, 0.16 mmol) was placed in Schlenk reactor. A mixture of $CuBr_2$ (3.55 mg, 0.16 mmol), Me_6TREN (3.69 mg, 0.02 mmol) and DMSO (0.785 mL) was added to the reactor and after this a mixture of MA (3.14 mL, 34.8 mmol), EBiB (30.62 mg, 0.16 mmol) and BMIM-PF_6 (0.785 mL) was also added to the Schlenk that was sealed and frozen in liquid nitrogen. The Schlenk reactor containing the reaction mixture was deoxygenated with four freeze-vacuum-thaw cycles and purged with nitrogen. The reactor was placed in a water bath at 30 °C with stirring (700 rpm). During the polymerization, different reaction mixture samples were collected by using an airtight syringe and purging the side arm of the Schlenk reactor with nitrogen. The samples were analyzed by ^{1}H NMR spectroscopy to determine the monomer conversion and by GPC, to determine the $M_{n,GPC}$ and $Đ$ of the polymers.

Chain extension experiment of –Br terminated PMA

A PMA-Br macroinitiator obtained with a typical $Na_2S_2O_4$/$CuBr_2$/Me_6TREN-catalyzed SARA ATRP reaction was precipitated in a cold hexane (ice bath). The polymer was then dissolved in THF and filtered through a sand/alumina column, to remove traces of the catalyst, and was reprecipitated in cold hexane. The polymer was dried under vacuum until constant weight. The purified monomer (MA) (4.18 mL, 46.5 mmol) was added to the –Br terminated PMA macroinitiator ($M_{n,GPC}$ = 6.90 x 10^3; $Đ$ = 1.05 , 641 mg, 0.09 mmol) in a Schlenk reactor. A mixture of BMIM-PF_6 (2.09 mL), DMSO (2.09 mL) (solvents previously bubbled with nitrogen for about 15 min), $Na_2S_2O_4$ (16.2 mg, 0.09 mmol), $CuBr_2$ (3.47 mg, 0.009 mmol) and Me_6TREN (3.58 mg, 0.009 mmol) was added to the reactor. The Schlenk was placed in the water bath at 30 °C with stirring (700 rpm) for 3h.

UV/Vis spectroscopy of $Na_2S_2O_4$/$CuBr_2$/Me_6TREN in BMIM-PF_6/DMSO = 50/50 (v/v)

$Na_2S_2O_4$ (50.0 mg, 0.250 mmol) were placed in a quartz UV/Vis cuvette, equipped with a magnetic stirrer, and purged with nitrogen. DMSO (1.25 mL), BMIM-PF_6 (1.25 mL), $CuBr_2$ (5.6 mg, 0.025 mmol) and Me_6TREN (5.8 mg, 0.025 mmol) were mixed in a vial and bubbled with nitrogen for about 15 min to remove oxygen. This solution was then added to the UV/Vis cuvette which was sealed under nitrogen. The cuvette was placed in a stirrer plate and placed in the spectrophotometer for spectra acquisition at specific times. The absorbance was measured at different times, in the 350-1100 nm range at room temperature.

Determination of $E_T(30)$ in BMIM-PF_6/DMSO mixtures

Different BMIM-PF_6/DMSO mixtures (5.0 mL) were prepared and small amounts of Reichardt's dye 30 (0.138 mg, 50 μM) were added. These solutions were then added to the UV/Vis cuvette and placed in the spectrophotometer for spectra acquisition. The absorbance was measured, in the 350-1100 nm range at room temperature. The $E_T(30)$ values of different BMIM-PF_6 mixtures were determined according to the expression $E_T(30) = 28591.5/\lambda_{abs,máx}(nm)$.[2]

Results

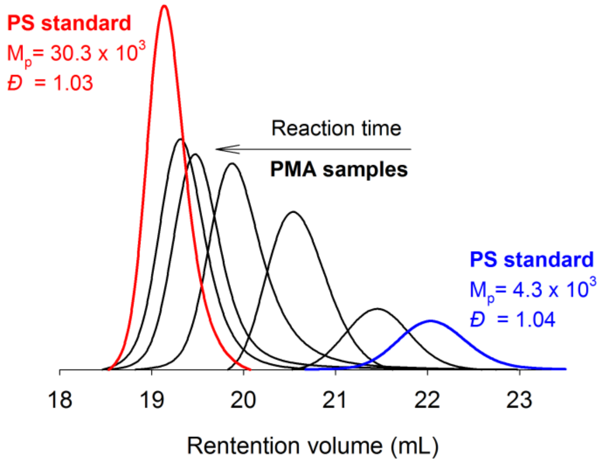

Figure S1. Chromatograms of PS standards (red and blue lines) and PMA samples (black lines) collected during the SARA ATRP of MA catalyzed by $Na_2S_2O_4/CuBr_2/Me_6TREN$ in BMIM-PF_6/DMSO = 50/50. Conditions: $[MA]_0/[solvent] = 2/1$ (v/v); $[MA]_0/[EBiB]_0/[Na_2S_2O_4]_0/[CuBr_2]_0/[Me_6TREN]_0 = 222/1/1/0.1/0.1$ (molar); T = 30 °C.

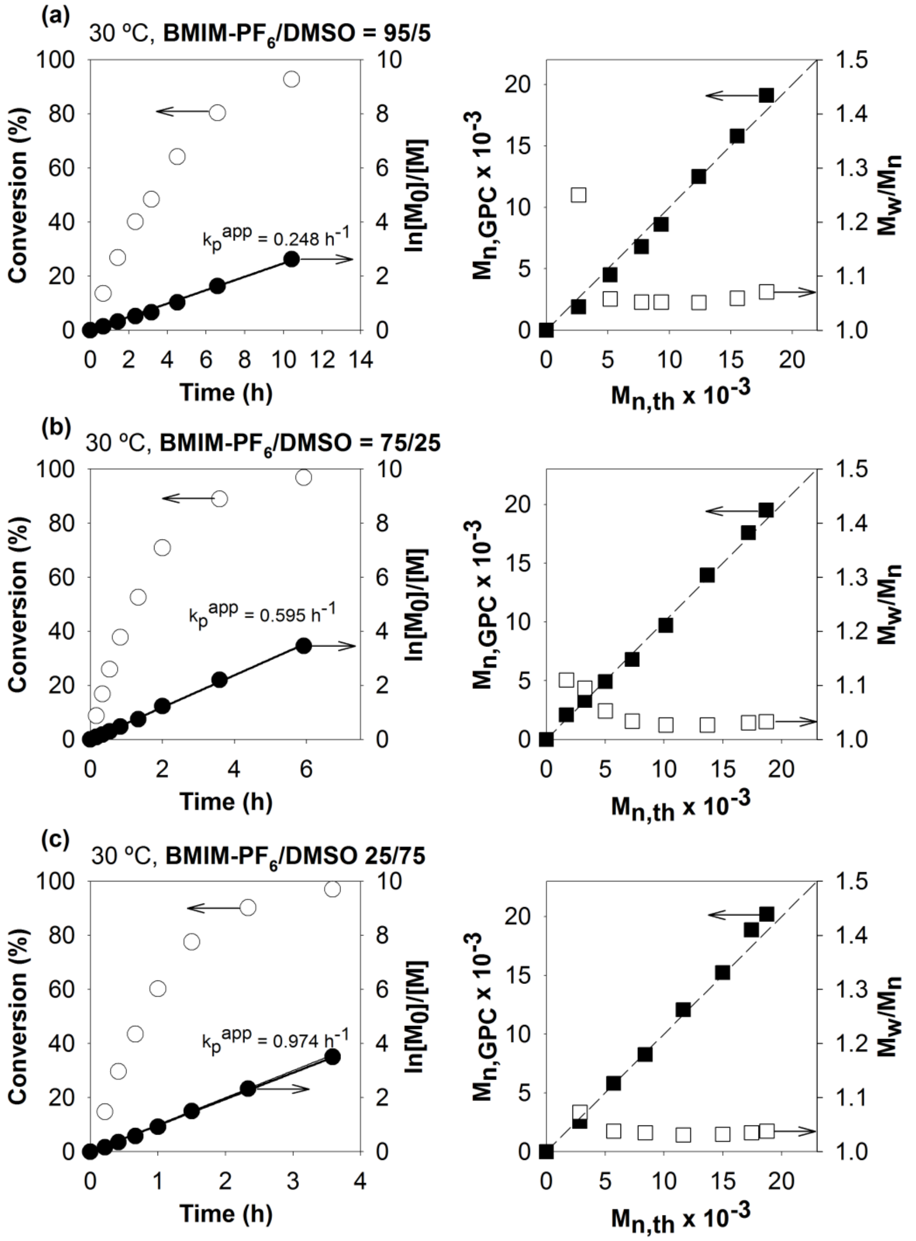

Figure S2. Kinetic plots of conversion and $\ln[M]_0/[M]$ *vs*. time and plots of number average molecular weights ($M_{n,GPC}$) and *Đ* (M_w/M_n) *vs*. theoretical number average molecular weights ($M_{n,th}$) for the SARA ATRP of MA catalyzed by $Na_2S_2O_4/CuBr_2/Me_6TREN$ in (a) BMIM-PF_6/DMSO = 95/5, (b) BMIM-PF_6/DMSO = 75/25 and (c) BMIM-PF_6/DMSO = 25/75.

Conditions: $[MA]_0/[solvent] = 2/1$ (v/v); $[MA]_0/[EBiB]_0/[Na_2S_2O_4]_0/[CuBr_2]_0/[Me_6TREN]_0 = 222/1/1/0.1/0.1$ (molar); T = 30 °C.

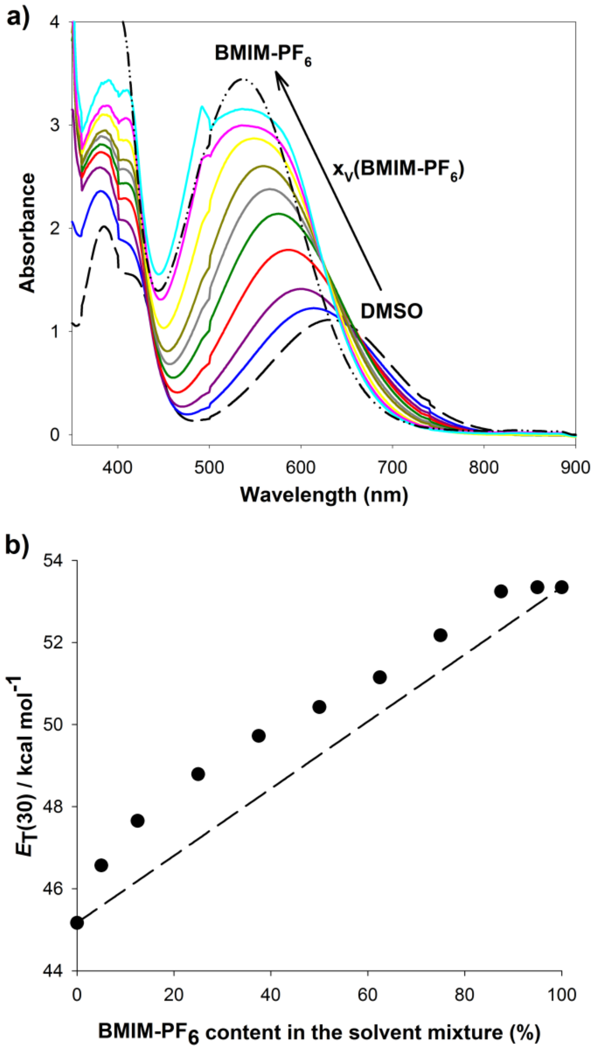

Figure S3. a) UV-Vis spectra in different BMIM-PF$_6$/DMSO mixtures with Reichardt's dye 30 (50 µM); b) Experimental $E_T(30)$ value in different BMIM-PF$_6$/DMSO mixtures (the dashed line represents the predicted $E_T(30)$).

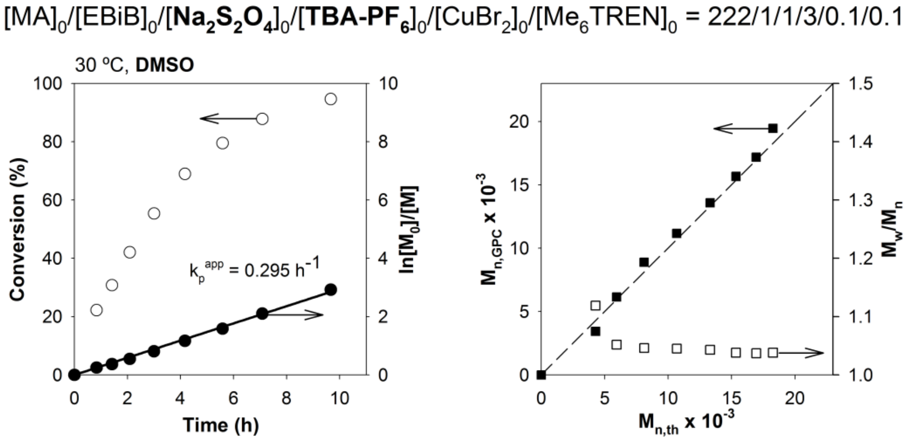

Figure S4. Kinetic plots of conversion and ln$[M]_0/[M]$ *vs*. time and plots of number average molecular weights ($M_{n,GPC}$) and *Đ* (M_w/M_n) *vs*. theoretical number average molecular weights ($M_{n,th}$) for the SARA ATRP of MA catalyzed by $Na_2S_2O_4$/TBA-PF_6/$CuBr_2$/Me_6TREN in DMSO. Conditions: $[MA]_0/[solvent] = 2/1$ (v/v); $[MA]_0/[EBiB]_0/[Na_2S_2O_4]_0/[TBAPF_6]_0/[CuBr_2]_0/[Me_6TREN]_0 = 222/1/1/3/0.1/0.1$ (molar); T = 30 °C.

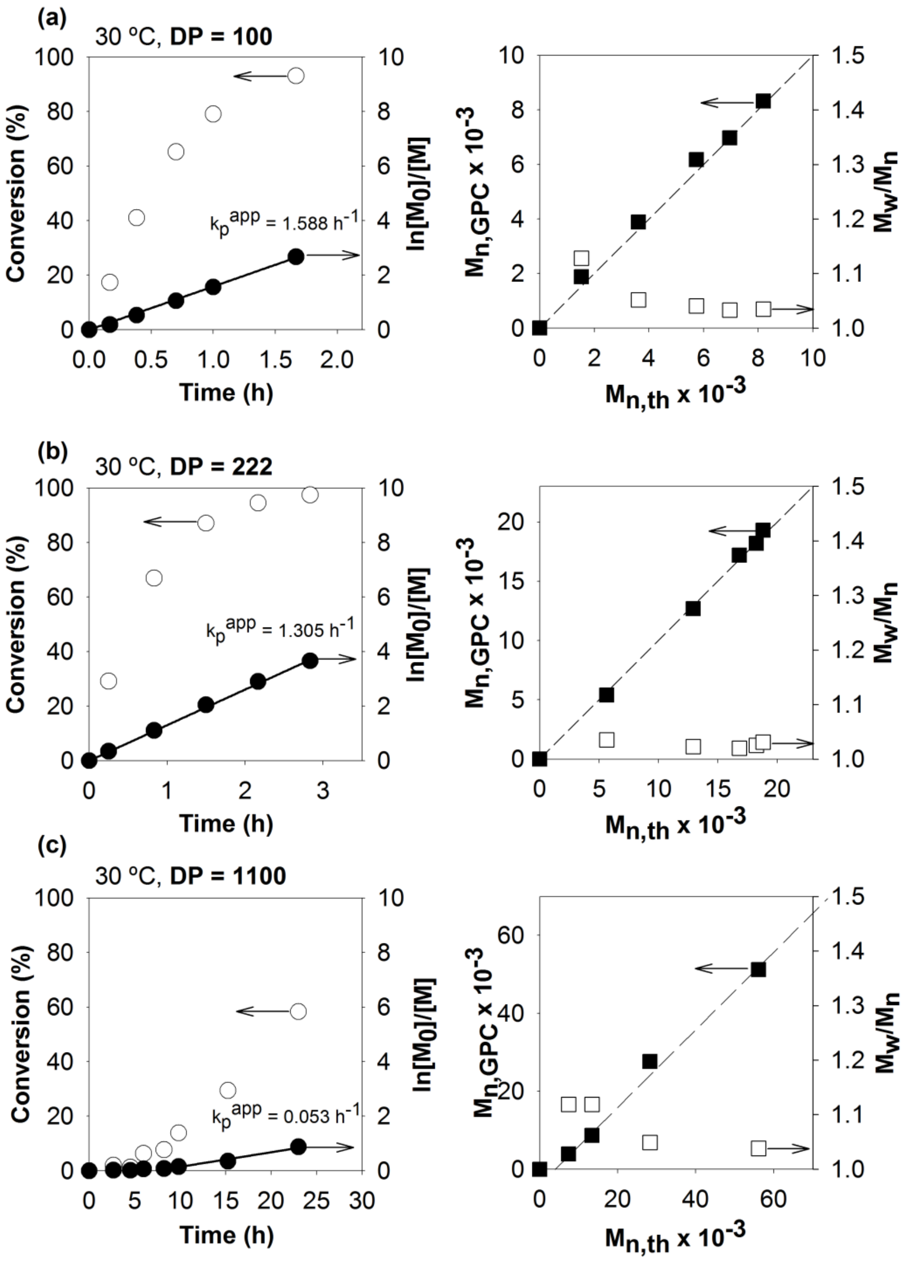

Figure S5. Kinetic plots of conversion and ln[M]$_0$/[M] *vs*. time and plots of number average molecular weights (M$_{n,GPC}$) and *Đ* (M$_w$/M$_n$) *vs*. theoretical number average molecular weights (M$_{n,th}$) for the SARA ATRP of MA catalyzed by $Na_2S_2O_4$/$CuBr_2$/Me$_6$TREN in BMIM-PF$_6$/DMSO = 50/50 (v/v) for different targeted DP values: (a) DP = 100; (b) DP = 222; (c) DP = 1100. Conditions: [MA]$_0$/[solvent] = 2/1 (v/v); [MA]$_0$/[EBiB]$_0$/[$Na_2S_2O_4$]$_0$/[$CuBr_2$]$_0$/[Me$_6$TREN]$_0$ = DP/1/1/0.1/0.1 (molar); T = 30 °C.

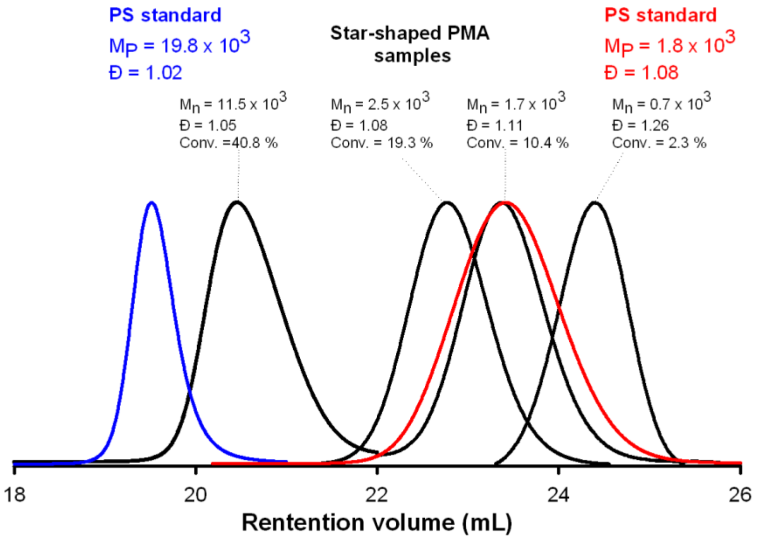

Figure S6. Chromatograms of PS standards (red and blue lines) and star-shaped PMA samples (black lines) collected during the SARA ATRP of MA catalyzed by $Na_2S_2O_4/CuBr_2/Me_6TREN$ in BMIM-FPF$_6$/DMSO = 50/50 (v/v). Conditions: $[MA]_0/[solvent]$ = 2/1 (v/v); $[MA]_0/[4f\text{-}BiB]_0/[Na_2S_2O_4]_0/[CuBr_2]_0/[Me_6TREN]_0$ = 400/1/1/0.4/0.4 (molar); T = 30 °C

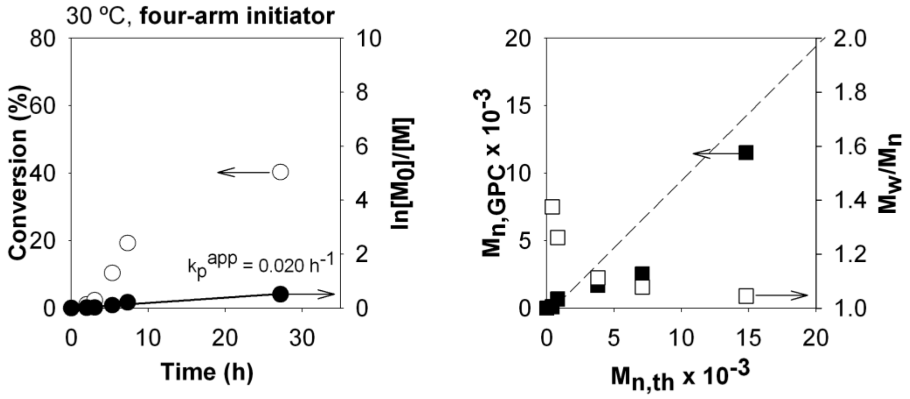

Figure S7. Kinetic plots of conversion and $\ln[M]_0/[M]$ *vs*. time and plots of number average molecular weights ($M_{n,GPC}$) and $Đ$ (M_w/M_n) *vs*. theoretical number average molecular weights ($M_{n,th}$) for the SARA ATRP of MA initiated by a four-arm initiator and catalyzed by $Na_2S_2O_4/CuBr_2/Me_6TREN$, in BMIM-PF$_6$/DMSO = 50/50 (v/v) for a targeted DP of 400. Conditions: $[MA]_0/[solvent]$ = 2/1 (v/v); $[MA]_0/[4f\text{-}BiB]_0/[Na_2S_2O_4]_0/[CuBr_2]_0/[Me_6TREN]_0$ = 400/1/1/0.4/0.4 (molar); T = 30 °C.

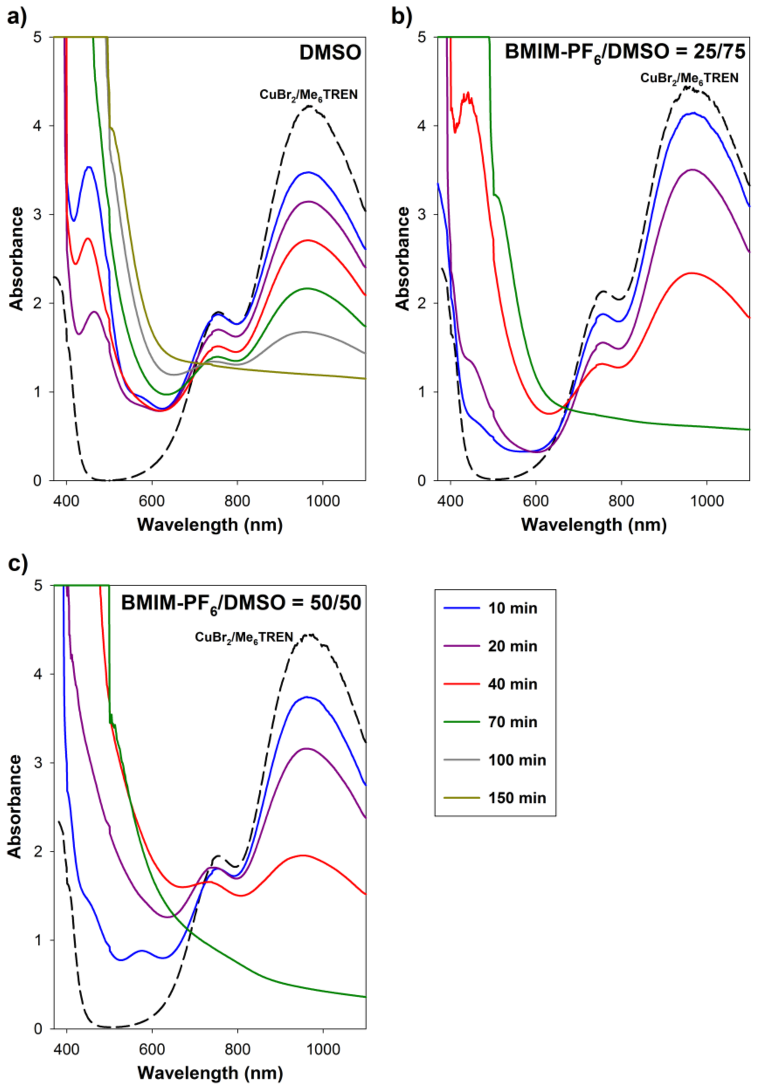

Figure S8. UV-Vis spectra of reduction of CuBr$_2$/Me$_6$TREN by $Na_2S_2O_4$ in a) pure DMSO, b) BMIM-PF$_6$/DMSO (25/75) and c) BMIM-PF$_6$/DMSO (50/50) at 30 °C.

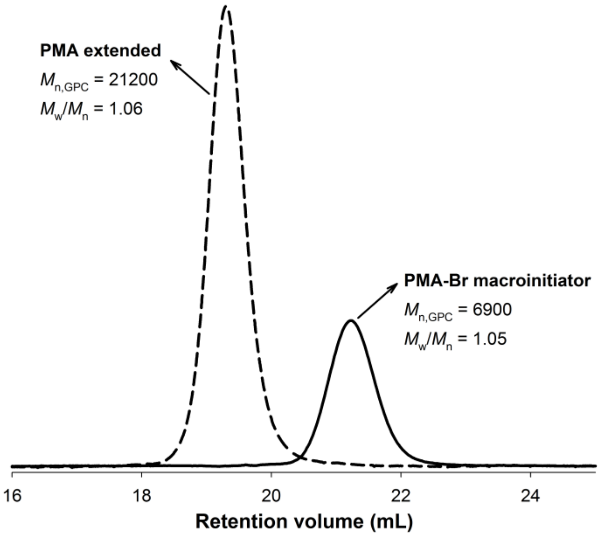

Figure S9. GPC traces of the PMA before (right curve) and after the chain extension (left curve) experiment.

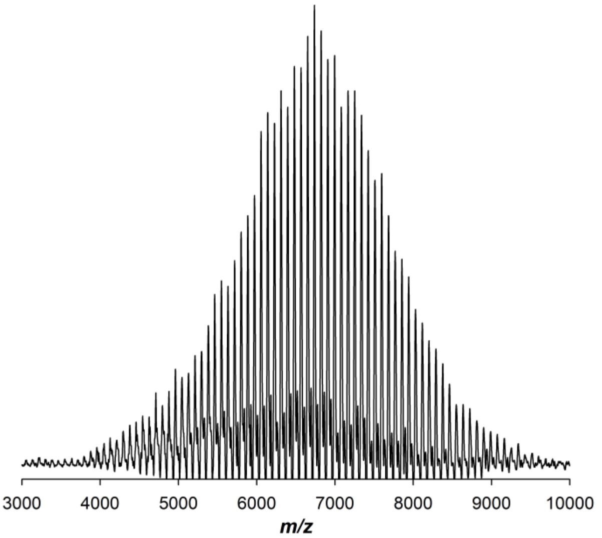

Figure S10. MALDI-TOF-MS in the linear mode (using HABA as matrix) of PMA-Br ($M_{n,GPC}$ = 6.9 x 10^3, *Đ* = 1.05) obtained by SARA ATRP of MA catalyzed by $Na_2S_2O_4$/$CuBr_2$/Me_6TREN, in BMIM-PF_6/DMSO = 50/50 (v/v). Conditions: $[MA]_0$/[solvent] = 2/1 (v/v); $[MA]_0/[EBiB]_0/[Na_2S_2O_4]_0/[CuBr_2]_0/[Me_6TREN]_0$ = 222/1/1/0.1/0.1 (molar); T = 30 °C.

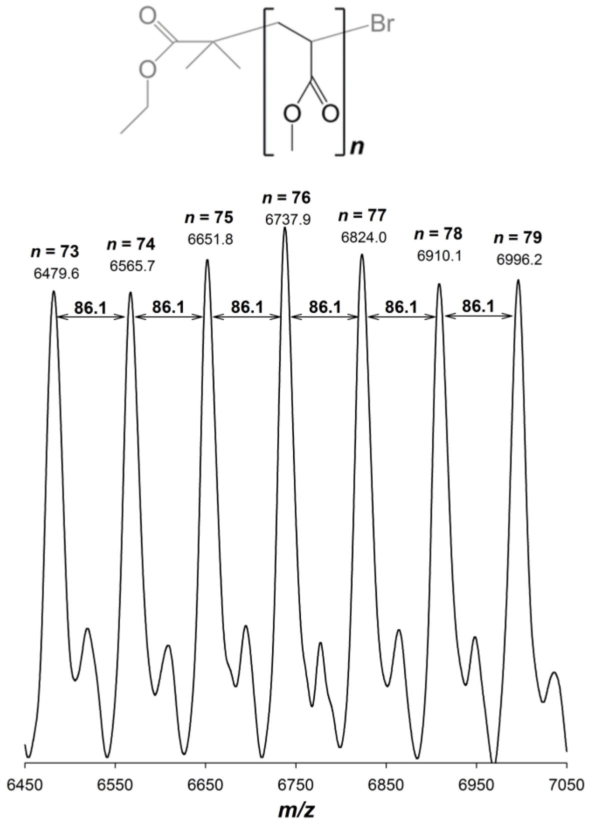

Figure S11. Enlargement of the MALDI-TOF-MS from m/z 6450 to 7050 of PMA-Br ($M_{n,GPC}$ = 6.9 x 10^3, *Đ* = 1.05) obtained by SARA ATRP of MA catalyzed by $Na_2S_2O_4/CuBr_2/Me_6TREN$, in BMIM-$PF_6$/DMSO = 50/50 (v/v). Conditions: $[MA]_0/[solvent]$ = 2/1 (v/v); $[MA]_0/[EBiB]_0/[Na_2S_2O_4]_0/[CuBr_2]_0/[Me_6TREN]_0$ = 222/1/1/0.1/0.1 (molar); T = 30 °C.

MALDI-TOF-MS technique was used to determine the chemical structure of PMA synthetized by SARA ATRP. In the experiment, both HABA and DHB were tested as matrices, but only the HABA matrix gave a clearly resolved spectrum (Figures S10 and S11). Figure S10 shows the MALDI-TOF-MS of PMA-Br in the linear mode with m/z ranging from 3000 to 10000. Enlargement of the m/z 6450-7050 range is presented in the Figure S11. It is important note that the main peaks are separated by an interval corresponding to a MA repeating unit (86.1 mass unit). The highest peaks, presented in the Figures S10 and S11, are attributed to a polymer chain R-$(MA)_n$-Br, where R-Br is the initiator EBiB (6479.6 = 195.05 + 73×86.09, where 195.05 and 86.09 correspond, respectively, to the molar mass of EBiB and MA).

The structure and the end-chain functionality of PMA-Br polymer obtained by SARA ATRP polymerization was studied by ^{1}H NMR.

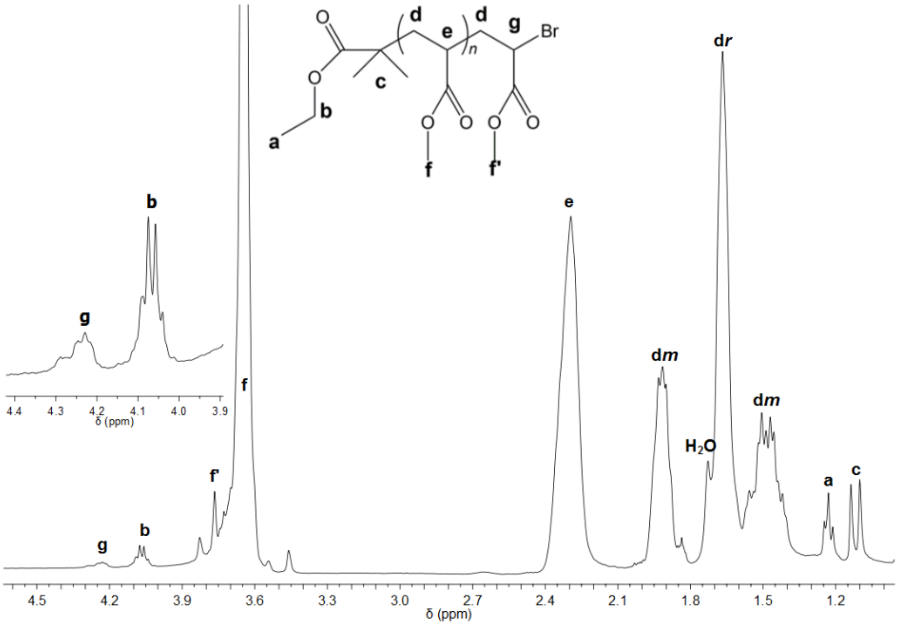

Figure S12. ^{1}H NMR spectrum, in $CDCl_3$, of PMA-Br obtained at high conversion ($M_{n,GPC}$ = 6900, $Đ$ = 1.05, $M_{n,NMR}$ = 6600; active chain-end functionality = 92%). The PMA is atactic: [dr] = [dm] = 0.5.

In the ^{1}H NMR analysis the protons chemical shifts were assigned (Figure S12) according to the references: (e, g, f, f'),$^{3\text{-}5}$ (a, b, c),$^{3, 6}$ (dr, dm).$^{3, 7\text{-}10}$ The spectrum reveals resonance at 1.7 ppm due to water trace in $CDCl_3$ that makes the signal of protons dr partially overlapped with the water signal. Chain-end functionality, in percentage, was calculated as follows: % funct. = [I(g)/(I(c)/6)] x 100%; where I(g) represents the integral of PMA terminal bromo chain-end –CH_2-CH_gBr-CO_2Me at 4.2-4.3 ppm and I(c) the integral of initiator fragment –CH(CH_{c3})$_2$-CO_2Et at 1.15-1.05 ppm. The molar mass of PMA polymer was also calculated from NMR results using the equation $M_{n,NMR} = [\ [I(e)/I(g)] + 1] \times\ MW_{MA} + MW_{EBiB}$, where I(e) represents the integral of the C-H proton of the PMA main chain –CH_2-CH_e-CO_2Me at 2.2-2.4 ppm and I(g) the integral of the active-end chain –CH_gBr at 4.2-4.3 ppm. By measuring the integrals of signals dm and dr the fractions of syndiotactic and isotactic diads (dr and dm respectively) were calculated.

References

1. Ciampolini, M.; Nardi, N. *Inorg. Chem.* **1966,** 5, (1), 41-44.

2. Sarkar, A.; Trivedi, S.; Baker, G. A.; Pandey, S. *J. Phys. Chem. B* **2008,** 112, (47), 14927-14936.

3. Mendonca, P. V.; Serra, A. C.; Coelho, J. F. J.; Popov, A. V.; Guliashvili, T. *Eur. Polym. J.* **2011,** 47, (7), 1460-1466.

4. Lligadas, G.; Ladislaw, J. S.; Guliashvili, T.; Percec, V. *J. Polym. Sci., Part A: Polym. Chem.* **2007,** 46, (1), 278-288.

5. Percec, V.; Guliashvili, T.; Ladislaw, J. S.; Wistrand, A.; Stjerndahl, A.; Sienkowska, M. J.; Monteiro, M. J.; Sahoo, S. *J. Am. Chem. Soc.* **2006,** 128, (43), 14156-14165.

6. Hasneen, A.; Kim, S. J.; Paik, H.-j. *Macromol. Res.* **2007,** 15, (6), 541-546.

7. Coelho, J. F. J.; Carvalho, E. Y.; Marques, D. S.; Popov, A. V.; Goncalves, P. M.; Gil, M. H. *Macromol. Chem. Phys.* **2007,** 208, (11), 1218-1227.

8. Coelho, J. F. J.; Carvalho, E. Y.; Marques, D. S.; Popov, A. V.; Percec, V.; Goncalves, P. M. F. O.; Gil, M. H. *J. Polym. Sci., Part A: Polym. Chem.* **2007,** 46, (2), 421-432.

9. Coelho, J. F. J.; Gois, J.; Fonseca, A. C.; Carvalho, R. A.; Popov, A. V.; Percec, V.; Gil, M. H. *J. Polym. Sci., Part A: Polym. Chem.* **2009,** 47, (17), 4454-4463.

10. Tabuchi, M.; Kawauchi, T.; Kitayama, T.; Hatada, K. *Polymer* **2002,** 43, (25), 7185-7190.

Appendix E – Article “Sulfolane – an Efficient and Universal Solvent for Copper Mediated Atom Transfer Radical (co)Polymerization of Acrylates, Methacrylates, Styrene and Vinyl Chloride.”

The content of this Appendix are published in J. P. Mendes, F. Branco, C. M. R. Abreu, P. V. Mendonça, A. C. Serra, A. V. Popov*, et al.*, "Sulfolane: an Efficient and Universal Solvent for Copper-Mediated Atom Transfer Radical (co)Polymerization of Acrylates, Methacrylates, Styrene, and Vinyl Chloride," *ACS Macro Letters,* pp. 858-861, 2014.

Sulfolane – an Efficient and Universal Solvent for Copper-Mediated Atom Transfer Radical (co)Polymerization of Acrylates, Methacrylates, Styrene and Vinyl Chloride.

Joana P. Mendes†, Fabio Branco†, Carlos M. R. Abreu†, Patrícia V. Mendonça†, Arménio C. Serra†, Anatoliy V. Popov‡, Tamaz Guliashvili*† and Jorge F. J. Coelho†*

† CEMUC, Department of Chemical Engineering, University of Coimbra, 3030-790 Coimbra, Portugal

‡ Department of Radiology, University of Pennsylvania, Philadelphia, Pennsylvania 19104, United States

ABSTRACT: A very fast and controlled atom transfer radical (co)polymerization (ATRP) of acrylates, methacrylates, styrene and vinyl chloride is reported in a single dipolar aprotic solvent, sulfolane, with the use of ppm amount of the copper catalyst. The observed rates of polymerization (k_p^{app}) of the monomers studied are similar to those reported using dimethylsulfoxide (DMSO) and other polar solvents typically employed in single electron transfer (SET)-mediated atom transfer radical polymerization (ATRP) processes. As proof-of-concept, ABA type block copolymers of polystyrene-*b*-poly(vinyl chloride)-*b*-polystyrene and poly(methyl acrylate)-*b*-poly(vinylchloride)-*b*-poly(methyl acrylate) were prepared for the first time using a reversible deactivation radical polymerization (RDRP) method in a single solvent. The quantitative preservation of halide chain-ends was confirmed by ^{1}H NMR and MALDI-TOF analysis as well as by the complete shift of the GPC traces. The results presented establish an innovative and robust system to afford a vast portfolio of (co)polymers in a single widely used industrial solvent.

Atom transfer radical polymerization (ATRP) is a versatile, efficient and robust method that has opened unprecedented opportunities to synthesize (co)polymers with controlled molecular weight, composition, architecture, high chain-end functionality and low dispersity (*Đ*).[1] ATRP is mediated by a dynamic equilibrium between dormant alkyl halide chains and growing radicals, which is catalyzed by a transition metal/ligand complex.[2] Traditionally, metal catalyst concentration greater than 10000 parts per million (ppm) were required to perform normal ATRP reactions. Recently, new variations of ATRP systems have been developed, namely activators regenerated by electron transfer (ARGET) ATRP,[3] initiators for continuous activator regeneration (ICAR) ATRP,[4] electrochemically mediated (*e*-ATRP) ATRP[5] and supplemental activator and reducing agent (SARA) ATRP.[6, 7] These new techniques allow the use of very low concentrations of metal catalyst (< 100 ppm), maintaining the control over the polymerization. Among these methods, SARA ATRP has demonstrated to be a very attractive technique using heterogeneous[7-9] zerovalent metal catalysts as both supplemental activator and reducing agent that can be easily removed from the reaction medium.[6-11] Also, Food and Drug Administration (FDA) approved inorganic sulfites, in combination with small amounts of soluble copper, proved to successfully mediate the SARA ATRP of several monomers in eco-friendly conditions.[12-16]

SARA ATRP has been used for the preparation of well-defined block copolymers in various solvents, such as water,[17] alcohol/water mixtures,[8, 13, 15, 18] and anisole.[12] However, due to solubility issues and system particularities, it is sometimes difficult to find appropriate solvents to perform copolymerization of a wide range of monomers using the same ATRP system without polymer isolation.

The SARA ATRP (originally called as SET living radical polymerization or SET-LRP) of activated and non-activated monomers catalyzed by copper complexes has become very popular method for the preparation of complex polymer architectures. It should be noted that the proposed mechanisms of SET-LRP and SARA ATRP processes are based on the same elemental microsteps,[19] the only difference being the identification of the major/minor contributing reactions.

Dimethyl sulfoxide (DMSO) has proven to be a suitable solvent for the SARA ATRP of methyl acrylate (MA)[11] and methyl methacrylate (MMA),[11] as well as for the non-activated monomer vinyl chloride (VC). For the polymerization of other relevant monomers such as styrene (St), DMSO is not an appropriate solvent due to the very poor solubility of polystyrene in this solvent. Usually, St is polymerized in dimethylformamide (DMF),[7] toluene,[20] anisole[21] or in bulk.[22] Thus, the possibility of having a single universal solvent for the preparation of well-defined block copolymers able to polymerize a wide range of monomer families is highly desirable. Other disadvantage of using DMSO in ATRP reactions is the very low efficiency of universal ATRP initiators such as sulfonyl chloride derivatives (e.g.:

tosyl chloride), due to their rapid reaction at room temperature.[23] Since the first report of ultrafast synthesis of high molar mass polymers mediated by SET-LRP in DMSO, the careful selection of solvent in addition to metal catalyst/monomer/initiator /polymer systems has become a very important issue for the successful control of ATRP polymerization.

Sulfolane (2,3,4,5-tetrahydrothiophene-1,1-dioxide) is a dipolar aprotic industrial solvent commonly used in organic synthesis, gas purification and oil refining.[24] This solvent is completely miscible with water and with most polar and several nonpolar solvents (except alkanes). It is also completely miscible with aromatic hydrocarbons and can also dissolve polystyrene. Compared to other dipolar aprotic solvents, sulfolane presents several advantages, such as: high dipole moment, high relative permittivity and a high Hildebrand solubility parameter.[2, 8, 9, 15, 24, 25] Therefore, an elevated solvency power for the reactions involving polarizable intermediated (like in SET mediated reactions, for example) is expected when using sulfolane as the solvent. Sulfolane is also very stable towards various reactive organic and inorganic solvents and reagents and has the lowest penetration trough skin parameter (compared to other dipolar aprotic solvents).[24] While sulfolane is widely used in organic synthesis and step-growth polymerizations in place of DMSO, DMF or other solvents, this solvent has never been reported as a suitable solvent for the ATRP or related developments.

In this communication, we present for the first time the use of sulfolane as the single solvent for the successful Cu(0)-mediated SARA ATRP of MA, MMA, St and VC. Several reaction parameters were investigated in the polymerization of each monomer to allow good control. As a proof-of-concept, the reported system was used to prepare PMA-*b*-PVC-*b*-PMA (PMA: poly(methyl acrylate); PVC: poly(vinyl chloride) and PS-*b*-PVC-*b*-PS (PS: polystyrene) block copolymers.

Preliminary experiments were carried out for the SARA ATRP of MA catalyzed by Cu(0) wire in sulfolane (Table 1, entries 1-3 and Figure 1). For the purpose of comparison, DMSO was also used under the same reaction conditions because this solvent is often used in the SARA ATRP of the most studied model monomers MA, MMA and VC (by the so-called SET-LRP).[2, 6, 20] The results presented in Figure 1 show that the level of control achieved is similar for both solvents, affording the synthesis of PMA with very low *Đ* (~ 1.05). The conversions reached are very high and the polymerization kinetics are of first-order with respect to monomer conversions.

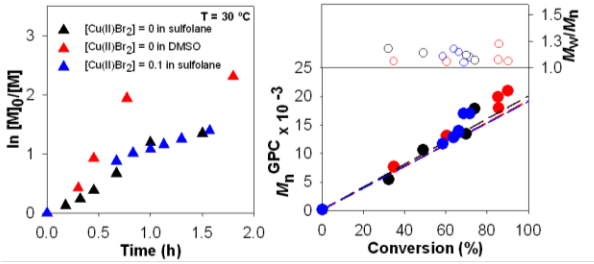

Figure 1. Kinetic plots of conversion and ln$[M]_0/[M]$ *vs*. time (left) and plot of number-average molecular weights (M_n^{GPC}) and *Đ* (M_w/M_n) *vs*. conversion (right) for the SARA ATRP of MA catalyzed by Cu(0) wire/Cu(II)Br_2/Me_6TREN in sulfolane (black and blue symbols) or DMSO (red symbols) at 30 °C. Conditions: $[MA]_0$/[solvent] = 2/1 (v/v); $[MA]_0/[EBiB]_0$/Cu(0) wire/[Cu(II)Br_2]/$[Me_6TREN]_0$ = 222/1/Cu(0) wire/0 or 0.1/1.1 (molar); Cu (0): d = 1 mm, l = 5 cm.

The influence of the target DP was investigated (Table 1, entries 2-4). It is remarkable to note that even for DP = 1100, the *Đ* value of PMA is very low (1.04). This low value indicates clearly that in the system reported herein, the contribution of side the reactions is minimal.

The reduction of Cu(II)Br_2/Me_6TREN by Cu(0) is known to be an important factor in the reaction kinetics.[2] The study of this process in sulfolane and DMSO by UV-vis spectroscopy (Figure S1) reveals no major differences in between both solvents.

The use of sulfolane as solvent was extended to the SARA ATRP of MMA, St and VC (Table S1, entries 5-16 and Figure 2). The necessary adjustments in the polymerization conditions were done regarding the initiator, ligand, ratio monomer/sulfolane and temperature taking into account the structure of each monomer.[6, 15, 20] Figure 2 demonstrates the possibility of synthesizing poly(methyl methacrylate) (PMMA), PS and PVC with controlled molecular weights, by SARA ATRP in sulfolane. The rate of polymerization is of first-order with respect to the monomer conversion and the final *Đ* of the polymers is similar to the best values reported in the literature[6, 15, 20] for different monomers. In the case of MMA polymerization the induction period observed (Figure 2a) was eliminated by adding Cu(II)Br_2 in the beginning of the polymerization, in accordance with the previous results reported by our research group.[6]

The kinetic data obtained for the different monomers is particularly relevant for St (Figure 2b, Figure S2 and Table S1, entry 10-13). Different issues hamper its controlled synthesis, such as: low propagation rate compared to acrylates, thermal self-initiation, occurrence of irreversible termination reactions, vitrification and poor solubility of most catalysts.[9] The results presented herein report the synthesis of PS under mild reaction conditions using a common solvent applied to other monomer families, which opens a portfolio of opportunities for the straightforward synthesis of block copolymers using PS segments.[9]

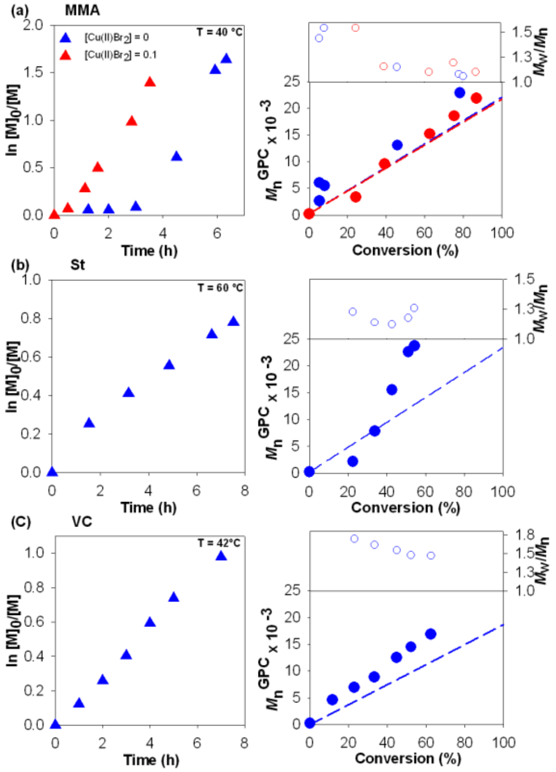

Figure 2. Kinetic plots of conversion and ln[M]$_0$/[M] *vs.* time and plot of number-average molecular weights (M_n^{GPC}) and $Đ$ (M_w/M_n) *vs.* conversion for the SARA ATRP of (a) MMA, (b) St and (c) VC using Cu(0) wire as a supplemental activator and reducing agent in sulfolane. Conditions: (a) $[MMA]_0/[EBPA]_0/Cu(0)$ wire/ $[Cu(II)Br_2]_0/[bpy]_0$ = 222/1/Cu(0) wire/0 (blue) or 0.1 (red)/2.2 (molar), $[MMA]_0/[Sulfolane]$ = 1/1 (v/v) and T = 40 ºC; (b) $[St]_0/[EBiB]_0/Cu(0)$ wire/$[PMDETA]_0$ = 222/1/Cu(0) wire/1.1 (molar), $[St]_0$/[Sulfolane] = 2/1 (v/v) and T = 60 ºC; (c) $[VC]_0/[CHBr_3]_0/[Cu(0)\ wire]_0/\ [TREN]_0$ = 222/1/ Cu(0) wire/1.1, $[VC]_0/[Sulfolane]$ = 1/1and T = 42 ºC; Cu (0): d = 1 mm, l = 5 cm.

The structure of the obtained polymers was assessed by ^{1}H NMR and MALDI-TOF analysis (Fig S3 - S8). The “living” nature of the polymers chain-ends was confirmed by carrying out successful chain extension experiments using PMA, PMMA and PS macroinitiators (Figure S9-S11). As a proof-of-concept, macroinitiators of α,ω-di(bromo)PVC were used to afford block copolymers of PMA-*b*-PVC-*b*-PMA and PS-*b*-PVC-*b*-PS using Me$_6$TREN and PMDETA as ligands, respectively (Figure 3). Figure 3 shows the movement of the low molecular weight PVC GPC trace (conv.$_{VC}$ = 48.4%, M_n^{th} = 5500, M_n^{GPC} = 9100, $Đ$ = 1.55) towards high molar mass PMA-*b*-PVC-*b*-PMA (conv.$_{MA}$ = 86.5%, M_n^{th} = 53800, M_n^{GPC} = 59400, $Đ$ = 1.87) and PS-*b*-PVC-*b*-PS (conv.$_{St}$ = 57.5%, M_n^{th} = 45000, M_n^{GPC} = 63300, $Đ$ = 2.34) block copolymers. Nevertheless, the movement is not complete either because the system is not optimized or due to the previously mentioned issues regarding the RDRP of styrene. The structure of the block copolymers was confirmed by ^{1}H NMR (Fig S12 – S13). These results prove the “living” character of the PVC and the possibility of using the reported system in the synthesis of unique block copolymers. It should be mentioned that to the best of our knowledge, the preparation of block copolymers containing PVC and PS blocks by sequential addition of the appropriated monomers by any RDRP method has never been reported.

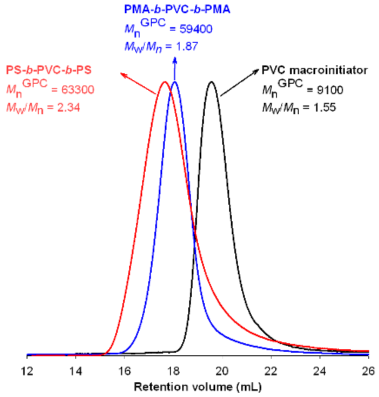

Figure 3. GPC traces of the Br-PVC-Br (conv.$_{VC}$ = 48.4%, M_n^{th} = 5500, M_n^{GPC} = 9100, $Đ$ = 1.55) macroinitiator (black line), and the PMA-*b*-PVC-*b*-PMA (conv.$_{MA}$ = 86.5%, M_n^{th} = 53800, M_n^{GPC} = 59400, $Đ$ = 1.87) (blue line) and PS-*b*-PVC-*b*-PS (conv.$_{St}$ = 57.5%, M_n^{th} = 45000, M_n^{GPC} = 63300, $Đ$ = 2.34) block copolymers (red line).

In an attempt to push the potential of the system, the PMA-*b*-PVC-*b*-PMA was synthesized using the “one-pot” chain extension approach (Figure 4).

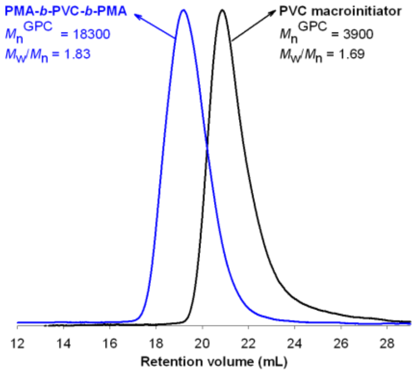

Figure 4. GPC traces of the Br-PVC-Br (conv.$_{VC}$ = 62.2%, M_n^{th} = 3000, M_n^{GPC} = 3900, $Đ$ = 1.69) macroinitiator (right curve), and the PMA-*b*-PVC-*b*-

PMA (conv.$_{MA}$ = 85.7%, M_n^{th} = 17800, M_n^{GPC} = 18300, $Đ$ = 1.83) block copolymer (left curve) prepared by "one-pot" SARA ATRP chain extension.

The GPC traces presented in Figure 4 proves the remarkable advantage of using a single solvent to afford the controlled polymerization of different families of monomers. By using a straightforward procedure involving no purification steps, it is possible to afford well-controlled polymeric structures. The results summarized in Table S1 demonstrate that by adjusting the catalytic complexes and the initiator it is possible to afford a controlled polymerization of MA, MMA, St and VC by SARA ATRP in sulfolane. The presented values regarding k_p^{app}, conversion and $Đ$ are in agreement with the best results reported in the literature for each monomer individually.[6, 15, 20]

In conclusion, the results presented herein establish an innovative and robust system to assess a vast portfolio of well-defined polymers and block copolymers using a common industrial solvent, and employing at the same time low amounts of soluble copper.

ASSOCIATED CONTENT

Supporting Information. Materials, techniques, procedures, kinetic data, ^{1}H NMR spectra, MALDI-TOF data and UV-vis spectroscopic study of the catalytic systems. This material is available free of charge via the Internet at http://pubs.acs.org.

AUTHOR INFORMATION

Corresponding Author

* Jorge F. J. Coelho – Email address: jcoelho@eq.uc.pt.
* Tamaz Guliashvili – Email address: tamazguliasvili@yahoo.com

Author Contributions

The manuscript was written through contributions of all authors. / All authors have given approval to the final version of the manuscript. / ‡These authors contributed equally Funding

Sources

The authors declare no competing financial interest

ACKNOWLEDGMENT

PVM acknowledges FCT-MCTES for her PhD scholarship (SFRH/BD/69152/2010). C.M.R.A. acknowledges FCT-MCTES for his Ph.D. scholarship (SFRH/BD/88528/2012). The authors acknowledge FCT-MCTES for funding (PTDC/EQU-EPR/098662/2008 and PTDC/EQU-EPR/114354/2009). The MALDI-TOF-MS data were obtained by Dr. Manuel Marcos Garcia and Dr. Paula Alvarez Chaver at Unidad de Espectrometria de Masas do Servicio de Determinación Estructural, Proteómica y Genómica, Centro de Apoyo Científico y Tecnologico a la Investigación (CACTI, University of Vigo, Spain). The ^{1}H NMR data were obtained at the Nuclear Magnetic Resonance Laboratory of the Coimbra Chemistry Centre (http://www.nmrccc.uc.pt), University of Coimbra, supported in part by grant REEQ/481/QUI/2006 from FCT, POCI-2010 and FEDER, Portugal.

REFERENCES

1. Matyjaszewski, K.; Tsarevsky, N. V. *J Am Chem Soc* 2014, 136, (18), 6513-6533.
2. Guliashvili, T.; Mendonça, P. V.; Serra, A. C.; Popov, A. V.; Coelho, J. F. J. *Chem-Eur J* 2012, 18, (15), 4607-4612.
3. Jakubowski, W.; Matyjaszewski, K. *Angew Chem* 2006, 118, (27), 4594-4598.
4. Matyjaszewski, K.; Jakubowski, W.; Min, K.; Tang, W.; Huang, J.; Braunecker, W. A.; Tsarevsky, N. V. *P Natl Acad Sci* 2006, 103, (42), 15309-15314.
5. Magenau, A. J. D.; Strandwitz, N. C.; Gennaro, A.; Matyjaszewski, K. *Science* 2011, 332, (6025), 81-84.
6. Mendonca, P. V.; Serra, A. C.; Coelho, J. F. J.; Popov, A. V.; Guliashvili, T. *Eur Polym J* 2011, 47, (7), 1460-1466.
7. Zhang, Y.; Wang, Y.; Matyjaszewski, K. *Macromolecules* 2011, 44, (4), 683-685.
8. Cordeiro, R. A.; Rocha, N.; Mendes, J. P.; Matyjaszewski, K.; Guliashvili, T.; Serra, A. C.; Coelho, J. F. J. *Polym Chem* 2013, 4, (10), 3088-3097.
9. Rocha, N.; Mendonca, P. V.; Mendes, J. P.; Simoes, P. N.; Popov, A. V.; Guliashvili, T.; Serra, A. C.; Coelho, J. F. J. *Macromol Chem Phys* 2013, 214, (1), 76-84.
10. Abreu, C. M. R.; Mendonca, P. V.; Serra, A. C.; Coelho, J. F. J.; Popov, A. V.; Guliashvili, T. *Macromol Chem Phys* 2012, 213, (16), 1677-1687.
11. Bortolamei, N.; Isse, A. A.; Magenau, A. J. D.; Gennaro, A.; Matyjaszewski, K. *Angew Chem Int Edit* 2011, 50, (48), 11391-11394.
12. Gois, J. R.; Rocha, N.; Popov, A.; Guliashvili, T.; Matyjaszewski, K.; Serra, A. C.; Coelho, J. *Polym Chem* 2014, 3919–3928.
13. Gois, J. R.; Konkolewicz, D.; Popov, A.; Guliashvili, T.; Matyjaszewski, K.; Serra, A. C.; Coelho, J. *Polym Chem* 2014, 4617–4626.
14. Mendes, J. P.; Branco, F.; Abreu, C. M. R.; Mendonça, P. V.; Popov, A. V.; Guliashvili, T.; Serra, A. C.; Coelho, J. F. J. *ACS Macro Lett* 2014, 544-547.
15. Abreu, C. M. R.; Serra, A. C.; Popov, A. V.; Matyjaszewski, K.; Guliashvili, T.; Coelho, J. F. J. *Polym Chem* 2013, 4, (23), 5629-5636.
16. Abreu, C. M. R.; Mendonca, P. V.; Serra, A. C.; Popov, A. V.; Matyjaszewski, K.; Guliashvili, T.; Coelho, J. F. J. *ACS Macro Lett* 2012, 1, (11), 1308-1311.
17. Konkolewicz, D.; Krys, P.; Góis, J. R.; Mendonça, P. V.; Zhong, M.; Wang, Y.; Gennaro, A.; Isse, A. A.; Fantin, M.; Matyjaszewski, K. *Macromolecules* 2014, 47, (2), 560-570.
18. Mendonca, P.; Konkolewicz, D.; Averick, S.; Serra, A. C.; Popov, A.; Guliashvili, T.; Matyjaszewski, K.; Coelho, J. *Polym Chem* 2014, DOI: 10.1039/C4PY00707G.
19. Konkolewicz, D.; Wang, Y.; Krys, P.; Zhong, M.; Isse, A. A.; Gennaro, A.; Matyjaszewski, K. *Polym Chem* 2014, 4396-4417.
20. Percec, V.; Guliashvili, T.; Ladislaw, J. S.; Wistrand, A.; Stjerndahl, A.; Sienkowska, M. J.; Monteiro, M. J.; Sahoo, S. *J Am Chem Soc* 2006, 128, (43), 14156-14165.
21. Tom, J.; Hornby, B.; West, A.; Harrisson, S.; Perrier, S. *Polym Chem* 2010, 1, (4), 420-422.
22. Jakubowski, W.; Kirci-Denizli, B.; Gil, R. R.; Matyjaszewski, K. *Macromol Chem Phys* 2008, 209, (1), 32-39.
23. Boyle, R. E. *J Org Chem* 1966, 31, (11), 3880-3882.
24. Tilstam, U. *Org Process Res Dev* 2012, 16, (7), 1273-1278.
25. Abreu, C. M. R.; Mendonça, P. V.; Serra, A. C.; Coelho, J. F. J.; Popov, A. V.; Gryn'ova, G.; Coote, M. L.; Guliashvili, T. *Macromolecules* 2012, 45, (5), 2200-2208.

Appendix F – SI of the article "Sulfolane – an Efficient and Universal Solvent for Copper Mediated Atom Transfer Radical (co)Polymerization of Acrylates, Methacrylates, Styrene and Vinyl Chloride."

The content of this Appendix are published in J. P. Mendes, F. Branco, C. M. R. Abreu, P. V. Mendonça, A. C. Serra, A. V. Popov, *et al.*, "Sulfolane: an Efficient and Universal Solvent for Copper-Mediated Atom Transfer Radical (co)Polymerization of Acrylates, Methacrylates, Styrene, and Vinyl Chloride," *ACS Macro Letters*, pp. 858-861, 2014.

Supporting Information for

Sulfolane – an Efficient and Universal Solvent for Copper Mediated Atom Transfer Radical (co)Polymerization of Acrylates, Methacrylates, Styrene and Vinyl Chloride.

Joana P. Mendes†, Fabio Branco†, Carlos M. R. Abreu†, Patrícia V. Mendonça†, Anatoliy V. Popov‡, Arménio C. Serra†, Tamaz Guliashvili*† and Jorge F. J. Coelho†*

† CEMUC, Department of Chemical Engineering, University of Coimbra, 3030-790 Coimbra, Portugal

‡ Department of Radiology, University of Pennsylvania, Philadelphia, Pennsylvania 19104, United States

Table of Contents

Experimental Section…………………………………………………………..….S2
Table S1 – Kinetic data for the SARA ATRP of MA, MMA, St and VC …..……S9
Comproportionation experiments………...……………………………………...S10
Kinetics plots of SARA ATRP of St………..………………………………….....S11
^{1}H NMR specta of homopolymers……………………………………...….S12
MALDI-TOF of homopolymers…………………………...……………..S16
Chain extensions……………………………………………………………….….S18
^{1}H NMR spectra of block copolymers………..……………………...…….…..S21

Experimental Section

Materials

Copper(II) bromide ($CuBr_2$) (+ 99 % extra pure, anhydrous; Acros), copper(II) chloride ($CuCl_2$) (max. 0.0008 % AS; Merck), zerovalent iron powder (Fe(0)) (99 %, ~ 70 mesh, Acros), metallic copper (Cu(0) wire) (≥ 99.9 %; Sigma-Aldrich), deuterated chloroform ($CDCl_3$) (+ 1 % tetramethylsilane (TMS); Euriso-top), deuterated tetrahydrofuran (THF-d_8) (99.5 %; Euriso-top), dimethyl sulfoxide (DMSO) (+ 99.8 % extra pure; Acros), sulfolane (+ 99 %; Acros), ethyl 2-bromoisobutyrate (EBiB) (98 %; Aldrich), p-toluenesulfonyl chloride (TsCl) (98 %; Merck), ethyl α-bromophenylacetate (EBPA) (97 %; Aldrich), bromoform ($CHBr_3$) (+ 99 % stabilized; Acros), tris(2-aminoethyl)amine (TREN) (96 %; Sigma-Aldrich), N,N,N′,N′′,N′′-pentamethyldiethylenetriamine (PMDETA) (99 %; Aldrich), 2,2′-bipyridine (bpy) (> 99 %, Acros) polystyrene (PS) standards (Polymer Laboratories), 2-(4-hydroxyphenylazo)benzoic acid (HABA) (99.5 %; Sigma-Aldrich) and 2,5-dihydroxybenzoic acid (DHB) (> 99 %; Sigma-Aldrich) were used as received. High-performance liquid chromatography (HPLC) grade THF (Panreac) was filtered (0.2 µm filter) under reduced pressure before use.

Methyl acrylate (MA) (99 % stabilized; Acros), methyl methacrylate (MMA) (99 % stabilized; Acros) and styrene (Sty) (+ 99 %; Sigma-Aldrich), were passed over a sand/alumina column before use to remove the radical inhibitors. Vinyl chloride (VC) (99 %) was kindly supplied by CIRES Lda, Portugal.

Me_6TREN was synthesized according to the procedure described in the literature.[1]

Metallic copper (Cu(0), d = 1 mm, Sigma Aldrich) was washed with nitric acid and subsequently rinsed with acetone and dried under a stream of nitrogen.

Synthesis

Typical procedure for the $[Cu(0)]_0/[CuBr_2]_0/[Me_6TREN]_0$ = Cu(0) wire/0.1/1.1 catalyzed SARA ATRP of MA (DP = 222)

Cu(0) wire (590 mg) and a mixture of $CuBr_2$ (3.51 mg, 0.02 mmol), Me_6TREN (39.76 mg, 0.17 mmol) and sulfolane (1.58 mL) (previously bubbled with nitrogen for about 15 minutes) were placed in a Schlenk tube reactor. A mixture of MA (3.16 mL, 34.90 mmol) and EBiB (30.62 mg, 0.16 mmol) was added to the reactor that was sealed, by using a rubber septum, and frozen in liquid nitrogen. The Schlenk tube reactor containing the reaction mixture was deoxygenated with four freeze-vacuum-thaw cycles and purged with nitrogen. The reactor was placed in a water bath at 30 ºC with stirring (700 rpm). During the polymerization, different reaction mixture samples were collected by using an airtight syringe and purging the side arm of the Schlenk tube reactor with nitrogen. The samples were analyzed by ^{1}H NMR spectroscopy to determine the monomer conversion and by GPC, to determine the average-number molecular weight (M_n^{GPC}) and dispersity ($Đ$) of the polymers.

Typical procedure for the $[Cu(0)]_0/[CuBr_2]_0/[bpy]_0$ = Cu(0) wire/0.1/2.2 catalyzed SARA ATRP of MMA (DP = 222)

For a typical polymerization of MMA, a mixture of Cu(0) wire (240 mg), $CuBr_2$ (3.16 mg, 0.014 mmol), bpy (46.38 mg, 0.30 mmol) and sulfolane (3.21 mL) (previously bubbled with nitrogen for about 15 minutes) was placed in a Schlenk tube reactor. A solution of EBPA (33.95 mg, 0.14 mmol) in MMA (3.21 mL, 30.0 mmol) was added to the reactor that was sealed, by using a rubber septum, and frozen in liquid nitrogen. The Schlenk tube reactor containing the reaction mixture was deoxygenated with four freeze-vacuum-thaw cycles and purged with nitrogen. The reactor was placed in a water bath at 40 ºC with stirring (700 rpm). During the polymerization, different reaction mixture samples were collected by using an airtight syringe and purging the side arm of the Schlenk tube reactor with nitrogen. The samples were analyzed by ^{1}H NMR spectroscopy to determine the monomer conversion and by GPC, to determine the M_n^{GPC} and $Đ$ of the polymers.

Typical procedure for the $[Cu(0)]_0/[CuBr_2]_0/[PMDETA]_0$ = Cu(0) wire/0/1.1 catalyzed ATRP of St (DP = 222)

A mixture of Cu(0) wire (335 mg), PMDETA (25.00 mg, 0.14 mmol) and sulfolane (1.66 mL) (previously bubbled with nitrogen for about 15 minutes) was placed in a Schlenk tube reactor. A solution of EBiB (25.27 mg, 0.13 mmol) in St (3.31 mL, 28.80 mmol) was added to the reactor that was sealed, by using a rubber septum, and frozen in liquid nitrogen. The Schlenk tube reactor containing the reaction mixture was deoxygenated with four freeze-vacuum-thaw cycles and purged with nitrogen. The reactor was placed in a water bath at 30 ºC with stirring (700 rpm). During the polymerization, different reaction mixture samples were collected by using an airtight syringe and purging the side arm of the Schlenk tube reactor with nitrogen. The samples were analyzed by ^{1}H NMR spectroscopy to determine the monomer conversion and by GPC, to determine the M_n^{GPC} and $Đ$ of the polymers.

Typical procedure for the $[Cu(0)]_0/[CuCl_2]_0/[PMDETA]_0$ = Cu(0) wire/0.1/1.1 catalyzed ATRP of St (DP = 222)

A mixture of $CuCl_2$ (2.30 mg, 0.013 mmol), PMDETA (24.73 mg, 0.14 mmol) and sulfolane (1.66 mL) (previously bubbled with nitrogen for about 15 minutes) was placed in a Schlenk tube reactor. A mixture of St (3.31 mL, 28.8 mmol) and $CHBr_3$ (34.73 mg, 0.13 mmol) was added to the reactor. Cu(0) wire (315 mg) was inserted in the reactor that was sealed, by using a rubber septum, and frozen in liquid nitrogen. The Schlenk tube reactor containing the reaction mixture was deoxygenated with four freeze-vacuum-thaw cycles and purged with nitrogen. The reactor was placed in an oil bath at 60 ºC with stirring (700 rpm). During the polymerization, different reaction mixture samples were collected by using an airtight syringe and purging the side arm of the Schlenk tube reactor with nitrogen. The samples were analyzed by ^{1}H NMR spectroscopy to determine the monomer conversion and by GPC, to determine the M_n^{GPC} and $Đ$ of the polymers.

Typical procedure for the $[Cu(0)]_0/[TREN]_0$ = Cu(0) wire/1 catalyzed SARA ATRP of VC (DP = 222)

A 50 mL Ace glass 8645#15 pressure tube, equipped with bushing and plunger valve, was charged with a mixture of $CHBr_3$ (86.43 mg, 0.33 mmol), TREN (50.19 mg, 0.33 mmol), Cu(0) wire (283 mg) and sulfolane (5 mL) (previously bubbled with nitrogen for about 15 min). The precondensed VC (5 mL, 72.8 mmol) was added to the tube. The exact amount of VC was determined gravimetrically. The tube was closed, submerged in liquid nitrogen and degassed through the plunger valve by applying reduced pressure and filling the tube with N_2 about 20 times. The valve was closed, and the tube reactor was placed in a water bath at 42 ºC with stirring (700 rpm). The reaction was stopped by plunging the tube into ice water. The tube was slowly opened, the excess of VC was distilled, and the mixture was precipitated into methanol. The polymer was separated by filtration and dried in a vacuum oven until constant weight to produce. The monomer conversion were determined gravimetrically. GPC was used for the determination of PVC´s M_n^{GPC} and $Đ$.

Typical procedure for chain extension of –Br terminated PMA

A PMA-Br macroinitiator obtained from a typical $Cu(0)/CuBr_2/Me_6TREN$-catalyzed SARA ATRP reaction was precipitated in water. The polymer was then dissolved in acetone, filtered through a sand/alumina column, to remove traces of the catalyst, and reprecipitated in water. The polymer was dried under vacuum until constant weight. MA (1.05 mL, 11.60 mmol) was added to the –Br terminated PMA macroinitiator (M_n^{GPC} = 4600 g.mol^{-1}; $Đ$= 1.16, 53.44 mg, 0.01 mmol) in a Schlenk tube reactor. A mixture of sulfolane (0.53 mL previously bubbled with nitrogen for about 15 min), Me_6TREN (2.94 mg, 0.01 mmol), and Cu(0) wire (233 mg) was added to the reactor that was sealed, by using a rubber septum, and frozen in liquid nitrogen. The Schlenk tube reactor containing the reaction mixture was deoxygenated with four freeze-vacuum-thaw cycles and purged with nitrogen. The Schlenk tube was placed in the water bath at 30 ºC with stirring (700 rpm) for 1.5 h.

Typical procedure for chain extension of –Br terminated PMMA

A PMMA-Br macroinitiator obtained from a typical Cu(0)/$CuBr_2$/Me_6TREN-catalyzed SARA ATRP reaction was precipitated in methanol. The polymer was then dissolved in THF, filtered through a sand/alumina column, to remove traces of the catalyst, and reprecipitated in methanol. The polymer was dried under vacuum until constant weight. (MMA (1.0 mL, 9.4 mmol) was added to the –Br terminated PMMA macroinitiator (M_n^{GPC} = 10 700 g.mol^{-1}; $Đ$= 1.05, 200.9 mg, 0.02 mmol) in a Schlenk tube reactor. A mixture of sulfolane (1.0 mL previously bubbled with nitrogen for about 15 min), bpy (6.45 mg, 0.04 mmol), and Cu(0) wire (230 mg) was added to the reactor that was sealed, by using a rubber septum, and frozen in liquid nitrogen. The Schlenk tube reactor containing the reaction mixture was deoxygenated with four freeze-vacuum-thaw cycles and purged with nitrogen. The Schlenk tube was placed in the water bath at 40 ºC with stirring (700 rpm) for 3.5 h.

Typical procedure for chain extension of –Br terminated PS

A PS-Br macroinitiator obtained from a typical Cu(0)/PMDETA catalyzed SARA ATRP reaction was precipitated in methanol. The polymer was then dissolved in THF, filtered through a sand/alumina column, to remove traces of the catalyst, and reprecipitated in methanol. St (0.55 mL, 4.8 mmol) was added to the –Br terminated PS macroinitiator (M_n^{GPC} = 3960 g.mol^{-1}; $Đ$= 1.36, 85.64 mg, 0.022 mmol) in a Schlenk tube reactor. A mixture of sulfolane (0.55mL previously bubbled with nitrogen for about 15 min), PMDETA (4.12 mg, 0.022 mmol) and Cu(0) wire (326 mg) was added to the reactor that was sealed, by using a rubber septum, and frozen in liquid nitrogen. The Schlenk tube reactor containing the reaction mixture was deoxygenated with four freeze-vacuum-thaw cycles and purged with nitrogen.The Schlenk tube reactor was placed in the oil bath at 60 ºC with stirring (700 rpm) for 7.5 h.

Typical procedure for the synthesis of PMA-*b*-PVC-*b*-PMA block copolymers by $[Cu(0)]_0/[Me_6TREN]_0$ = Cu(0) wire/1.1 catalyzed SARA ATRP

The α,ω-di(bromo)PVC macroinitiator was obtained from a typical Cu(0) wire/TREN catalyzed SARA ATRP reaction. After precipitation in methanol, the polymer was then dissolved in THF, filtered through a sand/alumina column, to remove traces of the catalyst, and reprecipitated in methanol again. The polymer was dried under vacuum until constant weight. A mixture of MA (3.0 mL, 33.3 mmol) and α,ω-di(bromo)PVC macroinitiator (M_n^{GPC} = 9100; $Đ$= 1.55; 505 mg, 0.056 mmol), previously dissolved in sulfolane (3.0 mL), was added to the recator.

Cu(0) wire (282 mg) and Me_6TREN (14.6 mg, 0.061 mmol) were added to the reactor that was sealed, by using a rubber septum, and frozen in liquid nitrogen. The Schlenk tube reactor was deoxygenated by five freeze-pump thaw cycles and purged with nitrogen. Then the reactor was placed in a water bath at 30 ºC with stirring (700 rpm). The reaction was stopped after 3 h and the mixture was analyzed by ^{1}H NMR spectroscopy in order to determine the MA conversion and by GPC, to determine the M_n^{GPC} and $Đ$ of the PMA-*b*-PVC-*b*-PMA block copolymer.

Typical procedure for the synthesis of PS-*b*-PVC-*b*-PS block copolymers by $[Cu(0)]_0/[PMDETA]_0$ = Cu(0) wire/1.1 catalyzed SARA ATRP

The α,ω-di(bromo)PVC macroinitiator was obtained from a typical Cu(0) wire/TREN catalyzed SARA ATRP reaction. After precipitation in methanol, the polymer was then dissolved in THF, filtered through a sand/alumina column, to remove traces of the catalyst, and reprecipitated in methanol. The polymer was dried under vacuum until constant weight. A mixture of St (3.0 mL, 26.1 mmol) and –Br terminated PVC macroinitiator (M_n^{GPC} = 9100; $Đ$= 1.55; 396 mg, 0.043 mmol), previously dissolved in sulfolane (3.0 mL), was added to the recator that was sealed, by using a rubber septum, and frozen in liquid nitrogen. Cu(0) wire (2842 mg) and PMDETA (8.6 mg, 0.048 mmol) were added to the reactor. The Schlenk tube reactor was deoxygenated by five freeze-pump thaw cycles and purged with nitrogen. Then the reactor was placed in an oil bath at 60 ºC with stirring (700 rpm). The reaction was stopped after 16 h and the mixture was analyzed by ^{1}H NMR spectroscopy in order to determine the St conversion and by GPC, to determine the M_n^{GPC} and $Đ$ of the PS-*b*-PVC-*b*-PS block copolymer.

Typical procedure for the synthesis of PMA-*b*-PVC-*b*-PMA block copolymers by "one-pot" $[Cu(0)]_0/[TREN]_0$ = Cu(0) wire/1 catalyzed SARA ATRP

A 50 mL Ace glass 8645#15 pressure tube, equipped with bushing and plunger valve, was charged with a mixture of $CHBr_3$ (230.14 mg, 0.87 mmol), TREN (133.16 mg, 0.87 mmol), Cu(0) wire (291.7 mg) and sulfolane (3.0 mL) (previously bubbled with nitrogen for about 15 min). The precondensed VC (3.0 mL, 43.7 mmol) was added to the tube. The exact amount of VC was determined gravimetrically. The tube was closed, submerged in liquid nitrogen and degassed through the plunger valve by applying reduced pressure and filling the tube with nitrogen about 20 times. The valve was closed, and the tube reactor was placed in a water bath at 42 °C with stirring (700 rpm). After 2 h, the reaction was stopped by plunging the tube into ice water. The tube was slowly opened and the excess VC was distilled. The monomer conversion were determined gravimetrically (62.2 %), and the M_n^{GPC} = 3900 and $Đ$= 1.69 were determined by GPC analysis in THF. A mixture of sulfolane (15.7 mL) and MA (15.7 mL, 174.8 mmol) was added to the same 50 mL Ace glass 8645#15 pressure tube (without any purification of the α,ω-di(bromo)PVC macroinitiator). The tube was closed, submerged in liquid nitrogen and degassed through the plunger valve by applying reduced pressure and filling the tube with nitrogen about 20 times. The valve was closed, and the tube reactor was placed in a water bath at 42 °C with stirring (700 rpm). The reaction was stopped after 1 h and the mixture was analyzed by ^{1}H NMR spectroscopy in order to determine the MA conversion and by GPC, to determine the M_n^{GPC} and $Đ$ of the PMA-*b*-PVC-*b*-PMA block copolymer.

UV-vis spectroscopic study of the catalytic systems

Cu(0) wire (l = 5 cm, d = 1 mm) and a magnetic stirrer were placed in a quartz UV-vis cell and purged with nitrogen. A mixture of $CuBr_2$ (4.2 mg, 19 µmol) and Me_6TREN (47.5 mg, 0.21 mmol) in the solvent (2.5 mL of DMSO or sulfolane) was bubbled with nitrogen for 20 min, to remove the oxygen. This solution was then added to the cuvette, which was sealed under nitrogen. The cuvette was placed in a water bath at 30 ºC and several UV-vis spectra were recorded at different reaction times, in the 350 – 1100 nm range.

Techniques

The chromatographic parameters of the samples were determined using high performance gel permeation chromatography (GPC); Viscotek (Viscotek TDAmax) with a differential viscometer (DV); right-angle laser-light scattering (RALLS) (Viscotek); low-angle laser-light scattering (LALLS) (Viscotek) and refractive index (RI) detectors. The column consisted of a PL 10 mm guard column (50 × 7.5 mm^2) followed by one Viscotek T200 column (6 µm), one MIXED-E PLgel column (3 µm) and one MIXED-C PLgel column (5 µm). A HPLC dual piston pump was set at a flow rate of 1 mL/min. The eluent, THF, was previously filtered through a 0.2 µm filter. The system was also equipped with an on-line degasser. The tests were done at 30 ºC using an Elder CH-150 heater. Before the injection (100 µL), the samples were filtered through a polytetrafluoroethylene (PTFE) membrane with 0.2 µm pore. The system was calibrated with narrow PS standards. The *dn/dc* was determined as 0.063 for PMA, 0.105 for PVC, 0.185 for PS and 0.089 for PMMA. The M_n^{GPC} and $Đ$ of the synthesized polymers and block copolymers were determined by multidetectors calibration using OmniSEC software version: 4.6.1.354.

400 MHz ^{1}H NMR spectra of the reaction mixture samples of MA, MMA and St polymerizations were recorded on a Bruker Avance III 400 MHz spectrometer, with a 5-mm TIX triple resonance detection probe, in $CDCl_3$ with TMS as an internal standard.

600 MHz ^{1}H NMR spectra of the reaction mixture samples of VC polymerization were recorded with a Varian VNMRS 600 MHz spectrometer, with a warm 3 mm PFG triple resonance indirect detection probe, in THF-d_8 with TMS as an internal standard. Monomer conversions were determined by integration of monomer and polymer peaks using MestRenova software version: 6.0.2-5475.

The PMA and PVC samples were dissolved in THF at a concentration of 10 mg/mL for the MALDI-TOF-MS analysis and DHB and HABA (0.05 M in THF) were used as matrices. The dried-droplet samples preparation technique was used to obtain a 1:1 ratio (sample/matrix); an aliquot of 1 µL of each sample was directly spotted on the MTP AnchorChip TM 600/384 TF MALDI target, BrukerDaltonik (Bremen Germany) and, before the sample dried, 1 µL of matrix solution in THF was added and the mixture was dried at room temperature, to allow matrix crystallization. External mass calibration was performed with a peptide calibration standard (PSCII) for the range 700-3000 (9 mass calibration points), 0.5 µL of the calibration solution and matrix previously mixed in an Eppendorf tube (1:2, v/v) were applied directly on the target and allowed to dry at room temperature. Mass spectra were recorded using an Autoflex III smartbeam 1 MALDI-TOF-MS mass spectrometer BrukerDaltonik (Bremen Germany) operating in the linear and reflectron positive ion mode. Ions were formed upon irradiation by a smartbeam laser using a frequency of 200 Hz. Each mass spectrum was produced by averaging 2500 laser shots collected across the whole sample spot surface by screening in the range m/z 500-13000 for PVC and in the range m/z 500-23000 for PMA. The laser irradiance was set to 35-40 % (relative scale 0-100) arbitrary units according to the corresponding threshold required for the applied matrix systems.

The ultraviolet-visible (UV-vis) studies were performed with a Jasco V-530 spectrophotometer. The analyses were carried in the 350 – 1100 nm range at 30 ºC.

Table S1. Kinetic data for the SARA ATRP of MA, MMA, St and VC. Conditions: $[monomer]_0/[EBiB]_0/[Cu(0)\ wire]_0/[Ligand]_0$=222/1/1/1.1. $[Monomer]_0/[Solvent]$= 2/1 (v/v);

Entry	*Polymer*	$[M]_0/[I]_0/[Cu(0)\ wire^a]_0/[CuX_2]_0/[L]_0$ *(molar)*	*T (°C)*	k_p^{app} (h^{-1})	*Time (h)*	*Conv. (%)*	M_n^{th} $x10^{-3}$	M_n^{GPC} $x10^{-3}$	*Đ*
1	*PMA*	$[MA]_0/[EBiB]_0/[Cu(0)]_0/[CuBr_2]_0/[Me_6TREN]_0=222/1/\ Cu(0)/0/1.1$	*30*	*0.900*	*1.35*	*80.8*	*15.5*	*16.6*	*1.05*
2	*PMA*	$[MA]_0/[EBiB]_0/[Cu(0)]_0/[CuBr_2]_0/[Me_6TREN]_0=222/1/Cu(0)/0.1/1.1$	*30*	-	*1.30*	*71.6*	*13.7*	*17.0*	*1.10*
3	*PMA*	$[MA]_0/[EBiB]_0/[Cu(0)]_0/[CuBr_2]_0/[Me_6TREN]_0=100/1/Cu(0)/0.1/1.1$	*30*	-	*1.17*	*72.9*	*6.5*	*4.6*	*1.16*
4	*PMA*	$[MA]_0/[EBiB]_0/[Cu(0)]_0/[CuBr_2]_0/[Me_6TREN]_0\ =1100/1/Cu(0)/0/1.1$	*30*	*0.660*	*3.27*	*86.5*	*73.3*	*78.4*	*1.04*
5	*PMA*	$[MA]_0/[EBiB]_0/[Cu(0)]_0/[CuBr_2]_0/[Me_6TREN]_0\ =222/1/Cu(0)/0/1.1$	*30*	*1.048*	*1.50*	*74.05*	*14.9*	*17.9*	*1.07*
6	*PMMA*[b]	$[MMA]_0/[EBPA]_0/[Cu(0]_0/[CuBr_2]_0/[bpy]_0\ =222/1/Cu(0)/0/2.2$	*40*	*0.489*	*6.33*	*80.5*	*17.8*	*25.5*	*1.06*
7	*PMMA*[b]	$[MMA]_0/[EBPA]_0/[Cu(0)]_0/[CuBr_2]_0/\ [bpy]_0\ =222/1/Cu(0)/0.1/2.2$	*40*	*0.410*	*4.05*	*87.0*	*18.9*	*21.9*	*1.10*
8	*PMMA*[b]	$[MMA]_0/[TsCl]_0/[Cu(0)]_0/[CuBr_2]_0/[bpy]_0\ =222/1/Cu(0)/0/2.2$	*40*	*0.161*	*7.62*	*76.6*	*16.9*	*25.8*	*1.21*
9	*PMMA*[b]	$[MMA]_0/[EBPA]_0/[Cu(0)]_0/[CuBr_2]_0/[bpy]_0=\ 80/1/Cu(0)/0/2.2$	*40*	-	*2.83*	*95.0*	*7.8*	*10.7*	*1.05*
10	*PS*	$[St]_0/[EBiB]_0/[Cu(0)]_0/[CuBr_2]_0/[PMDETA]_0\ =222/1/\ Cu(0)/0/1.1$	*30*	*0.022*	*44.6*	*58.5*	*13.7*	*63.4*	*1.27*
11	*PS*	$[St]_0/[EBiB]_0/[Cu(0)]_0/[CuBr_2]_0/[PMDETA]_0\ =222/1/\ Cu(0)/0/1.1$	*60*	*0.112*	*7.52*	*54.3*	*12.7*	*23.7*	*1.26*
12	*PS*	$[St]_0/[EBiB]_0/[Cu(0)]_0/[CuBr_2]_0/[PMDETA]_0\ =222/1/\ Cu(0)/0/1.1$	*90*	*0.240*	*4.15*	*64.5*	*15.0*	*42.8*	*1.24*
13	*PS*	$[St]_0/[CHBr_3]_0/[Cu(0)]_0/[CuCl_2]_0/[PMDETA]_0=222/1/Cu(0)/0.1/1.2$	*60*	*0.104*	*5.42*	*37.6*	*8.3*	*12.0*	*1.18*
14	*PVC*[b]	$[VC]_0/[CHBr_3]_0/[Cu(0)]_0/[CuBr_2]_0/[TREN]_0\ =222/1/Cu(0)/0/1.1$	*42*	*0.141*	*6.5*	*62.5*	*12.1*	*16.9*	*1.48*
15	*PVC*[b]	$[VC]_0/[CHBr_3]_0/[Cu(0)]_0/[CuBr_2]_0/[TREN]_0\ =222/1/Cu(0)/0/1.1$	*30*	-	*16.0*	*55.8*	*11.0*	*14.2*	*1.49*
16	*PVC*[b]	$[VC]_0/[CHBr_3]_0/[Cu(0)]_0/[TREN]_0\ =100/1/Cu(0)/0/1.1$	*42*	-	*2.0*	*48.4*	*5.5*	*9.1*	*1.55*
17	*PVC*[b]	$[VC]_0/[CHBr_3]_0/[Cu(0)]_0/[TREN]_0\ =50/1/Cu(0)/0/1.1$	*42*	-	*1.5*	*62.2*	*3.0*	*3.9*	*1.69*

[a] Cu(0) wire: d = 1 mm, l = 5 cm;

[b] $[monomer]_0/[solvent]$= 1/1

Comproportionation experiments

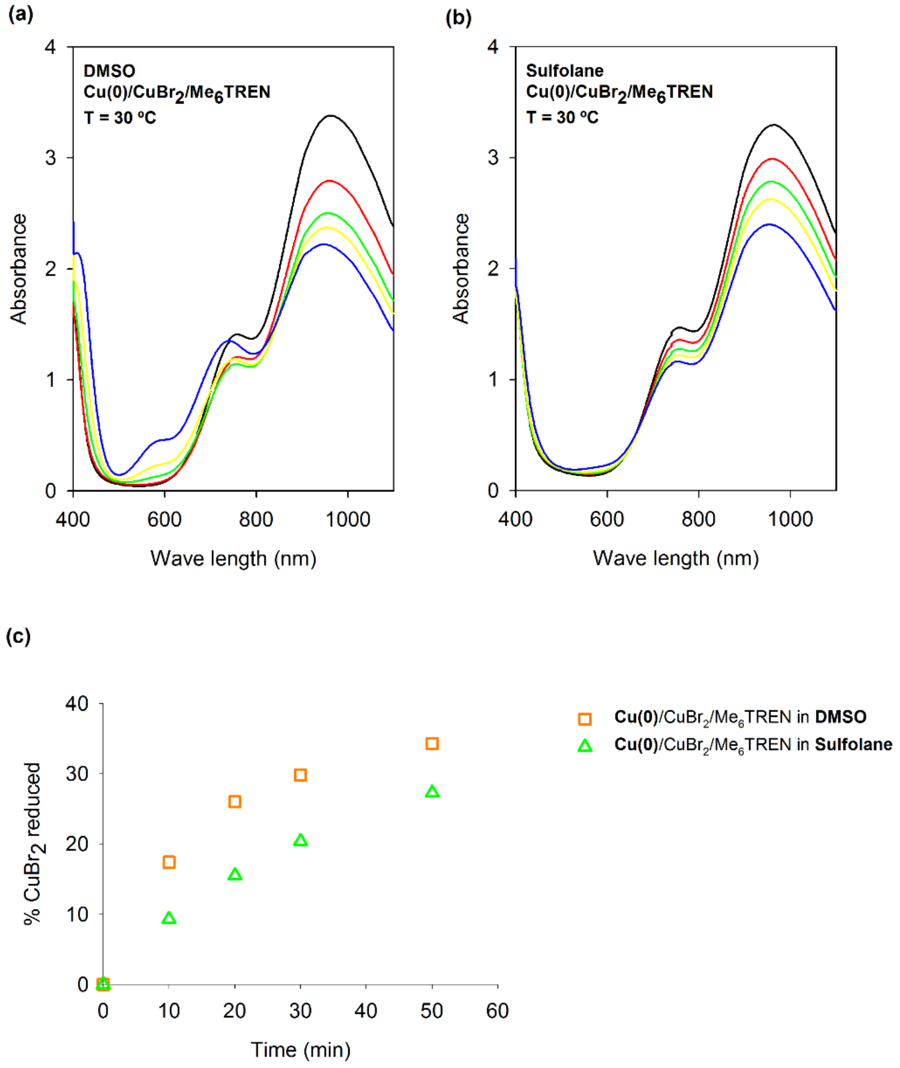

Figure S1. Evolution of UV−vis spectra in comproportionation experiments at 30 ºC: (a) Cu(0) wire: *l* = 5 cm and *d* = 1 mm, $[CuBr_2]_0$ = 7.50 mM and $[Me_6TREN]_0$ = 82.5 mM in DMSO (2.5 mL); (b) Cu(0) wire: *l* = 5 cm and *d* = 1 mm, $[CuBr_2]_0$ = 7.50 mM and $[Me_6TREN]_0$ = 82.5 mM in sulfolane (2.5 mL); (c) Percentage of $CuBr_2$ reduced during the comproportionation of Cu(0) and $CuBr_2$ in DMSO or sulfolane at 30 ºC. The values were determined by UV-vis spectroscopy.

Kinetic plots of SARA ATRP of St

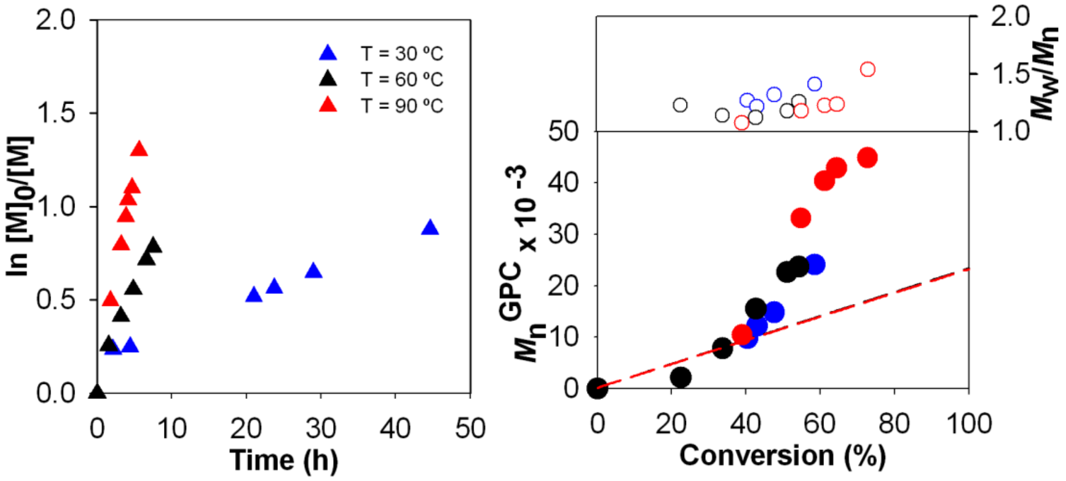

Figure S2 - a) Kinetic plots of ln$[M]_0/[M]$ *vs.* time and plot of number-average molecular weights (M_n^{GPC}) and $Đ$ (M_w/M_n) *vs.* conversion for the SARA ATRP of St using Cu(0) wire as supplemental activator and reducing agent in sulfolane at 30 ºC (blue symbols), 60 ºC (black symbols) and 90 ºC (red symbols) . Conditions: $[St]_0/[solvent]$ = 2/1 (v/v); $[St]_0/[EBiB]_0$/Cu(0)wire /$[PMDETA]_0$ = 222/1/Cu(0) wire/1.1 (molar); Cu (0): d = 1 mm, l = 5 cm.

^{1}H–NMR spectra of homopolymers

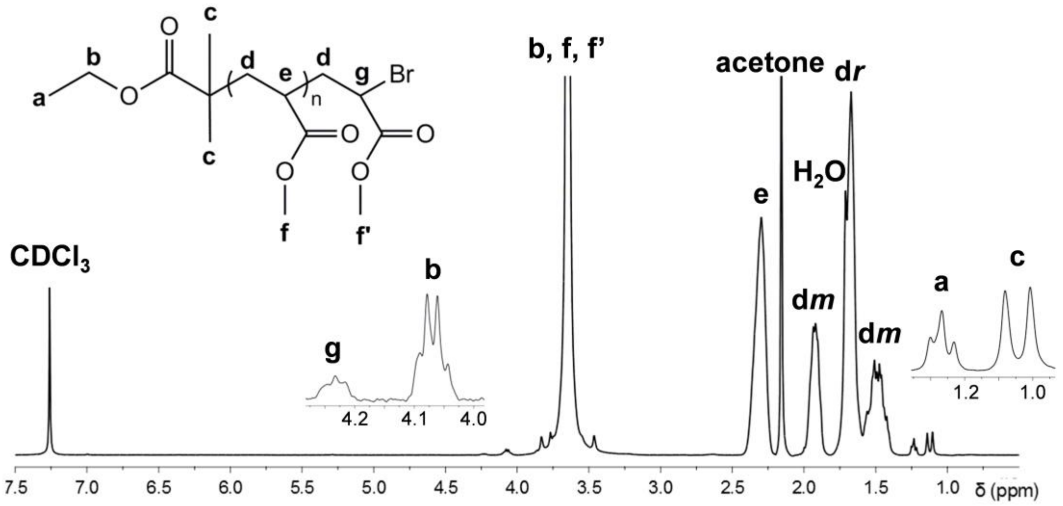

Figure S3. ^{1}H NMR spectrum of PMA-Br (M_n^{GPC} = 15.9 x 10^3; Đ =1.08) in $CDCl_3$.

The structure of PMA was confirmed by ^{1}H NMR spectrum that is shown in Figure S3. The assignment of proton resonances was realized according to the references: (e, g, f, f’)[2-4], (a, b, c)[2, 5], (d*r*, d*m*).[2, 6-9] The ^{1}H NMR spectrum reveals the resonance of the repeating unit CH_2-CH-CO_2Me: d (1.4-2.0 ppm), e (2.35-2.4 ppm) and f (3.6-3.75 ppm), respectively. The resonance of the terminal group CHBr-CO_2Me is also present at 4.2-4.35 ppm (g) and 3.75-3.85 ppm (f’), respectively. The initiator fragments (containing protons a, b and c) are revealed at 1.2-1.25 ppm, 4.05-4.1 ppm and 1.05-1.15 ppm.

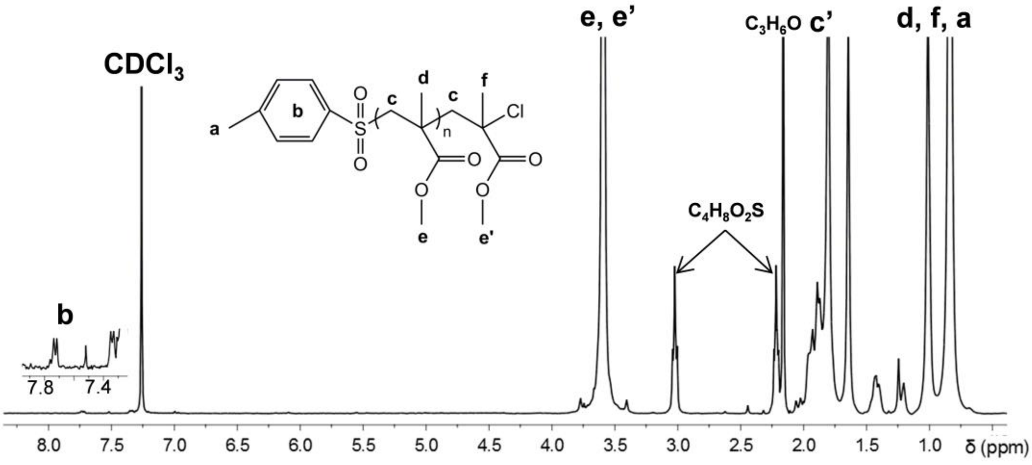

Figure S4. ^{1}H NMR spectrum of PMMA-Br (M_n^{GPC} = 52500; $Đ$ =1.46) in $CDCl_3$.

^{1}H NMR technique was used to confirm the PMMA-Br structure and the spectrum is shown in Figure S4. The assignment of the proton resonances was realized according to references: (a, b)[10], (c, d e, e’, f).[11] The ^{1}H NMR spectrum reveals the resonance of the repeating unit $CH_2CCH_3COOCH_3$: d (0.75-1.0 ppm) and e (3.5-3.75 ppm). The resonance of the terminal group is also present at 1.75-2.0 ppm. The initiator fragments are revealed through the resonance of protons at 1.25 ppm and 7.36 - 7.74 ppm respectively from the methyl and phenyl group.

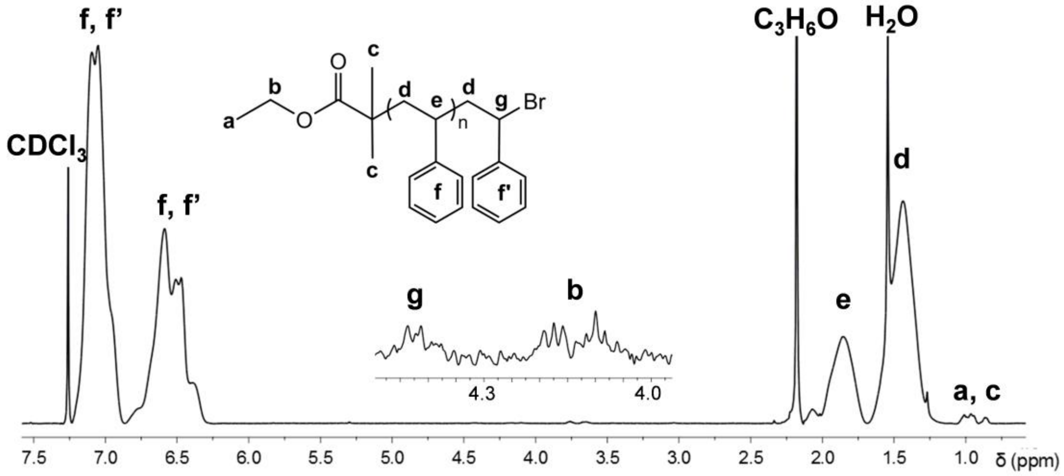

Figure S5. ^{1}H NMR spectrum of PS-Br (M_n^{GPC} = 24.7 x 10^3; $Đ$ = 1.24) in $CDCl_3$.

The structure and the presence of the chain-end functionality of PS-Br polymer was evaluated by 400 MHz ^{1}H NMR spectroscopy. The initiator fragment is revealed by the appearance of the resonance peaks of protons a, b and c, at 0.90-1.05 ppm, 4.0-4.25 ppm and 0.7-0.9 ppm, respectively. The spectrum reveals the presence of the repeating unit CH_2-CHPh by the aromatic protons peaks at 6.25-7.5 ppm (f). The chain-end functionality is confirmed by the resonance of proton e, adjacent to bromine, at 4.35-4.5 ppm from CH_2-CHPhBr terminal group.[12]

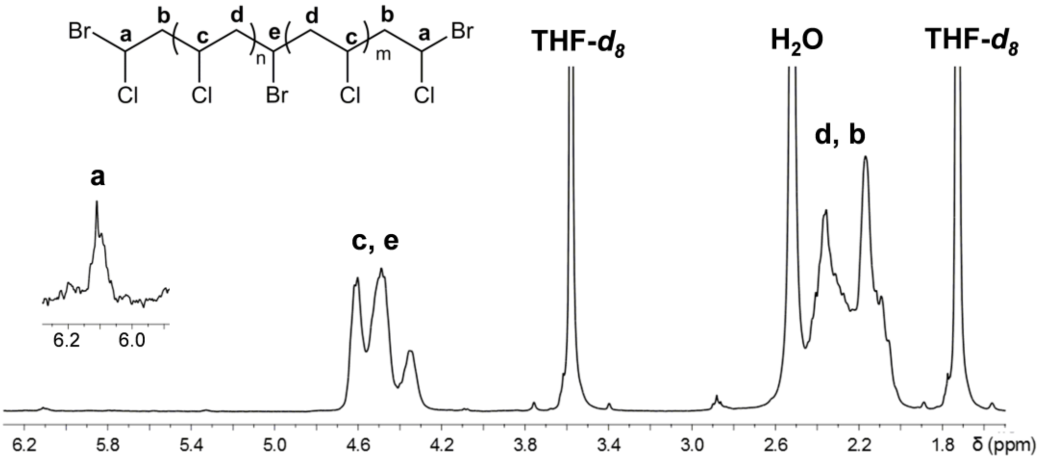

Figure S6. The ^{1}H NMR spectrum of Br-PVC-Br (M_n^{GPC} = 9100; $Đ$ = 1.55) in THF-d_8.

The structure of α,ω-di(bromo)PVC was analyzed by 400 MHz ^{1}H NMR spectroscopy and the spectrum is shown in the Figure S6 . The assignment of the proton resonances was realized according to the references: (a, d, e)[13] and (b, d)[13, 14]. The ^{1}H NMR spectrum reveals the resonance of the repeating unit CH_2-CHCl: 2.0-2.4 ppm (b) and 4.3-4.7 ppm (c). The resonance of the terminal group CH_2-CHClBr is also present at 2.0-2.7 ppm (d) and 6.05-6.15 ppm (e). The initiator fragments (a) is overlapped with the repeating unit signals in the range of 4.3-4.7 ppm.[13] Through the magnification of the region between 5.4 ppm and 6.5 ppm, it is possible to detect that only the diastereomeric –CHClBr (6.1 ppm) chain-ends were formed, since the signal from the diastereomeric –$CHBr_2$ at 6.0 ppm does not appear.[13]

MALDI – TOF homopolymers

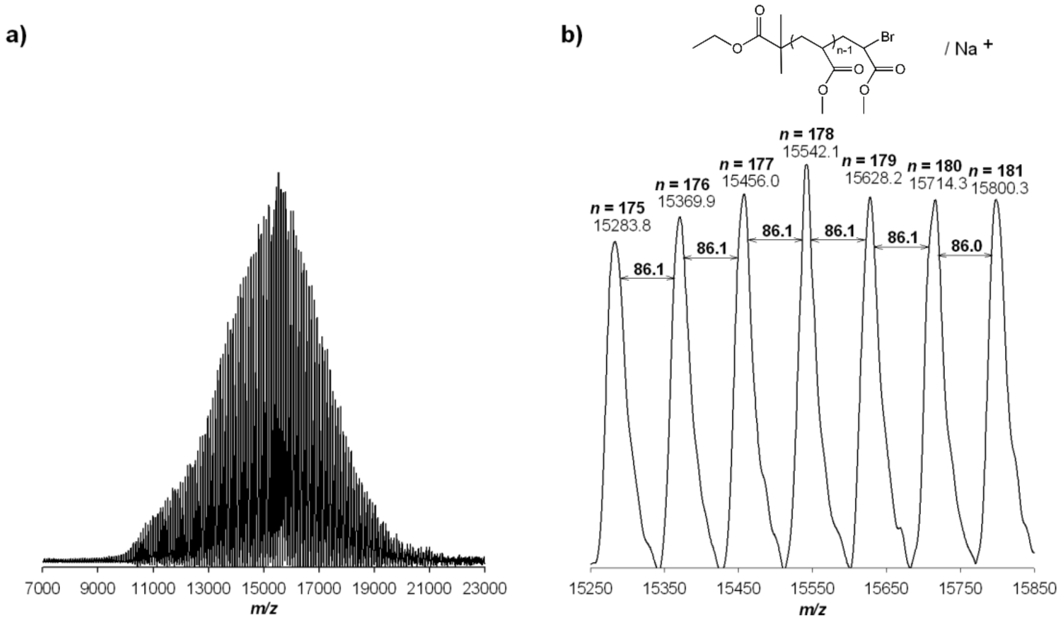

Figure S7. (a) MALDI-TOF-MS in the linear mode (using HABA as matrix) of PMA-Br (M_n^{GPC} = 15900, Đ = 1.08); (b) Enlargement of the MALDI-TOF-MS from m/z 15250 to 15850 of PMA-Br .

The MALDI-TOF-MS spectrum of PMA was acquired with two different matrices, HABA and DHB, but only HABA gave a clearly resolved spectrum (Figure S7 a) and b). MALDI-TOF-MS of PMA-Br with m/z ranging from 7000 to 23000 in linear mode is shown in Figure S7 a). Figure S7 b) shows the enlargement of the m/z 15250-15850 range. Importantly, the main peaks are separated by an interval corresponding to a monomer MA repeating unit (86.1 mass units). Figure S7 shows peaks that are attributed to a PMA-Br polymer chain, with ion formed of single alkali metal adduct $[R\text{-}(MA)_n\text{-}Br + Na^+]^+$, where R-Br is the initiator EBiB (15283.8 = 195.05 + 175 × 86.09 + 22.99, where 195.05, 86.09 and 22.99 correspond to the molar mass of EBiB, MA and Na^+, respectively).

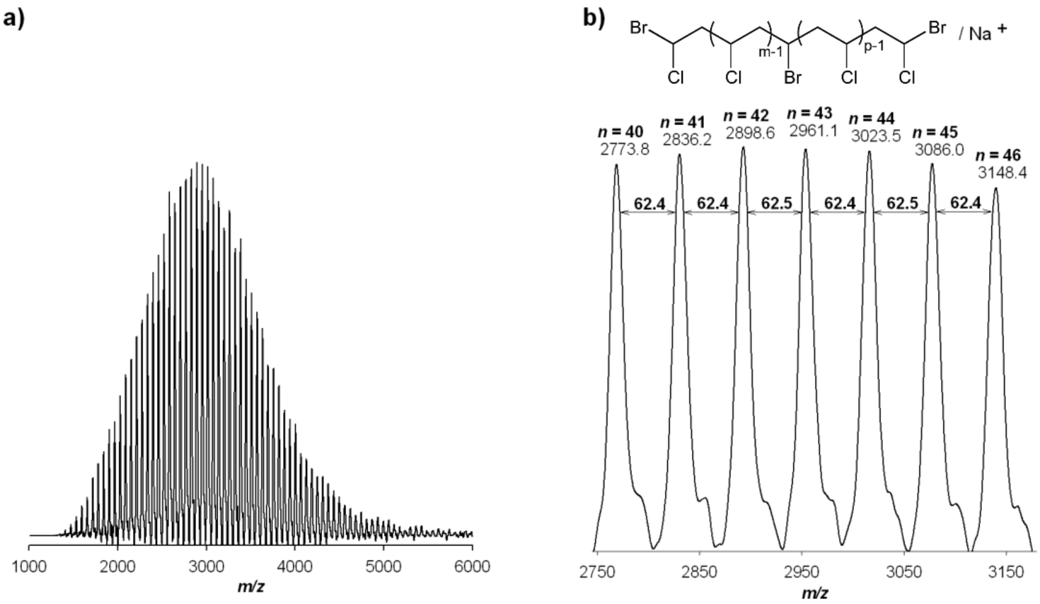

Figure S8. (a) MALDI-TOF-MS in the linear mode (using HABA as matrix) of Br-PVC-Br (M_n^{GPC} = 9100, *Đ* = 1.55); (b) Enlargement of the MALDI-TOF-MS from m/z 2750 to 3200 of Br-PVC-Br .

Again, for the MALDI-TOF-MS of Br-PVC-Br only HABA matrix allowed to obtain a clearly resolved spectrum (Figure S8 a) and b)). Figure S8 b) shows the enlargement of the m/z 2750-3200 range in linear mode. The higher peaks are separated by an interval that corresponds to a VC repeating unit (62.5 mass units). The peaks obtained from MALDI-TOF-MS analysis are attributed to a polymer chain [Br-$(PVC)_m$-CHBr-$(PVC)_p$-Br + Na^+]$^+$, where ‘m + p’ correspond to the degree of polymerization ‘n’ (2773.8 = 252.73 + 40 × 62.45 + 22.99, where 252.73, 62.45 and 22.99 correspond to the molar mass of initiator $CHBr_3$, VC and Na^+, respectively). The MALDI-TOF-MS confirmed the well-controlled PVC structure obtained using sulfolane as the solvent for the polymerization reactions.

To prove the “living” nature of the –Br chain-ends, chain extensions and block copolymerizations were carried out using different macroinitiators. Figure S9, Figure S10 and Figure S11 show the complete movement of the GPC traces of PMA-Br, PS-Br and PMMA-Br macroinitiators towards high molecular weights, resulting from the reinitiation of the –Br chain-ends using the respective monomers. The results presented in Figure S10 are particularly relevant since they demonstrate the high chain-end functionality of the PS prepared by SARA ATRP in sulfolane. Usually, PS is known for having poor chain-end functionality at high monomer conversion due to termination reactions.

Chain Extensions

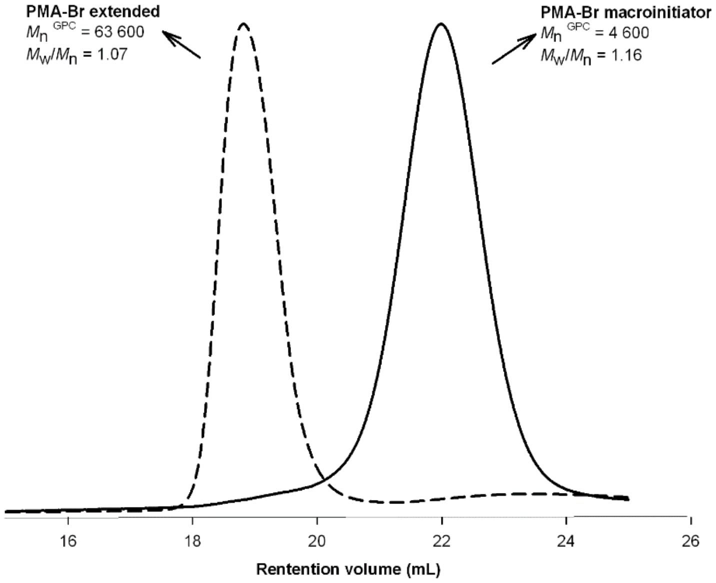

Figure S9 - Displacement of the GPC trace (RI signal) of a –Br-terminated PMA, obtained by SARA ATRP (solid line), towards high molecular weight values after a chain-extension experiment (dashed line). Conditions: $[MA]_0/[solvent] = 2/1$ (v/v); $[MA]_0/[EBiB]_0/Cu(0)$ wire $/[Me_6TREN]_0 = 222/1/$ Cu(0) wire /1.1 (molar); Cu (0): d = 1 mm, l = 5 cm.

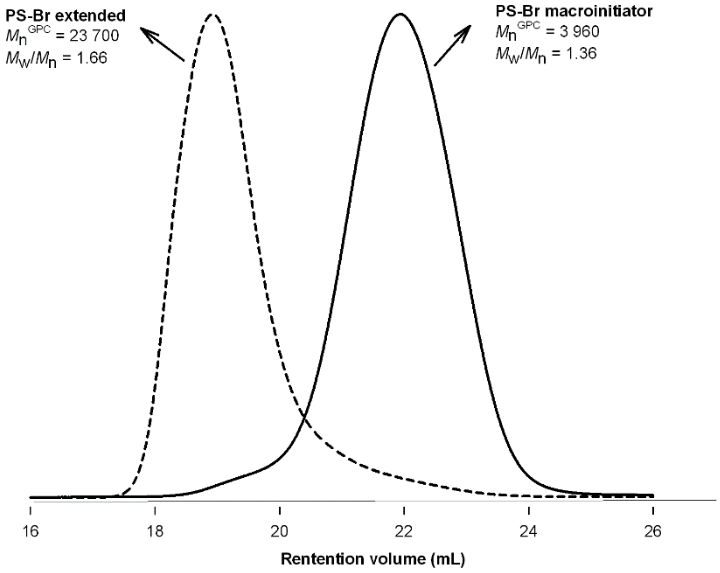

Figure S10 - Displacement of the GPC trace (RI signal) of a –Br-terminated PS obtained by SARA ATRP (solid line) towards high molecular weight values after a chain-extension experiment (dashed line). Conditions: $[St]_0/[solvent] = 2/1$ *(v/v);* $[St]_0/[EBiB]_0/Cu(0)\ wire/[PMDETA]_0 = 222/1/Cu(0)\ wire/1.1$ *(molar); Cu (0): d = 1 mm, l = 5 cm.;*

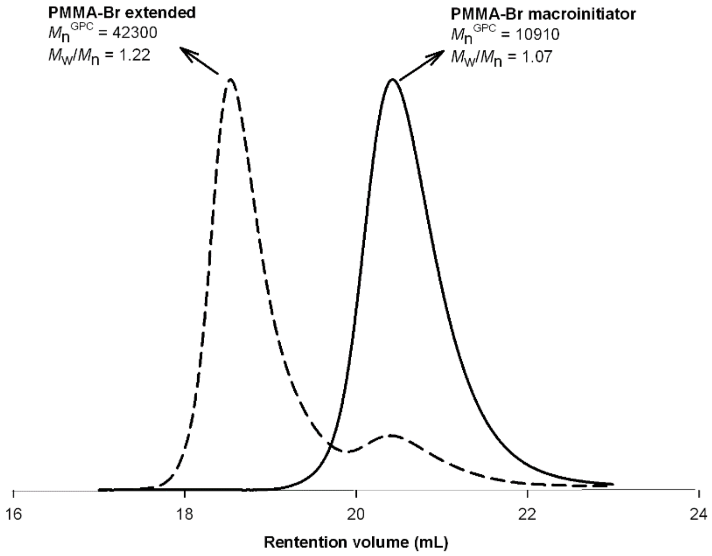

Figure S11 - Displacement of the GPC trace (RI signal) of a –Br-terminated PMMA obtained by SARA ATRP (solid line) towards high molecular weight values after a chain-extension experiment (dashed line). Conditions: $[MMA]_0/[solvent]$ = 2/1 (v/v); $[MMA]_0/[EBPA]_0/Cu(0)wire/[PMDETA]_0$ = 222/1/Cu(0) wire/1.1 (molar); Cu (0): d = 1 mm, l = 5 cm.

^{1}H NMR spectra of block copolymers

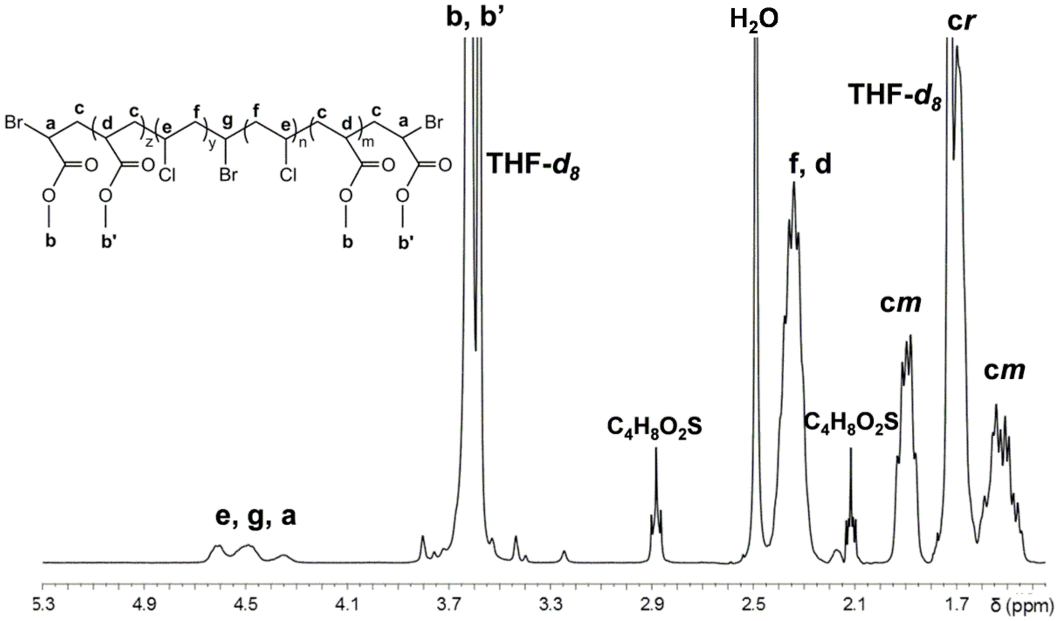

Figure S12. The ^{1}H NMR spectrum of PMA-*b*-PVC-*b*-PMA block copolymer (M_n^{GPC} = 59400; $Đ$ = 1.87) in THF- d_8.

The PMA-*b*-PVC-*b*-PMA structure was studied by ^{1}H NMR spectroscopy and spectrum is presented in Figure S12. The presence of the PMA block is confirmed by the appearance of the signals: 3.5-3.7 ppm (f and f', 3H), 1.4-2.0 ppm (d) and 2.0-2.45 (e). The presence of the PVC block is confirmed by the signal at 4.3-4.7 ppm, corresponding to the resonance of the repeating unit CH_2-CHCl. The d*r* signal is overallaped with the THF-d_8 signal, which avoided the determination of the syndiotactic and isotactic diads (d*r* and d*m* respectively) fractions.

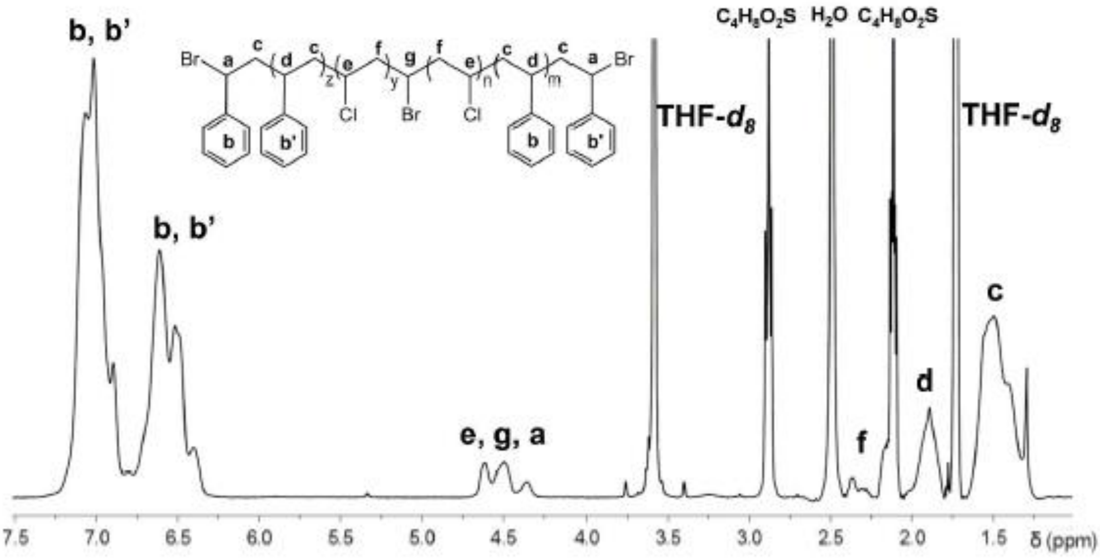

Figure S13. ^{1}H NMR spectrum of PS-*b*-PVC-*b*-PS block copolymer (M_n^{GPC} = 63300; $Đ$ = 2.34) in THF-d_8.

Figure S13 shows the ^{1}H NMR spectrum of the PS-*b*-PVC-*b*-PS block copolymer. The presence of the vinyl chloride repeating unit is revealed by the resonances of CH_2-CHCl: 2.0 -2.40 ppm (b), that is partially overlapped with the sulfolane and water signals, and 4.25-4.7 ppm (c). The styrene repeating unit is revealed by the resonance of the protons (d) at 1.25-2.0 ppm and (f) at 6.25-7.25 ppm.

References

1. Ciampolini, M.; Nardi, N. *Inorg Chem* **1966,** 5, (1), 41-44.
2. Mendonca, P. V.; Serra, A. C.; Coelho, J. F. J.; Popov, A. V.; Guliashvili, T. *Eur Polym J* **2011,** 47, (7), 1460-1466.
3. Lligadas, G.; Ladislaw, J. S.; Guliashvili, T.; Percec, V. *J Polym Sci Pol Chem* **2008,** 46, (1), 278-288.
4. Percec, V.; Guliashvili, T.; Ladislaw, J. S.; Wistrand, A.; Stjerndahl, A.; Sienkowska, M. J.; Monteiro, M. J.; Sahoo, S. *J Am Chem Soc* **2006,** 128, (43), 14156-14165.
5. Hasneen, A.; Kim, S.; Paik, H.-j. *Macromol. Res.* **2007,** 15, (6), 541-546.
6. Coelho, J. F. J.; Mendonça, P. V.; Popov, A. V.; Percec, V.; Gonçalves, P. M. O. F.; Gil, M. H. *J Polym Sci Pol Chem* **2009,** 47, (24), 7021-7031.
7. Coelho, J. F. J.; Carvalho, E. Y.; Marques, D. S.; Popov, A. V.; Percec, V.; Gonçalves, P. M. F. O.; Gil, M. H. *J Polym Sci Pol Chem* **2008,** 46, (2), 421-432.
8. Coelho, J. F. J.; Carvalho, E. Y.; Marques, D. S.; Popov, A. V.; Goncalves, P. M.; Gil, M. H. *Macromol Chem Phys* **2007,** 208, (11), 1218-1227.
9. Tabuchi, M.; Kawauchi, T.; Kitayama, T.; Hatada, K. *Polymer* **2002,** 43, (25), 7185-7190.
10. Gurr, P. A.; Mills, M. F.; Qiao, G. G.; Solomon, D. H. *Polymer* **2005,** 46, (7), 2097-2104.
11. Gong, S.; Ma, H.; Wan, X. *Polym Int* **2006,** 55, (12), 1420-1425.
12. Rocha, N.; Mendonca, P. V.; Mendes, J. P.; Simoes, P. N.; Popov, A. V.; Guliashvili, T.; Serra, A. C.; Coelho, J. F. J. *Macromol Chem Phys* **2013,** 214, (1), 76-84.
13. Sienkowska, M. J.; Rosen, B. M.; Percec, V. *J Polym Sci Pol Chem* **2009,** 47, (16), 4130-4140.
14. Abreu, C. M. R.; Mendonça, P. V.; Serra, A. C.; Coelho, J. F. J.; Popov, A. V.; Gryn'ova, G.; Coote, M. L.; Guliashvili, T. *Macromolecules* **2012,** 45, (5), 2200-2208.

Appendix G – Reactions Tables for the different modifications realized to GO

- **Esterification reaction based on the Lee method (-OH groups)**

Table G1. Amounts and ratios used to determine the quantities of reactants used in esterification reactions, following the work reported [24].

	Reactant	Amount		Ratio	
Lee method [24]	GO	1.00	g		-
	BIBB	30.00	mL		-
		55.80	g	55.80	g BIBB/g GO
		0.24	mol		-
	TEA	20.00	mL		-
		14.52	g	14.52	g TEA/g GO
		0.14	mol	0.59	mol TEA/mol BIBB
	Dry DMF	30	mL	33.33	mg GO/mL DMF
Example for Br_G10	GO	0.60	g		-
	BIBB	18.00	mL		-
		33.48	g	55.80	g BIBB/g GO
		0.146	mol		-
	TEA	12.00	mL		-
		8.71	g	14.52	g TEA/g GO
		0.086	mol	0.59	mol TEA/mol BIBB
	Dry DMF	20	mL	30.00	mg GO/mL DMF
Br_G11	GO	0.50	g		-
	BIBB	7.50	mL		-
		13.96	g	27.90	g BIBB/g GO
		0.061	mol		-
	TEA	0.061	mol	1/1	mol TEA/mol BIBB
		8.457	mL		-
	Dry DMF	25.00	mL	20.00	mg GO/mL DMF

- **Esterification reaction based on the Yang method (-COOH and -OH groups)**

Table G2. Amounts and ratios used to determine the quantities of reactants used in esterification/amidation reactions, following the work reported in the literature [23].

	Reactant	Amount		Ratio	
Yang method [23]	GO	1.00	g		-
	1,3-diaminopropane	3.80	mL		-
		3.37	g	3.37	g/g GO
		0.046	mol		-
	NHS	3.42	g	3.42	g NHS/g GO
		0.030	mol		-
	EDC.HCl	5.75	g	5.75	g EDC/g GO
		0.030	mol		-
	BIBB	6.20	mL		-
		11.53	g	11.53	g BIBB/g GO
		0.050	mol		-
	TEA	10.50	mL		-
		7.62	g	7.62	g TEA/g GO
		0.075	mol	1.50	mol TEA/mol BIBB
	Dry DMF	250	mL	4.00	mg GO/mL DMF
Our experiments	GO	0.100	g		-
	1,3-diaminopropane	0.38	mL		-
		0.337	g	3.37	g/g GO
	NHS	0.342	g	3.42	g NHS/g GO
		0.0030	mol		-
	EDC.HCl	0.575	g	5.75	g EDC/g GO
		0.0030	mol		-
	BIBB	0.620	mL		-
		1.153	g	11.53	g BIBB/g GO
		0.0050	mol		-
	TEA	1.050	mL		-
		0.762	g	7.62	g TEA/g GO
		0.0075	mol	1.50	mol TEA/mol BIBB
	Dry DMF	25.00	mL	4.00	mg GO/mL DMF

- **Preliminary polymerization reactions**

Table G3. Amounts of monomers, catalyst and ligands used in some of the articles found. Research for typical ratios of catalysts and ligands used in the literature.

Ref	Reactant	Amount		Ratio	
[26]	GO-Br	100	mg		-
	DMAEMA	2000	mg	20	mg DMAEMA/mg GO
		2.14	mL		-
	CuBr	15.00	mg	0.15	mg CuBr/mg GO
		0.10	mmol		-
	PMDETA	0.10	mmol	1/1	mol PMDETA/mol CuBr
		21.00	µL		-
	DMF	5	mL	20.00	mg GO/mL DMF
[25]	GO-Br	200	mg		-
	SS	200	mg	1	mg SS/mg GO
		210	µL		-
	CuBr	28.00	mg	0.14	mg CuBr/mg GO
		0.20	mmol		-
	PMDETA	0.20	mmol	1/1	mol PMDETA / mol CuBr
		42.17	µL		-
	DMF	4	mL	50.00	mg GO/mL DMF
[24]	GO-Br	100	mg		-
		0.115	mmol		-
	Sty	4530	mg	45.30	mg Sty/mg GO
		5	mL		-
		43.49	mmol	379.74	mol Sty/mol Br
	Cu(0)	wire			
	TREN	75.00	µL		-
		73.28	mg	0.73	mg TREN/mg GO
		0.50	mmol	4.37	Mol TREN/mol Br
	DMF	5	mL	20.00	mg GO/mL DMF
				1/1	Sty/DMF (v/v)

Table G3. (Continued)

	Reactant	Amount		Ratio	
[23]	GO-Br	200	mg		-
		0.0112	mmol		-
	DMAEMA	0.011	mmol		-
		1400	mg	7.00	mg DMAEMA/mg GO
		1.50	mL		-
	CuBr	16.00	mg	0.08	mg CuBr/mg GO
		0.11	mmol	10.00	mol CuBr/mol Br
	PMDETA	67.00	µL		-
		0.32	mmol	2.88	mol PMDETA/mol CuBr
[54]	GO-Br	500	mg		-
	EBiB	0.65	mmol		-
	Sty	27.18	g	54.36	mg MA/mg GO
		30	mL		-
		260.97	mmol	100/0.5	mol Sty/mol EBiB
	CuBr	188.00	mg	0.38	mg CuBr/mg GO
		1.31	mmol	1/0.5	mol CuBr/mol EBiB
	PMDETA	274	µL		-
		1.31	mmol	1/1	mol PMDETA/mole CuBr
	DMF	10	mL	50.00	mg GO/mL DMF
[56]	GO-Br	25	mg		-
	MA	2870	mg	114.72	mg MA/mg GO
		3.00	mL		-
	CuCl	100	mg	4.00	mg CuCl/mg GO
		1.01	mmol		-
	$CuCl_2$	50	mg	2.00	mg $CuCl_2$/mg GO
		0.37	mmol	0.37	mol $CuCl_2$/mol CuCl
	PMDETA	100	µL		-
	DMF	20	mL	1.25	mg GO/mL DMF

Table G4. Amounts and ratios used to determine the quantities of reactants used in preliminary polymerization reactions, following the work developed by Gonçalves and co-workers [10].

	Reactant	**Amount**		**Ratio**	
Reference paper [10]	GO-Br	200	mg		-
	MMA	2800	mg	14.02	mg MMA/mg GO
		3.00	mL		-
	CuBr	38.73	mg	0.19	mg CuBr/mg GO
		0.27	mmol		-
	DMF	6.00	mL	33.33	mg GO/mL DMF
				1/2	MMA/DMF (v/v)
Our experiments	GO-Br	47	mg		-
	MA	660	mg	14.02	mg MA/mg GO
		689.11	µL		-
	CuBr	9.10	mg	0.19	mg CuBr/mg GO
		0.063	mmol		-
	Cu(0) wire	5	cm		-
	CuBr2	0.006	mmol	0.1/1	mol CuBr2/ mol CuBr
		1.42	mg		-
	Me_6TREN	0.070	mmol	1.1/0.1	mol Me_6TREN / mol $CuBr_2$
		18.65	µL	-	-
	DMF	1.38	mL	33.33	mg GO/mL DMF

In the case of CuBr/Me_6TREN catalytic system it was calculated the ratio between the mass of CuBr and the mass of GO used by Gonçalves [10] and based on this ratio the amount of CuBr was determined as a function of the mass of GO used in this work. The amount of Me_6TREN was determined having in mind the defined CuBr/Me_6TREN molar ratio 1/1.1 [101, 102, 110].

For the Cu(0) wire/$CuBr_2$/Me_6TREN catalytic system a similar strategy was followed, however additional considerations were necessary. The amount of $CuBr_2$ and Me_6TREN used were also determined from the CuBr quantities used in the literature [10]. It is already known that to have a good control over the polymerization the important parameter is the ratio between the soluble Cu^{I} ($\boldsymbol{Cu^{I}L_{n}}$) and Cu^{II} ($\boldsymbol{XCu^{II}L_{n}}$) species present in the system and not only the absolute amounts of CuBr and CuBr$_2$ used. This relation can be defined by the following equation [144]:

$$R_p = k_p[M][P^{\cdot}] = k_p[M]k_{ATRP}\frac{[PX][\boldsymbol{Cu^{I}L_{n}}]}{[\boldsymbol{XCu^{II}L_{n}}]}$$

In Figure 9 is shown the ATRP mechanism which support the equation presented above.

The ratio of CuBr$_2$ normally used as starting point is 0.1 relatively to the moles of initiator [101, 102, 110]. In this stage of the work, the moles of initiator were unknown and, because of this, the amounts of CuBr$_2$ were defined based on the moles of CuBr used in the paper used as reference [10]. As previous, was assumed that the relation between CuBr and initiator moieties used by the authors was 1/1, as employed in several reports [54, 70, 71].

In short, the amount of CuBr$_2$ was defined base on the amount of CuBr defined by Gonçalves [10] and the CuBr/CuBr$_2$ ratio of 1/0.1. The amount of Me$_6$TREN was defined in order to obtain a molar ratio of 0.1/1.1 between the CuBr$_2$ species and the ligand species. All the molar ratios between the different species were defined having as base previous works developed in the ATRP research area [100-102, 110].

- **SARA ATRP of Sty catalysed by Cu(0) wire/TREN based on the literature [24]**

Table G5. Amounts and ratios used to determine the quantities of reactants used in SARA ATRP of Sty catalysed by Cu(0) wire/TREN [24].

	Reactant	**Amount**		**Ratio**	
Using exactly the same amounts	GO-Br	100	mg		-
		0.072	mmol		-
	Sty	4530	mg	45.30	mg Sty/mg GO
		5	mL		-
		43.49	mmol	602	mol Sty/mol Br
	Cu(0) wire	5	cm		-
	TREN	75.00	µL		-
		73.28	mg	0.73	mg TREN/mg GO
		0.50	mmol	7	mol TREN/mol Br
	DMF	5	mL	20.00	mg GO/mL DMF
				1/1	Sty/DMF (v/v)
Example for a target DP = 500	GO-Br	50	mg		-
		0.036	mmol		-
	Sty	18.05	mmol	500	mol Sty/mol Br
		1880	mg		-
		2.08	mL		-
	Cu(0) wire	5	cm		-
	TREN	37.50	µL		-
		36.64	mg	0.73	mg TREN/mg GO
		0.25	mmol	7	mol TREN/mol Br
	DMF	2.5	mL	20.00	mg GO/mL DMF

- **SARA ATRP of MA from the surface of GO catalysed by Cu(0) wire/Me$_6$TREN in DMF at 60 ºC**

Table G6. Amounts and ratios used to determine the quantities of reactants used in SARA ATRP of MA catalysed by Cu(0) wire/Me$_6$TREN from the surface of GO.

	Reactant	Amount		Ratio	
Without sacrificial initiator	GO-Br	100	mg		-
		0.051	mmol		-
	MA	25.52	mmol	500	mol MA/mol Br
		1880	mg		-
		2.08	mL		-
	Cu(0) wire	5	cm		-
	Me$_6$TREN	0.056	mmol	1.1	mol Me$_6$TREN/mol Br
		15.01	µL		-
		12.94	mg		-
	DMF	5	mL	20.00	mg GO/mL DMF
With sacrificial initiator	GO-Br	100	mg		-
		0.051	mmol		-
	EBiB	0.051	mmol	1.0	mol EBiB/mol Br
		7.49	µL		-
	MA	51.04	mmol	500	mol MA/mol (Br + EBiB)
		4390	mg		-
		4.60	mL		-
	Cu(0) wire	5	cm		-
	Me$_6$TREN	0.112	mmol	1.1	mol Me$_6$TREN/mol (Br + EBiB)
		30.01	µL		-
		25.53	mg		-
	DMF	5.00	mL	20.00	mg GO/mL DMF

Appendix H – Preliminary reactions results

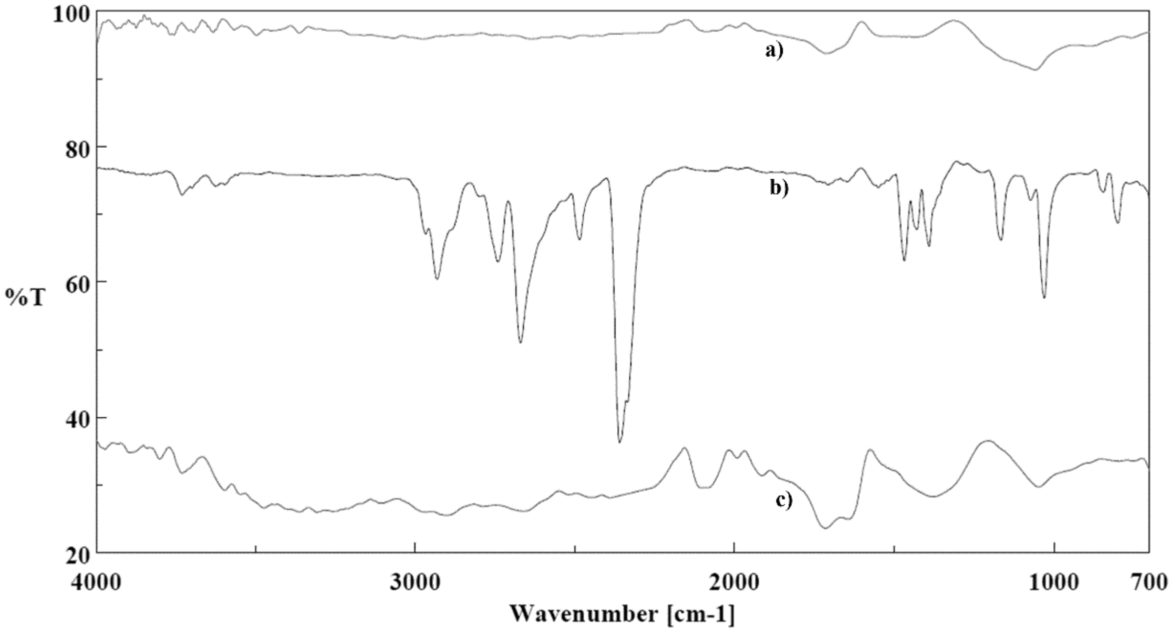

Figure H1. IR spectrum of a) Original GO, Oxi_Porto1; b) Esterification/amidation product Br_G01 and c) Esterification product Br_G02.

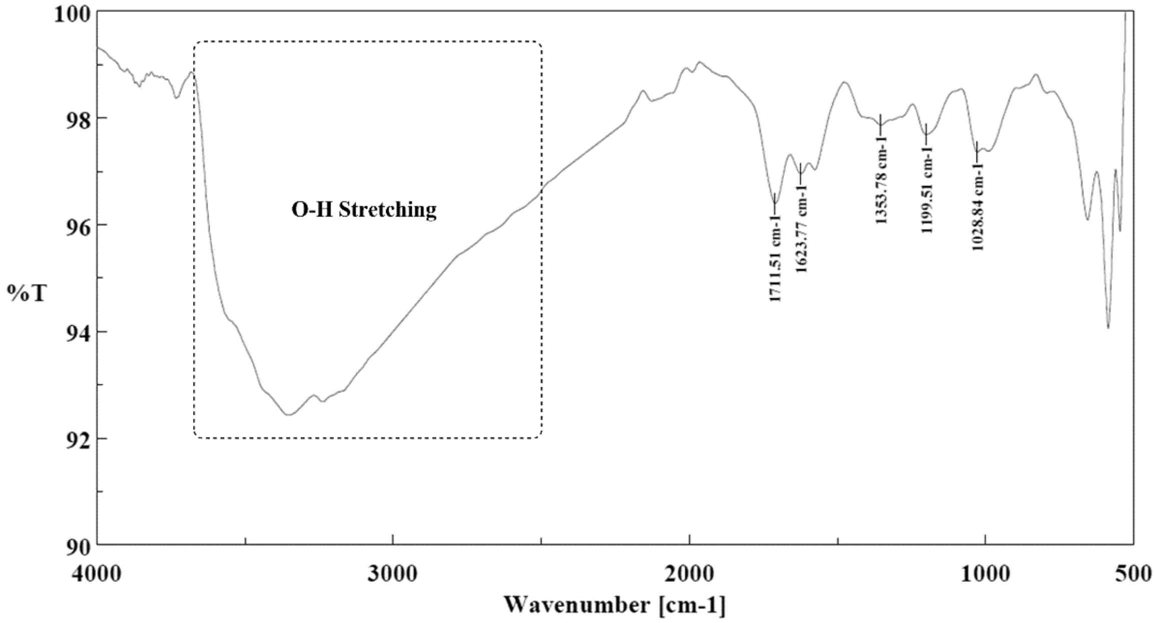

Figure H2. IR spectrum of Original GO Oxi_Porto2.

In IR spectrum of GO Oxi_Porto 2 (Figure H2) a strong and wide band in the range of 2500-3680 cm^{-1} is clearly visible, attributed to O-H stretching vibration from hydroxyl and carboxyl groups [23, 56]. This band is the most obvious indicator of the presence of hydroxyl groups in GO's surface. The peaks at 1711 and 1624 should illustrate the presence of C=O stretching vibration from carboxyl groups and C=C from aromatic skeletons of GO, respectively [13, 56, 61, 62, 118]. Finally, the three small peaks at 1354, 1200 and 1029 cm^{-1} should indicate the presence of C-OH groups, epoxy (C-O-C) and alkoxy (C-O) groups respectively [56, 118].

The TGA curve (Figure H3) revealed a first weight loss of 11% near to 100 ºC, which is mainly associated to the loss of water molecules that were adsorbed in the structure of GO [24, 56]. The main weight loss was observed in the range of 115 and 373 ºC. This weight loss of about 32% was attributed to the decomposition of the labile oxygenated species like hydroxyl, carboxyl and epoxy groups that were released in the form of carbon oxides, namely CO and CO_2 [24, 61, 62].

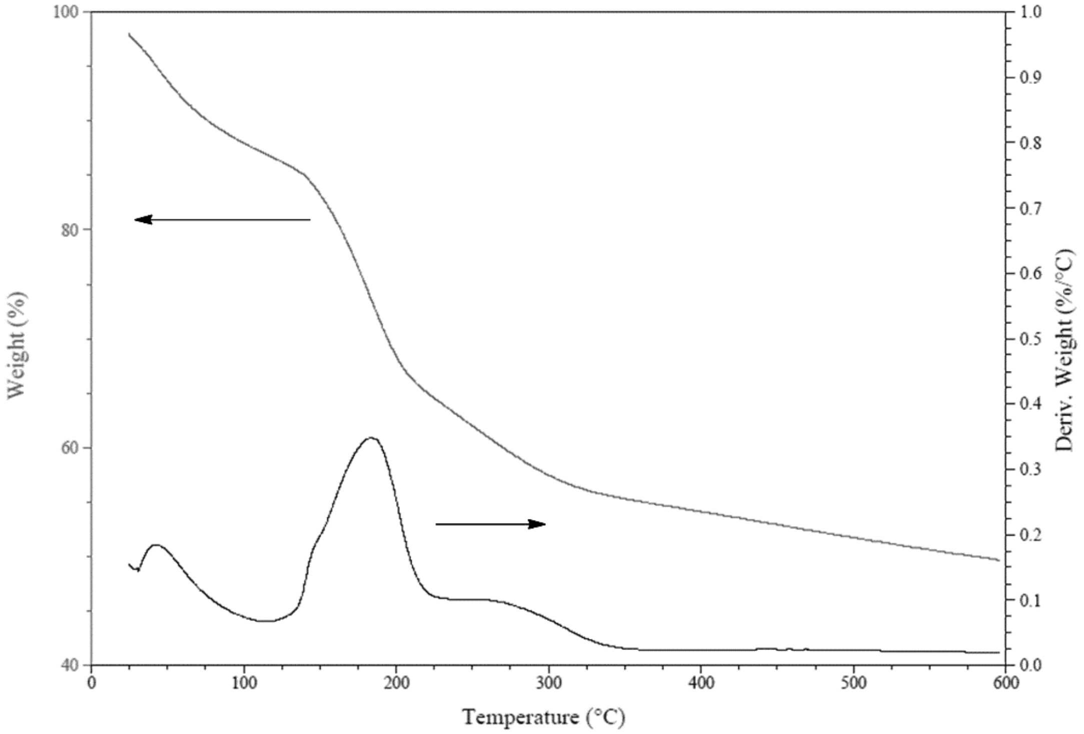

Figure H3. TGA curves of Original GO Oxi_Porto2.

In Figure H4 and Figure H5 are presented the FTIR and TGA results, respectively, obtained for the esterification products Br_G03, Br_G04 and Br_05.

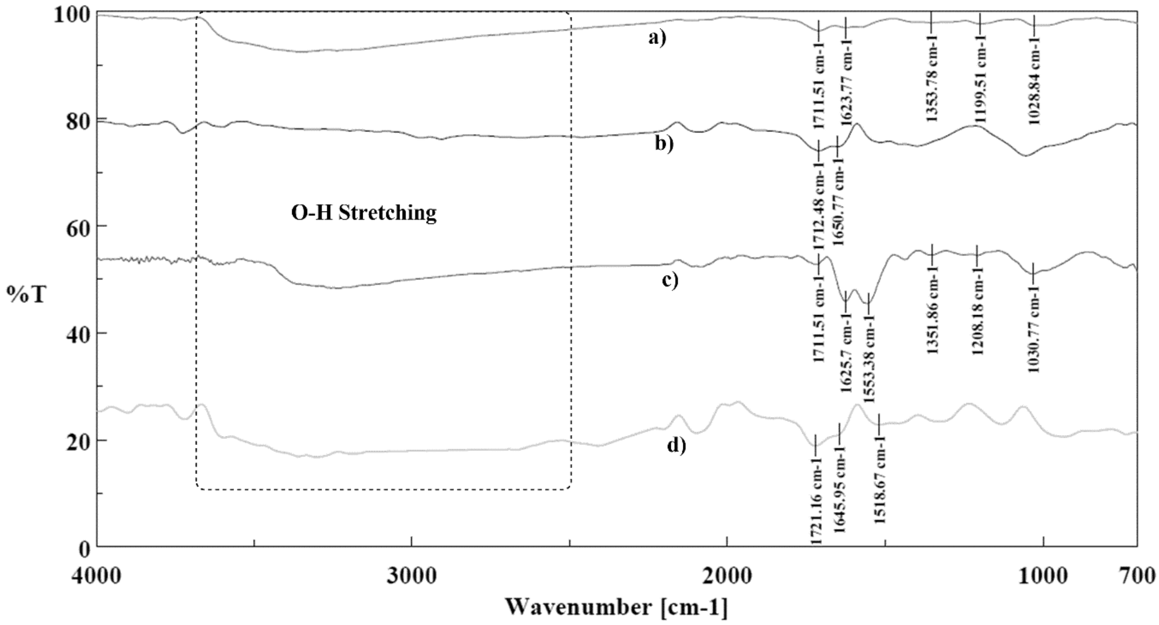

Figure H4. IR spectrum of a) Original GO Oxi_Porto2; b) Esterification product Br_G03; c) Esterification/amidation product Br_G04 and d) Esterification product Br_G05.

The O-H stretching vibration band disappeared when the Lee method [24] was used, indicating the replacement of -OH groups by the initiator molecules (Figure H4, curve b)). Instead, when the Yang method [23] was used only a slightly decrease in the O-H stretching vibration was observed (Figure H4, curve c)) probably indicating that the first method caused a greater functionalization of GO with BIBB molecules. Regarding the other peaks their analysis wasn't so obvious. In this phase of the work it was not possible to clearly understand the modifications observed in such peaks, as result of its low intensities and poor definitions. Considering this, the analysis of the success of the reactions was evaluated having as main focus the O-H stretching vibration band.

The TGA curves (Figure H5) also revealed modifications in GO. When the Lee method was employed the weight change measured was considerably lower than the weight loss observed in original GO (weight loss of Oxi_Porto2 was of about 48%, as for the weight losses of Br_G03 and Br_G05 samples were of about 24% and 29% respectively). On the other hand when both carboxyl and hydroxyl groups were modified a higher weight loss (about 40%) was measured. Additionally, the esterified products Br_G03 and Br_G05 only revealed one weight loss region, contrarily to the Br_G04 esterification/amidation samples in which two main weight loss regions around 200 ºC and 400 ºC could be observed.

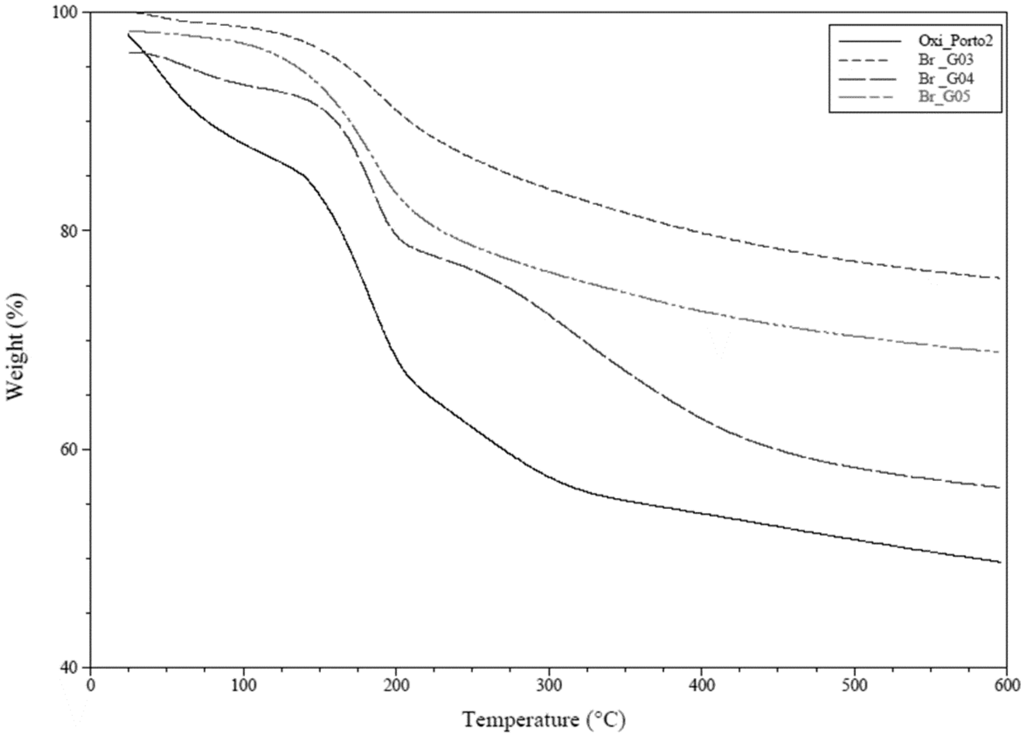

Figure H5. TGA curves of a) Oxi_Porto2 (solid line); b) Esterification product Br_G03 (short dashed line); c) Esterification/amidation product Br_G04 (long dashed line) and d) Esterification product Br_G05 (broken double dashed line).

The lower weight loss observed for the samples Br_G03 and Br_G05, compared to the original GO, indicated that most part of the water adsorbed in the GO's structure was removed, since there was not observed weight loss around 100 ºC. The weight changes of such samples were due to the decomposition of the functional groups attached to the surface of GO, including the initiator moieties. Also in the TGA curve of the sample Br_G04, there was no weight loss around 100 ºC, revealing, again, that the water absorbed in the GO was removed during the modification reactions. In this sample the two weight loss regions observed indicated the presence of different species and linkages existing in the GO's surface. The first weight loss observed was associated to the decomposition of oxygen containing species present in GO and the second to the amines attached to the surface of GO, by the first amidation reaction.

The TGA results were in agreement with the results reported in the literature, revealing that the two types of functionalization reactions were probably successful [23-26].

Figure H6 and Figure H7 show the IR spectra and TGA results, respectively, of the original GO Oxi_Porto2 and esterification product Br_G06 and Br_G07.

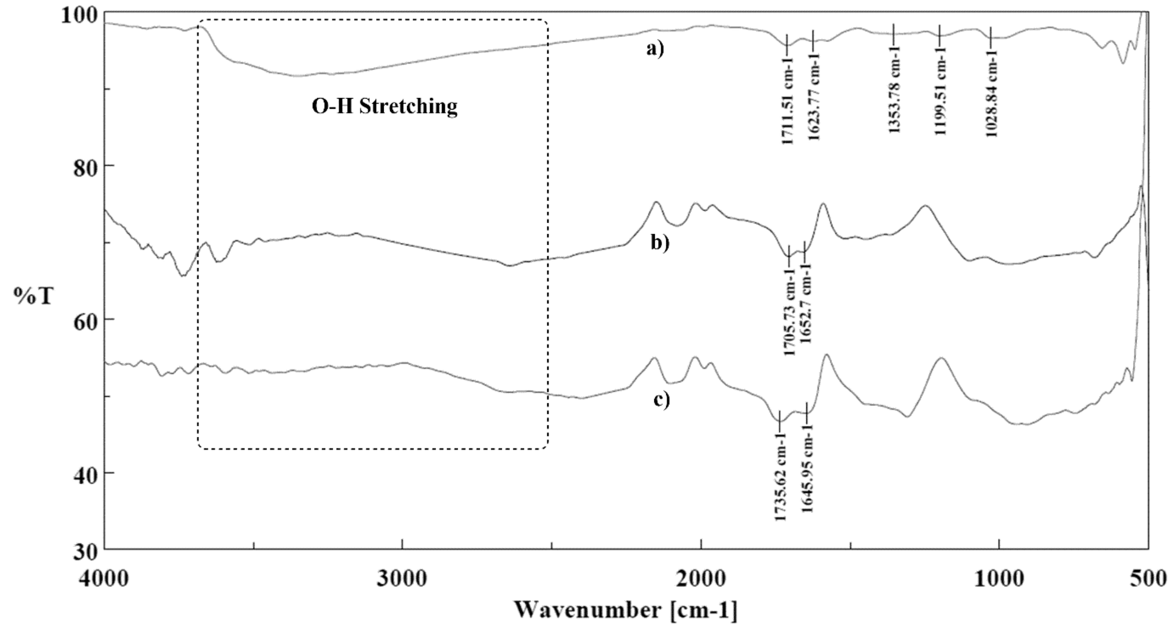

Figure H6. IR spectrum of a) Original GO Oxi_Porto2; b) Esterification product Br_G06 and c) Esterification product Br_G07.

The results obtained in esterification reactions Br_G06 and Br_G07 were the same as the ones obtained in previous esterification reactions Br_G03 and Br_G05. The characteristic O-H vibration band from hydroxyl groups disappeared and new peaks appeared at about 1500-1700 cm^{-1} probably attributed to the formation of new C=O bonds, from ester linkages. The TGA decomposition pattern was also identical, identifying only one weight loss zone attributed to the remaining oxygen containing species and to the degradation of the ester bonds. The weight losses observed were 31% and 24.3% for esterification products Br_G06 and Br_G07, respectively. With this, was proved one more time the reproducibility of the esterification reactions carried out.

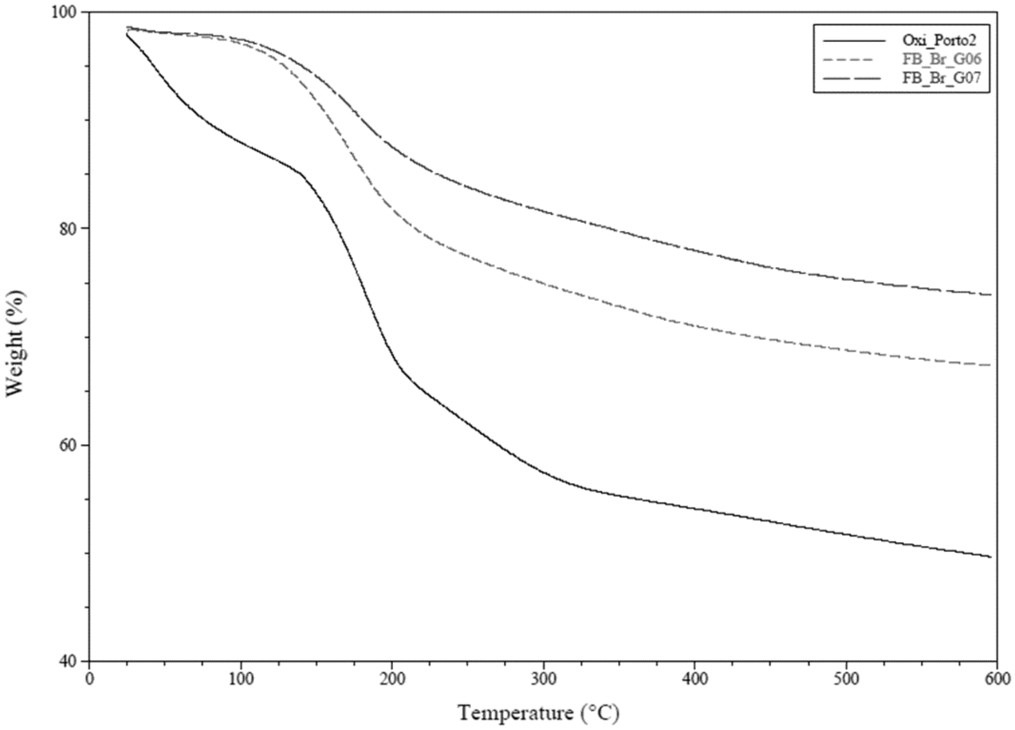

Figure H7. TGA curves of original GO Oxi_Porto2, esterification product Br_G06 and esterification product Br_G07.

In the Figure H8 and Figure H9 are presented comparisons between the FTIR results as well as the TGA results obtained for the two raw materials used, Oxi_Porto2 and FB_NIT.

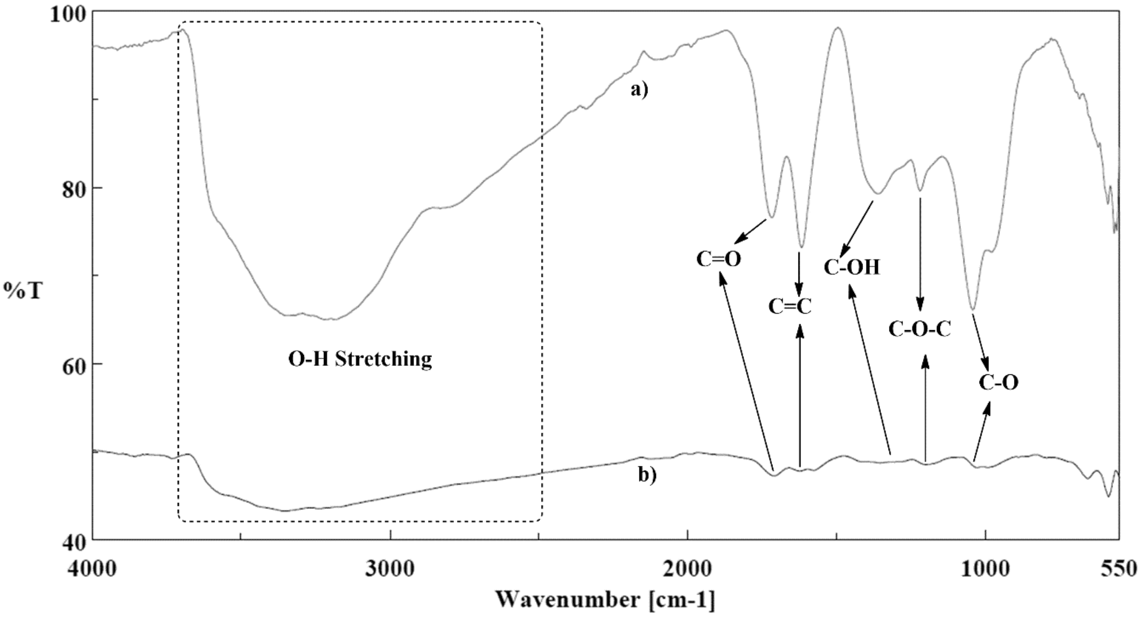

Figure H8. Comparison between a) FB_NIT and b) Oxi_Porto2.

The FTIR-ATR and TGA results, presented in Figure H8 and Figure H9, clearly showed that GO Oxi_Porto2 was significantly different from the purchased FB_NIT. In regard to the IR spectra all the main groups (O-H, C=O, C-OH, C-O-C and C-O) can be found in both raw material IR spectra, however the intensity of the peaks and the respective definition was much higher in the FB_NIT spectrum. These differences could be attributed to the lower degree of oxidation of the GO Oxi_Porto2. The TGA curves of the two GOs (Figure H9) presented the same decomposition pattern, with similar weigh losses (FB_NIT about 47% and Oxi_Porto2 at 48 %). However, in FB_NIT the weight loss between 200 and 300 ºC was much more abrupt, as can be seen through the derivative of weight loss respecting the temperature. This more abrupt weight loss can be ascribed to the presence of more labile oxygen-containing groups, like hydroxyl groups.

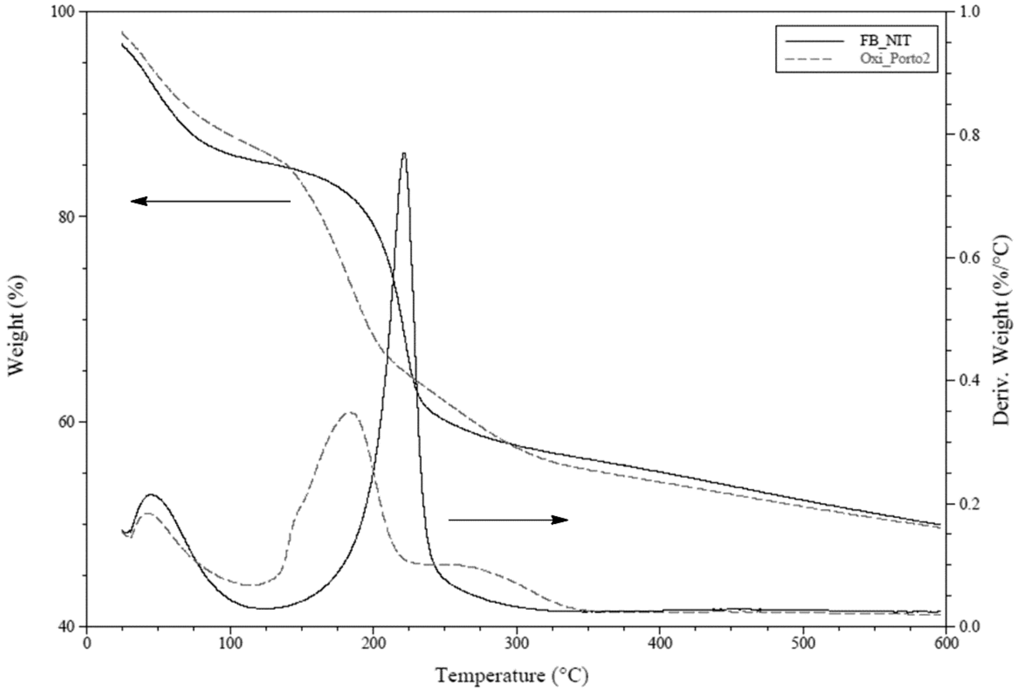

Figure H9. Comparison between TGA curves of GO FB_NIT and Oxi_Porto2.

Figure H10, Figure H11 and Table H1 show the XPS results measured for the product of the esterification/amidation reaction Br_G09, in which was reproduced the Yang method [23].

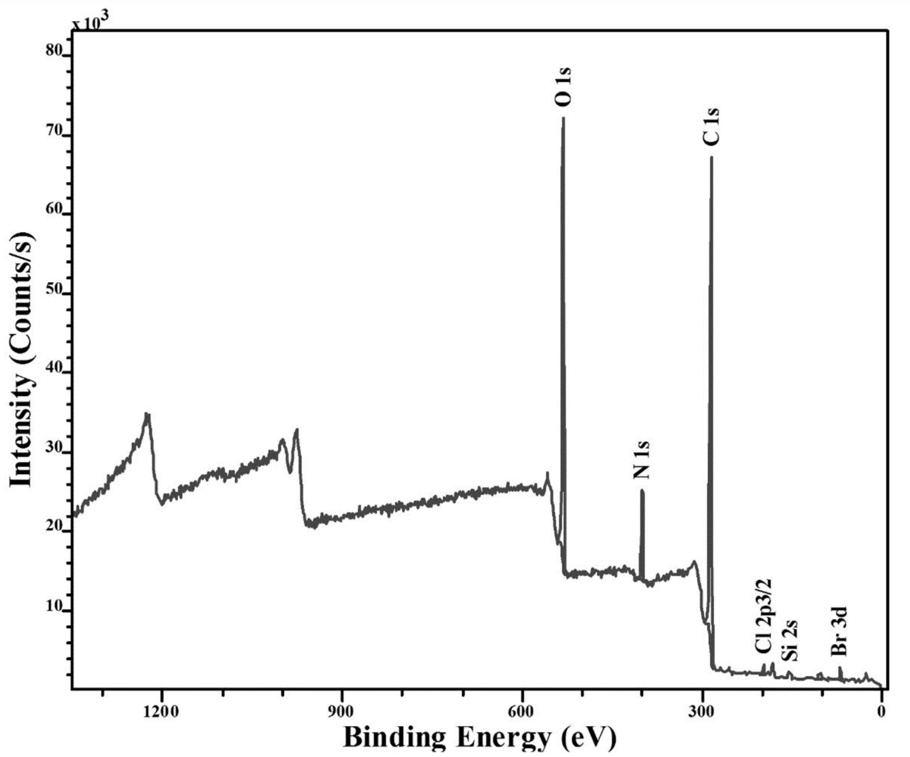

Figure H10. XPS spectrum of esterifications/amidation product Br_G09.

As result of the elemental quantification realized from the study of the spectrum acquired for the esterification/amidation product Br_G09 (Figure H10) the content of bromine in the sample was determined to be 3.35% (w/w). However, the Br3d high resolution spectrum, (Figure H11) revealed that from the total bromine content measured, 81.12% was covalently bonded to the GO surface, which means that in 100 mg of GO, 0.034 mmol of Bromine were covalently bonded.

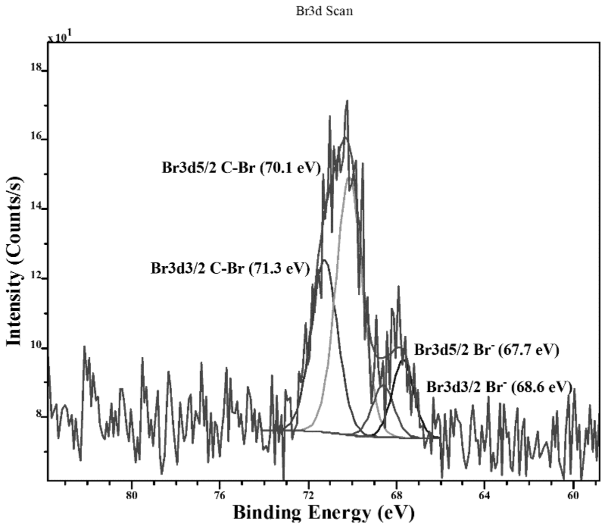

Figure H11. Br3d High resolution spectrum of Br_G09 esterification/amidation product.

In addition to the presence of Bromine also other minority elements were detected (Table H1) namely Nitrogen (N), Silicon (Si), sulphur (S) and chlorine (Cl). The increase in the amount of nitrogen percentage, in the modified product compared to the original GO, supports the attachement of 1,3-diaminepropane molecules to the surface of GO, indicating that also the first amidation reaction was successful. The appearance of Cl atoms was due to some traces of reactants that remained from the amidation/esterification reactions.

Table H1. Elemental quantification obtained from the XPS analysis conducted to the esterifications amidation product Br_G09.

Code	%	C	O	Br	Si	S	N	Cl	O/C Ratio
FB_NIT	atom	65.40	31.65	-	1.55	0.59	0.81	-	0.484
	w/w	57.52	37.08	-	3.19	1.39	0.83	-	-
Br_G09	atom	70.11	19.37	0.58	2.05	-	7.09	0.80	0.276
	w/w	60.86	22.40	3.35	4.16	-	7.18	2.05	-

Regarding the majoritary elements, namely carbon (C) and oxygen (O), the XPS results revealed an increase in the percentage of carbon atoms and, consequently, a decrease in the oxygen percentage. These changes were probably due to the attachment of new molecules, to the surface of GO, with more carbons than oxygen atoms, resulting in a decrease of the O/C ratio.

Figure H12 shows a comparison between one IR spectrum acquired conducting the FTIR analysis using the ATR mode and using KBr pellets. The samples submitted to the analysis were from the esterification product Br_G10.

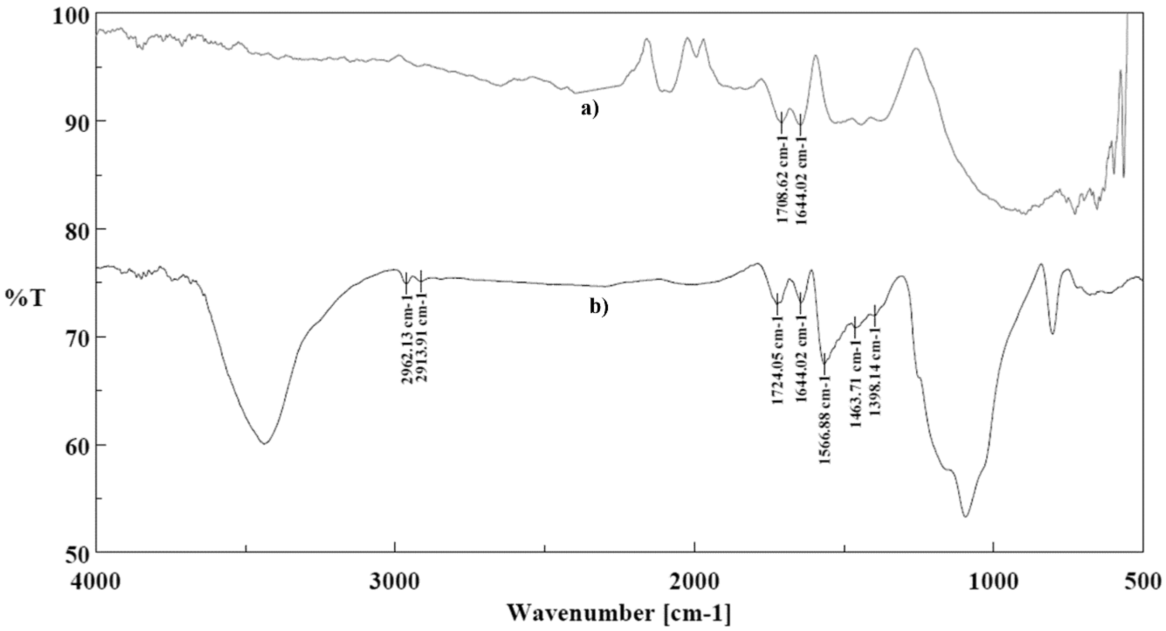

Figure H12. Comparison between the IR spectra from the esterifications product Br_G10 acquired using the FTIR analysis in a) ATR mode and b) KBr mode.

Appendix I – NanoInnova Technologies analysis

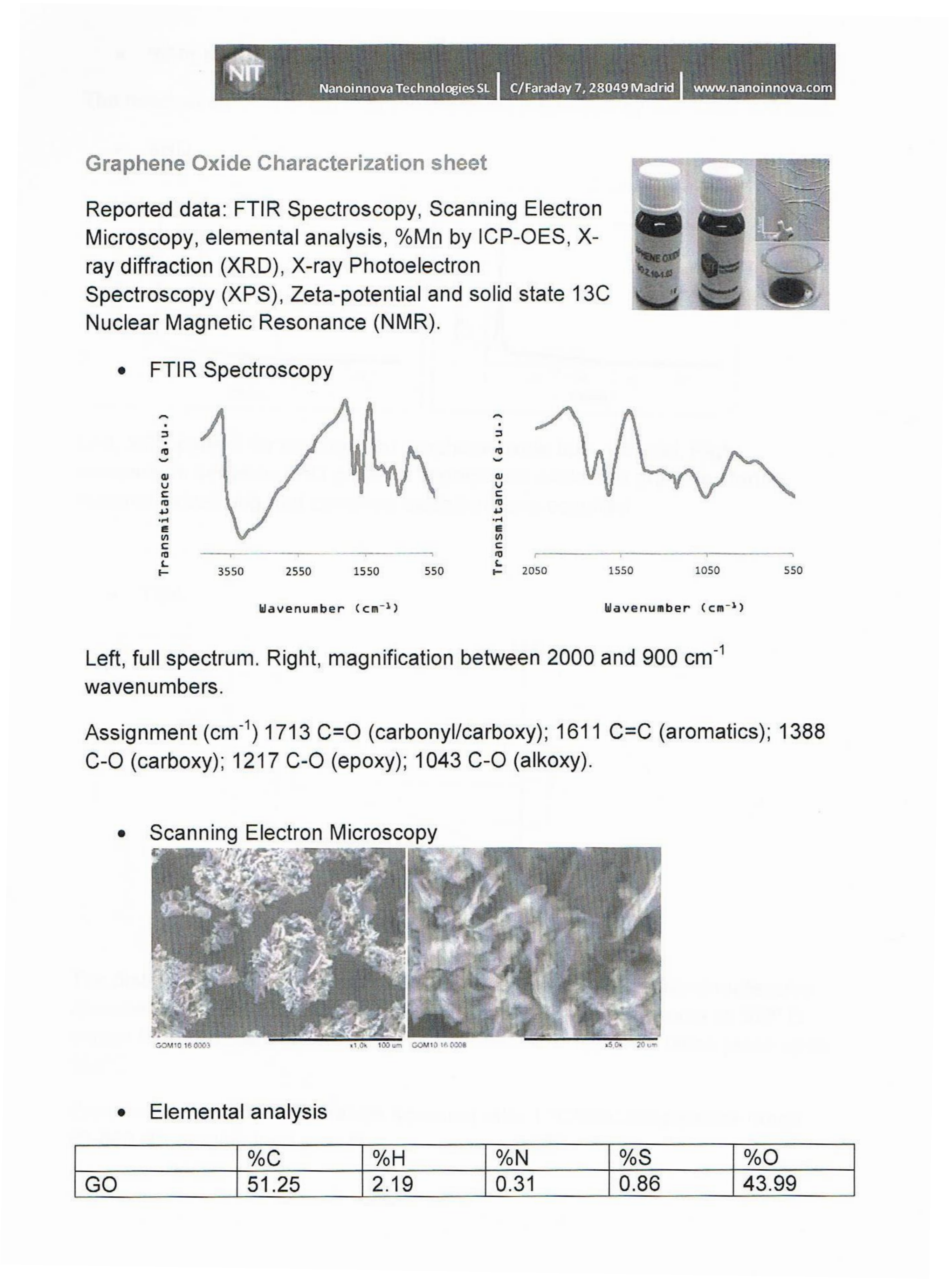

NIT Nanoinnova Technologies SL | C/Faraday 7, 28049 Madrid | www.nanoinnova.com

Graphene Oxide Characterization sheet

Reported data: FTIR Spectroscopy, Scanning Electron Microscopy, elemental analysis, %Mn by ICP-OES, X-ray diffraction (XRD), X-ray Photoelectron Spectroscopy (XPS), Zeta-potential and solid state 13C Nuclear Magnetic Resonance (NMR).

- FTIR Spectroscopy

Transmitance (a.u.)
3550
2550
1550
550
Wavenumber (cm⁻¹)
Transmitance (a.u.)
2050
1550
1050
550
Wavenumber (cm⁻¹)

Left, full spectrum. Right, magnification between 2000 and 900 cm^{-1} wavenumbers.

Assignment (cm^{-1}) 1713 C=O (carbonyl/carboxy); 1611 C=C (aromatics); 1388 C-O (carboxy); 1217 C-O (epoxy); 1043 C-O (alkoxy).

- Scanning Electron Microscopy

GOM10 16 0003
x1,0k 100 um
GOM10 16 0008
x5,0k 20 um

- Elemental analysis

	%C	%H	%N	%S	%O
GO	51.25	2.19	0.31	0.86	43.99

- %Mn by ICP-OES

The residual amount of Mn in graphene oxide measured by ICP-OES is 0.05%.

- XRD

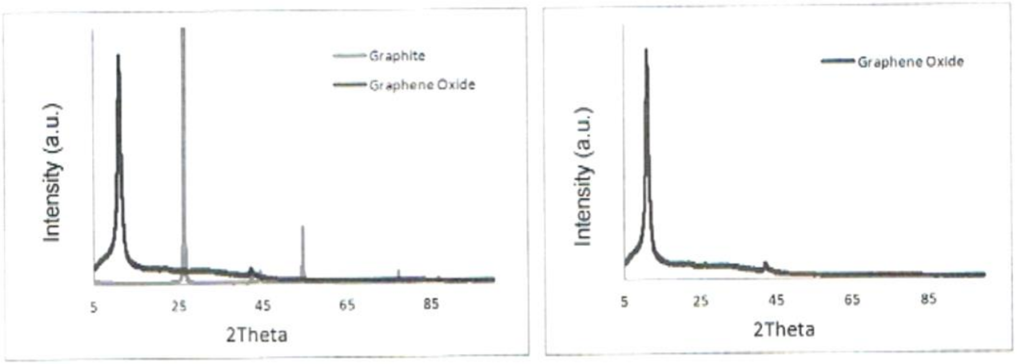

Left, XRD pattern for as-prepared graphene oxide bulk material. Right, comparison between XRD patterns of graphene oxide and graphite starting material evidencing that complete oxidation have occurred.

- TGA

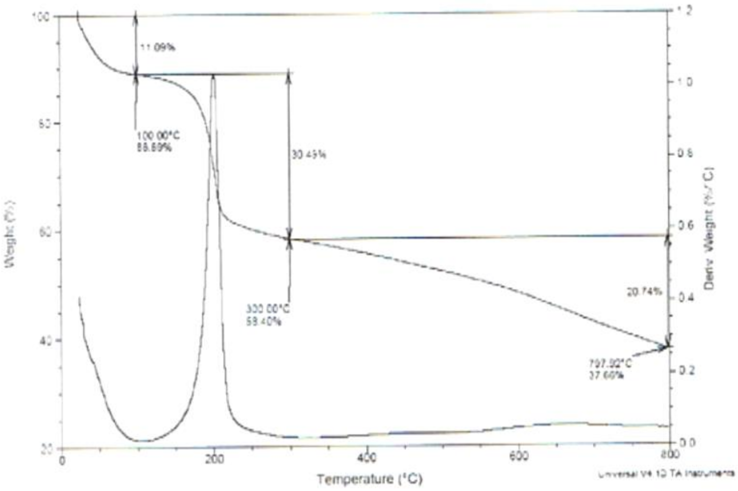

The first 11.9% mass loss (approx 100º C) it is due to water solvent molecules absorbed into the GO bulk material, the following 30.49% decrease at 300º C stands for GO decarboxylation process, further decomposition takes place up to 800ºC.

Experiment settings: temperature scanning rate: 1 ºC/min; temperature range 20-800 ºC; purging inert gas: N_2

- XPS

	C1s	**O1s**	**O/C atomic ratio**
GO	284.8 (38) 286.6 (54) 288.3 (8)	530.9 (21) 532.5 (79)	0.655

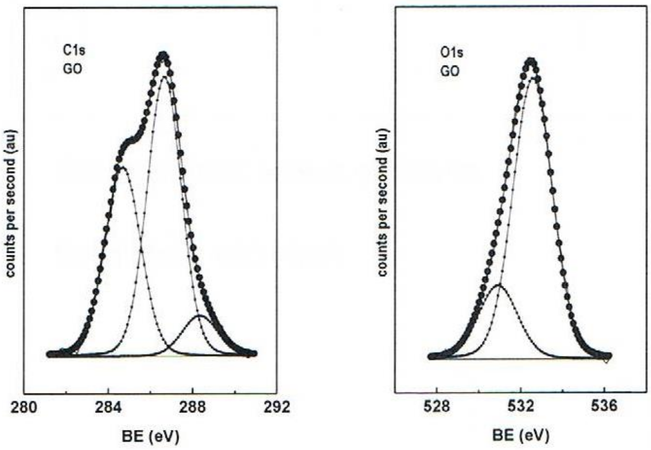

Binding energies (eV) and deconvoluted peaks (%) for C1s, O1s core levels.

Assignment (eV): 284.8 C-C 530.9 C=O
286.6 C-O 532.5 C-O
288.3 C=O

- AFM

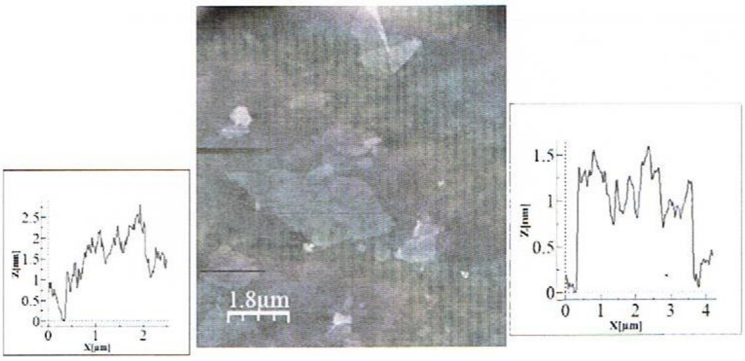

AFM topographic image and magnification of GO deposited onto a silicon wafer. The high profile of the observed GO flakes correlates accordingly calculated values (0.7-1.2 nm).

- Zeta-potential

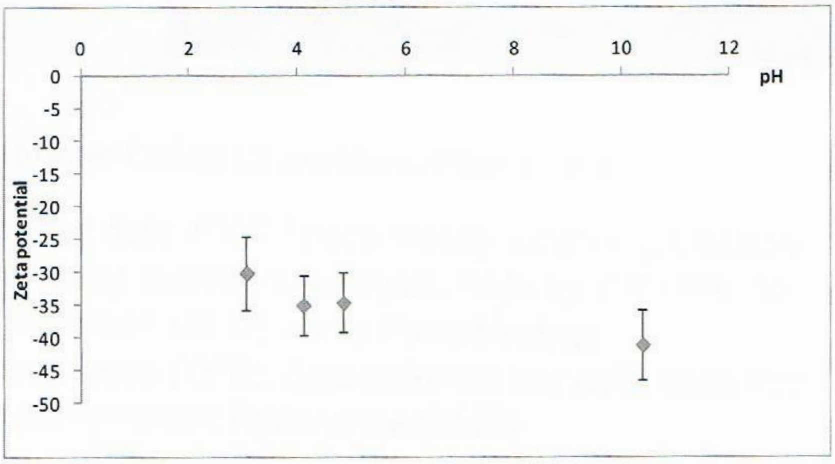

Zeta-potential versus pH curve.

- Solid state 13C NMR

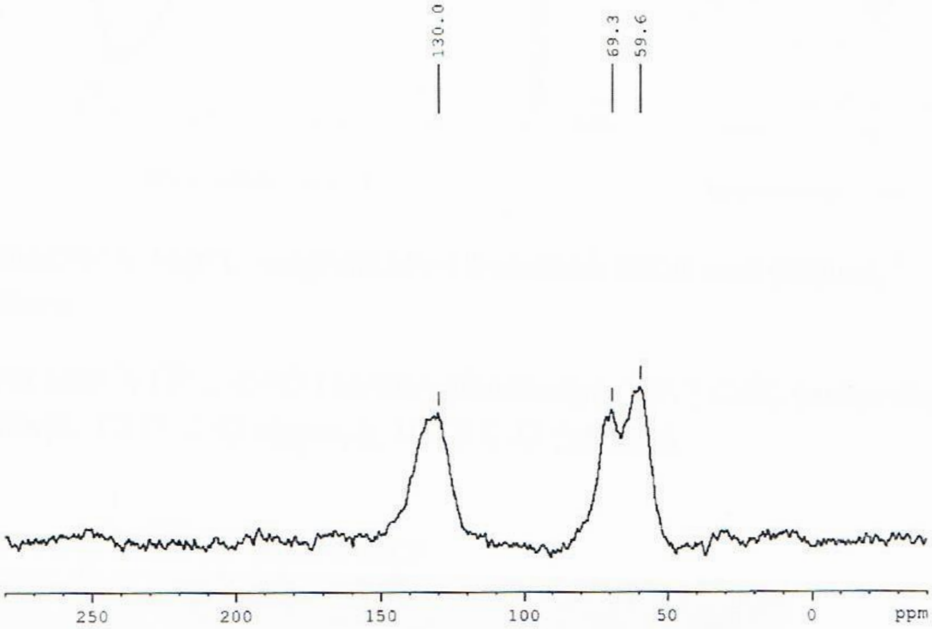

Appendix J – Control tests to esterification reaction

Throughout the work some difficulties were found in the interpretation of the IR spectra from the diverse esterification products. The changes observed in such spectra were drastic when compared with the spectrum of the original GO, namely FB_NIT. As mentioned in the body of this dissertation, the spectra acquired when the FTIR analysis was employed in ATR mode had broad peaks, with poor-definition and of difficult identification. To overcome these problems, the FTIR analysis were carried out in KBr mode, i.e., the samples were mixed with dried KBr powder and were compressed in order to obtain compact pellets. In addition, to understand the origin of the modifications observed, two control tests were conducted. In the test number one, named as Br_teste01, the reaction were carried out as all the other esterification reactions (using the same temperature, same reactant ratios, etc) but only was added to the reaction medium TEA, the catalyst used in esterification reactions. Instead, in the test number two (Br_teste02), TEA was not used, only BIBB was added to the reaction, maintained all the other variables as in the other esterification reactions.

Figure J1 and Figure J2 show the FTIR and TGA plots obtained from the characterization realized to the products of the two esterification control tests.

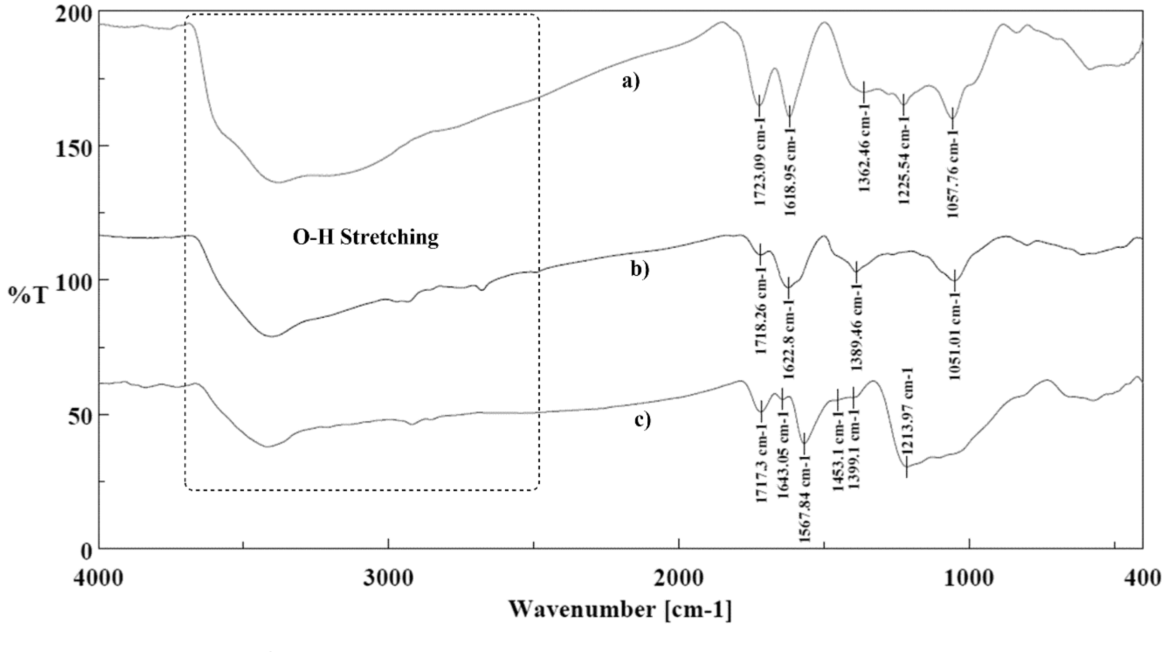

Figure J1. IR spectrum of a) FB_NIT; b) Control test nº 1 (only TEA) and c) Control test nº 2 (only BIBB).

Through the comparison between the IR spectrum of the GO FB_NIT and the IR spectra of the control test products (Figure J1) was possible to conclude that both TEA and BIBB promoted changes in the structure of GO, reacting with some of the oxygen-containing species presented in the GO's surface.

When was added to the reaction medium only TEA (Figure J1, curve b)) the intensity of the IR peaks due to C=O vibration from the carboxyl/carbonyl groups at 1718 cm^{-1} (1723 cm^{-1} in original GO curve a)) and due to C-O vibration from epoxy groups (1226 cm^{-1} in the original GO curve a)) decreased, remaining all the other peaks (from hydroxyl and alkoxy groups and from the aromatic skeletons) practically unchanged. In our point of view, such modifications in the referred IR peaks are ascribed to reactions that probably occurred between the carboxyl acid and epoxy groups of GO and the esterification catalyst, TEA.

The decreasing observed was explained based on the C=O vibration peak having in mind an acid-base reaction described as follow. The tertiary amine reacted with the carboxyl acids from the GO through an acid-base reaction producing a quaternary ammonium salt and decreasing the number of carboxyl groups present in the surface of the carbon nanomaterial. In this reaction, protons of –OH groups from the carboxyl acids were caught by TEA acting as a proton acceptor and producing the quaternary salt [$COO^- NEt_3H^+$] [122]. The formation of this salt, shift the C=O vibration peak to lower wave lengths (around 1600 cm^{-1}), as result of the formation of carboxylat ions [123]. A similar reaction can had occurred with the epoxy groups, however, the reaction mechanism was not understood as the mechanism that justify the changes observed in the IR peaks resulting from the carboxyl groups [122].

In Figure J1 (curve c)) is presented the IR spectrum obtained from the product of the control test number two (Br_teste02) in which was added to the reaction medium only BIBB. As expected, the modifications observed in the IR spectrum relatively to the spectrum of original GO were higher than the modifications observed when was used only TEA. Most of the peaks suffered important modifications, namely the O-H stretching vibration band that considerably reduced its intensity. The decreasing observed in the intensity of the O-H vibration band was associated to the substitution of the –OH groups by the initiator moieties, producing new ester linkages ($-O-CO-C(CH_3)_2Br$). Having in mind that the esters formed, as result of the esterification reaction, were esters bonded to the aromatic skeletons of GO (conjugated esters) the C=O vibration peak from the new ester linkages should appear at low wave lengths, around 1700-1600 cm^{-1}. Considering this information, the new peak that appeared at 1643 cm^{-1} (Figure J1, curve c)) was associated to the new ester bonds. The presence of initiator molecules was also evaluated by two peaks at 1453 and 1399 cm^{-1} that were ascribed to the C-C vibration bonds existing in the structure of the initiator molecules (alkanes structure) [123]. Also is possible to see in curve c) (Figure J1) small peaks in the region of 3000-2500 cm^{-1} probably due to C-H vibrations from the methyl groups presented in BIBB molecules [123]. The BIBB structure is exposed in Appendix O.

Additionally, the peak at 1568 cm^{-1} was associated to the C=C vibration from the aromatic rings of the GO structure. Having as base some articles, the shift observed in this peak relatively to the C=C vibration peak shown in the IR spectrum of the original GO was due to some reduction of the oxygen functionality that may occurred during the esterification reaction and due to some interaction between the new attached molecules and the aromatic skeletons [24-26].

The C=O vibration peak from the carboxyl/carbonyl groups (at 1723 cm^{-1} in original GO curve a) and 1717 cm^{-1} in Br_teste02 curve c)) was the peak that suffered less modifications, revealing that BIBB molecules didn´t reacted significantly with the carboxyl and carbonyl groups.

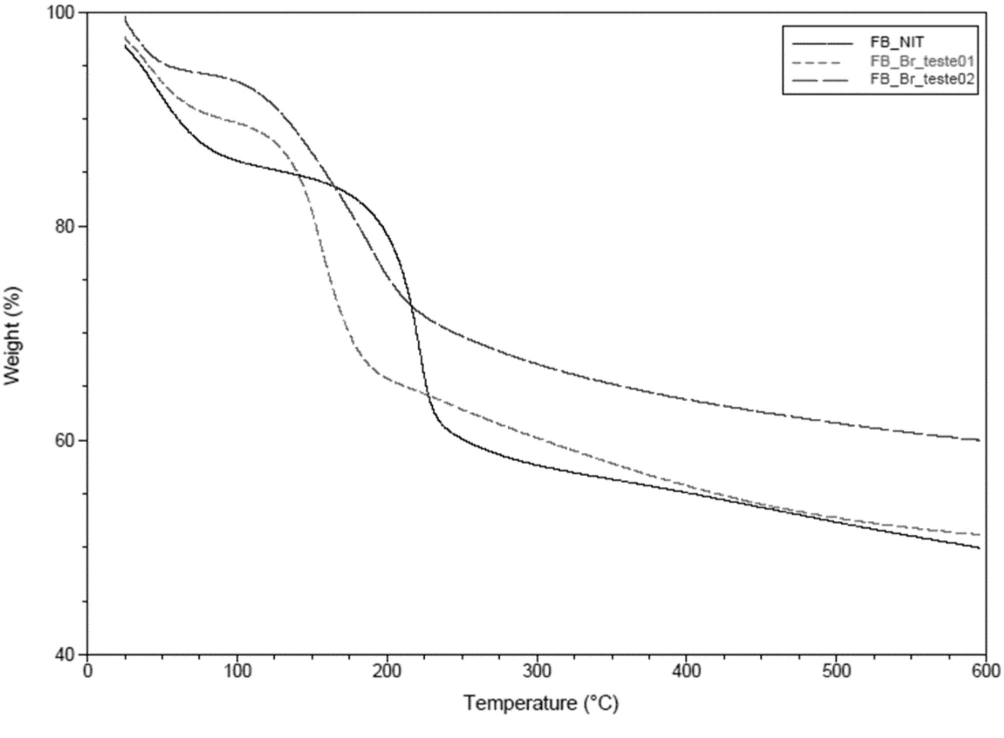

Figure J2. TGA curves of GO FB_NIT (solid line), control test nº 1 (only TEA, short dash line) and control test nº 2 (only BIBB, long dash line).

The TGA results (Figure J2) revealed that when was used only TEA either the weight loss behaviour as the total weight loss obtained were similar to the registered for the original GO. In the TGA analysis realized to the purchased GO was determined a total weight loss of about 47% while the weight loss of the product resulting from the test number one was of about 46%.

In the other hand, the weight loss observed for the product of the control test number two, in which was added only initiator molecules, was of about 40%, considerably lower than the previous.

The TGA results alongside with the FTIR spectra confirm that the BIBB was the reactant responsible for the major modifications observed in GO when submitted to esterification reactions. In short, when BIBB was used the FTIR spectrum changed drastically, disappearing the O-H vibration band and appearing new peaks in the region between 1800-800 cm^{-1}. The weight loss was considerably lower as result of the removal of the adsorbed water, during the esterification reactions.

The results obtained for the test number two were compared with the results obtained for the two main esterification reactions, aiming to confirm the analysis realized above. In Figure J3 and Figure J4 are presented the IR spectrum and the TGA results obtained for the different products, respectively.

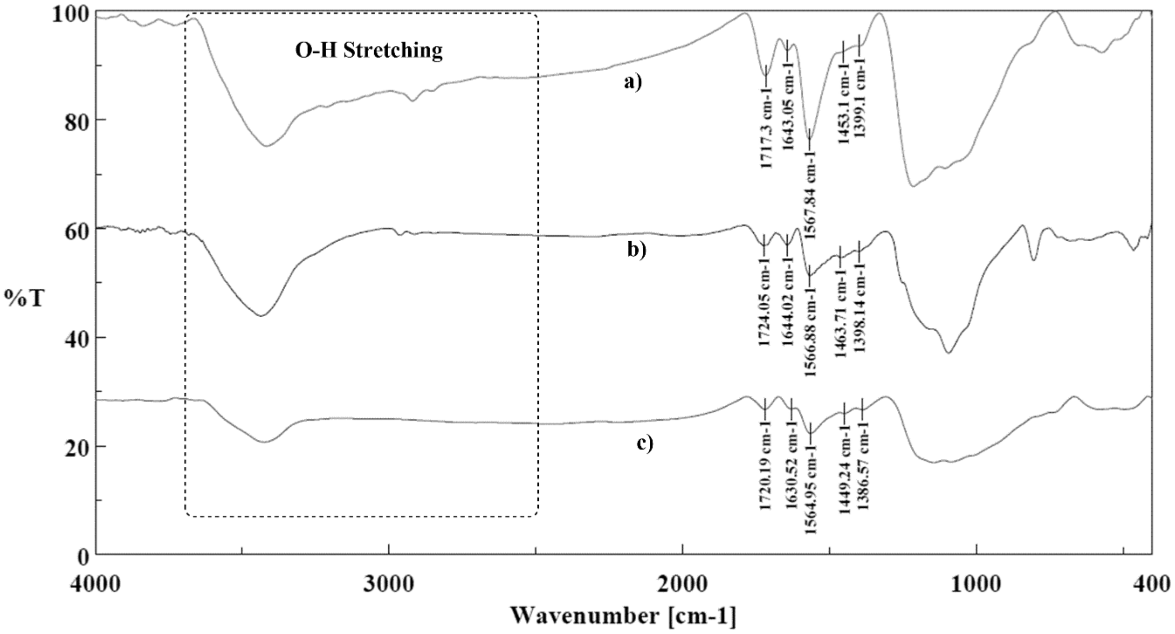

Figure J3. IR spectrum of a) Control test nº 2; b) Esterification product Br_G10 and c) Esterification product Br_G11.

As expected, the results presented in the Figure J3 and Figure J4 revealed that the modifications observed in the three products (Br_test02, Br_G10 and Br_G11) are very similar and support the analysis of the IR spectrum previously exposed. In all IR spectra were observed a decreasing/disappearance in the O-H stretching vibration band and the new peaks appeared in the same wavelengths region. In the cases in which TEA was used along with BIBB (Figure

J3, curves b) and c)) the O-H band disappeared and the C=O vibration peak at about 1720 cm^{-1}, as result of the carbonyl/carboxyl groups of GO, decreased. While, when BIBB was employed without TEA (Figure J3, curve a)) the O-H vibration band was yet visible and the C=O vibration peak at about 1717 cm^{-1} remain with higher intensity when compared with the other esterified products (Figure J3, curves b) and c)). These results support the idea that TEA react with carboxyl acid groups existing in the GO's surface and also prove its catalytic effect in the esterification reactions.

In addition to the similarities observed in the IR results also TGA curves were very similar. The decomposition patterns were similar, with the main weight losses observed between about 120 and 400 ºC. The weight losses measured were of about 40% for test number two product, 37% for the esterified Br_G10 product and 42% for the Br_G11 product.

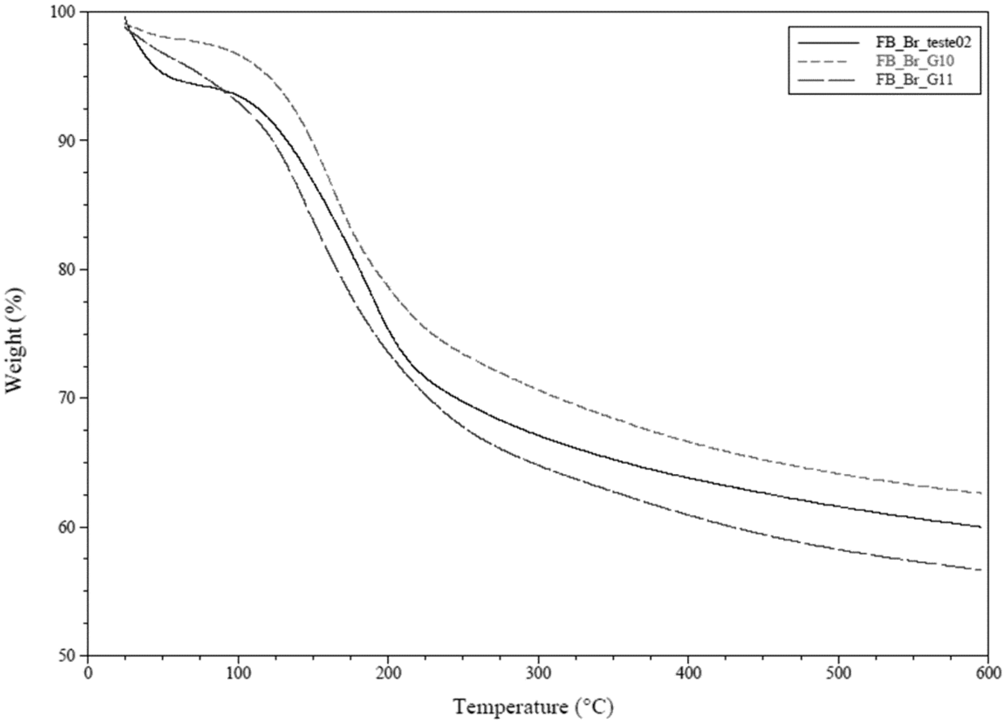

Figure J4. TGA curves of control test nº 2, esterification product Br_G10 and esterification product Br_G11.

Appendix K – Main esterification reactions

In this Appendix are shown the FTIR, TGA, and XPS results for the second main esterification reaction conducted during this work (Figure K1 to Figure K3 and Table K1).

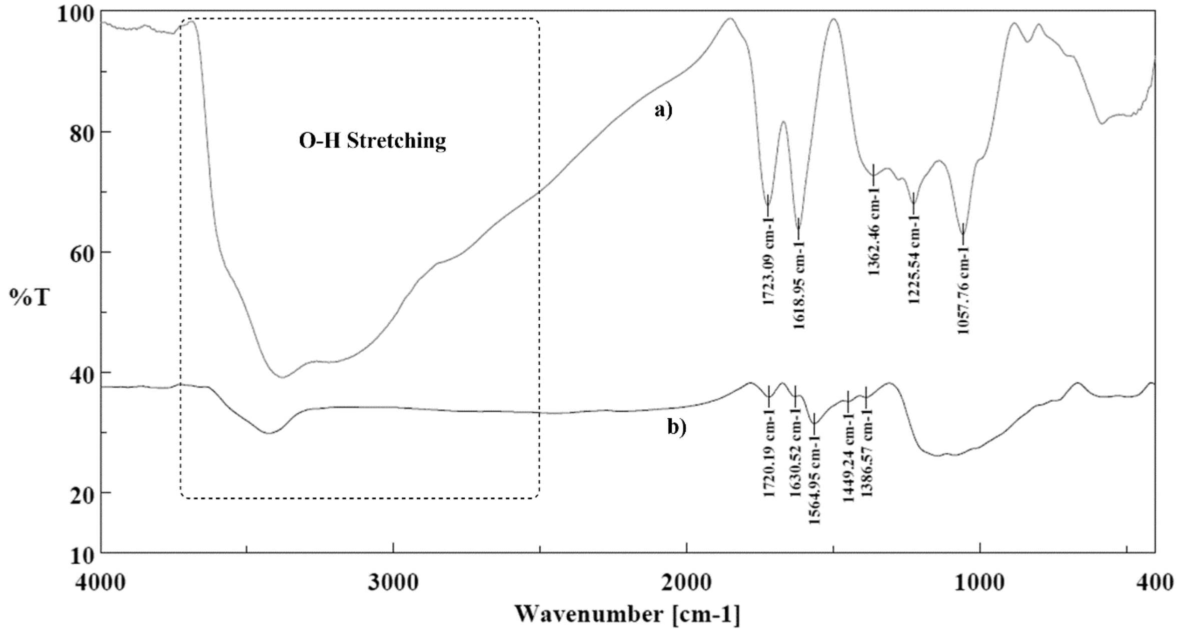

Figure K1. IR spectrum of a) GO FB_NIT and b) Esterification product Br_G11.

As mentioned in the body of the dissertation, the results acquired through the different characterization techniques realized to the esterified product Br_G11 were very similar to the results of the previous esterification reaction, Br_G10. In the FTIR spectrum of the esterified GO (Figure K1, curve b)) the O-H vibration band was not visible, indicating that the hydroxyl groups existing in the GO surface were replaced by the BIBB molecules. Additionally, new peaks appeared at 1631, 1449 and 1387 cm^{-1}. The peak at 1631 cm^{-1} was attributed to the C=O vibration from the new conjugated ester and the other two peaks were attributed to the C-C vibration from the alkane structure of BIBB molecules attached to the GO’s surface [123]. The peak at 1565 cm^{-1} was due to the C=C vibration of the aromatic skeletons from the GO. The C=O peak from carbonyl/carboxyl groups was also visible at 1720 cm^{-1} but with less intensity than in the spectrum of original GO (Figure K1, curve a)) as result of the reaction that probably occurred between TEA and carboxyl acid groups of GO.

TGA results, shown in Figure K2, revealed that great part of the adsorbed water was removed during the esterification reaction, since was not observed weight loss around 100ºC. The main weight loss of the GO-Br was measured between 120ºC and 400ºC and the total weight loss determined was of about 42%. The TGA curve of the product Br_G11 is in agreement with the literature [24].

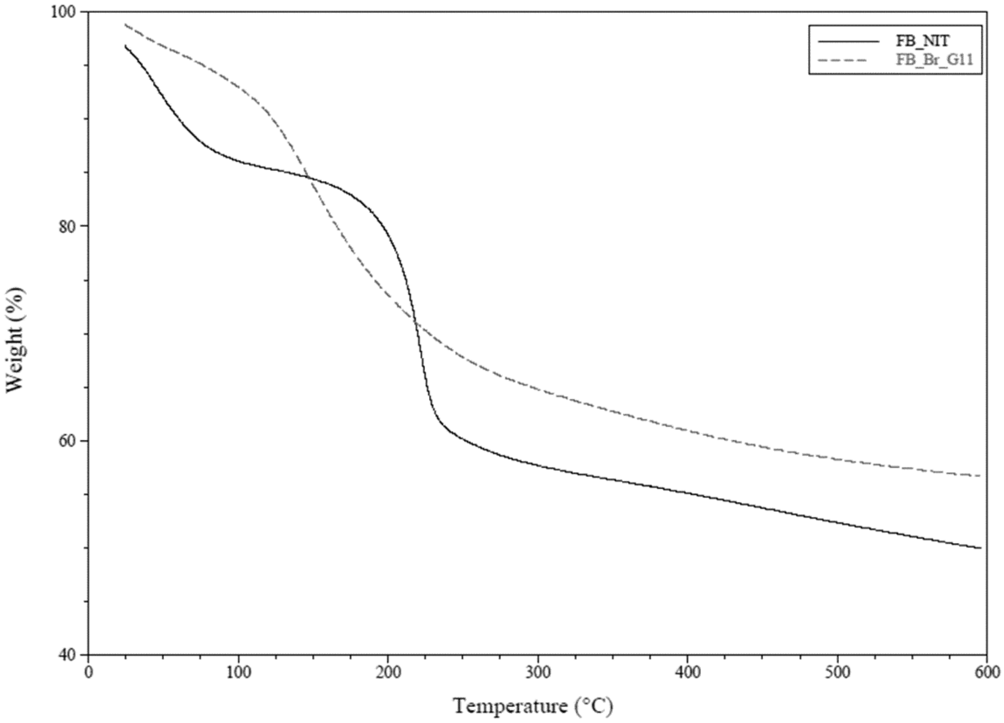

Figure K2. TGA curves of original GO (solid line) and esterifications product Br_G11 (dashed line).

Finally, the XPS analysis confirmed the FTIR and TGA results, revealing that initiator molecules were covalently bonded to the surface of GO.

Table K1. Elemental quantification obtained from the XPS analysis for the esterifications product Br_G11.

Code	%	C	O	Br	Si	S	N	O/C Ratio
FB_NIT	atom	65.40	31.65	-	1.55	0.59	0.81	0.484
	w/w	57.52	37.08	-	3.19	1.39	0.83	-
Br_G11	atom	81.68	14.54	0.87	0.72	-	2.19	0.178
	w/w	73.54	17.44	5.21	1.52	-	2.30	-

Through the elemental quantification, realized from the survey spectrum (Figure K3 and Table K1) was determined a total bromine content of 5.21% (w/w). The Br3d high resolution spectrum, portrayed in the body of the work, revealed that 78.27% of the total bromines were covalently bonded to the GO surface, which means that in 100 mg of GO were present 0.051 mmol of Br. Additionally, other minority elements were found, namely silicon (Si), sulphur (S) and nitrogen (N). One more time, the percentage of nitrogen increased revealing that some TEA reacted with the oxygen-containing species of GO.

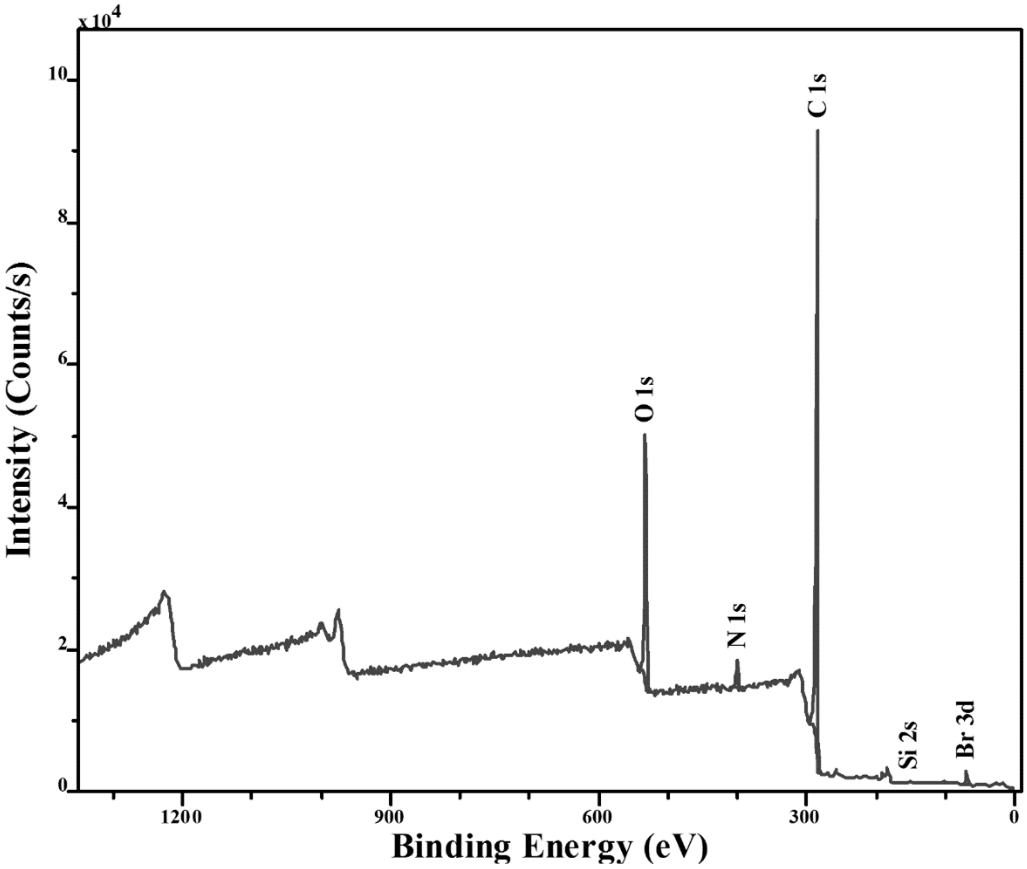

Figure K3. XPS spectrum of the esterified GO Br_G11.

As verified with the product from the esterification reaction Br_G10, the percentage of carbon atoms increased (from 57.52% (w/w) in original GO to 73.54% (w/w) in esterified product Br_G11), contrarily to the oxygen percentage that decreased (from 37.08% (w/w) in original GO to 17.44% (w/w) in esterified product Br_G11).

Interestingly, when less BIBB was used and less BIBB was covalently attached to the surface of graphene oxide less was the decreasing observed in the O/C ratio. This can means that the BIBB can be the responsible for the decreasing of the oxygen functionality of the GO as result of its reaction with the oxygen-containing species.

Appendix L – Preliminary polymerization reactions characterization

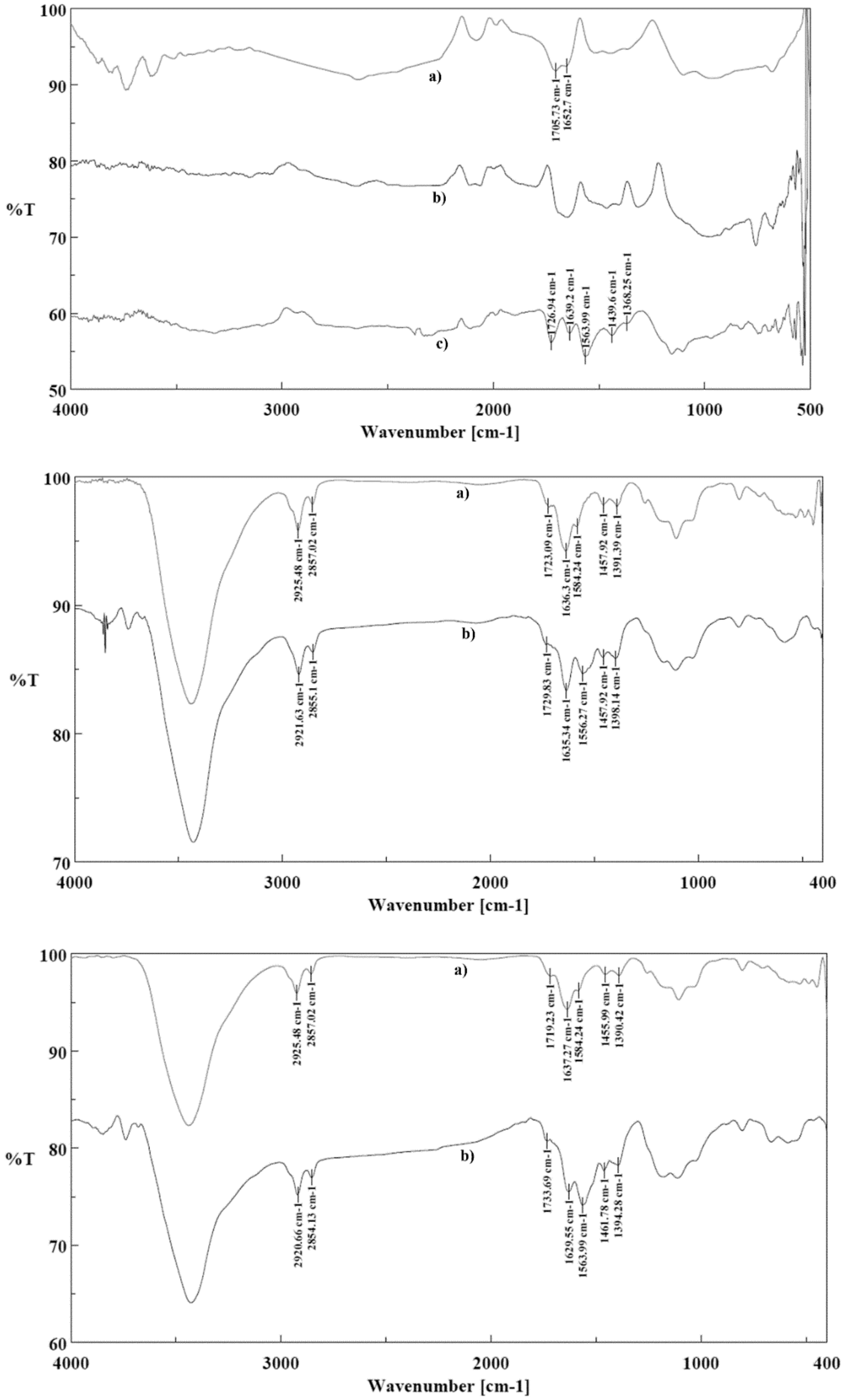

Figure L1. FTIR spectra obtained for the different polymerization preliminary reactions. a) (top) esterified product Br_G06; a) (middle) esterified product Br_G07; a) (bottom) esterified product Br_G08. b) (top) and b) (middle) product obtained from the ATRP of MA catalysed by CuBr:Me$_6$TREN in DMF at 30ºC and c) (top) and b) (bottom) product obtained from the SARA ATRP of MA catalysed by Cu(0):CuBr$_2$:Me$_6$TREN in DMF at 30 ºC.

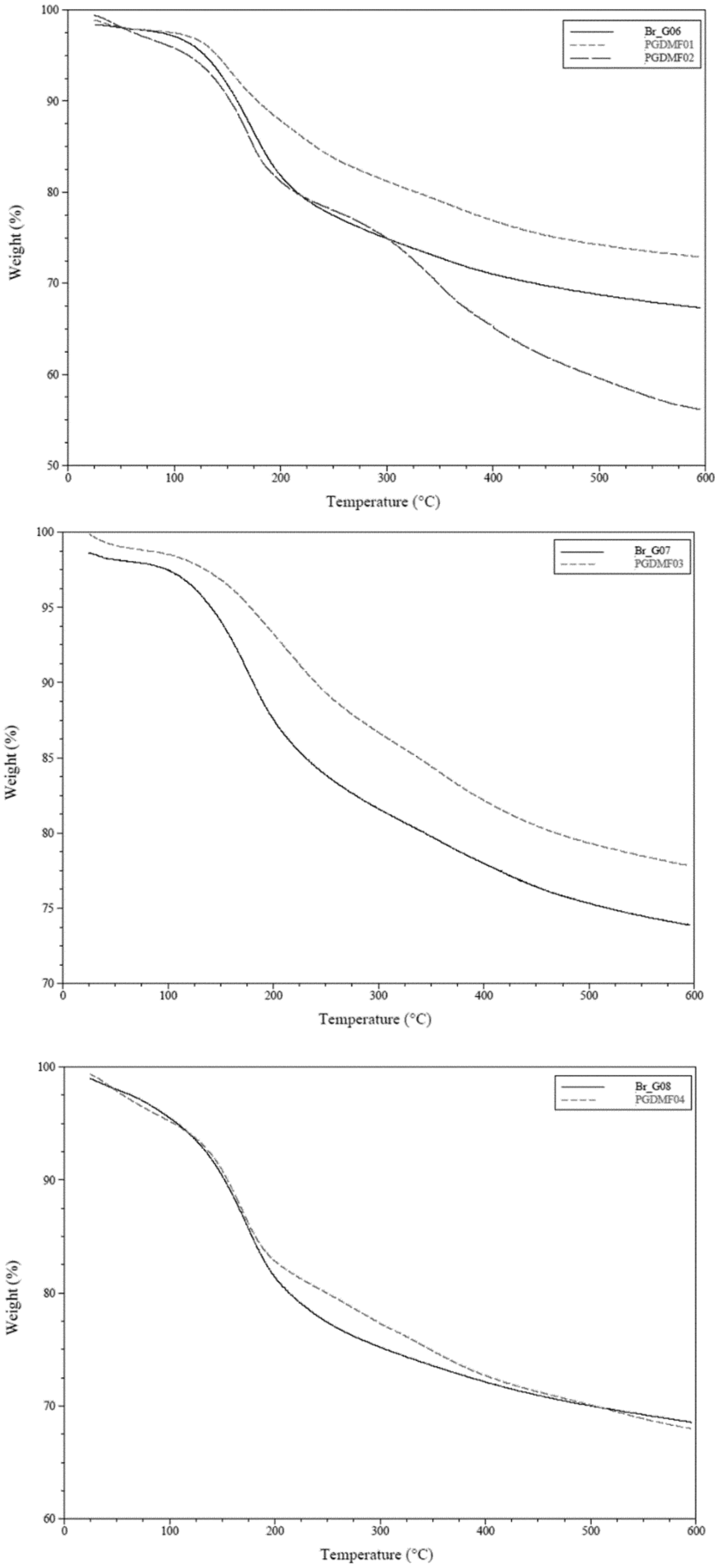

Figure L2. TGA results obtained for the different polymerization preliminary reactions. (solid line, top) esterified product Br_G06; (solid line, middle) esterified product Br_G07; (solid line, bottom) esterified product Br_G08. (short dashed line, top) and b) (dashed line, middle) products obtained from the ATRP of MA catalysed by CuBr:Me$_6$TREN in DMF at 30ºC and (long dashed line, top) and (dashed line, bottom) products obtained from the SARA ATRP of MA catalysed by Cu(0):CuBr$_2$:Me$_6$TREN in DMF at 30 ºC.

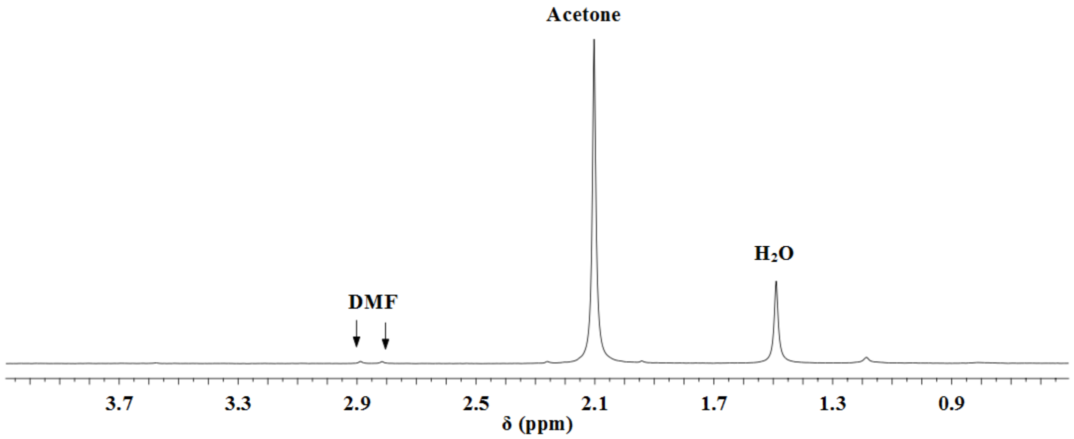

Figure L3. Typical ^{1}*H NMR acquired for the washed powders of the various preliminary polymerization reactions.*

Appendix M – Polymerization reactions, reproduction of one reported system

Figure M1 and Figure M2 show the FTIR, TGA, ^{1}H NMR results obtained for the precipitates recovered from the three type of reactions in which the procedures described by Lee were reproduced [24].

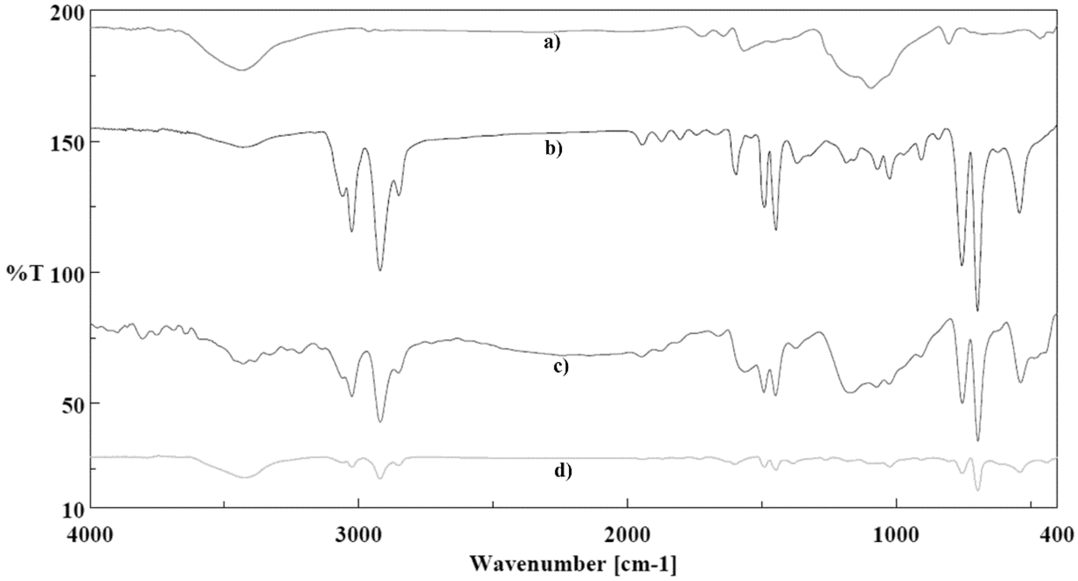

Figure M1. FTIR spectra of a) Esterified product GO-Br and of the precipitates obtained from the SARA ATRP of Sty catalyzed by Cu(0) wire/TREN in DMF at 80 ºC with different target DPs, b) DP = 602, c) DP = 250, d) DP = 500.

In the FTIR curves of the different precipitates (Figure M1, curves b), c) and d)) several characteristic peaks of PS were observed [54]. For example, the peaks around 3000 cm^{-1} are due to the C-H stretching vibration of the methylene groups from the PS[54].

TGA results presented in Figure M2 (left) revealed an abrupt weight loss around 400 ºC for all the precipitates. This weight loss and the respective decomposition patterns were attributed to the presence of PS [24]. Solution ^{1}H NMR was conducted in $CDCl_3$ (10 mg/mL) to confirm the structure of the synthetized polymer. For all the precipitates the ^{1}H NMR results proved that PS was yielded, since was possible to observe the peaks at 6.00-7.50 ppm as result of the **b** protons from the aromatics groups and at 2.0-1.25 ppm due to the presence of **a** protons from the structure of the PS chains (Figure M2, right) [24, 134].

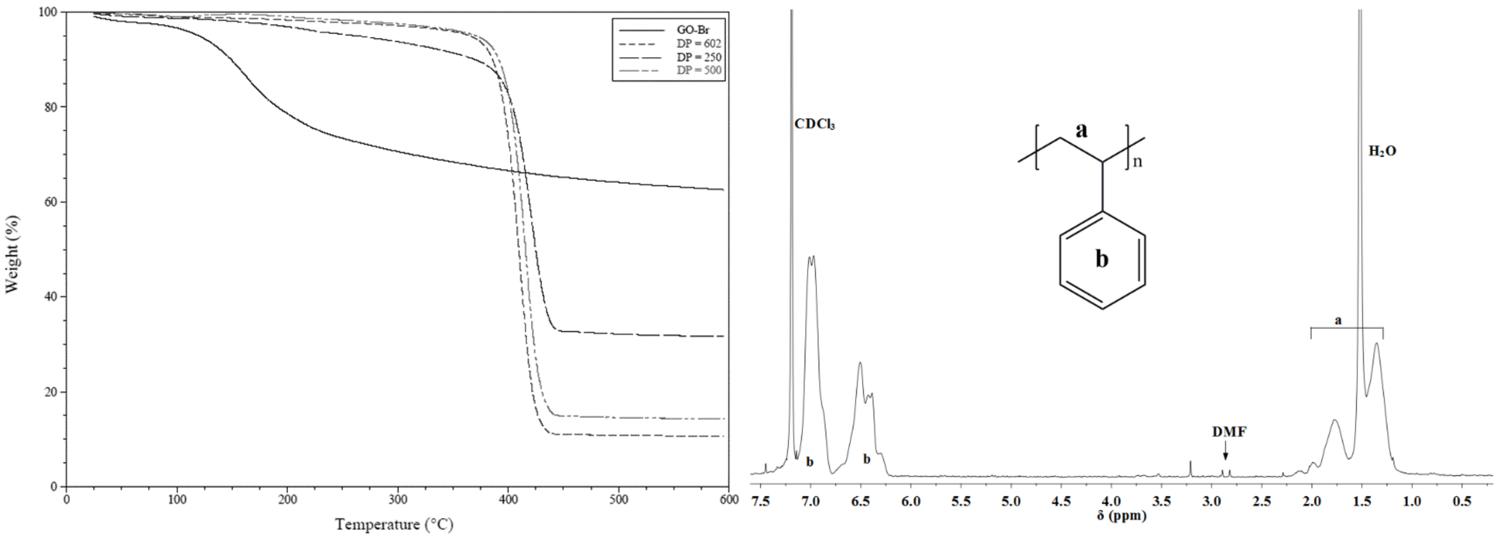

Figure M2. (Left) TGA curves obtained for the esterified GO used as raw material (solid line) and for the various precipitates obtained from the SARA ATRP of Sty in DMF at 80 ºC having different target DPs; DP = 602 (short dashed line), DP = 250 (long dashed line) and DP = 500 (broken double dashed line). (Right) Typical ^{1}H NMR obtained for the respective precipitates.

The analysis carried out to the precipitates revealed that PS was polymerized, however, after an exhaustively wash process realized to the precipitates was possible to conclude that these PS was detached from the surface of GO, as explained in the body of the dissertation. The PS recovered from the supernatants resulting from the washing process were analysed by GPC to evaluate the molecular weights as well as the dispersity values of the polymers. The GPC traces acquired for the products of the three type of reactions are presented in Figure M3.

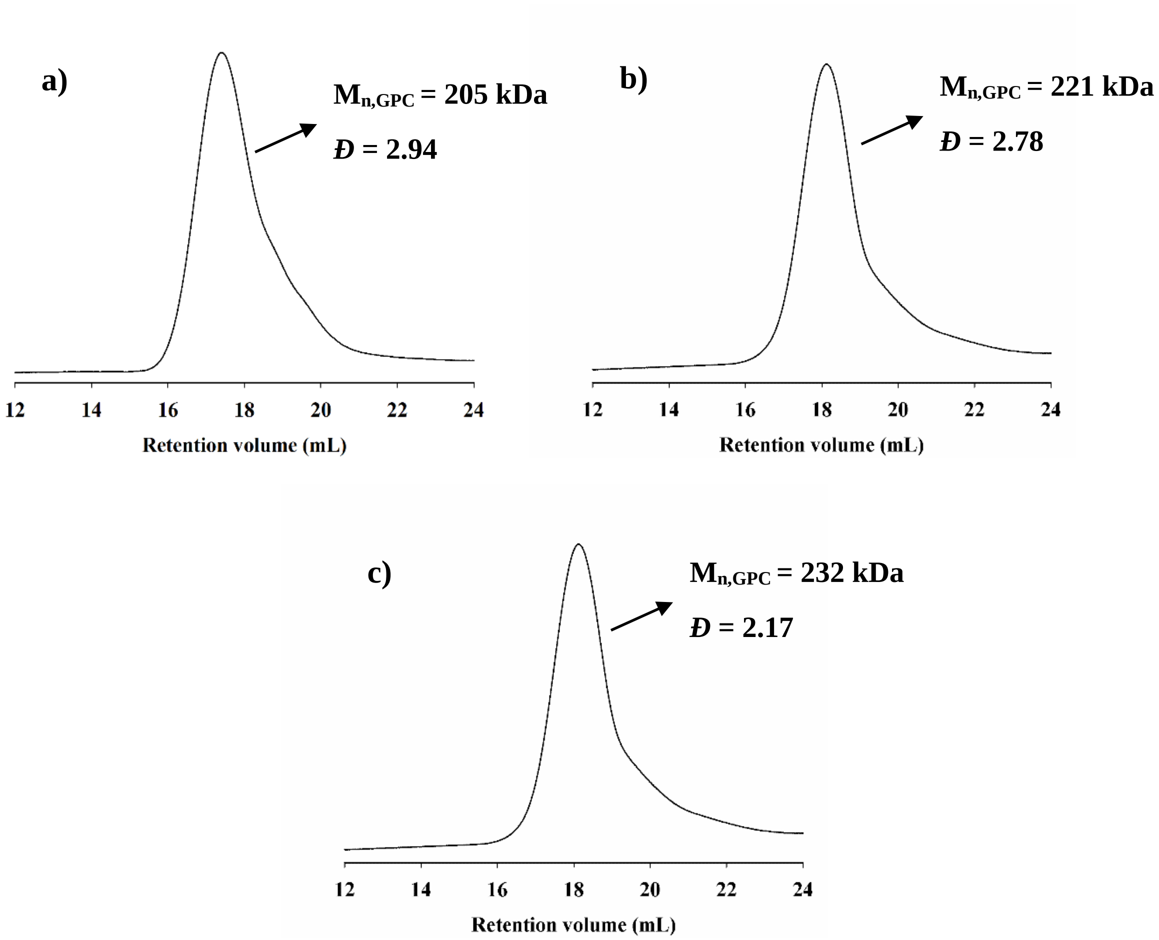

Figure M3. GPC traces of the polymers recovered from the supernatants with diferente target DPs; a) DP = 602, b) DP = 250 and c) DP = 500. The molecular weights, $M_{n,GPC}$*, and the dispersity values were calculated through the software OmniSEC using the TRiSEC calibration.*

Appendix N – "Grafting-from" in the presence of sacrificial initiator

As mentioned in the body of the dissertation SARA ATRP of MA experiments were carried out adding to the heterogeneous reaction mixtures sacrificial initiator. In this Appendix are shown the results obtained in such polymerizations.

Since some decades "free" initiator molecules have been employed in "grafting-from" CLRP from surfaces, namely from GO [54, 57, 58, 61, 62, 70, 71, 145]. Was reported that the use of sacrificial initiator can help in the control of the polymerization, namely in the beginning of the reaction [145]. The low concentrations of initiation moieties attached to the surfaces cannot generate a sufficient concentration of deactivator, also known as persistent radical, in solution to guarantee a controlled grafting reaction [146]. Additionally, according to the CLRP mechanism, free polymers initiated by sacrificial initiator owned almost the same molecular weight and dispersity values as those grafted onto the surface of the carbon macroinitiator [61, 62]. Husseman reported a comparison between GPC traces of free polymer chains and detached polymer brushes, polymerized in the same heterogeneous reaction, and proved that they owned similar molecular weights and dispersity values [145].

In research area of CLRP from graphene oxide were already reported diverse works in which sacrificial initiator was used to help in the control of the "grafting-from" reactions [54, 57, 58, 61, 62, 70, 71]. In some of the works the control achieved over the grafting polymerization was evaluated having as base the GPC and ^{1}H NMR results acquired for the free polymer chains polymerized in solution [54, 57, 58, 61, 62, 70, 71].

Considering the information acquired from the literature and aiming to improve the control over the "grafting-from" polymerization the sacrificial initiator methodology was tested. With this experiments we were also interested into to realize the complete evaluation of the control achieved in SARA ATRP of MA from GO in DMF catalysed by Cu(0) wire/Me$_6$TREN at 60 ºC, determining the monomer conversion and the $M_{n,th}$. Two experiments were realized using sacrificial initiator and collecting diverse samples of the reaction mixtures at pre-determined times. With the kinetic of the reactions was possible to evaluate the evolution of the polymerization with time. The samples were analysed through ^{1}H NMR and GPC techniques (Figure N1 to Figure N2). In the end of the reactions the recovered GO was exhaustively washed with DMF and THF, by successive centrifugation/redispersion cycles, dried in a vacuum oven at 40 ºC and evaluated by FTIR, TGA and ^{1}H NMR analysis (Figure N4 and Figure N5).

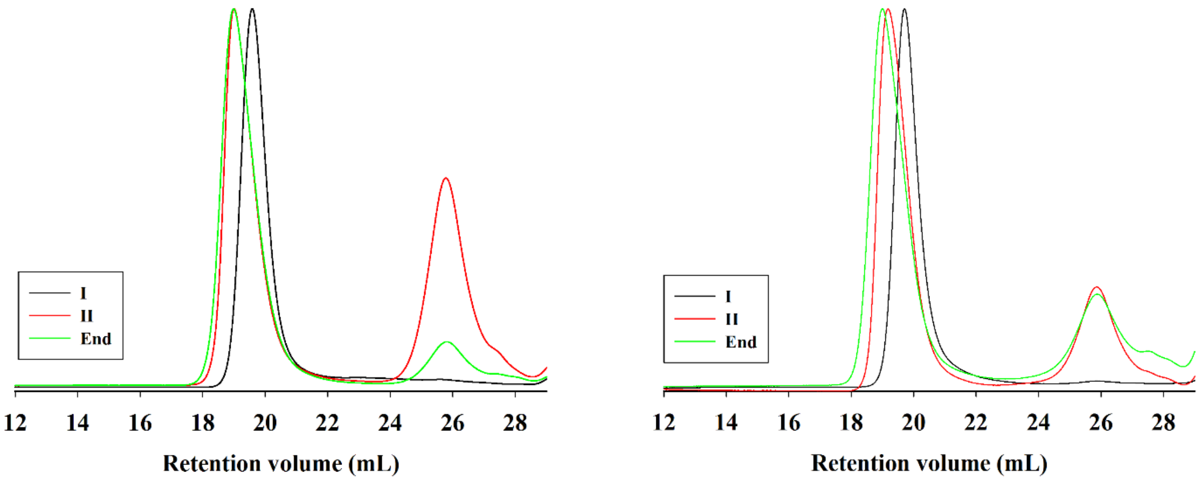

Figure N1. GPC traces of free PMA obtained in the SARA ATP of MA catalyzed by Cu(0) wire/Me6TREN in DMF at 60 ºC in heterogeneous medium. Kinetic points: (left) I – 2h, Mn,GPC= 28 kDa, Đ = 1.14 ; II – 4h, Mn,GPC= 53 kDa, Đ = 1.20; End – 7inh, Mn,GPC = 55 kDa, Đ = 1.33 and (right) I – 0.5h, Mn,GPC = 24 kDa, Đ = 1.16 ; II – 1h, Mn,GPC= 41 kDa, Đ = 1.15; End – 2h, Mn,GPC = 49 kDa, Đ =1.29 . The molecular weights and the dispersity values were measured in OmniSec software using the TriSec calibration.

In the plots presented in Figure N1 are shown the GPC traces of the two first and final samples collected, from both "grafting" reactions conducted in the presence of sacrificial initiator. The first reaction was conducted during 7 hours and the first samples were collected every 2 hours. As shown in Figure N1 (left), the GPC traces of the first sample collected, at 2h of reaction, revealed a low dispersity value (*Đ* = 1.14) and a number average molecular weight, $M_{n,GPC}$, of 28 kDa. After collecting the first sample, from the reaction medium, an unexpected increase of the viscosity of the reaction mixture was observed, causing the stop of the reaction after 7h. This increase of viscosity was unexpected because, in a polymerization without sacrificial initiator was never observed such significant increase even after 24h of reaction. Other interesting observation retired from the GPC traces of the first kinetic realized, was the appearance of a new peak at low molecular weights after the second sample collected.

From the ^{1}H NMR results was possible to determine the conversion, the theoretical number average molecular weight and the ln[M_0]/ln[M]. From the results (Figure N3) was possible to conclude that despite the monomer conversion was almost 100% (after 7h of reaction) and the first order-kinetic with respect to the monomer conversion achieved, the $M_{n,GPC}$ were considerably higher than the $M_{n,th}$.

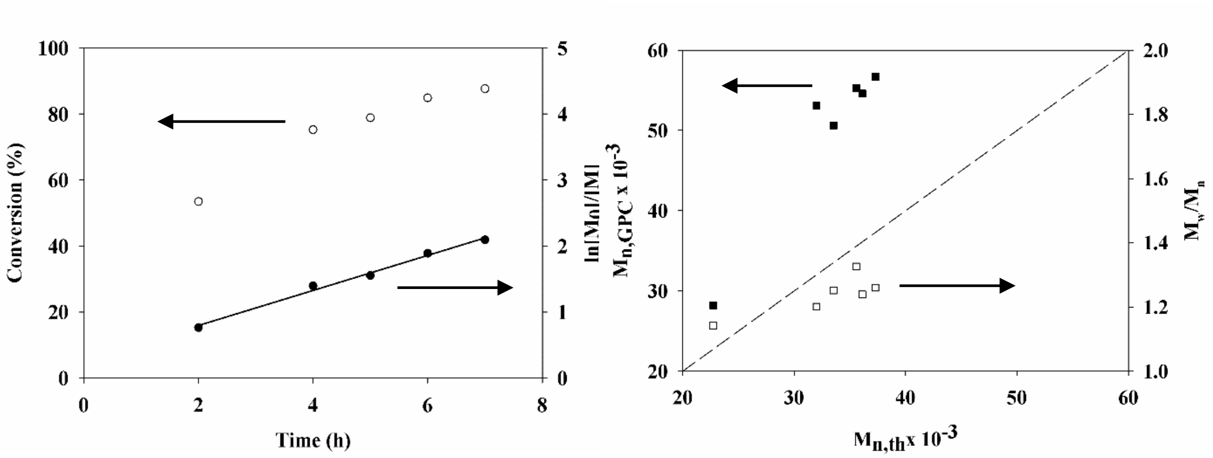

Figure N3. First reaction conducted with sacrificial initiator. (left) Kinetic plot of conversion and ln[M_0]/[M] vs Time and (right) plot of number average molecular weight, $M_{n,GPC}$, and dispersity values, Đ, vs theoretical number average molecular weight, $M_{n,th}$, for SARA ATRP of PMA catalysed with Cu(0) wire/Me6TREN in DMF at 60ºC.

Considering the results obtained from the first kinetic was supposed that the reaction could be faster when sacrificial initiator was added, since more active sites were available, leading to some decontrol in the final phase of the polymerization. With this in mind, a second “grafting-from” reaction with sacrificial initiator was conducted, however, the samples were collected in an earlier phase of the polymerization. Every 0.5h one sample was collected from the reaction mixture. Strangely, one more time, after collecting the first sample an increase in the reaction mixture was observed and the reaction had to be stopped after 2 hours. The GPC and ^{1}H NMR results were similar to the results obtained in the first kinetic conducted. The GPC trace of the first sample is a perfect peak and in the subsequently samples a second peak appeared at low molecular weights, as shown in Figure N1 (right). Also the $M_{n,GPC}$ were higher than the $M_{n,th}$, (Figure N2).

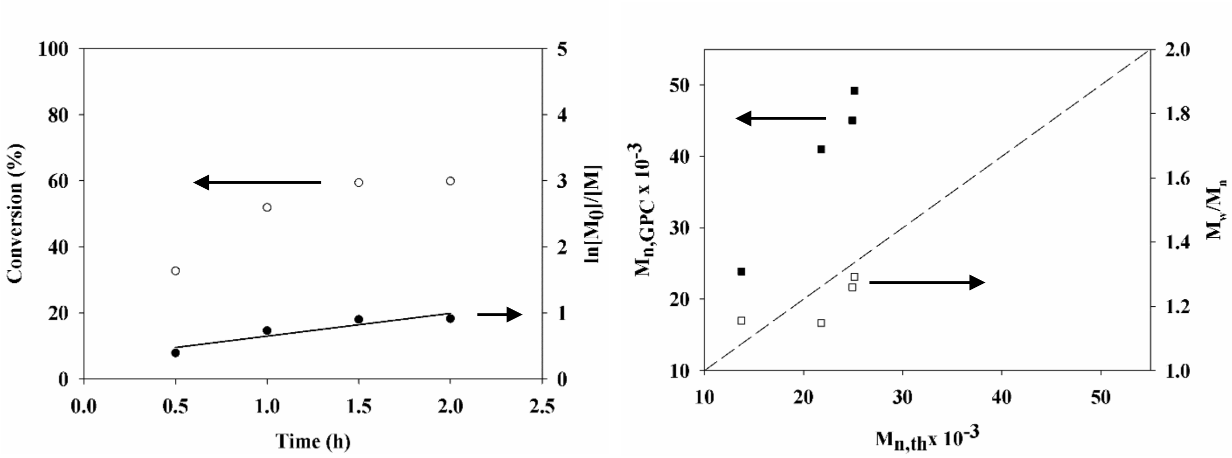

Figure N2. Second reaction conducted with sacrificial initiator. (left) Kinetic plot of conversion and ln[M_0]/[M] vs Time and (right) plot of number average molecular weight, $M_{n,GPC}$, and dispersity values, Đ, vs theoretical number average molecular weight, $M_{n,th}$, for SARA ATRP of PMA catalysed with Cu(0) wire/Me6TREN in DMF at 60ºC.

After these results, the products obtained from the two reactions were exhaustively washed with DMF and THF, by successive centrifugation/redispersion cycles, to remove the free polymer chains and evaluate if attached PMA was produced. The dried powders were analysed by FTIR, TGA and ^{1}H NMR and the results are shown in Figure N4 and Figure N5.

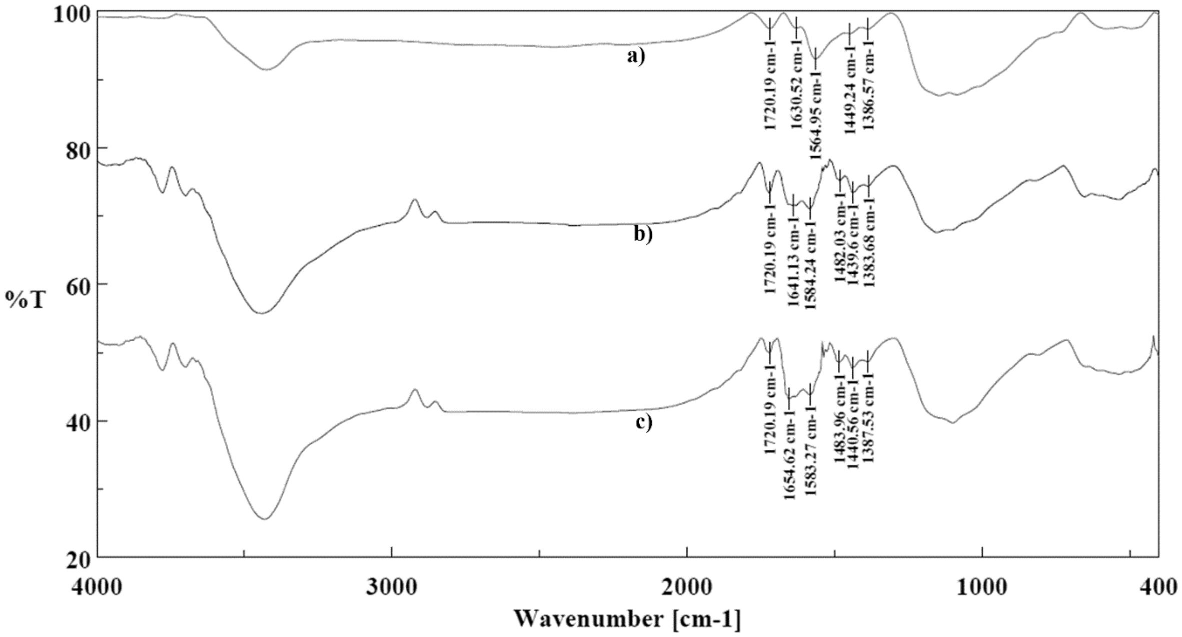

Figure N4. FTIR spectra pf a) GO-Br (Br_G11) and b), c) washed products obtained from the two SARA ATRP of MA in the presence of GO-Br using sacrificial initiator.

The results obtained from the FTIR, TGA and ^{1}H NMR analysis clearly proved that PMA brushes were not grown from the GO's surface. The C=O peak at 1720 cm^{-1} from ester groups remained unchanged, the weight loss measured was not higher when compared to the weight loss of the original GO and any peaks as result of the PMA protons appeared in the ^{1}H NMR spectra of the washed powders.

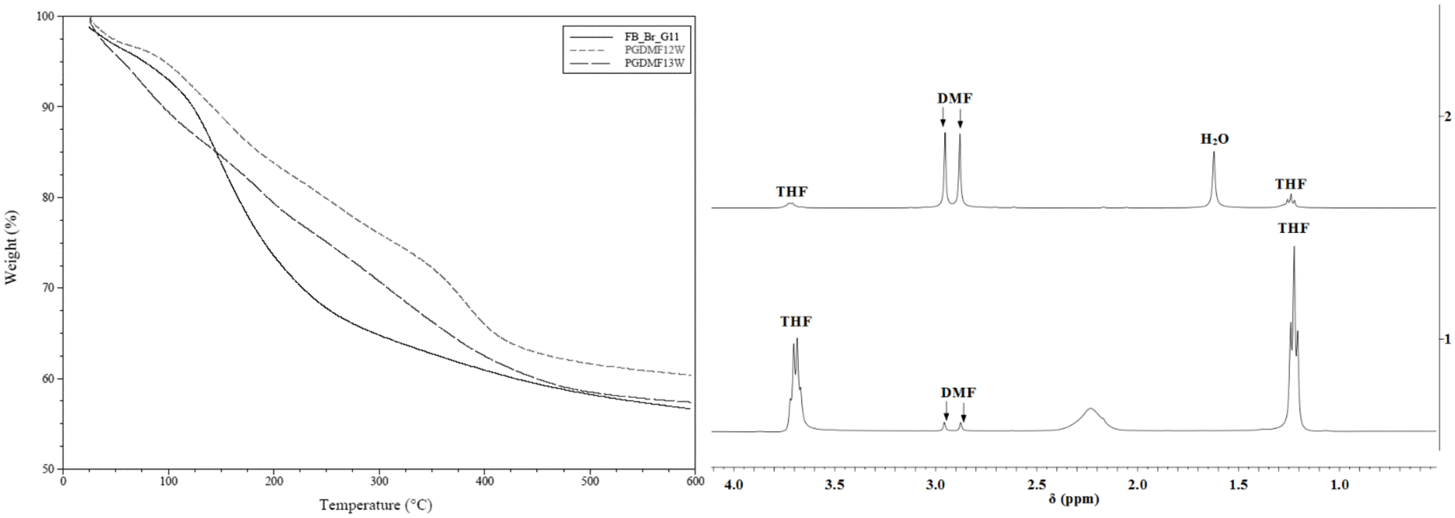

Figure N5. (Left) TGA curves obtained for the esterified GO used as raw material (solid line) and for the two washed products obtained from the SARA ATRP of MA catalysed by Cu(0) wire/Me_6TREN at 60 ºC. (Right) ^{1}H NMR obtained for the respective washed powders collected from the two polymerizations.

With all these results was concluded that when sacrificial initiator was used in the reaction medium, only detached PMA was obtained. Additionally, with these experiments also was demonstrated the efficiency of the washing process, since when only free polymer chains were produced was no observed evidences of PMA in the results, namely in the FTIR and ^{1}H NMR.

The scientific mechanism that led to the results exposed was not understood, since the phenomena is completely unusual. The failure in the attachment of PMA to the surface of GO in the presence of sacrificial initiator could be influenced by the kinetic employed. The increase in the viscosity of the reaction mixture as well as the appearance of a second peak in the GPC traces (at low molecular weights) were observed after collecting the first sample, in both reactions. The collecting of the samples could reduce the number of dormant species in the system, leading to an increase in the propagation rates. Also the easy accessibility of the free initiators when compared to the attached initiator could avoided the polymerization rates. In addition, the higher values of $M_{n,GPC}$ comparatively to the values of $M_{n,th}$ could resulted from the unique reaction occurred between the monomer and the sacrificial initiators, since less initiator sites than the expected were used for the polymerization.

In our opinions in the future works, to better understand the phenomena, should be carried out a reaction with sacrificial initiator without collect samples during the polymerization process. The free polymer chains should be only analysed in the end of the reaction. If the previous phenomena were not observed it means that the problem result from the kinetic conducted to the reactions.

Other suggestion, to improve the control over the grafting polymerization, is to add $CuBr_2$ in the beginning of the reaction to increase the concentration of the deactivator species in the earlier phases of the reactions.

Appendix O – Chemical structures

In this Appendix are presented the structures of the compounds used in the different reactions carried out during all the experimental work.

- **Esterification/amidation reactions**

Raw Material	**GO** 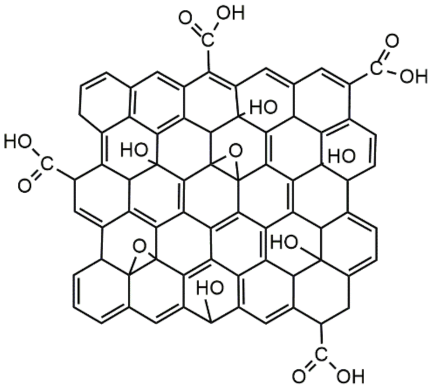
Reactants	BIBB 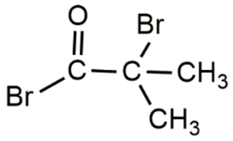 1,3-diaminepropane 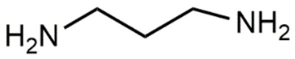
Catalysts	TEA 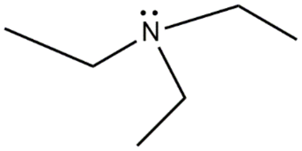 NHS 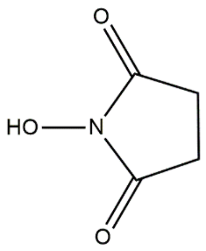 EDC.HCl 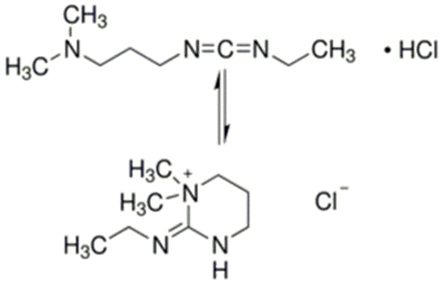
Solvents	DMF 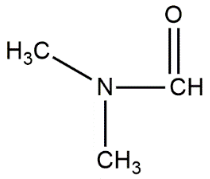

- **Polymerization reactions**

Macroinitiator / Initiator	**GO-Br** 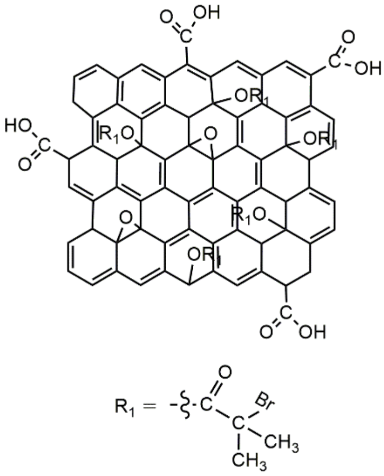 **EBiB** 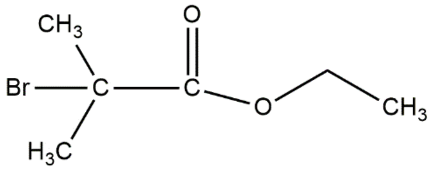
Monomers	MA 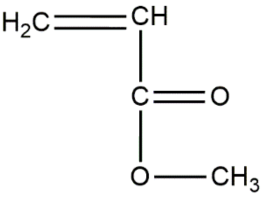 Sty 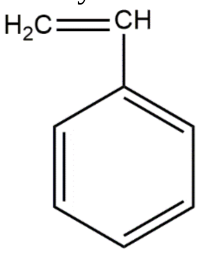
Catalysts	Cooper Bromide Cooper (II) Bromide Cu(0) wire
Ligands	TREN 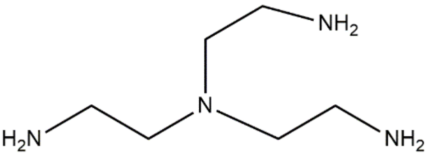 Me_6TREN 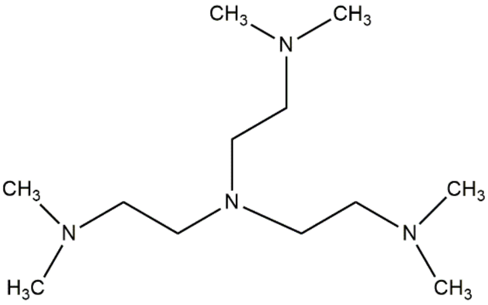
Solvents	DMF 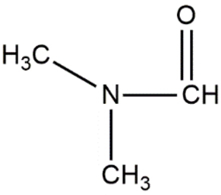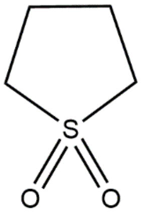 Sulfolane